Triarylamminium radical-cation complexes:

design and magnetic properties

and

Base-catalyzed hydrosilylation:

mechanism and substrate scope

Kseniya Revunova

A thesis submitted to the Department of Chemistry in partial fulfillment of the requirements for the degree of Doctor of Philosophy

Supervised by:

Professor Martin T. Lemaire

And

Professor Georgii I. Nikonov

Brock University,

St.Catharines, Ontario, Canada

Abstract

1. Triarylamminium radical-cation complexes.

The detailed study of manganese, copper and nickel metal-radical complexes with triarylamminium ligands was conducted.

Stable, neutral and pseudo-octahedral coordination monometallic complexes with simple monodentate 2,2`-bipyridine ligand containing a redox-active N,N`-(4,4`-dimethoxydiphenyl-amino) substituent were synthesized and fully characterized. The one-electron oxidation process and formation of persistent radical-cation complexes was observed by cyclic voltammetry and spectroelectrochemical measurements. Evans method measurements were performed with radical-cation complexes generated by chemical one-electron oxidation with $NOPF_6$ in acetonitrile. The experimental results indicate ferromagnetic coupling between metal and triarylamminium cation in manganese (II) complex and antiferromagnetic coupling in nickel (II) complex. This data is supported by DFT calculations which also lend weight to the π spin polarization mechanism as an operative model for magnetic exchange coupling.

Neutral bimetallic complexes with a new ditopic ligand were synthesized and fully characterized, including magnetic and electrochemical studies. Chemical oxidation of these precursor complexes did not generate radical-cations, but dicationic complexes, which was confirmed by UV-vis and EPR-experiments, as well as varied temperature magnetic measurements. DFT calculations for radical-cation complexes are included.

A synthetic pathway for polytopic ligand with multiple redox-active triarylamine sites was developed. The structure of the ligand is presumably suitable for π-spin polarization exchange model and allows for production of polymetallic complexes having high spin ground states.

2. Base-catalyzed hydrosilylation.

A simple reductive base-catalyzed hydrosilation of aldehydes and ketones was adapted to the use of the cheap, safe, and non-toxic polymethylhydrosiloxane (PMHS) instead of the common $PhSiH_3$ and $(EtO)_3SiH$, which present significant cost and safety concerns, respectively. The conversion of silane into pentacoordinate silicate species upon addition of a base was studied in details for the cases of phenyl silane and PMHS and is believed to be essential for the hydrosilylation process. We discovered that nucleophiles (a base or fluoride-anion) induced the rearrangement of PMHS and TMDS into light silanes: $MeSiH_3$ and Me_2SiH_2, respectively. The reductive properties of PMHS under basic conditions can be attributed to the formation of methyl silane and its conversion into a silicate species. A procedure for the generation of methyl silane and its use in further efficient reductions of aldehydes and ketones has been developed.

The protocol was extended to the selective reduction of esters and tertiary amides into alcohols and aldimines into amines with good isolated yields and reduction of heterocyclic compounds was attempted.

Acknowledgements

First of all, I would like to thank both my supervisors – Prof. M. Lemaire and Prof. G. Nikonov – for the opportunity to be part of their groups and projects, for teaching me, for their patience, for their support and encouragement. This thesis would not be possible without their guidance. Their working styles are no less different from each other than magnetism and catalysis are. While the research freedom within the defined project and valuable insights provided by Dr. Lemaire helped me to develop as an independent researcher, at the same time the limitless enthusiasm and intense working pace of Dr. Nikonov was a strong motivation for me. I deeply appreciate these two experiences and I learned a lot from both. Thank you.

I would like to thank my committee members – Prof. S. Rothstein, Prof. J. Atkinson, Prof. M. Pilkington – for their time and valuable suggestions. And my big thanks to Prof. H. Gordon, Faculty of Graduate Studies and Joanne Kremble for supporting my transfer to Prof. Nikonov's group. Prof. H. Gordon, Prof. T. Dudding, Prof. J. Atkinson and Prof. M. Pilkington are thanked for their participation in my candidacy examination. I also thank Prof. T. Yan for his work as a Graduate Program director.

I thank the Razavi group for assistance with magnetic measurements and Prof. A. Van der Est and Sam Mula for EPR experiments. Yong Wang is acknowledged for elemental analysis. Razvan Simionescu is thanked for numerous NMR experiments. I am very grateful to Tim Jones for mass spectrometry characterization and his kind support. I also thank our collaborators Prof. S. Gorelsky (University of Ottawa) for DFT calculations and Dr. Hilary Jenkins (McMaster University) for X-

Ray crystallography. Thanks to John and Jordan Vandenhoff for their artful glassware work and sense of humour.

I am grateful to all members of the Lemaire group for coworking and good lab experiences. I wish to thank the entire Nikonov group for being great mentors, colleagues and friends, in particular: Terry Chu, Nicolas McLeod, Sun-Hwa (Tori) Lee, Courtney Boone, Van Hung Mai and Kostia Piatrou. Big thanks to Terry Chu for proofreading this manuscript.

Since it is impossible to mention here everyone that I wish to, I want to thank all the research group members of the Chemistry department at Brock University, especially the Hudlicky, Metallinos, Pilkington, Stamatatos and Yan groups. It has been a privilege to work among so many talented people in such a friendly atmosphere full of ideas.

At last, I wish to thank my family and friends. And my husband, Sergey Vshyvenko, for all the things I do not want to misspeak with words.

Table of Contents

List of Tables

List of schemes

List of Figures

List of Abbreviations

0D	0-Dimensional
1D	1-Dimensional
2D	2-Dimensional
3D	3-Dimensional
Å	Angstrom
AFM	atomic force microscopy
bipy	bipyridyl
BM	Bohr Magneton
bu	butyl
^{o}C	Degree Celsius
CIDNP	chemically induced dynamic nuclear polarization
CV	cyclic voltammetry
d	doublet
dd	doublet of doublets
DC	Direct Current
DCM	dichloromethane
DFT	Density Functional Theory
DMF	dimethylformamide
DMSO	dimethylsulfoxide
ENDOR	electron nuclear double resonance
EPR	electron paramagnetic resonance
Et	ethyl

EXSY	exchange spectroscopy
g	gram
h	hour
h	Plank constant
hfac	hexafluoroacetylacetone
HOMO	highest occupied molecular orbital
Hz	Herz
INEPT	insensitive nuclei enhanced by polarization transfer
i-Pr	*iso*-Propyl
IR	infrared
J	coupling constant, magnetic exchange parameter
K	Kelvin
LUMO	lowest unoccupied molecular orbital
m	multiplet
M	molar
MFM	magnetic force microscopy
min	minutes
ml	milliliter
mmol	millimole
m.p.	melting point
MRI	magnetic resonance imaging
M_{sat}	saturation magnetization
MS	mass spectroscopy
NMR	nuclear magnetic resonance

nm	nanometer
NPA	natural population analysis
ORTEP	oak ridge thermal ellipsoid plot
OAc	acetate
PMAT	3,5-bis([N-(2-pyridinemethyl)amino]methyl)-4H-1,2,4-triazole
PMHS	polymethylhydrosiloxane
ppm	parts per million
PTM	polychlorotriphenylmethyl radical
py	pyridine
RT	room temperature
s	singlet
S	spin number
SCM	single chain magnet
SMM	single molecule magnet
SOMO	singly occupied molecular orbital
SQUID	superconducting quantum interference device
t	triplet
T	temperature
T_c	critical or Curie temperature
tacn	triazacyclononane
TBAF	tetrabutylammoniumfluoride
TEMPO	2,2,6,6-tetramethylpiperidin-l-oxyl
TFA	trifluoroacetic acid

$THBF_4$	thianthrenium tetrafluoroborate
THF	tetrahydrofuran
TLC	thin layer chromatography
TMDS	tetramethyldisiloxane
UV-vis	ultra violet-visible
V	volt
μ_B	Bohr magneton
μ_{eff}	effective magnetic moment
λ	wavelength
χ	magnetic succeptibility

List of Compounds

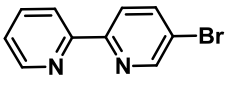

1.1

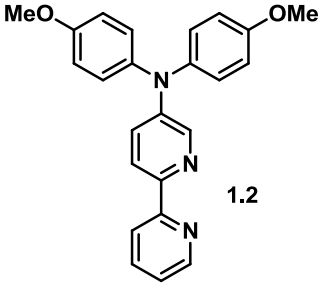

1.2

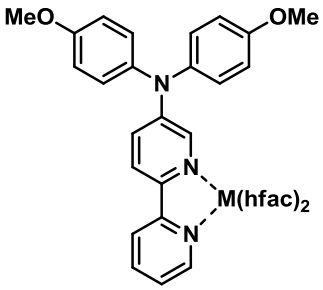

1.3 M = Mn (II)
1.4 M = Ni (II)
1.5 M = Cu (II)

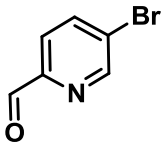

2.1

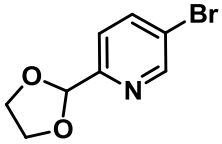

2.2

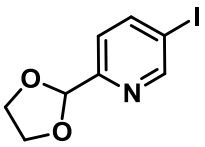

2.3

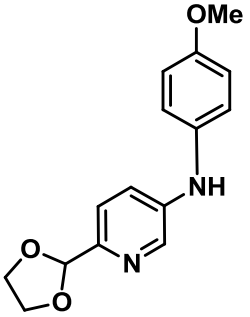

2.4

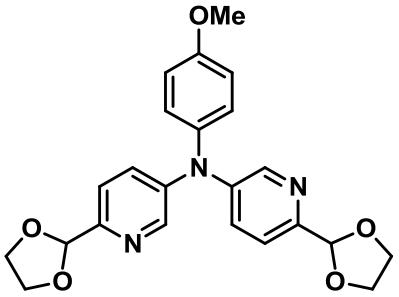

2.5

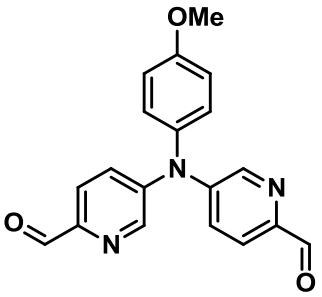

2.6

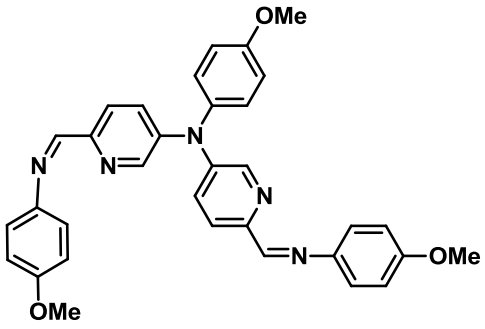

2.7

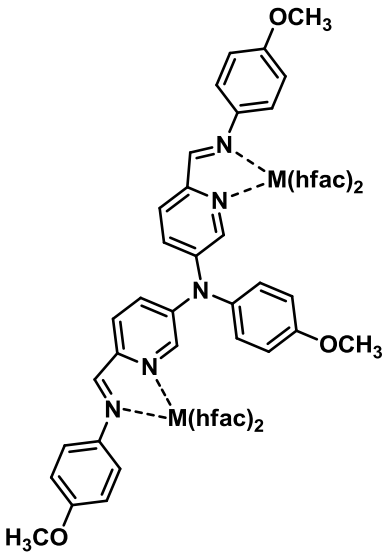

2.8 M = Mn (II)
2.9 M = Ni (II)
2.10 M = Cu (II)

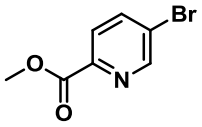

3.1

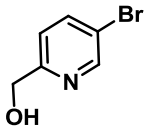

3.2

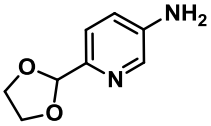

3.3

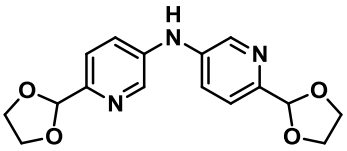

3.4

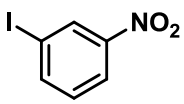

3.5

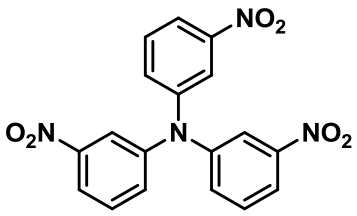

3.6

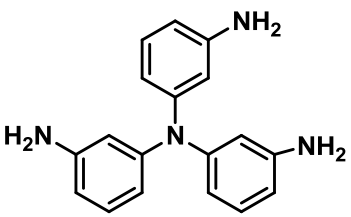

3.7

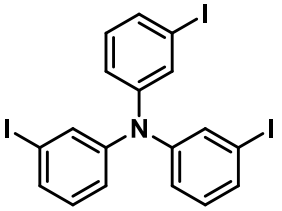

3.8

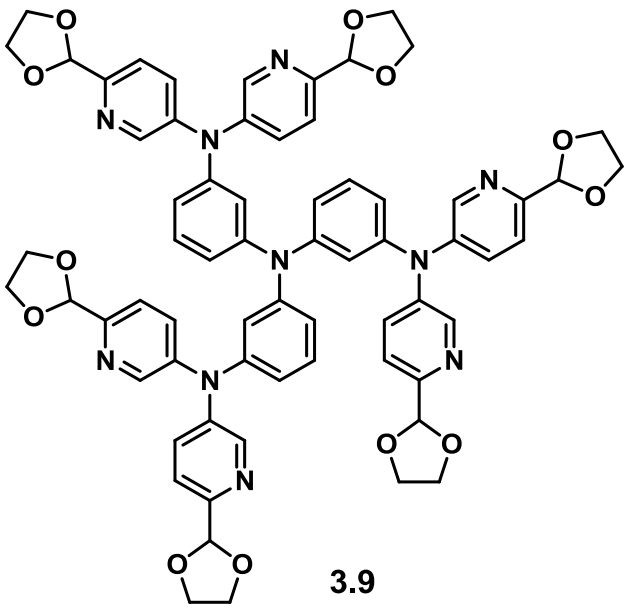

3.9

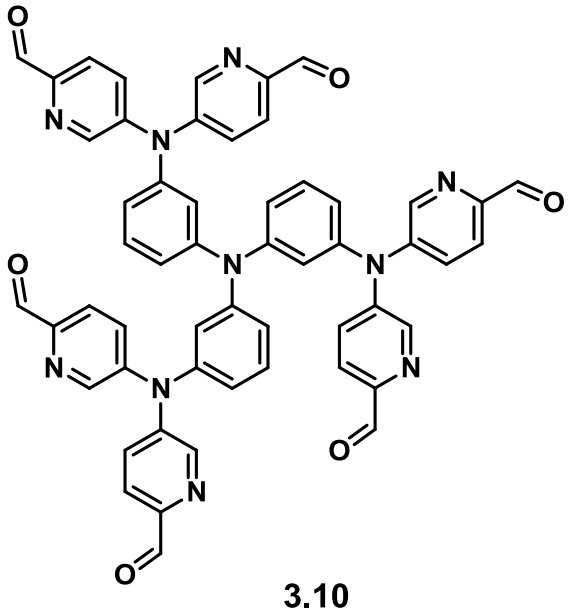

3.10

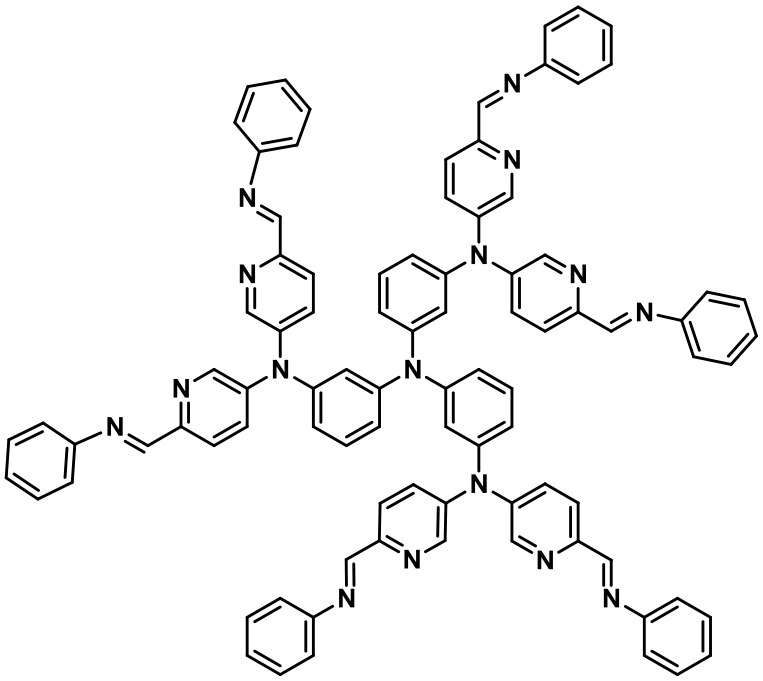

3.11

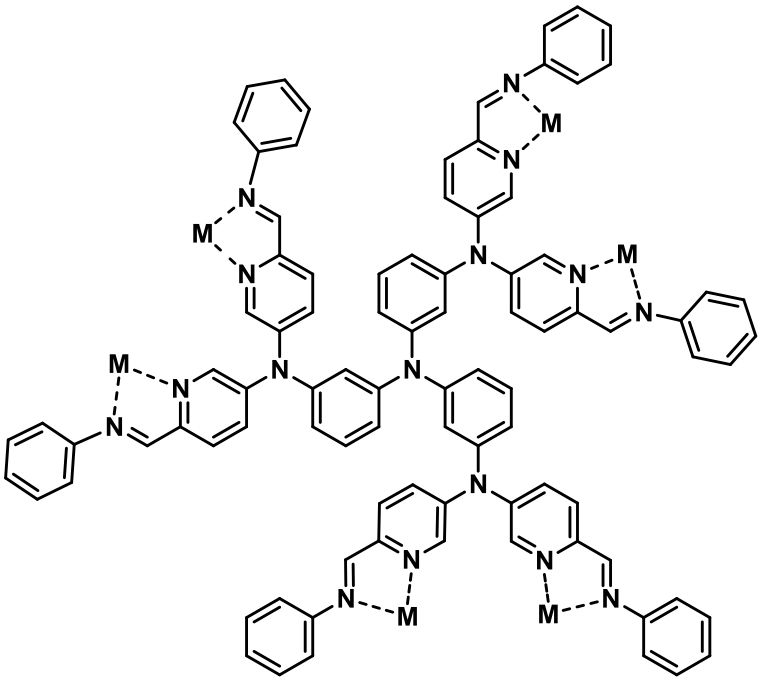

3.12 M = Mn (II)
3.13 M = Ni (II)
3.14 M = Cu (II)

1 Triarylamino radical-cation complexes

1.1 Introduction

The area of molecule-based magnets has developed significantly during last two decades, and the market of magnetic materials is estimated to reach $33 billion by 2018.[1] This resulted in discovery of magnets with ordering temperature close to ambient conditions, extremely high and low coercivities and high remanent and saturation magnetization values.[2] They have potential application in such areas as data storage materials, production of frictionless bearings, medical implants, magnetic separators, quantum computing, magnetic refrigerants, MRI contrast agents, acoustic devices, sensors and magnetic shielding.[2] However, the list of possible magnet application is not full yet. Current goals for the field of molecular magnets include the discovery of transparent insulating magnets, flexible magnets, photomagnets, ultra "hard" (very high coercivity) and soft (high permeability) magnets.[2]

This project is intended to synthesize and explore mono-, bi- and polymetallic triarylamminium-based radical-cation complexes.

1.2 Historical

Since the field of molecular magnets is extremely broad, the goal of this historical overview was not to make an extensive review, but to provide information about the key points of molecular magnetism and the metal-radical approach. In this respect, types of magnetic interaction, examples of molecular magnets as well as organic and metal-organic radicals will be discussed.

1.2.1 Magnetism.

1.2.1.1 Classical and molecular magnetism

The traditional meaning of magnetism, e.g. classical magnetism, is usually referred to co-operative spin-spin interaction of unpaired *d* or *f* - electrons in atom-based materials such as Fe, $SmCo_5$, $Nd_2Fe_{14}B$, etc, while in molecular magnets these interactions can involve unpaired electrons on σ and π molecular orbitals.[3] Atom-based materials are produced *via* high temperature metallurgical processes.[3] Design of molecular magnets assumes combination of unpaired spin-bearing molecular precursors in such a way that spin pairing does not happen.[2-4] The interaction between unpaired spins in molecular magnets can take place through bond or through space if it is allowed by design of molecular lattice.[3] Two general requirements for the design of molecular magnets are the presence of unpaired electrons on every molecule of the structure and parallel alignment of spins along a given direction.[3-4] Interaction of spins through bond or through space in all three directions between molecular units is highly important for magnetic properties of the compound.[3, 5]

1.2.1.2 Key parameters of molecular magnetism.[2, 5-6]

Magnetic properties depend on distribution of unpaired electrons and their movement pattern in the molecules. Similarly to the Earth – Sun system, each electron has both orbital and spin movement modes at the same time. Orbital mode can be described as rotation of electron around the nucleus, while spin mode is spinning of electron around its own axis. Since molecules may have not only one or two, but many unpaired electrons, the magnetic characteristics of the molecule can be described as the summarized magnetic characteristics of all its electrons. Many of those electrons are moving in couples with antiparallel spins within the couple.

Being exposed to an external magnetic field, this electron pair is capable of producing an internal magnetic field with vector direction opposite to the external one. The interaction between the weaker internal field (produced by electron pair) and the stronger external field directed oppositely leads to repelling of the sample to the weaker zone of the external magnetic field. This behaviour is called diamagnetism. Since in the molecules the number of fully occupied orbitals is prevalent, it means that there is a lot of diamagnetic behaviour in every molecular magnetic pattern. However, many species contain half-filled orbitals. Since the spin of the unpaired electron is not cancelled out, under external magnetic field it results in production of the internal field with the direction aligned to the external. In this case the sample will be "pulled" into the intense zone of the external field, and this pattern is called paramagnetism.

Paramagnets – structures containing unpaired electrons – can be classified into categories such as ferromagnets, antiferromagnets and ferrimagnets (**Figure 1**).

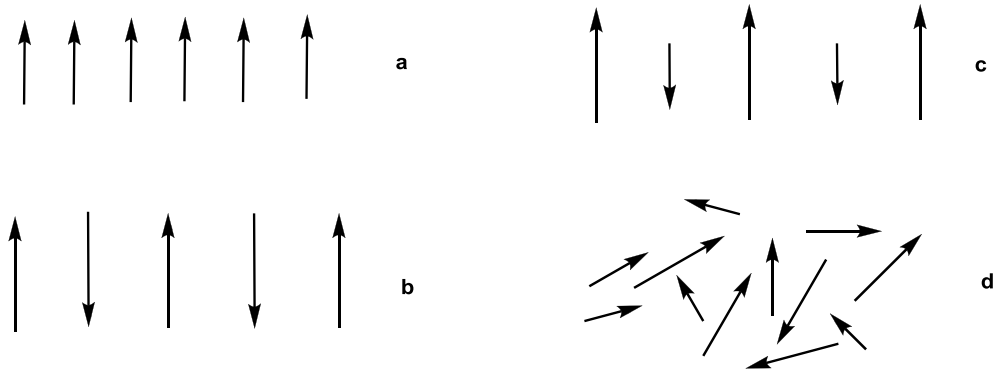

Figure 1: Spin alignment a-ferromagnets, b-antiferromagnets, c- ferrimagnets, d – paramagnets with disordered spins. (Adapted from references 2, 6-7)

In ferromagnets the unpaired spins are aligned, in antiferromagnets the unpaired spins are equal and antiparallel, and in ferrimagnets the spins of antiparallel modes are not equal (**Figure 1**).

Subsequently, the spin number $\boldsymbol{S}$ of a molecule is the sum of spins of all unpaired electrons (**Equation 1**), given the spin of one electron to be $\boldsymbol{M_s} = \pm\frac{1}{2}$

$$\boldsymbol{S} = \sum \boldsymbol{M_s} \quad \textbf{(1)}$$

The spin magnetic moment $\boldsymbol{\mu}$ of the molecule is represented in **Equation 2** (the orbital momentum is neglected):

$$\boldsymbol{\mu} = \mathbf{2}\sqrt{\boldsymbol{S}(\boldsymbol{S}+\mathbf{1})} \quad \textbf{(2)}$$

When ideal non-interacting spins are inserted into magnetic field $\boldsymbol{H}$, a net magnetic moment of magnetization, $\boldsymbol{M}$, is produced, which is proportional to $\boldsymbol{H}$ (**Equation 3**)

$$\boldsymbol{M} = \boldsymbol{\chi H} \quad \textbf{(3)}$$

The constant of proportionality in Eq.3, $\boldsymbol{\chi}$, is called the molar magnetic susceptibility and its temperature dependence can be characterized by the Curie expression (**Equation 4**):

$$\boldsymbol{\chi} = \frac{\boldsymbol{C}}{\boldsymbol{T}} \quad \textbf{(4)}$$

Where the Curie constant $\boldsymbol{C}$ can be expressed with such constants as Avogadro

number $\boldsymbol{N_A}$, the Lande factor $\boldsymbol{g}$, the Bohr Magneton $\boldsymbol{\mu_B}$ and the Boltzmann constant $\boldsymbol{k_B}$ (**Equation 5**)

$$\boldsymbol{C = \frac{N_A g^2 \mu_B^2 2S(S+1)+1)}{3k_B}} \quad \textbf{(5)}$$

When there is an effective parallel or antiparallel exchange field between spins caused by weak cooperative interactions with the neighbouring spins, it affects magnetic susceptibility, therefore the measured data will differ from the one predicted by Curie law. The Curie-Weiss law (**Equation 6**) can be used to express the magnetic susceptibility (**Equation 6**), where the Weiss constant is $\theta > 0$ for ferromagnets and $\theta < 0$ for antiferromagnets.

$$\boldsymbol{\chi = \frac{C}{T-\theta}} \quad \textbf{(6)}$$

The effective magnetic moment μ_B in this case can be described by **Equation 7**:

$$\boldsymbol{\mu_{eff} = \sqrt{\frac{3\chi k_B T}{N_A}} = 2.83\sqrt{\chi T}} \quad \textbf{(7)}$$

At the same time for the simple systems with $\boldsymbol{\theta = 0}$ effective magnetic moment does not depend on temperature (**Equation 8**)

$$\boldsymbol{\mu_{eff} = \mu_B\sqrt{g^2 S(S+1)}} \quad \textbf{(8)}$$

One of the most complete examples of magnetic behaviour dependence on the magnetization – applied magnetic field relation was found in [6] (**Figure 2**)

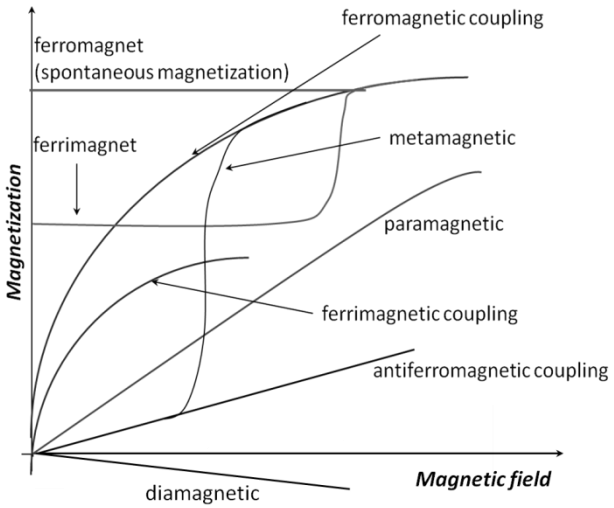

Figure 2: Relation between magnetization and applied magnetic field. Adapted from reference 6.

1.2.1.3 Spin polarization in molecular magnets.

There are few approaches for spin polarization prediction and modeling. The simplest one is based on an intraatomic Hund's rule, which states that electrons on the atom are most likely to have parallel spins, and on the fact that electrons participating in a chemical bond have antiparallel spins.[6]

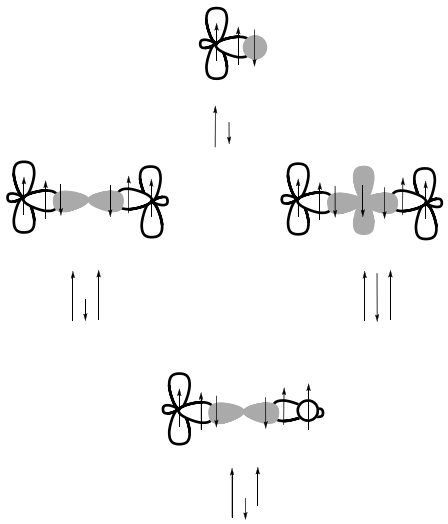

Figure 3: Representation of the spin polarization in the adjacent σ and π bonds. Adapted from reference 6.

It is also known that unpaired electron can polarize the pair of electrons in the adjacent σ or π bond, so that one of those two electrons will be located closer to one of the bond-forming atoms.[6] The radicals in the molecules are usually located at a distance from each other, which is long enough to prevent their coupling. At the same time if the distance is short enough so the radicals could be involved in cooperative interactions, their spins get aligned (**Figure 3**). For example, radical spins in the structure shown on **Figure 4** have ferromagnetic interactions because of metasubstituition pattern. At the same time ortho- or parasubstituted structure would have antiferromagnetic coupling mode because of an even number of atoms on a pathway between two radical-spin sites.[8]

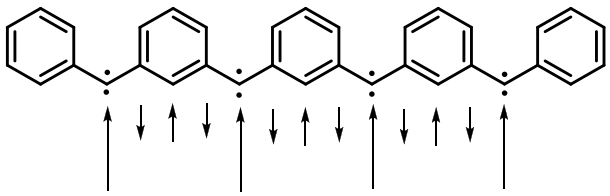

Figure 4: Spin polarization in polyradical structure.[6, 8a]

This approach was proposed and tested on polycarbene structures by Iwamura.[8a] He and his group were able to obtain tetracarbene with $\boldsymbol{S = 4}$, hexacarbenes with $\boldsymbol{S = 6}$ [8b] and even nonacarbenes with $\boldsymbol{S = 9}$ [9,6]. A number of other examples of this spin polarization model are presented in the discussion of organic radicals.

The mode of alignment strongly depends on the type of atoms and the number of chemical bonds between those spins and can be either ferromagnetic or antiferromagnetic.[6]

If this spin alignment occurs in the solid state, then bulk magnetism can be observed (**Figure 1**). Usually three-dimensional interactions are required to maintain bulk magnetic properties; however there are examples of 2D and even 1D interactions leading to the long-range magnetic order. [6]

The parameter characterizing spin-spin interactions is the $\boldsymbol{J}$ value or spin-coupling constant. For example, the Heisenberg Hamiltonian describing the system of two spins $\boldsymbol{S_1}$ and $\boldsymbol{S_2}$ is presented in **Equation 9**: [10]

$$\boldsymbol{H = -2JS_1S_2} \quad \textbf{(9)}$$

When spins are ferromagnetically coupled, $\boldsymbol{J} > 0$, and $\boldsymbol{J} < 0$ for antiferromagnetically coupled systems. [10] When more than two spins are involved, especially in polyradical systems, **Equation 9** is transformed into **Equation 10**: [10]

$$\boldsymbol{H = -2\sum J_{ij}\, S_iS_j} \quad (10)$$

In this case spin-spin interaction may be related to either inter- or intramolecular interactions.

Intramolecular interactions may show four possible values of coupling constant: $\boldsymbol{-J \gg kT}$, $\boldsymbol{S = 0}$ (even number of spins) or $\boldsymbol{S = \frac{1}{2}}$ (odd number of spins) – strong antiferromagnetic coupling; $\boldsymbol{J \gg kT}$, $\boldsymbol{S = \frac{number\ of\ spins}{2}}$ – strong ferromagnetic coupling; $\boldsymbol{|J| \ll kT}$, $\boldsymbol{S = \frac{1}{2}}$ – very weak ferromagnetic or antiferromagnetic coupling; $\boldsymbol{J \approx kT}$ - weakly coupled polyradicals, all possible geometrical configuration of the structure must be taken into account for coupling characterization. [10]

Intermolecular interactions can be observed in solids as well as sometimes in dilute, frozen solutions. Their existence brings a lot of additional steps and parameters into magnetic characterization and is generally accounted for using the Weiss constant; however study of these interactions is essential for further development of molecular magnets with high bulk magnetic characteristics. [10]

The spin-spin interactions in dinuclear (or polynuclear) complexes can be described with the famous Bleaney-Bowers equation (**Equation 11**), where $\boldsymbol{N_a}$ is accounted for temperature-independent molar paramagnetic parameter[11]:

$$\boldsymbol{\chi_M = \frac{2g^2N\beta^2}{3kT}(1 + \frac{1}{3}e^{J/kT})^{-1} + N_a} \qquad \textbf{(11)}$$

This approach is widely used for the study of binuclear systems by analyzing low temperature susceptibility data.

For example, in a binuclear copper (II) system, where each metallic site has one unpaired electron ($\boldsymbol{S = \frac{1}{2}}$), the possible types of spin-spin interaction include ferromagnetic ($\boldsymbol{J > 0,\ \ S = 1}$) and antiferromagnetic ($\boldsymbol{J < 0,\ S = 0}$) coupling as well as a case of two non-interacting independent spins ($\boldsymbol{J = 0}$). Schematic representation of magnetic behaviour for each case is shown on **Figure 5**:

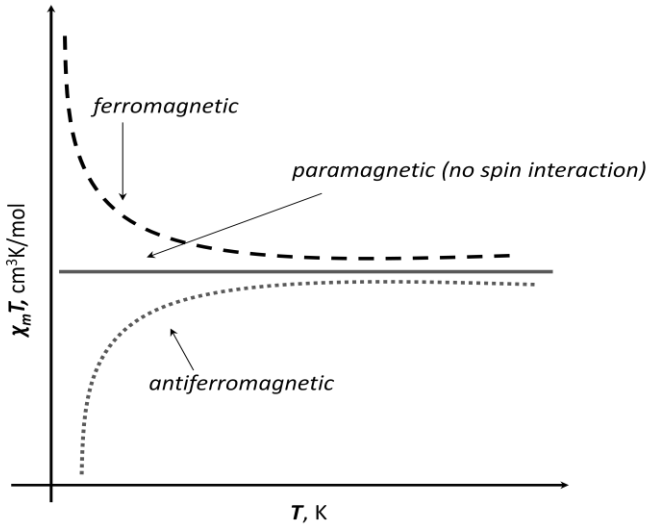

Figure 5: Schematic drawing of magnetic succeptibility×temperature vs temperature plots for binuclear systems with ferromagnetic and antiferromagnetic spin interaction, the paramagnetic interaction assumes two independent spins with no interaction.

Out of these three systems, the one featuring ferromagnetic coupling is considered high-spin. **Equation 7** can be used for calculation of effective magnetic moment $\boldsymbol{\mu_{eff}}$ and this data can be used in **Equation 8** to obtain the actual number of the unpaired electrons.

$$\boldsymbol{M = Ng\mu_\beta S \cdot B_s(y)} \quad \textbf{(12)}$$

$$\boldsymbol{B_s(y) = \frac{2S+1}{2S}\coth\left(\frac{2S+1}{2S}y\right) - \frac{1}{2S}\coth\left(\frac{1}{2S}y\right)} \quad \textbf{(13)}$$

$$\boldsymbol{y = \frac{g\mu_\beta SH}{kT}} \quad \textbf{(14)}$$

Another way to get information about the spin number value is through the Brillouin function (**Equations 12-14**)[12] calculations performed with the data, obtained in a series of experiment where the saturation magnetization is determined by varying the magnetic field at low temperatures (**Figure 6**)

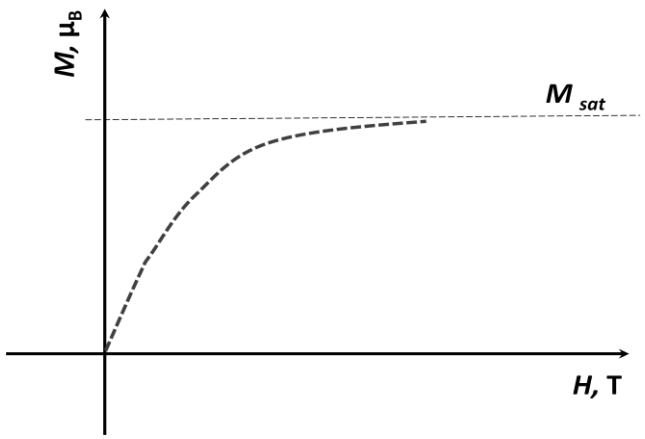

Figure 6: Schematic drawing of saturation magnetization experiment.

The ferri- or ferromagnetic property can be also confirmed *via* a low-temperature magnetization vs magnetic field experiment (also see **Equation 3**), which shows a hysteresis loop pattern with distinct, almost vertical parallel sides (**Figure 7**).

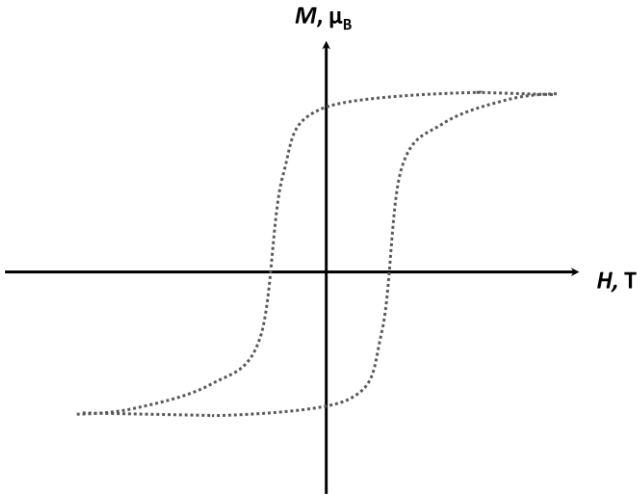

Figure 7: A schematic drawing of data representation for high-spin system in low temperature magnetization/magnetic field experiment.

1.2.1.4 Characterisation of magnetic materials.

Magnetic materials can be characterized by their response to the applied magnetic field.[6]

SQUID, super conducting quantum interference device, is a flux method that allows for measurement of magnetization $\boldsymbol{M}$ as a function of temperature $\boldsymbol{T}$ and applied static magnetic field $\boldsymbol{H}$. Therefore, magnetic susceptibility $\boldsymbol{\chi}$ can be obtained as $\boldsymbol{\chi = \frac{M}{H}}$.[10] The temperature range used for these measurements is usually between the liquid helium temperature (~ 2 K) and room temperature (~ 300 K), however high temperature SQUID-devices are also known.[5] A schematic diagram of the SQUID magnetometer is presented on **Figure 8**. The sample is slowly moved through the superconducting pick up coil in a constant magnetic field, maintained with a superconducting shield. The signal is integrated by counting voltage steps.[13]

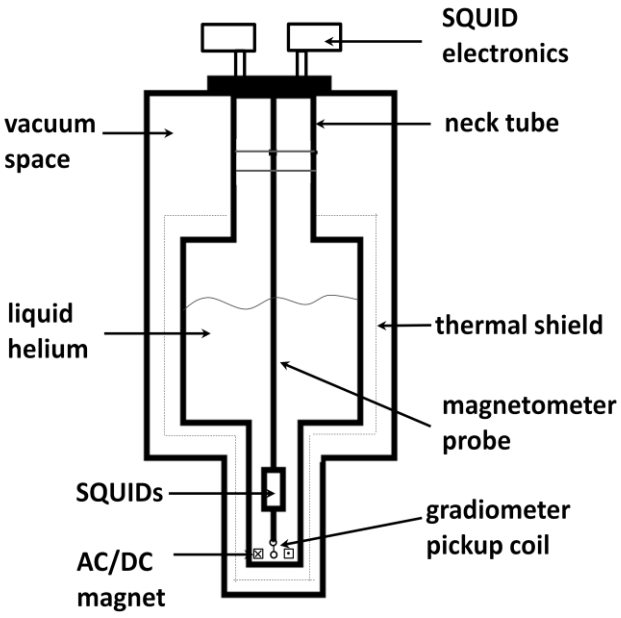

Figure 8: Schematic representation of the SQUID magnetometer.
Adapted from reference 14.

NMR techniques, such as the Evans method, are successfully used in the characterization of magnetic compounds for measuring the effective magnetic moment and determination of the number of unpaired electrons. The method was proposed by Dennis Evans in 1959. [15] The magnetic susceptibility can be found as a function of temperature in deuterated solvents by measuring the shift difference between the solvent or standard compound with and without the presence of the studied paramagnetic sample in a ^{1}H NMR spectrum. The experimental set up can be maintained by use of a special NMR-tube with coaxial insert NMR-tube or a regular NMR-tube with a sealed capillary insert. The inner tube contains solvent or the standard compound in solution, while the outer tube is filled with the solution of the paramagnetic species or vice versa. In the original work of Evans magnetic susceptibility was calculated with **Equation 15**:[15a]

$$\boldsymbol{\chi = \frac{3\Delta f}{2\pi f m} + \chi_0 + \frac{\chi_0(d_0 - d_s)}{m}} \qquad \textbf{(15)}$$

Where $\boldsymbol{\Delta f}$ is the observed frequency shift, in $^{cycles}/_{sec}$ or *Hz*, $\boldsymbol{f}$ is the frequency at which the proton resonances are being studied, in $^{cycles}/_{sec}$ or *Hz*, $\boldsymbol{m}$ is the mass of the substance studied per 1 ml of solution, in g, $\boldsymbol{\chi_0}$ is the mass susceptibility of the solvent, in $^{cm^3}/_{g}$, and finally the $\boldsymbol{d_0}$ and $\boldsymbol{d_s}$, solvent and solution density, in $^{g}/_{cm^3}$.

In modern NMR equipment the applied magnetic field is usually parallel to the sample tube axis, while in Evans case the magnetic field vector was perpendicular to the tube axis. In this case **Equation 11** can be transformed into **Equation 16**:[16]

$$\chi = \frac{-3\Delta f}{4\pi f m} + \left[\chi_0 + \frac{\chi_0(d_0 - d_s)}{m}\right] \quad \textbf{(16)}$$

As the concentrations used are relatively low and therefore the densities of solvent and solution are very close, then solution density can be assumed by $d_s = d_0 + m$ and, subsequently,[16a]

$$\chi = \frac{-3\Delta f}{4\pi f m} \quad \textbf{(17)}$$

For the effective magnetic moment calculation (**Equation 14**) the obtained mass magnetic susceptibility χ is transformed into molar susceptibility and corrected by its diamagnetic component with Pascal constants to $\chi_{m'}$ [16a]

$$\mu_{eff} = 2.82\sqrt{\chi_{m'} T} \quad \textbf{(18)}$$

EPR (or ESR) spectroscopy is one of the most useful techniquess for obtaining information about unpaired spins. The method is based on exciting electron spins under an applied strong magnetic field. It was used for triplet excited state ($S = 1$) detection and is commonly applied for $S > 0$ states studied in bi- and polyradicals.[10] While this method is a reliable source of qualitative information, its quantitative application such as spin number counting for polyradicals study is limited since determination of hyperfine coupling constant *A* is difficult for $S > \frac{1}{2}$. In polyradicals with $|J| \ll kT$ the electron-electron spin coupling may be observed by EPR/ESR techniques.[10]

The Faraday balance, Evans balance and Gouy balance are simple and similar devices used for the measurement of mass magnetic susceptibility.[5, 18] For example, in the Gouy balance method (**Figure 9**) a cylindrical sample attached to a

sensitive analytical balance is inserted into magnetic field, and the force produced due to sample magnetization is measured.[18b]

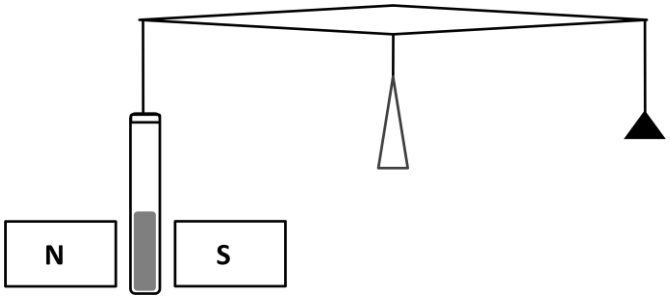

Figure 9: Schematic drawing of Gouy balance. Adapted from reference 13.

Out of data obtained with the balance the magnetic susceptibility can be calculated with **Equation 19:**[18b]

$$\chi = \frac{2g(m_2 - m_1)}{AB^2} \quad \textbf{(19)}$$

Where m_2 and m_1 are masses of the sample with and without applied magnetic field respectively, A is cross-sectional area of the sample and B is the magnetic field.[18b]

Mössbauer spectroscopy is based on recoilless emission and resonant absorption of γ–radiation by an atomic nuclei.[19] It allows for determination of magnetic order temperature by studying the temperature variation of the magnetic hyperfine field. [20] This technique is extremely helpful in the characterization of spin cross-over compounds (especially bi- and polynuclear), for detection of high and low spin states, metal-to-metal electron transfer phenomenon and glass transitions.[21] For example, Mössbauer method was successfully used in the study of dinuclear iron complex, such that the data obtained showed thermal spin transition from double high-spin state to high-spin plus low-spin state but no mixture of double high and

double low states was detected (**Figure 10**).[21] Although Mössbauer spectroscopy is usually considered as a method for studying of ^{57}Fe compounds, its application can be extended to certain isotopes of other metals such as lanthanides, nickel, tungsten, osmium, zinc, silver, ruthenium, platinum, etc.[22]

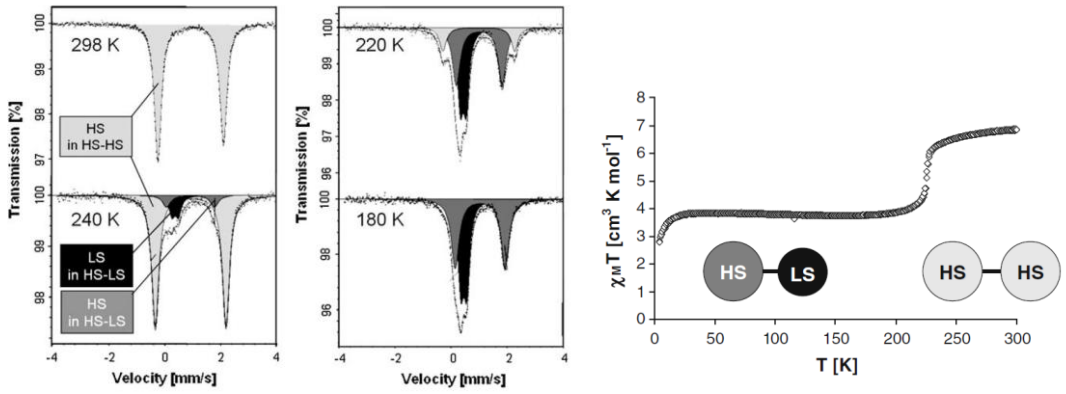

Figure 10: Mossbauer spectra of $[Fe^{II}_2(PMAT)_2](BF_4)_4 \cdot DMF$ at various temperatures (left), magnetic susceptibility*T vs temperature plot (right). Reprinted with permission from reference [23]. Copyright © 2005 Royal Society of Chemistry.

Other methods to study magnetic properties include but are not limited to chemically induced dynamic nuclear polarization (CIDNP),[10] electron nuclear double resonance (ENDOR),[10] neutron scattering,[10] thermal analysis,[5] closed circuit magnetization measurements with hysteresisgraph,[5] etc. Electronic properties of magnetic compounds can be also studied by UV-vis and IR spectroscopy. Electrochemistry is used for oxidation-reduction characterization as well.

1.2.2 Molecule-based magnets.

Compared to traditional magnets, molecular magnets have a wider range of interesting features and advantages, such as: low density, mechanical flexibility, low-temperature processability, high strength, modulation/tuning of properties by means of organic chemistry, solubility, low environmental contamination, compatibility with polymers for composites, biocompatibility, high magnetic susceptibilities high

magnetizations, high remanent magnetizations, low magnetic anisotropy, transparency, semiconducting and/or insulating dc electrical, conductivity.[2] Molecular magnets can be categorized in a number of different ways such as by the type of architectural arrangement, magnetic interactions, size, number of metallic centers, coordination pattern, spin number, synthetic pathway, ligand type, etc. In this work a few families of molecular magnets will be briefly discussed while the main attention will be focused on organic and metal-organic radical magnets.

1.2.3 Types of molecular-based magnets

1.2.3.1 Single molecule magnets

Unlike traditional bulk magnets with atomic structure, in single molecule magnets (SMM) each molecule acts as a magnet due to the presence of unpaired electrons in the partially filled *d*-orbitals of transition metals while its organic core prevents magnetic contacts with neighbouring molecules.[24] The first SMM reported was a mixed valence manganese cluster $[Mn_{12}O_{12}(O_2CMe)_{16}(H_2O)_4]$ with $Mn^{III}_8Mn^{IV}_4$ ratio and ground spin of $S = 10$ (**Figure 11**).[24a, 25] In this molecule for central Mn^{III} atoms were weakly ferromagnetically coupled while the rest of Mn^{III} atoms were involved into antiferromagnetic $Mn^{III}Mn^{III}$ and $Mn^{III}Mn^{IV}$ interactions. These interactions are essential, because large metal clusters with large ground state number and with the symmetry not allowing for intramolecular metal-metal interactions cannot be considered as single molecule magnets.[25b] The well-known examples of SMMs are $[Fe_8O_2(OH)_{12}(tacn)_6]Br_8$ (where tacn = triazacyclononane), $[Mn_4O_3Cl(O_2CCH_3)_3(dbm)_3]$ (where dbm = dibenzoylmethane), $[Fe_4(OH)_6(dpm)_3]$ (where dpm =dipivaloylmethane).[25b, 26]

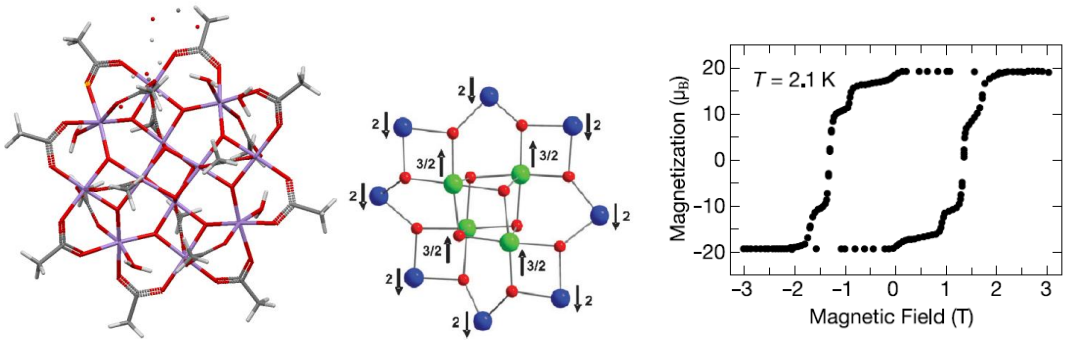

Figure 11: The structure (left), spin orientation (center) and magnetization vs magnetic field data (right) for $[Mn_{12}O_{12}(O_2CMe)_{16}(H_2O)_4]$. Adapted and reprinted with permission from reference [24a]. Copyright © 2009 Royal Society of Chemistry.

The following reports can be mentioned to name just a few of the most recent discoveries in the SMM field: lanthanide single-molecule magnets with fluorescent properties,[27] SMM cobalt complex with unusual fully reversible on/off switching for both anodic and cathodic states[28] from the Murugesu group, the first f-element nitrosyl complex exhibiting temperature-independent paramagnetism,[29] and the first report of spin-crossover SMM featuring light-actuated magnetic tristability phenomenon[30] from Long *et al*, etc.

1.2.3.2 Single chain magnets

Although the early approach to magnets design exploited 3-D structural organization, the discovery of SMMs led to 0-D arranged structures, since single molecule magnets tend to form isolated wheel-shaped structures and molecular clusters.[31] In 1963 Glauber suggested that cluster building blocks due to their ligand arrangement properties can form 1-D polymer chain-like structures, in which intrachain magnetic coupling values will largely exceed interchain interactions.[32] One of the first SCM (single chain magnets) was the cobalt complex $Co(hfac)_2[NIT(C_6H_4$*p*$-OMe)]$ (ligand shown on **Figure 12**) obtained by the Gatteschi

group in 2001.[32b] The 1D chain consisted of alternating cobalt (II) acetylacetonate and nitroxide radical parts. The complex exhibited slow relaxation of the magnetization and hysteresis effect where the chains acted as superparamagnetic nanowires.

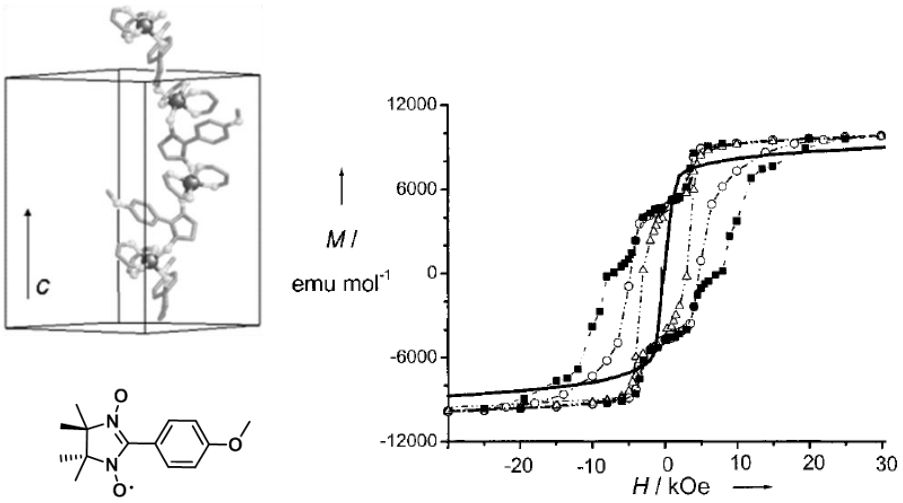

Figure 12: Chain structure (top left), nitroxide ligand (bottom left) and hysteresis effect of $Co(hfac)_2[NIT(C_6H_4p\text{-}OMe)]$ (right). Reprinted with permission from reference [32b]. Copyright © 2001 WILEY-VCH Verlag GmbH & Co. KGaA, Weinheim.

The weak interchain magnetic interactions, mentioned above, and significant easy-axis magnetic anisotropy originated from anisotropic building blocks are the main factors of SCMs. A number of various single chain magnets with bulky organic ligands have been reported up to the moment (**Figure 13**). Current challenges in the SCM field include production of multifunctional chains with additional properties such as conductivity, magnetostriction and higher blocking temperatures, obtaining of surface-anchored chains and SCM-based nanoparticles.[31]

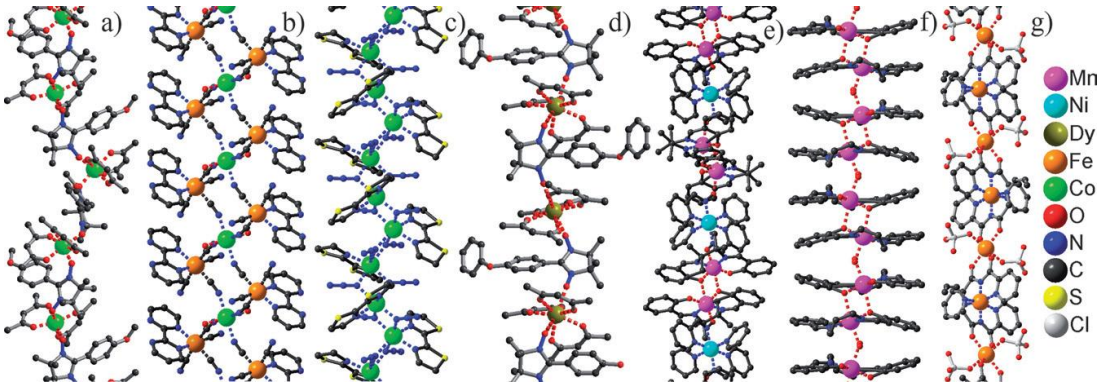

Figure 13: Examples of single-chain magnet structures. Reprinted with permission from reference 31. Copyright © 2008 Royal Society of Chemistry.

1.2.3.3 Polycyanometalates

The history of cyanocomplexes started with the discovery of Prussian Blue in 1704 by German painter Diesbach,[33] followed by structural studies conducted by Ludi and Gudel in 1973.[3] Since cyanometalates can coordinate to a variety of different metal ions, the number of structures known and studied up to the moment exceeds thousands, of which most exhibit magnetic properties.[34] The cyano-group bridges are known to maintain strong ferromagnetic or antiferromagnetic interactions [35] and high Curie temperatures.[3, 36]

Tricyanometalates are highly versatile motifs for construction of 0-D (SMMs) and 1-D (SCMs) magnetic architectures.[37] The 0-D metal clusters represent a variety of complex shapes (**Figure 14**) as well as simple linear clusters.[38]

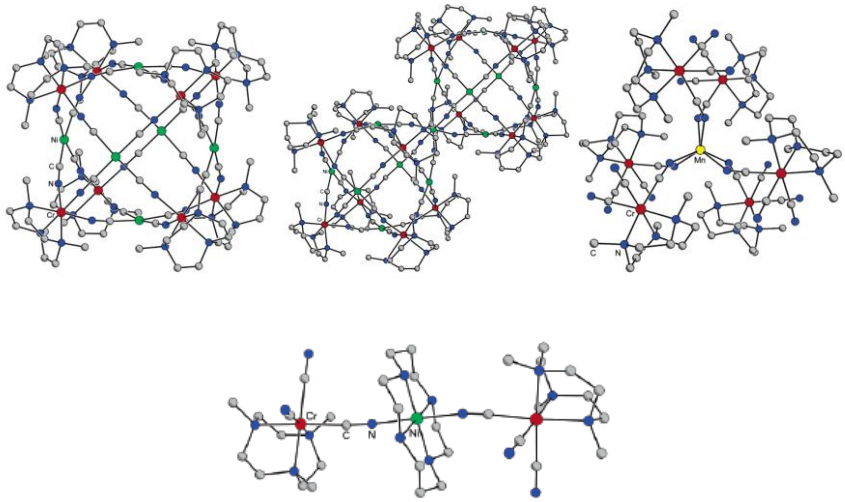

Figure 14: Top: left – Face-centered cubic cluster $[(Me_3tacn)_8Cr_8Ni_6(CN)_{24}]^{12+}$ [39], center – double face-centered cubic cluster $[(Me_3tacn)_{14}Cr_{14}Ni_{13}(CN)_{48}]^{20+}$ [39], right – trigonal prismatic cubic cluster $[(Me_3tacn)_6MnCr_6(CN)_{18}]^{2+}$ [40]. Bottom center: $[(Me_3tacn)_2(cyclam)NiCr_2(CN)_6]^{2+}$ [38-39]. Reprinted with permission from references 38-40. Copyright © 2000,2002,2005 American Chemical Society.

A large share in the field of molecular magnets belongs to Prussian Blue ($Fe^{III}_4[Fe^{II}(CN)_6]_3\times15H_2O$) analogues. Most metal hexacyanometallates have cubic 3D structure (**Figure 15**) where the cyanide groups bridge transition metal ions occupying the cube corners.[3]

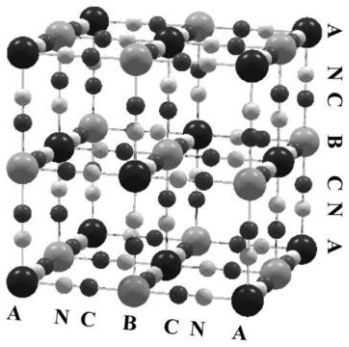

Figure 15: The 3-D-structure of Prussian Blue analogue. Reprinted with permission from reference 3. Copyright © 2009 Indian Academy of Sciences.

The hepta and octa- cyanates' coordination properties provide plenty of opportunities to create 0-D, 1-D, 2-D and 3-D structures.[3, 34] The first octacyanometalate hexanuclear complex containing octahedral cyanide-bridged core

surrounded by bipyridyl ligands was reported in 2000 by Sieklucka *et al*. (**Figure 16**, left) [41] followed by the first high spin cyanide-bridged Mn_9W_6 cluster with a full-capped cubane structure and $S = {}^{39}/_{2}$ (**Figure 16**, right).[42]

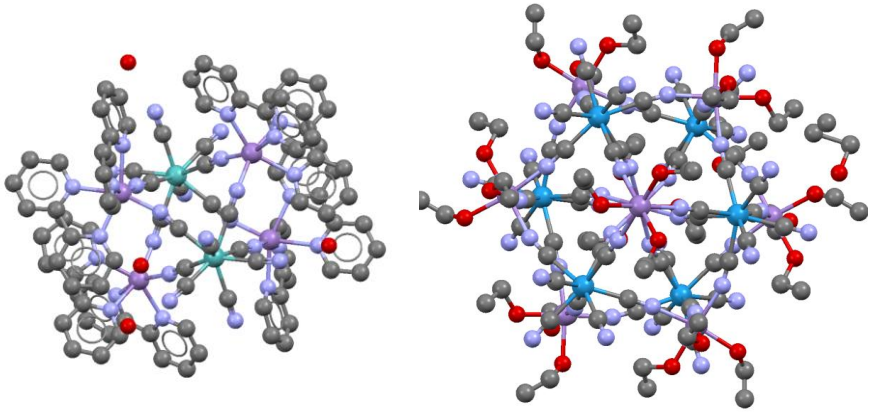

.

Figure 16: Structures of hexanuclear octacyanometalate complex[41] and cyanide-bridged Mn_9W_6 cluster[42]. Adapted with permission from references 41 and 42. Copyright © 2000 American Chemical Society.

The current challenges in polycyanometalates chemistry are focused on increasing the T_c, improvement of magnetic relaxation parameters, development of lanthanide-centered luminescent complexes, cross-over systems and multifunctional materials.[34]

1.2.3.5 Organic radicals.

Despite the generally high reactivity of organic radicals due to their open-shell structure and presence of unpaired electrons on the highest occupied molecular orbitals, persistent organic radicals can be obtained *via* protection of the paramagnetic center with bulky substituents.[43] (Note: In this part of historical review only organic radicals without coordinated metal ions will be discussed. The metal-radical approach will be considered in the following chapter.)

1.2.3.5.1 Organic monoradicals.

1.2.3.5.1.1 Triphenylmethyl radical.

Triphenylmethyl radical, the first open-shell organic radical, was discovered by Gomberg in 1900.[43-44] The ways to study its electronic properties were limited by the high reactivity of the compound. It became evident that two important factors that must be taken into account when designing a neutral molecular radical are the spin stabilization and ability to control the electronic structure which is critical for intermolecular interactions.[43] While spin stabilization can be achieved through introduction of sterics around the radical center, which helps to prevent dimerization and oxidation and enhances formation of crystal structures and intermolecular spin-spin interactions, at the same time, control of electronic properties can be realized by use of heteroatoms which also provide possibility to delocalize unpaired electrons through resonance.[43]

In polychlorinated triphenylmethyl radical the spin bearing central sp2-carbon is shielded by ortho-chlorines of the bulky polychlorophenyl substituents (**Figure 17**), which provides remarkable chemical and thermal stability as well as high magnetic characteristics.[43, 45]

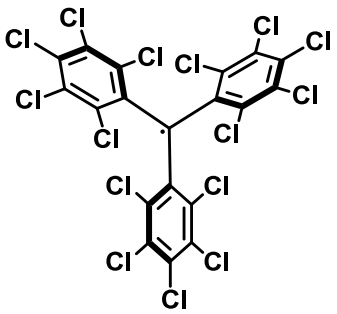

Figure 17: *Minus*-atropoisometric form of polychlorotriphenylmethyl (PTM) radical.[43]

1.2.3.5.1.2 Nitroxides, verdazyls and thiazyls

The approach for enhancing the electronic properties by including heteroatoms into the molecular structure is widely exploited for the development of stable radicals based on nitroxides, verdazyls and thiazyls (**Figure 18**).[43, 46]

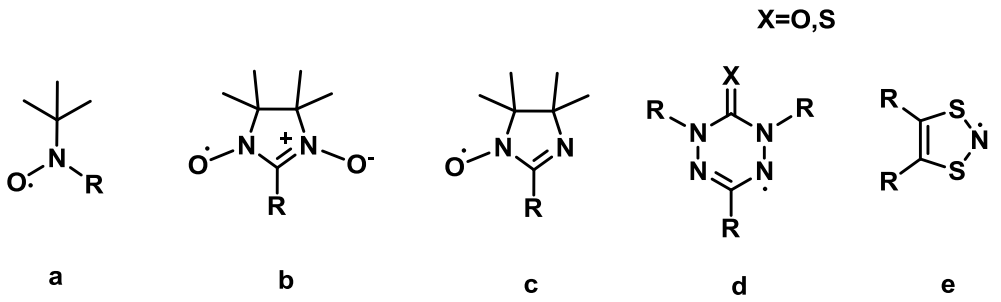

Figure 18: a – tert-butylnitroxide, b – α-nitronyl nitroxide, c – α-imino nitroxide, d – verdazyl, c – 1,3,2 – dithiazole radicals.[43, 46b]

Interest in nitroxide and verdazyl radicals, a popular object of study in late-1960s, massively rose again in the 1990s when radical crystalline compounds with distinct magnetic properties were obtained and studied.[43] Those were *p*-nitrophenyl α-nitronylnitroxide (**Figure 19**, a), which showed ferromagnetic interactions at a critical temperature 0.6 K [47], and *N,N′*-dioxy-l,3,5,7-tetramethyl-2,6-diazaadamantane (**Figure 19**, b), a biradical with two nitroxide functionalities, which maintained strong ferromagnetic intramolecular interactions at T_c = 1.48 K.[48]

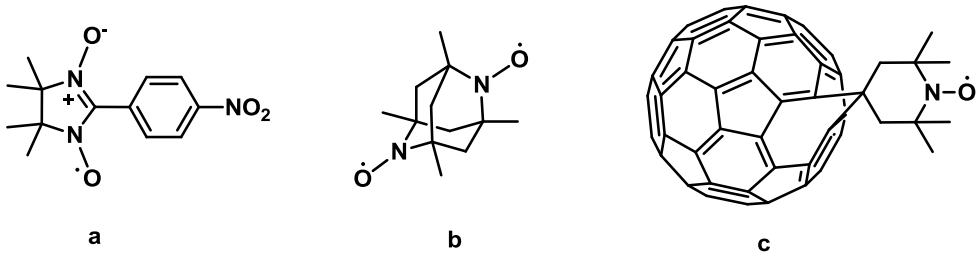

Figure 19: a – p-nitrophenyl α-nitronylnitroxide [47], b - *N,N′*-dioxy-l,3,5,7-tetramethyl-2,6-diazaadamantane - [48],c - C_{60}(TEMPO) [49].

The C_{60}(TEMPO) (**Figure 19**, c) – nitroxide species synthesized and studied by Nogami *et al.* – was one of the first radical-based magnetic materials reported.[43, 49]

1.2.3.5.1.3 Phenalenyl radical

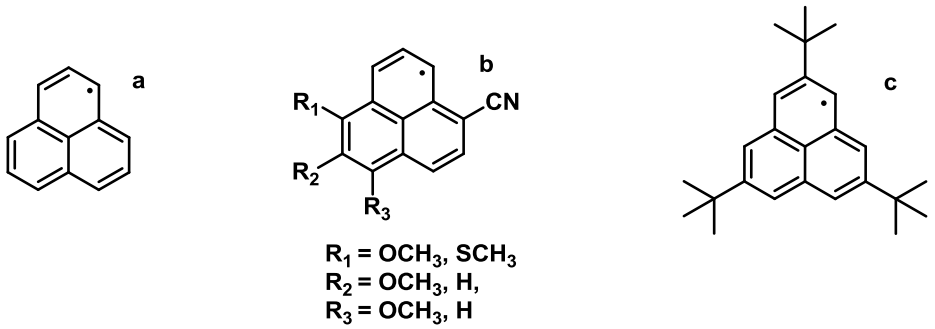

Figure 20: a- phenalenyl radical, b and c – radical, stabilized by various substituents.[50-51]

In phenalenyl radicals the unpaired electron is delocalized over the planar π-conjugated structure.[43] The efforts to stabilize the radicals *via* the introduction of donor and acceptor substituents[50] resulted in the isolation of an air stable, solid compound in 1999 (**Figure 20**).[43, 51]

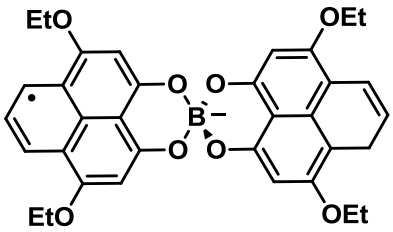

Figure 21: 3,7-ethoxy-substituted spirobiphenalenyl-boron neutral radical.[52]

Since phenalenyl core structures provide a lot of opportunities for the tuning of electronic properties, a number of phenalenyl-based magnetic materials with various conducting and optical properties[52] (**Figure 21**) were developed.

1.2.3.5.1.4 Triarylamine radical.

The magnetic properties of simple triarylaminium monoradicals (**Figure 22**) were studied with magnetic torsion balance and by solid state NMR spectroscopy of aminium salts by Watanabe *et al.* in 1975.[53] Strong antiferromagnetic intermolecular interactions were observed for chloroantimonates while data for perchlorates displayed Curie-Weiss behaviour down to 1.5 K.[53]

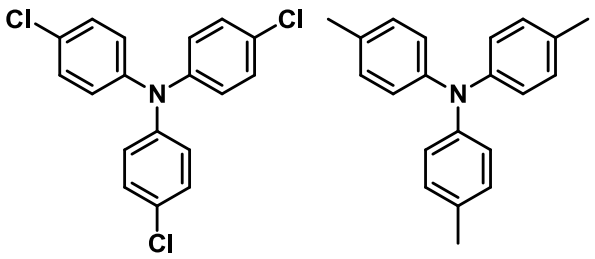

Figure 22: Neutral triarylamine radical precursors.[53]

A similar study was reported by Pearson and Walter in 1977.[54] The radical-cations were produced by oxidation of *tris*-parasubstituted triphenylamines (**Figure 23**) with silver perchlorate and the obtained hyperfine interaction data was analysed.

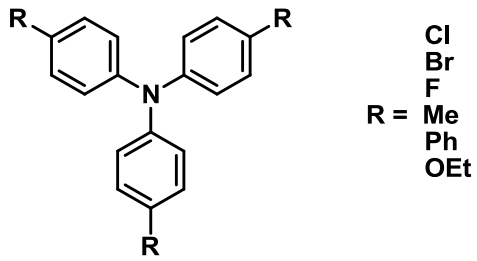

Figure 23: Neutral triarylamine radical precursors with various substituents.[54]

1.2.3.5.2 Diradicals

The study of diradicals is particularly important for magnetochemistry since it provides valuable information about spin-spin interactions and spin polarization.

Simple biradical structures such as trimethylene methane (**Figure 24**, a), and m-xylene (**Figure 23**, b) allow for ferromagnetic coupling while p- and o-xylene byradicals (**Figure 23**, c and d) have antiferromagnetic interactions.

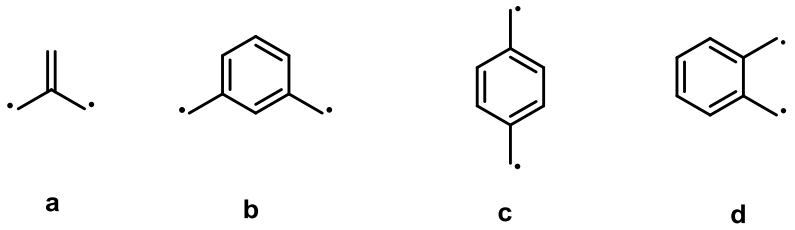

Figure 24: Simple organic biradicals.[10]

Other examples of simple biradicals include conjugated aromatic and non-aromatic systems. Biradicals with ferromagnetic coupling are presented on **Figure 25**. Since the current research project is intended to study the complexes with highest possible ground spin number, this chapter discussion will be focused on systems with ferromagnetic spin-spin interactions.

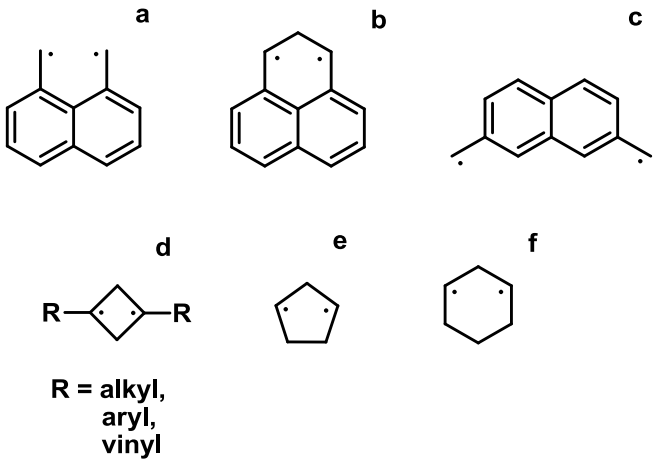

Figure 25: Biradicals based on conjugated systems.[10]

The easiest way to stable biradicals suggests combination of several stable monoradical units into one system.[10] Since the triphenylmethyl radical, mentioned

above, cannot be considered as stable, the same is true towards its biradical derivative, the Schlenk hydrocarbon (**Figure 26**, a). Therefore, stabilization of radical sites via steric protection with branched alkyl- and halogen- substituents can be used (**Figure 26**, b, c and d).[10, 55]

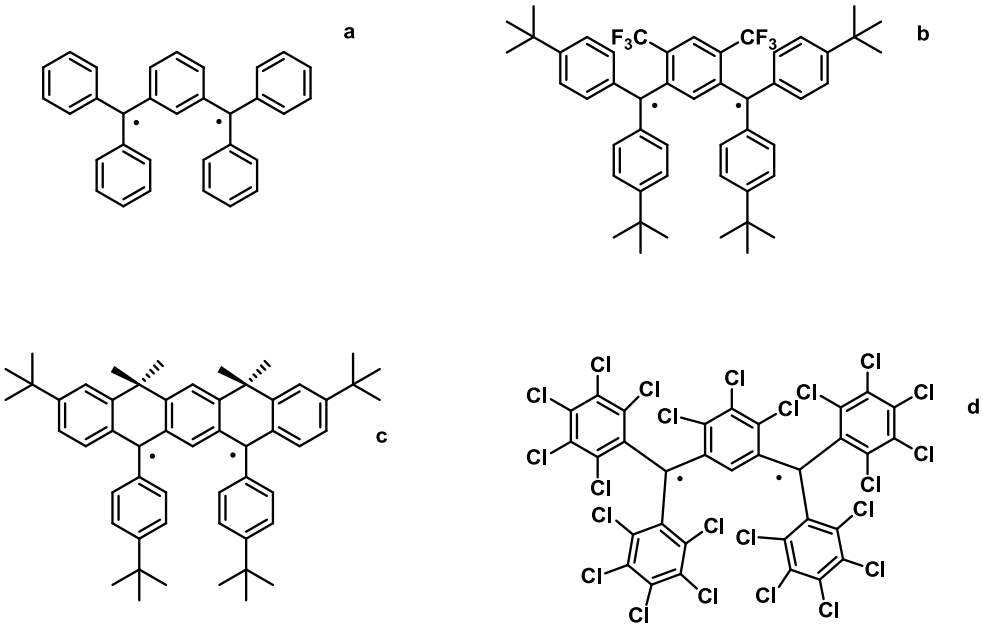

Figure 26: Organic biradicals with ferromagnetic spin coupling.[10]

The *bis*-triarylamine biradical-cation reported by Bushby *et al.* in 2007 (**Figure 27**)[56] exhibited strong ferromagnetic coupling between two amminium functionalities through the central metaterphenyl moiety. This work highlighted the importance of the bridging substituent. Thus, similar systems with bridging heterocycles, although expected to possess superior spin characteristics due to improved planarity, did not show such great results: the pyridine-based diradical was very unstable, and pyrimidine-based diradical was determined to have $\boldsymbol{S = 0}$. Both examples may be explained by the negative influence of heteroatoms on the

degeneracy of the singly occupied orbitals, which outweighs possible planarity benefits.[56]

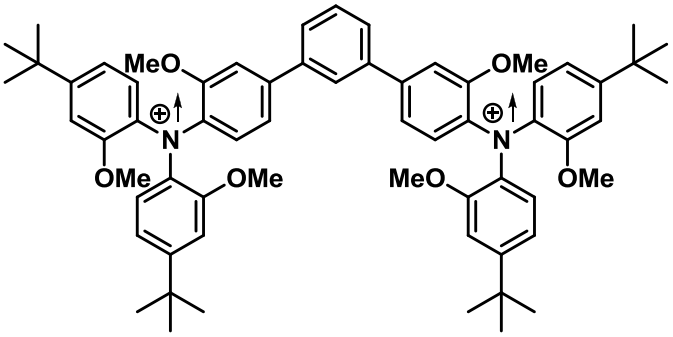

Figure 27: 1.34: N,N,N'',N''-tetrakis(4-tert-butyl-2-methoxyphenyl)-3,3''-dimethoxy[1,1';3',1'']terphenyl-4,4''-diamine diradical dication.[56]

A spiro-fused triarylaminium *bis*-(radical-cation) (**Figure 28**) with a triplet ground state was reported by the Tanaka group in 2003.[57] The magnetic measurements showed strong spin-spin ferromagnetic interactions between triphenylaminium sites even at room temperature.

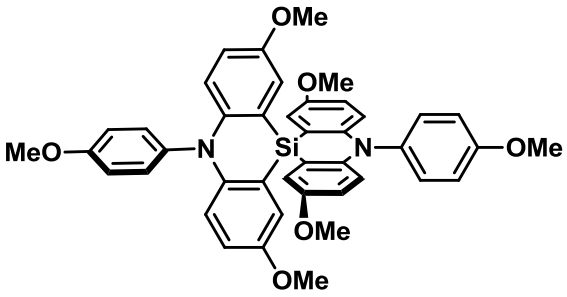

Figure 28: Neutral spiro-fused bis(triarylamine) radical precursor.[57b]

1.2.3.5.3 Tri- and tetraradicals

There are just a few basic directions in tri- and tetraradicals design: linear structures assembled out of meta-connected benzenes (**Figure 29**, a), 1,3,5-connected

benzenes (**Figure 29**, b), star-branched structures (**Figure 29**, c) and "closed loop" structural sets (**Figure 29**, d).[10]

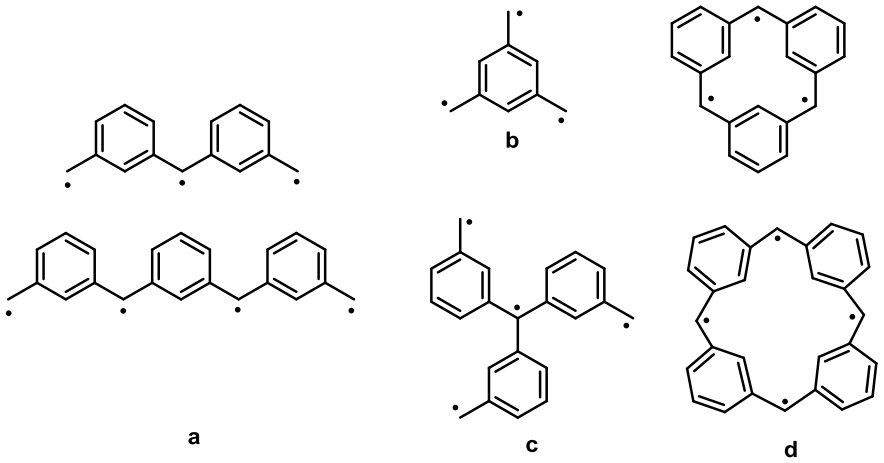

Figure 29: Simple organic tri- and tetraradicals.[10]

Each approach can be advanced via the methods mentioned above such as steric shielding with bulkier alkyl and halogen substituents, as well as the introduction of heteroatoms into the structure (**Figure 30**).[10]

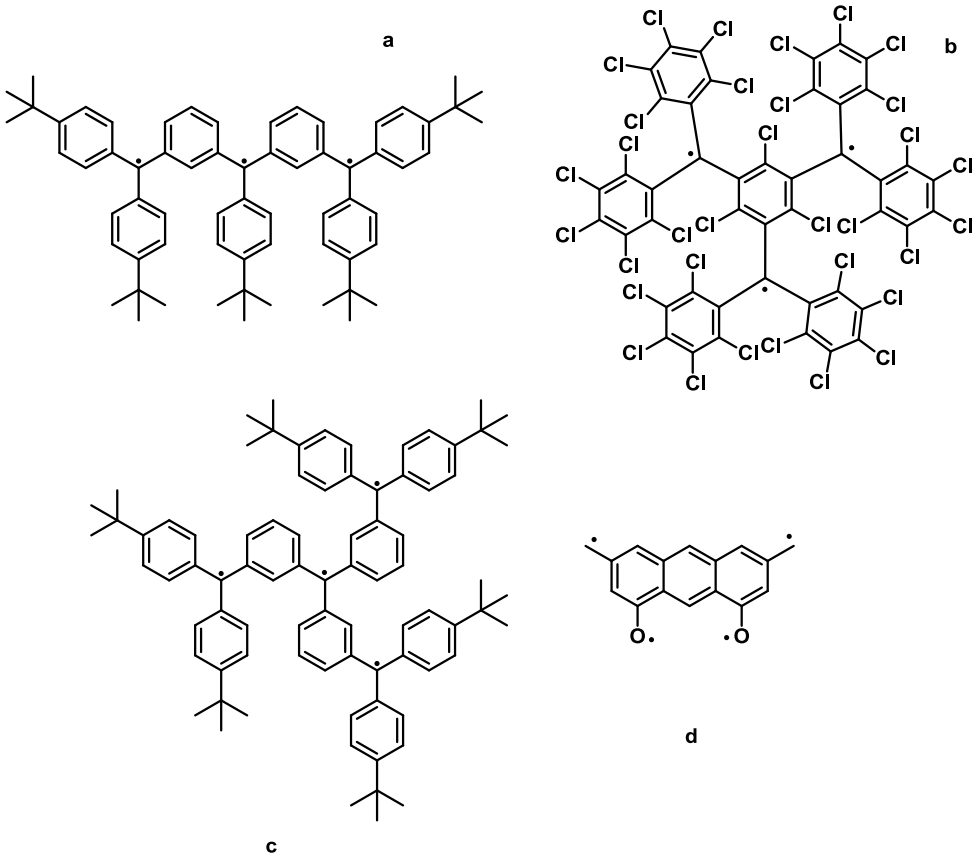

Figure 30: Stable organic tri- and tetrarardicals.[10]

The tetraradical (**Figure 30**, d) has quintet ground state (S = 2) and the radical units within the system are strongly ferromagnetically coupled.[10, 58]

A *para*-phenylene-bridged spirobi(triarylamine) dimer was reported in 2010.[59] This work continued the previous biradical project[57a] by producing a homologous structure with four triarylaminium sites (**Figure 31**). Expected to exhibit interesting tetraradical behaviour, the system did show a three-wave oxidation pattern on electrochemical measurements by losing one, another one and another two electrons stepwise. However, the structure was unstable and rapidly decomposed into a complex mixture of tri- and mono(radical-cations) and diamagnetic quinoid dication.[59]

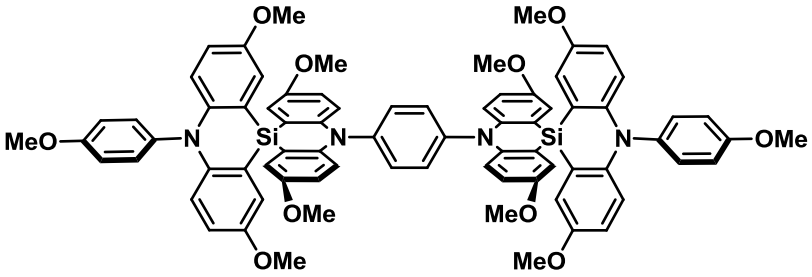

Figure 31: Para-phenylene-bridged spirobi(triarylamine) dimer (neutral form).[59]

1.2.3.5.4 Polyradicals

Star-branched and dendritic polyradicals can be designed based on the strategies used for tetraradicals. Starbranched decaradical (**Figure 32**, a)[60], reported by Rajca *et al*. in 1992 showed $\boldsymbol{S = 5}$, supported by NMR and ESR spectroscopy, however, weak antiferromagnetic coupling through space between branches should be anticipated as well.[10, 60]

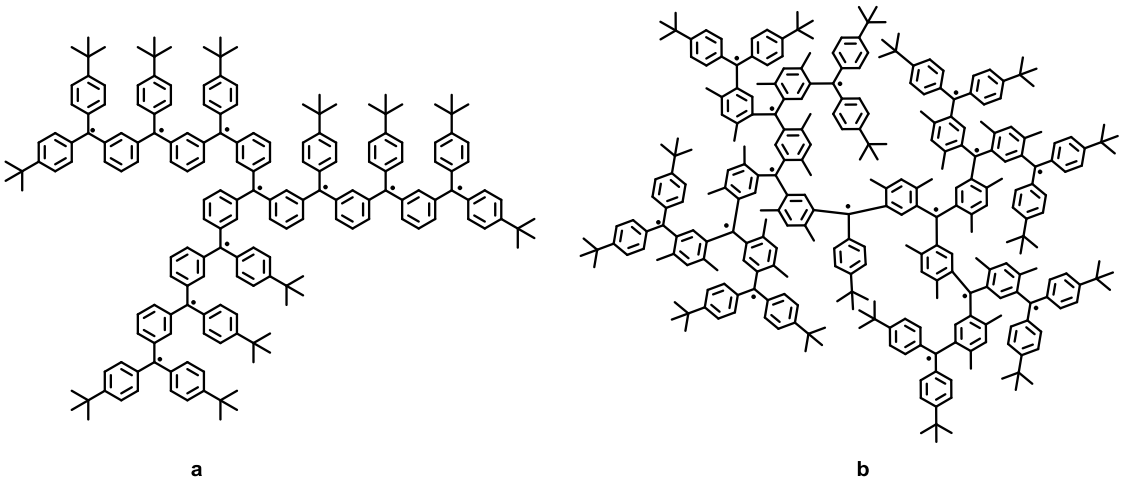

Figure 32: a - starbranched decardical[60] b - dendridic pentadecaradical[61].

Despite conformational defects and molecular tendency to fold into random 3D structure, magnetic studies of the pentadecaradical **(Figure 32**, b**)** showed average

$\boldsymbol{S = \frac{7}{2}}$.[61] However, it was shown that spin coupling significantly depends on the occurrence of defects.[10]

One of the most significant achievements in polyradical field belongs to the Rajca group. A polymer consisting of macrocyclic ($\boldsymbol{S = 2}$) and cross-linking ($\boldsymbol{S = \frac{1}{2}}$) modules with $\boldsymbol{S_{total} = 5000}$ was reported in 2001.[62]

1.2.3.5.4.1 Triarylamminium polyradicals

1.2.3.5.4.1.1 Linear Triarylamminium polyradicals

Although the idea to produce long linear triarylamminium polyradicals with higher values of spin number from mono or diradical precursor building blocks is tempting, efforts to realize it in practice were very challenging.[63]

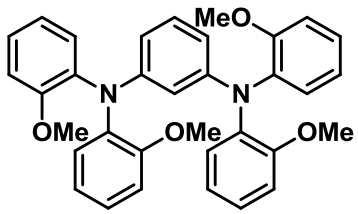

Figure 33: Neutral Schlenk hydrocarbon-based diradical dication precursor.[63]

Despite the fact that block model analogue of Schlenk hydrocarbon (**Figure 33**) forms a diradical dication upon oxidation, efforts to obtain homologous tetraradical tetracations in both linear and cyclic forms (**Figure 34**, a and b) were not fruitful.

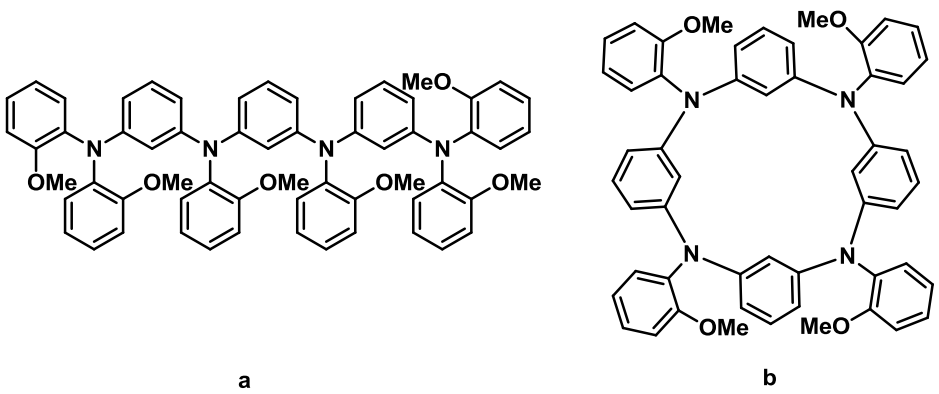

Figure 34: Potential precursors for tetraradical tetracation.[63]

The reason for that is the fact that only coextensive unpaired spins contribute to the high spin numbers while disjoint radical-cations, although easily producible and of good stability, tend to exist separately from each other without significant spin-spin interactions (**Figure 35**).

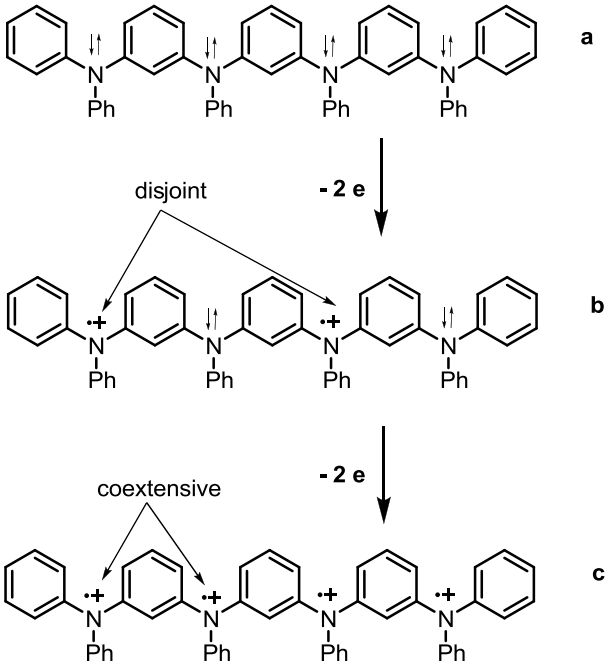

Figure 35: Formation of disjoint and coextensive radical cations via stepwise oxidation. Adapted from reference [63].

While producing a diradical dication out of precursors shown on **Figure 33** requires an extra effort compared to formation of its monoradical-cation, due to the necessity of changing the mild oxidant $THBF_4$ to the stronger $NOBF_4$, these enforced oxidation measures did not result in obtaining either tri- and tetraradicals. This fact may be explained by insufficient oxidative capacity of $NOBF_4$ or possible rapid dimerization of the freshly formed polyradicals.[56]

1.2.3.5.4.1.1 Branched Triarylamminium polyradicals

The study of hyperbranched poly(1,2,(4)-phenylenevinyleneanisylamine polyradical-cation (**Figure 36**), reported by Nishide and Fukuzaki in 2005, showed that it is a multiplet molecule with $\boldsymbol{S = \frac{7}{2}}$ (DP (degree of polymerisation) = 12, spin concentration 0.65) at room temperature. The authors also noted the high stability of the polyradical: in acidic conditions (TFA) where the half-life exceeded 3 weeks at room temperature, which was significantly longer than that of a linear amminium polyradical (1.8 weeks). The low viscosity of polymer solution and data obtained by atomic and magnetic force microscopies revealed the globular structure with distribution of single molecules per globule and distinct magnetic gradient response on the AFM position. It is interesting that when oxidation of precursor with 0.5 equivalent of thianthrene tetrafluoroborate was done resulting in 0.35 spin concentration, the preferred location of tryarylamminium spin radicals was determined to be in the centre of dendritic globule leading to high spin number values.[64]

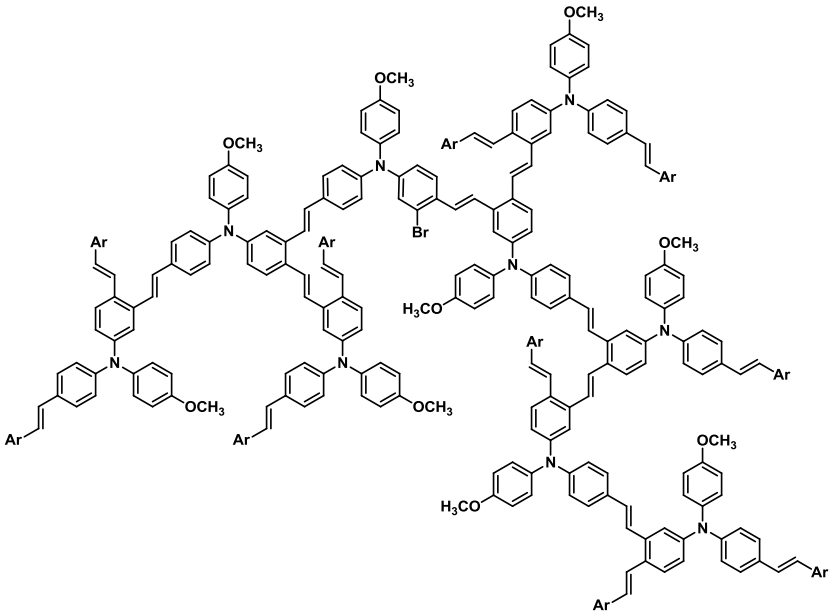

Figure 36: Hyperbranched poly(1,2,(4)-phenylenevinyleneanisylamine (neutral form).[64]

The radical-cation properties of triarylamines have not only interesting magnetic properties, but also exhibit interesting electroactivity. Thus triarylamine-based starburst polymers (**Figure 37**) show reversible electrooxidation pattern as well as very distinct electrochromism in near-infrared and visible light regions depending on the formation of mono- and bi- radical-cations.[65]

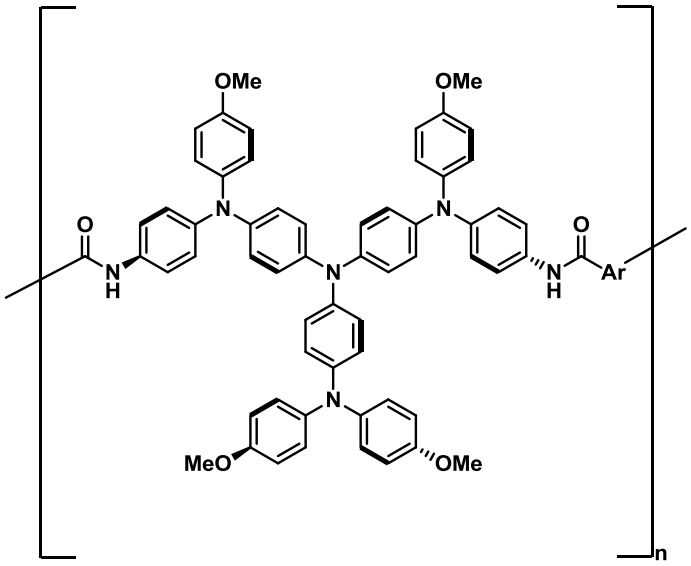

Figure 37: Starburst triarylamino polymers.[65]

1.2.3.4 Metal-radical approach.

The metal-radical approach is a well-developed concept of building molecular magnets in such way that transition-metal ions with unpaired d-electrons are coordinated to the stable free radical ligands. Since there is a direct magnetic coupling between the metal ion and radical,[4b] prediction of magnetic behaviour of the molecule as well as the design of new molecular magnets with desired properties became possible.

The following types of organic radicals were used as ligands for producing various high-spin molecules: nitroxides, verdazyls, dithiadiazolyls and semiquinones.[66]

1.2.3.4.1 Nitroxides

There are a few different kinds of nitroxide radical complexes with different magnetic properties.

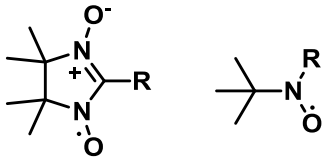

Figure 38: Nitronyl and aminoxyl ligands.[66]

Nitronyls and aminoxyls (**Figure 38**) bind to the metal ion through the oxygen atom. In this case spin pairing usually happens and only few exceptions were reported.[66-67] Since nitronyls have good bridging properties and are also known to maintain antiferromagnetic interactions with coordinated metal ions, their metal complexes often form ferromagnetic-alternating chain-type structures.[66, 68]

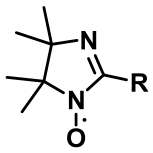

Figure 39: Iminonitroxide ligand.[66]

Iminonitroxides (**Figure 39**) exhibit different coordination patterns. Species coordinated through the oxyl group usually show antiferromagnetic interactions with metals except for lanthanides and axially coordinated square-planar copper (II). At the same time coordination through the nitrogen site leads to strong ferromagnetic interactions with copper, nickel and cobalt and strong antiferromagnetic coupling with Mn (II) (**Figure 40**).[65, 68] It must be mentioned that in all iminonitroxide complexes the ligand does not possess a bridging moiety, which significantly limits the number of obtained and studied structures.

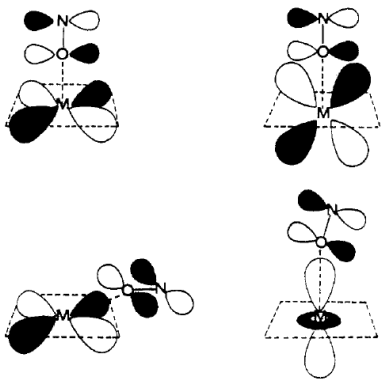

Figure 40: Possible interactions between molecular orbitals of nitroxide and metal ion.[7]
Reprinted with permission from reference 7. Copyright © 1989 American Chemical Society.

Iwamura *et al.*[69] studied mononuclear *bis*-hfac complexes of manganese (II), copper (II) and zinc (II) with 4-(N-tert-butylaminoxyl)-2,2`-bipyridine (**Figure 41**). In these complexes the metal was coordinated to bipyridine and not to the aminoxyl site, however complexes featured through bond ferromagnetic (copper, $J = +68.7$ cm^{-1})

and antiferromagnetic (manganese, $J = -20.2$ cm^{-1}) interaction between metal and aminoxyl radicals.

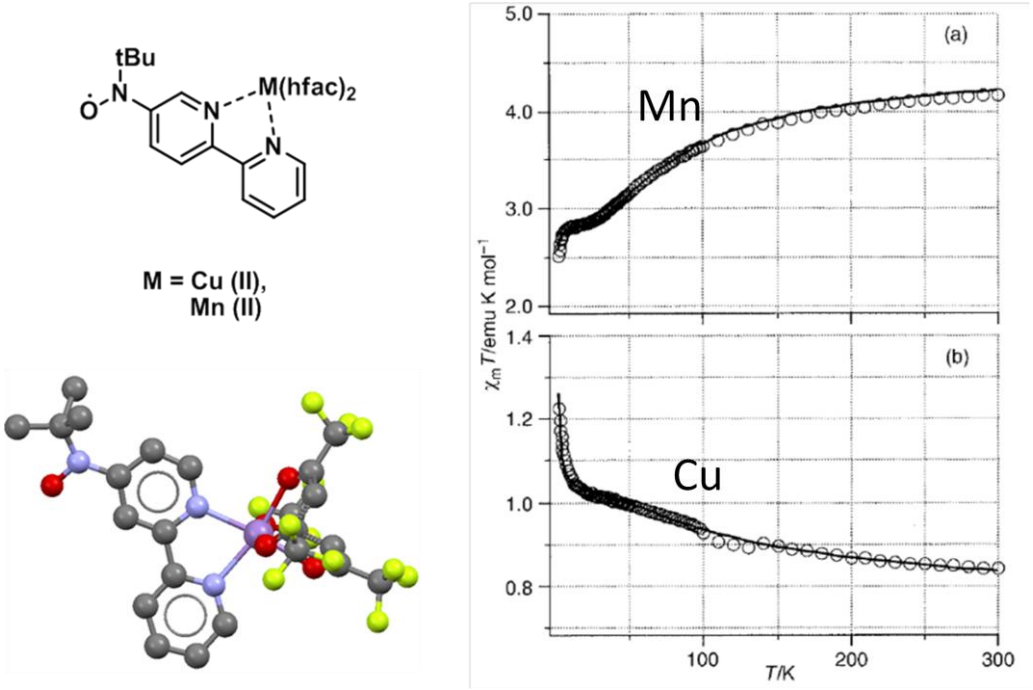

Figure 41: Scheme of manganese and copper complexes (top left), structure of manganese complex (bottom left) and χT vs T plot for manganese and copper (right) complexes. Adapted and reprinted with permission from reference 69. Copyright © 2000 Royal Society of Chemistry.

1.2.3.4.2 Verdazyls

Verdazyls (**Figure 42**) are one of the moisture- and air-stable classes of organic radicals and their structure provides many opportunities for synthetic modifications. There are three ways for the verdazyl radical to couple to another spin center: through bond, through space and to the coordinated metal ion.[46a] In this section only verdazyl-metal interactions will be considered.

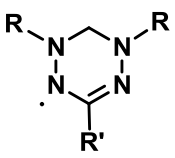

Figure 42: Verdazyl ligand.

Verdazyls have a similar coupling pattern to nitroxides (considering the case when the radical in verdazyl belongs to the bidentate metal-chelate system, thus SOMO π-orbital of the radical is perpendicular to the metal-ligand coordination bonds); the interactions are ferromagnetic and strong with Cu (II), Co (II) and Ni (II) and antiferromagnetic with Mn (II).[66]

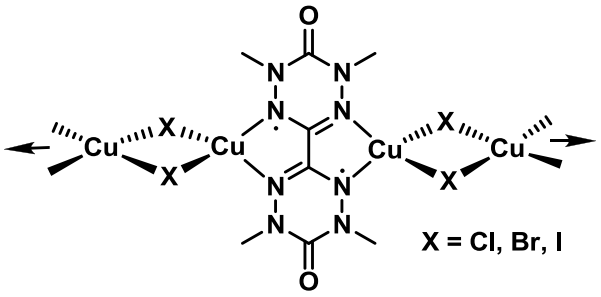

Figure 43: Brook's copper verdazyl complex.[70]

The first verdazyl complex with copper (I) was reported by Brook in 1997 (**Figure 43**).[46a, 70] The attachment of two diamagnetic Cu (I) ions to each biradical unit resulted in one-dimensional coordination polymer with strong intramolecular and interchain as well as weak intrachain interactions.[70]

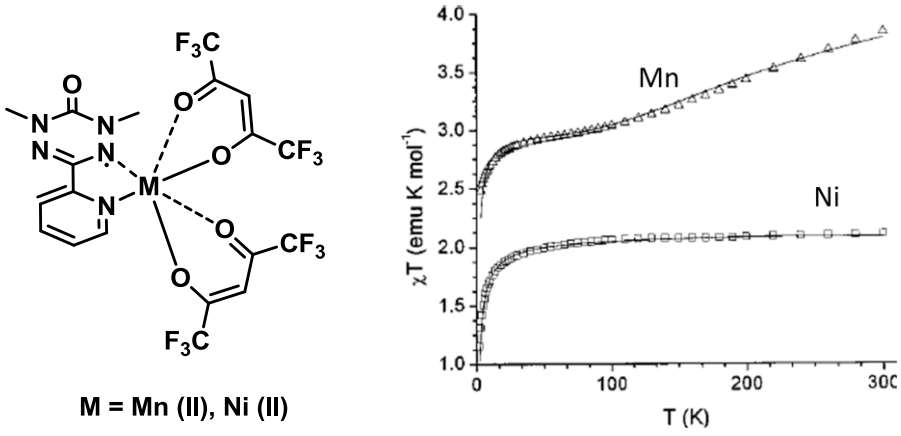

Figure 44: Hicks' verdazyl paramagnetic complexes (left) and their χT vs T plots. Reprinted and adapted with permission from reference 71. Copyright © 2000 American Chemical Society.

The first verdazyl complex with paramagnetic transition metals was reported by Hicks in 2000 (**Figure 44**).[46a, 71] The manganese complex demonstrated moderately antiferromagnetic interaction while nickel-ligand coupling in the nickel complex was strongly ferromagnetic.

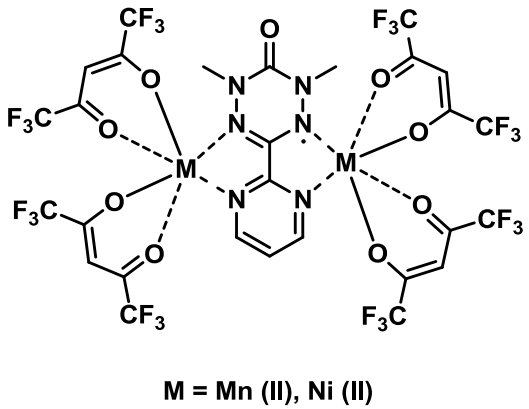

Figure 45: Hicks' verdazyl bimetallic complexes.[72]

A bimetallic nickel complex with a bridging ligand was obtained by the Hicks's group in 2001 (**Figure 45**).[72] Interpretation of magnetic measurements led to the conclusion that the spins of both metal ions are parallel and together they are antiparallel to the radical spin on the nitrogen site ($J = -48$ cm^{-1}). This gave a large overall spin ground state of $\boldsymbol{S} = \frac{\mathbf{9}}{\mathbf{2}}$. Efforts to coordinate the same ligand with nickel resulted in bimetallic complex with ferromagnetic coupling ($J = +220$ cm^{-1}) between the metal ion and radical ($\boldsymbol{S} = \frac{\mathbf{5}}{\mathbf{2}}$).

1.2.3.4.3 Dithiadiazolyls

Extensive studies of dithiadiazolyl complexes were conducted in the Preuss group. The general trend of their magnetic behaviour can be described as being similar to the verdazyls while dimerization is very typical for thiazyl-type radicals.[66]

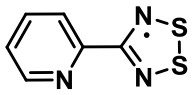

Figure 46: Preuss' dithiadiazolyl ligand.[73]

The first dithiadiazolyl complex was obtained in 2004 and showed ferromagnetic interaction with Co (II).[73] This work was later continued by obtaining complexes of Mn (II) and Cu (II) with the same ligand. The study of their magnetic and structural properties lead to the conclusion that copper and manganese complexes tend to form dimers while the cobalt complex is a monomer. The monomer-dimer equilibria was shown to affect magnetic behaviour of the compounds.[74] Unlike Mn (II) and Cu(II), new Ni (II) and Fe (II) complexes were not dimerized, while the iron complex was very unstable.[75]

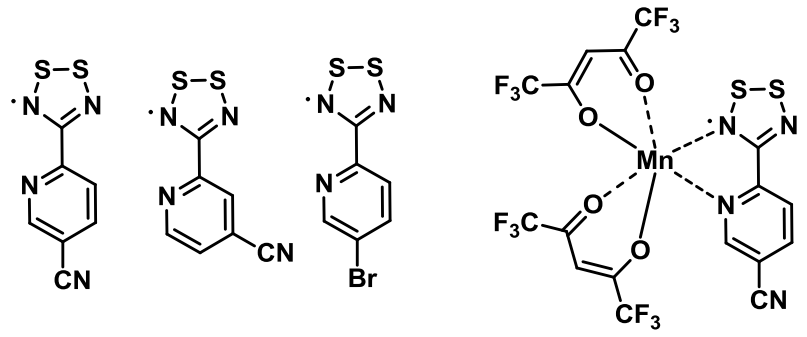

Figure 47: Substituted dithidiazolyl ligands and manganese complex.[76]

Since packing of complexes in the solid state leads to spin pairing and loss of desired spin-spin interactions between the metal center and ligand radical, efforts to prevent dimerization by changing the ligand structure were made. The standard dithiazolyl ligand was modified with cyano groups and halogen substituents (**Figure 47**).[76] This strategy allowed for the isolation of the non-dimerized manganese complex with weak antiferromagnetic coupling.

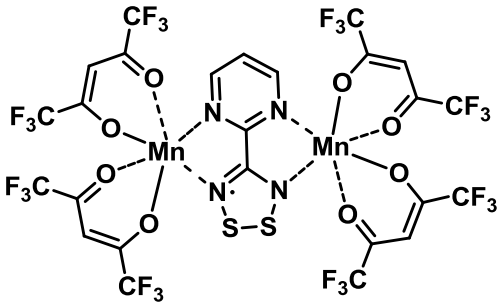

Figure 48: Binuclear dithiazolyl complex.[77]

Similar ligand with the pyrimidyl moiety instead of the pyridyl part was coordinated with two manganese metal centers to produce bimetallic complex with antiferromagnetic coupling between the ligand-centered spin and metal-centered spins (**Figure 48**).[77] This work was further extended to such metals as Co (II), Ni (II) and Zn (II).[78] Binuclear cobalt and nickel complexes demonstrated ferromagnetic coupling between metal centers and ligand spin. The zinc complex showed ligand spin behaviour only, which was expected due to the diamagnetic nature of zinc ions.

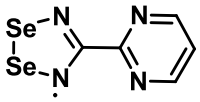

Figure 49: Selenium analogue of dithiazolyl ligand.[78]

Also the selenium-based analogue of this ligand was synthesized (**Figure 49**) to study the impact of chalcogen-oxygen interaction on magnetic behaviour of the complex.[78] It has to be mentioned that selenazyl complexes had magnetic properties similar to their sulfur-based alternatives. The ability of dithiazolyls to maintain magnetic interactions between two metal centers in one molecule and between the

ligand radical center and metals in other molecules was proposed in this publication as well.

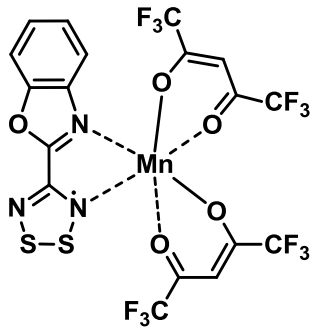

Figure 50: Manganese complex with oxygen-modified dithiazolyl ligand.[79]

In order to enhance magnetic interactions between the manganese center and ligand radical, further changes in the ligand structure were made. The shorter distances between the sulfur site of one molecule and oxygen on the hfac-site of another one significantly increased antiferromagnetic coupling between molecules (**Figure 50**).[79]

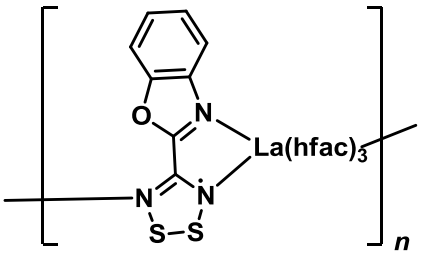

Figure 51: Dithiazolyl-based bridging polymer.[80]

The first dithiazolyl-based bridging polymer was recently reported (**Figure 51**).[80] The one-dimensional alternating polymer chain was shown to have ferromagnetic interactions between the ligand-radical units which were mediated through the coordinated diamagnetic lanthanide ion.

One of the most important directions in the development of dithiazolyl magnets will be finding efficient synthetic routes since at the moment synthesis of these ligands is quite complicated.[78] As well methods to prevent dimerization are of great importance.

1.2.3.4.4 Semiquinones

The *o*-semiquinone radicals are well-known.[66] Unfortunately, they have low stability and thus EPR is the primary method of radical detection in this class of compounds. The coordination to metal ions is known to improve radical stability.

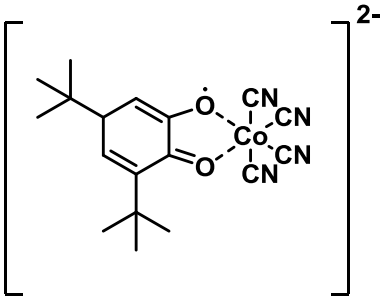

Figure 52: Cobalt (III) - semiquinone complex.[81]

One of the first air-stable semiquinone coordination compounds reported was octahedral cobalt (III) semiquinone complex (**Figure 52**).[81] The magnetic behaviour pattern of semiquinones lies between oxygen-coordinated nitroxides and nitrogen-coordinated verdazyl radicals. Despite their high coordination properties, semiquinones are not bridging ligands. Thus even in rare cases when coupling between the metal center and ligand is ferromagnetic, the spin values are still low.[66] This issue can be avoided by use of combined bi- and polyradical ligands containing other radical functionalities besides semiquinones such as nitroxides (heterospin or donor-acceptor biradicals[82]) or poly-*o*-semiquinones (homo-spin ligands[66]).

1.2.3.4.4.1 Heterospin semiquinones

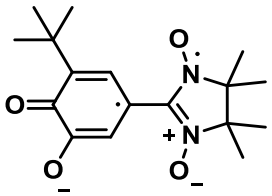

Figure 53: Heterospin semiquinone-nitroxide ligand.[83]

The heterospin ligand consisting of semiquinone and nitroxide parts (**Figure 53**) was coordinated to the Cu (II) ion.[83] Both parts of the ligand provided spin $S = \frac{1}{2}$ each, allowing the ligand to provide total $S = 1$, while the copper ion gave another $\frac{1}{2}$. Total spin number of complex was determined to be $\frac{3}{2}$ which means that metal and ligand have ferromagnetic spin interaction. This ligand was later coordinated to Mn (II), Co (II), Ni (II) and Zn.[84] Manganese, cobalt and pentacoordinated nickel had antiferromagnetic coupling with the ligand, while hexacoordinated Ni had ferromagnetic interactions, the same as copper. This work also contributed to the understanding of how significantly intraligand ferromagnetic interactions can increase stability of the high-spin state in transition metal complexes.

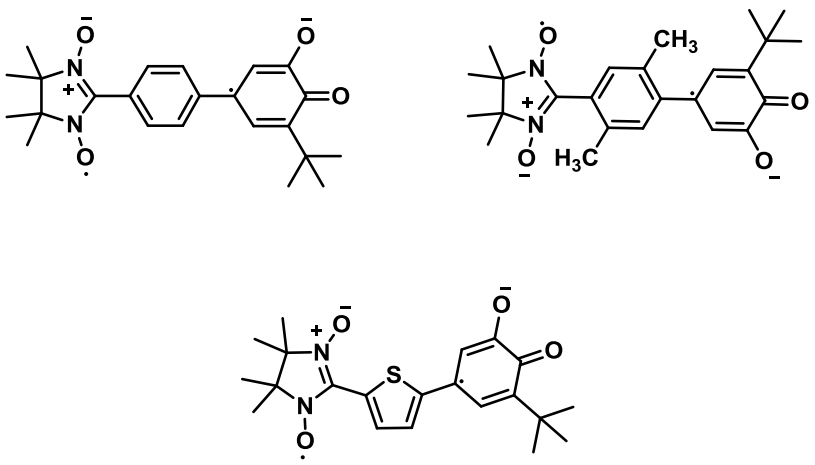

Figure 54: The donor-bridge-acceptor semiquinone ligands.[85]

The *donor – bridge – acceptor* class of ligands was developed and studied to explore the intraligand charge distribution and its effects on the magnetic properties of metal complexes (**Figure 54**).[82,85] The study concluded, that the most essential role in this stabilizing internal ligand function belongs to NN-LUMO – bridge-LUMO interactions.[85]

1.2.3.4.4.2 Homospin semiquinones

Bi- and polyradical structures containing more than one semiquinone motif provides a lot of varieties for designing polymetallic high-spin complexes.

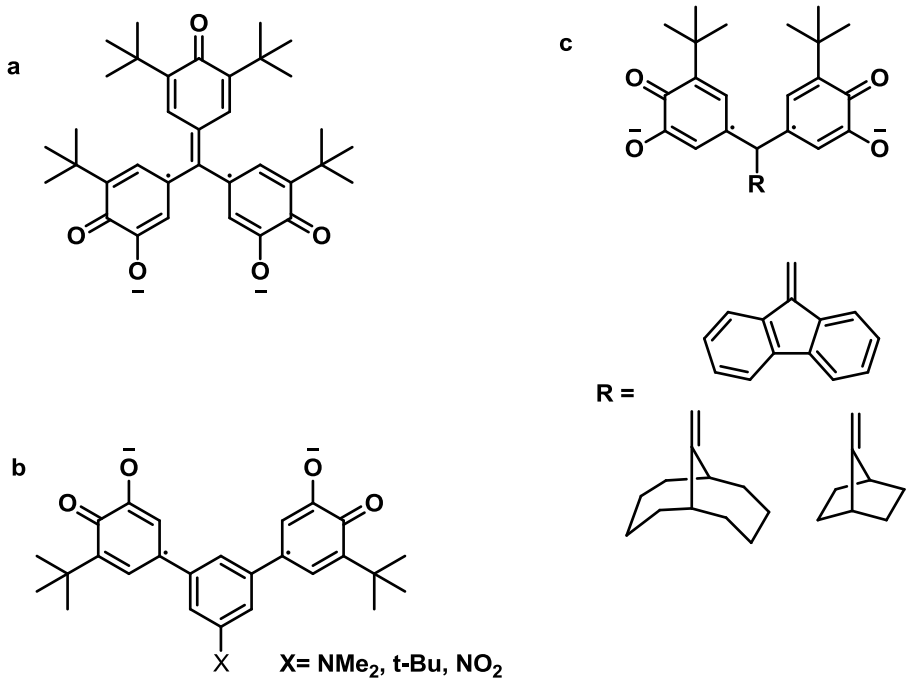

Figure 55: Biradical semiquinone ligands.[86]

One of the first stable biradicals was obtained by Yang in 1960 (**Figure 55**, a)[86a]. More recent studies were focused on producing ligands based on *m*-phenylene (**Figure 55**, b)[86d] and trimethylenemethane [86c, 87] (**Figure 55**, c) derivatives.[66] A study of a series of nearly conformationally identical biradicals with varied substituents[86d] revealed a highly important criteria for ligand design: the presence of electron-

withdrawing substituents (-NO_2) decreases the electron density in the bridging compartment and minimizes the ***J***-value of the singlet-triplet gap the most which provides excellent conditions for ferromagnetic coupling. The strong electron-donating group (-NMe_2) has a smaller influence on the singlet-triplet gap and finally the weak electron donating group (-tBu) has the least effect out of all three substituents toward the energy gap. Another biradical study explored magnetic exchange in trimethylenemethane-based cross-conjugated systems (**Figure 55**, c).[87] Similar to previous examples, it was discovered that intraligand coupling values correlate to angles between semiquinone rings which can be regulated by the structure of substituent. Also, a number of works on bimetallic complexes with bridging semiquinone ligands was published by Shultz *et al*.[85, 88]

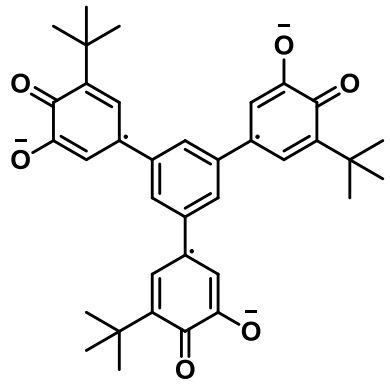

Figure 56: Tri-topic semiquinone ligand.[86b]

The bulkier tri-topic *tris*-semiquinone ligand (**Figure 56**) showed ferromagnetic coupling between semiquinone radicals when coordinated to Ni (II) and Mn (II) ions while metal-ligand coupling differed from antiferromagnetic with manganese to ferromagnetic with nickel.[86b]

Overall prediction of magnetic interactions in poly-*o*-semiquinones is complicated and many factors must be taken into consideration such as type, size and

location of substituents, position and properties of the bridging part of the ligand, possible conformational variations and accessibility of metal-binding sites for coordination.

1.2.3.4.5 Tetracyanoethylenides and Tetracyanoquinodimethanides.

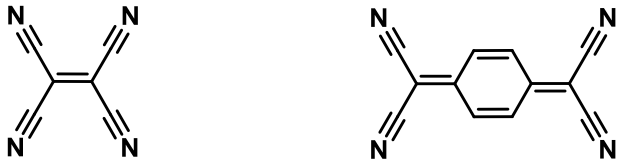

Figure 57: Tetracyanoethylene (TCNE) (left) and 7,7,8,8-tetracyano-*p*-quinodimethane (TCNQ) (right) neutral ligands.

The study of two closely related classes of 7,7,8,8-tetracyano-*p*-quinodimethane (TCNQ) and tetracyanoethylene (TCNE)- based magnetic compounds (**Figure 57**) at the moment may be considered as on one of the most successfull branches of molecular magnetism.

One of the early tetracyanoethylene magnetic complexes was reported by Miller *et al.* The charge transfer complex containing equimolar amounts of decamethylferrocene (donor) and tetracyanoethylene (acceptor) exhibited Curie-Weiss behaviour above 60 K while featuring ferromagnetic coupling between donor and acceptor units.[89] Further studies of TCNE complexes led to the discovery of TCNE-based first room-temperature magnet $V(TCNE)_x \cdot y(CH_2Cl_2)$ (x~2, y~1/2) which demonstrated ferrimagnetic behaviour, while its critical temperature could not be estimated since it exceeded the decomposition temperature of the complex at 350 K (**Figure 58**).[90]

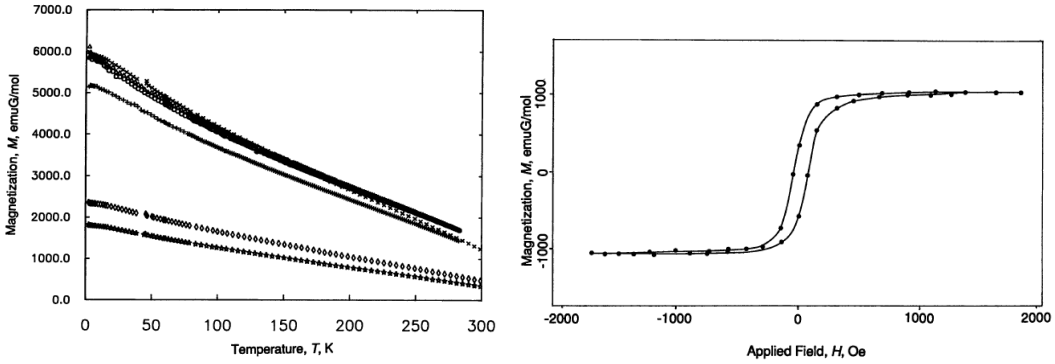

Figure 58: Magnetization vs temperature at various values of magnetic field (left) and hysteresis loop (right) for $V(TCNE)_x \cdot y(CH_2Cl_2)$. Reprinted with permission from reference 90. Copyright © 1991 The American Association for the Advancement of Science.

A variety of TCNE with different substituents by Yee *et al.* as well as Miller's methyl tricyanoethylenecarboxylates were reported later resulting in additional examples of room temperature magnets (**Figure 59**).[91]

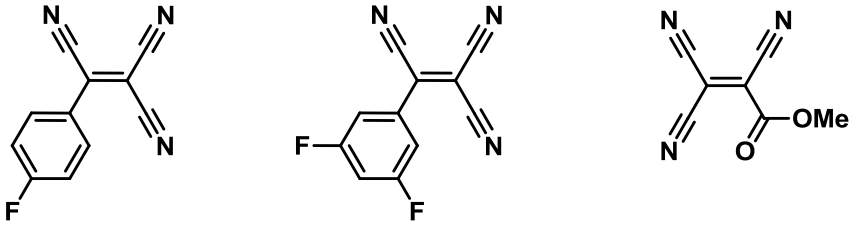

Figure 59: Mono- and disubstituted TCNE-type acceptors[91a] (left and center) and methyl tricyanoethylenecarboxylate[91b] (right).

The reports on TCNQ-based materials include decamethylmanganocenium 7,7,8,8- tetracyano-p-quinodimethanide bulk molecular ferromagnet with Curie temperature 6.2 K from 1990;[92] a study of solvation/desolvation dependent magnetism switching in $[Ru_2]_2$-TCNQ charge transfer systems;[93] characterization of manganese, iron, cobalt and nickel TCNQ complexes;[94] magnetic behaviour of metamagnetic and ferromagnetic phases of $[Fe(C_5Me_5)_2][TCNQ]$,[95] and

ferromagnetic interactions in sandwich-type networks of cerium (III) ions and 2,5-$TCNQX_2$ (X=Cl, Br) (**Figure 60**)[96].

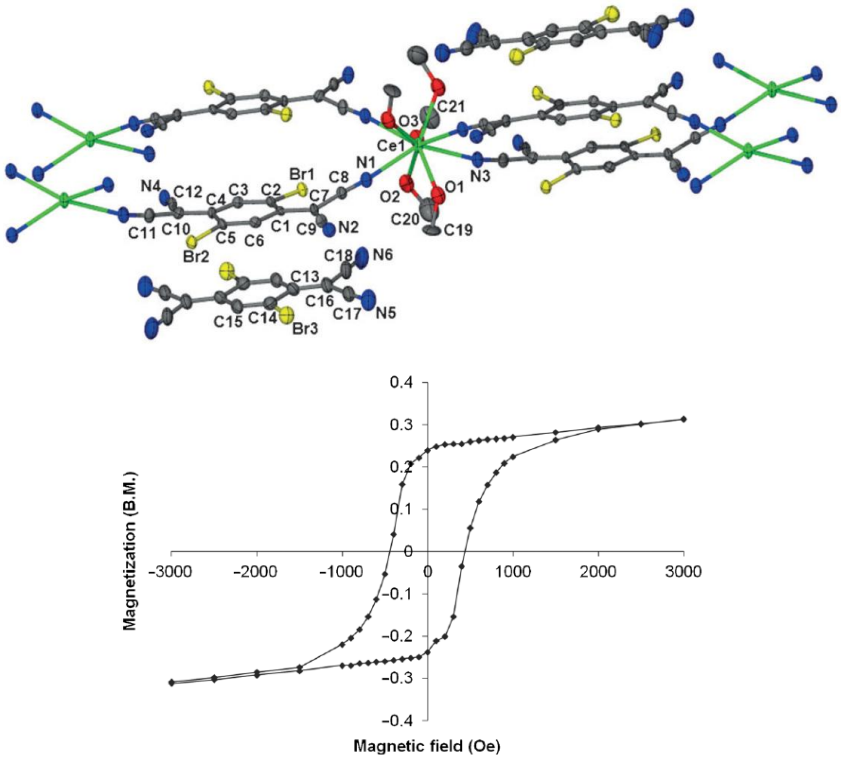

Figure 60: Structure (top) and hysteresis loop (bottom) for $[Ce(TCNQBr_2)_2(MeOH)_{4.5}(H_2O)_{0.5}]$-$[TCNQBr_2]$. Reprinted with permission from reference 96. Copyright © 2012 WILEY-VCH Verlag GmbH & Co. KGaA, Weinheim.

1.2.3.4.6 Triarylamines.

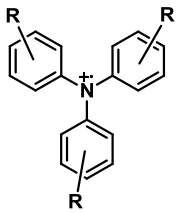

Figure 61: Triarylamine radical-cation ligand.

Though triarylamine radical-cations have been extensively studied,[97, 57b, 64, 98] there are just very few examples of triarylamine-metal complexes reported up to date.

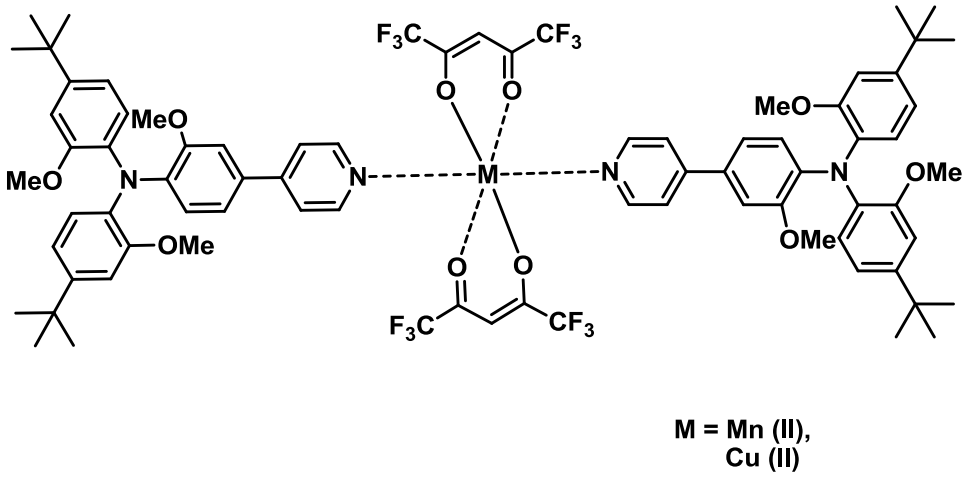

Figure 62: Bushby's bis-triarylamine complex (neutral).[99]

Bushby *et al.* in 2008 reported about persistent manganese and copper complexes with monodentate triarylamminium ligand $M(hfac)_2L_2$ (L = 4``,4```-di-tert-butyl-2`,2``, 2```trimethoxy-(4-(40-diphenylaminophenyl) pyridine)) (**Figure 62**).[99] A very weak antiferromagnetic coupling was observed, and since the study was intended to test the applicability of such radicals in coordination polymer magnets, Bushby characterised the system as non-promising. However it is highly possible that the values of spin coupling are low because of the long distance between triarylamminium radical and the metal center.

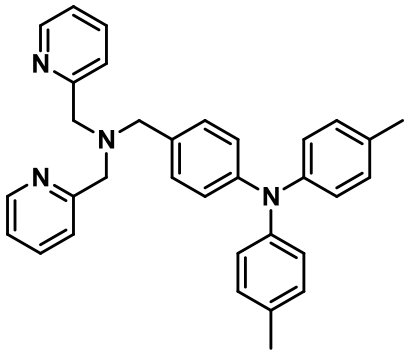

Figure 63: Yano's monotopic ligand (neutral form).[100]

Another triarylamminium copper complex was prepared by Yano *et al.*[100] and exhibited some magnetic interactions between the ligand radical and metal center, detected by EPR spectroscopy (ligand shown on **Figure 63**). Unfortunately, the nature of this interaction remains unknown.

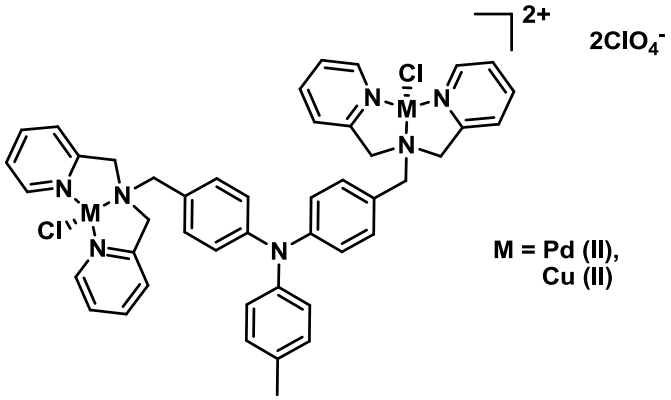

Figure 64: Yano's ditopic complex.[101]

This work was continued resulting in a bimetallic complex [101] with the open-shell geometry ligand (**Figure 64**). The EPR spectrum of the copper complex showed strong interaction with the triarylamminium site although the data obtained was not sufficient for any further interpretation and conclusions. In 2009 Yano *et al.* also reported a trinuclear complex with analogous structure[102] and the same conclusion regarding non-determined magnetic interactions.

The neutral Cr (III) triarylamine – salen complex[103] at room temperature showed only $\boldsymbol{S = \frac{3}{2}}$ which obviously must have been expected based on the structure with large distance between the amine and the metal center. No study of the oxidized complex was conducted, although the system by itself could be interesting for metal-radical interaction studies.

1.3 Results and discussion.

The monometallic complexes project was conducted at Brock University under the supervision of Prof. M. Lemaire in collaboration with Lemaire group members B. Djukich and S. Adugna. The X-ray structure studies were obtained by Dr. H. Jenkins (McMaster University). The DFT calculations were done by Dr. S. Gorelsky (University of Ottawa). The work was published in the following article: Persistent Metal Bis(Hexafluoroacetylacetonato) Complexes Featuring a 2,2′-Bipyridine Substituted Triarylamminium Radical Cation. S. Adugna, K. Revunova, B. Djukic, S. I. Gorelsky, H. A. Jenkins, M. T. Lemaire, *Inorganic Chemistry* **2010**, *49*, 10183-10190.[104]

The bimetallic complexes project was conducted at Brock University under the supervision of Prof. M. Lemaire. The DFT calculations were done by Dr. S. Gorelsky (University of Ottawa). The work was published as: Synthesis and coordination chemistry of a potential precursor to a triarylamminium radical cation ditopic ligand. K. Revunova, S. I. Gorelsky, M. T. Lemaire, *Polyhedron* **2013**, 52, 1118-1125.[105]

The dendrimer ligand project was conducted at Brock University under the supervision of Dr. M. Lemaire. The manuscript is in preparation.

1.3.1 Synthesis and study of monometallic complexes.

1.3.1.1 Goals and objectives.

This study of the magnetic properties of simple monometallic, monoradical-cation complexes is the first part of our triarylamminium project which was intended to explore the coordination chemistry of substituted triarylamminium radical-cations. These complexes are designed to place the metal centers in close proximity to the radical-cation sites to allow for extensive magnetic spin-spin interactions.

1.3.1.2 Ligand synthesis and coordination chemistry.

The ligand (**1.2**) was designed in order to keep the distance minimal between the amminium and metal spin sites. The bromo-substituted bipyridine part (**1.1**) was obtained via Negishi coupling[106] and attached to the N,N`-(4,4`-dimethoxydiphenyl)amine through palladium catalyzed Buchwald-Hartwig coupling.

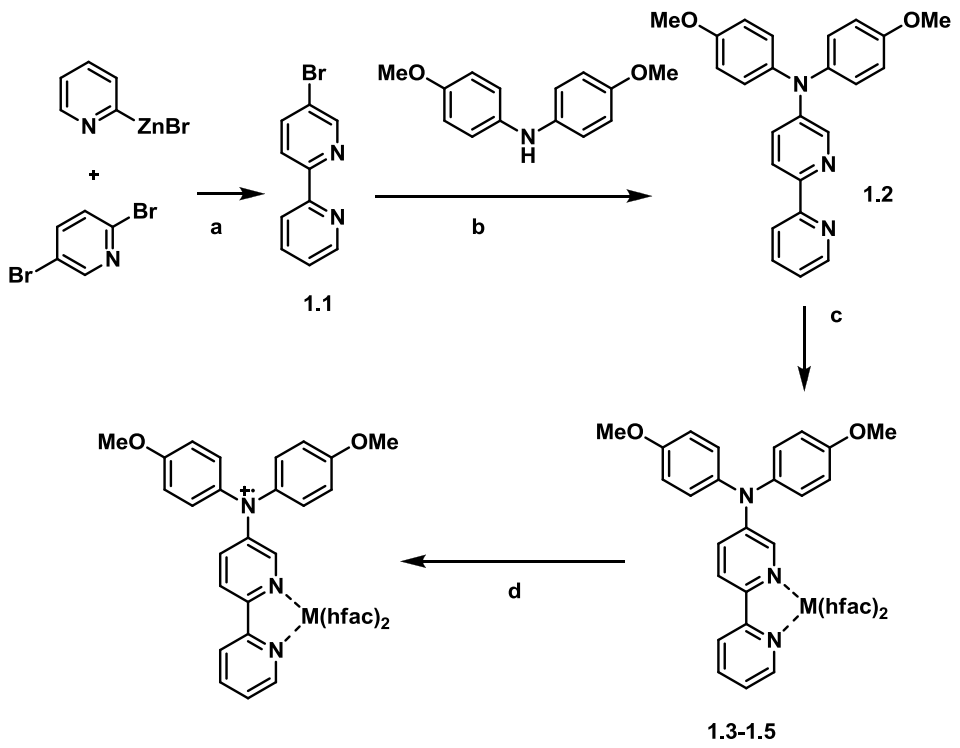

Scheme 1: Synthetic pathway. Reagents and conditions: a – 5 mol% $Pd(PPh_3)_4$, THF, RT, 33 h; b – 5.5 mol% $Pd(OAc)_2$, Cs_2CO_3, BINAP, Toluene, 95 ^oC, 35 h; c – $M(hfac)_2 \cdot xH_2O$ (M = Mn, Ni, Cu), hexanes/CH_2Cl_2, RT; d – $NOPF_6$, acetonitrile, RT.

The neutral coordination complexes of ligand **1.2** with $M(hfac)_2 \cdot xH_2O$ salts (M = Mn (**1.3**), Ni (**1.4**) and Cu (**1.5**)) were prepared simply by mixing metal salts and ligand in a hexanes/dichloromethane solution. All of the complexes were analytically pure microcrystals and had similar FT-IR absorption spectra.

X-ray quality crystals of **1.5** were obtained via slow evaporation of methanol solution. The obtained structure (**Figure 65**) confirmed the original suggestion of **1.2** acting as a bidentate ligand through nitrogen sites in the bipyridine functionality. The Cu^{2+} complex displays anticipated Jahn – Teller distorted, cis pseudo-octahedral coordination geometry. The neutral triarylamminium nitrogen center N3 is almost planar with a bond angle sum of 359.8°. The C-N bond between this center and bipyridine part is less than 1.4Å and is shorter than two other C-N bonds connecting N3 to *p*-methoxyphenylsubstituents (**Table 1**). Thus we were successful in obtaining a metal complex with short metal-radical distance. It is also in agreement with our suggestion about electron density delocalisation with bipyridine rings and interaction between metal and amminium part.

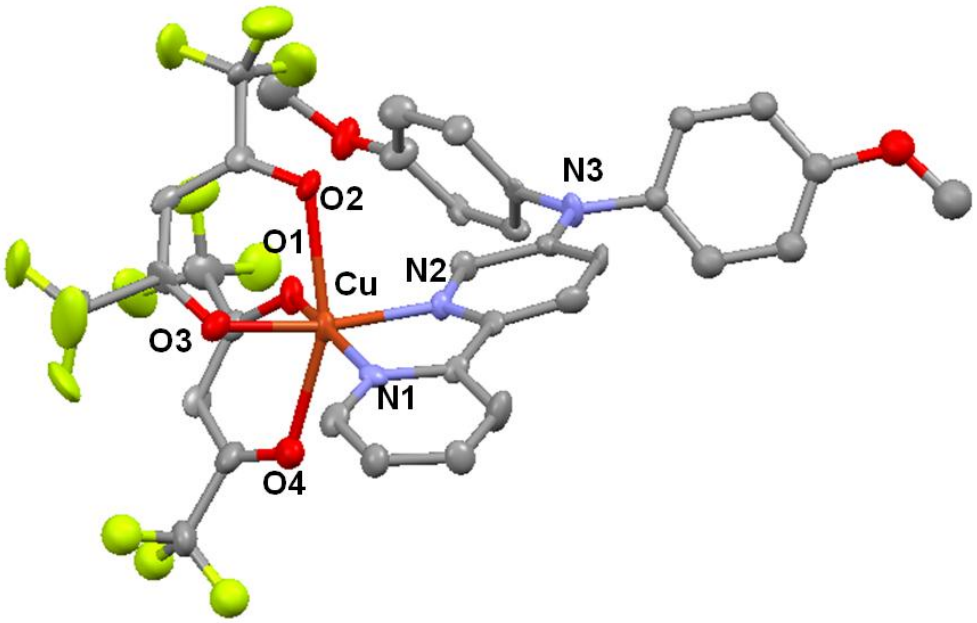

Figure 65: ORTEP diagram of the molecular structure of **1.5**.

Selected bond distances	Value (Å)	Selected angles	Value (^{o})
Cu(1)-O(2)	2.381(7)	O(1)-Cu(1)-N(1)	167.3(3)
Cu(1)-O(1)	1.988(6)	O(3)-Cu(1)-N(2)	164.7(3)
Cu(1)-O(3)	1.978(6)	O(2)-Cu(1)-O(4)	155.8(2)
Cu(1)-O(4)	2.294(7)	O(1)-Cu(1)-N(2)	92.3(3)
Cu(1)-N(1)	2.008(7)	O(3)-Cu(1)-N(1)	92.8(3)
Cu(1)-(N2)	2.007(7)	O(1)-Cu(1)-O(3)	96.1(3)
		N(1)-Cu(1)-N(2)	81.3(3)

Table 1: Selected parameters for structrure **1.5**.

The radical-cation complexes were generated in solution through one-electron chemical oxidation with $NOPF_6$. These complexes were stable under inert atmosphere and gradually decomposed in about an hour during UV-visible spectroscopy experiments. Exposure to air results in complex decomposition within several minutes.

1.3.1.3 Study of properties.

1.3.1.3.1 Electronic properties.

The electronic properties of the free ligand and complexes were studied by cyclic voltammetry (CV) and UV-visible spectroscopy.

1.3.1.3.1.1 Electrochemical properties.

All potentials were quoted and referenced to the ferrocene/ferrocenium couple. The anodic scan of ligand **1.2** shows two quasi-reversible waves at +0.5 and

+1.0 V, respectively. The reversibility of either anodic wave could not be improved by increasing the scan rate, which can be explained by formation of the radical cation with dication generation at a higher potential. A small peak at +0.7 V can be a sign of ligand decomposition due to an oxidation process. The cathodic scan does not show any reduction activity, which is expected since the ligand is not stabilized with coordinated metal ion. These observations are in agreement with electrochemical data reported for other triarylamines.[107]

Anodic scans for metal complexes (**1.3**-**1.5**) look similar to each other (**Figure 66**). The fact that the radical-cation formation ($E`_{ox1}$) is reversible for every complex, indicates the stabilization effect from the coordinated metal ion. Also since the ligands are more stable and harder to oxidize when coordinated to the metal ion, the potential of radical-cation formation is slightly higher than in ligand solution. Unlike the smooth CV for manganese (**1.3**) and nickel (**1.4**) complexes, the electrochemical data for copper compound (**1.5**) looks broader and some additional peaks of irreversible oxidation can be seen between values of $E`_{ox1}$ and $E`_{ox2}$ (it is not present at higher scan rates > 200 mV/s) which can be attributed to an oxidation of the side-product which decomposes and is not detectable at higher scan rates. All the complexes exhibit dication formation at potentials slightly higher than +1.0 V on anodic scans and some irreversible peaks at cathodic potentials over - 1.0V which may come from reduction of hfac and bipyridine.[107]

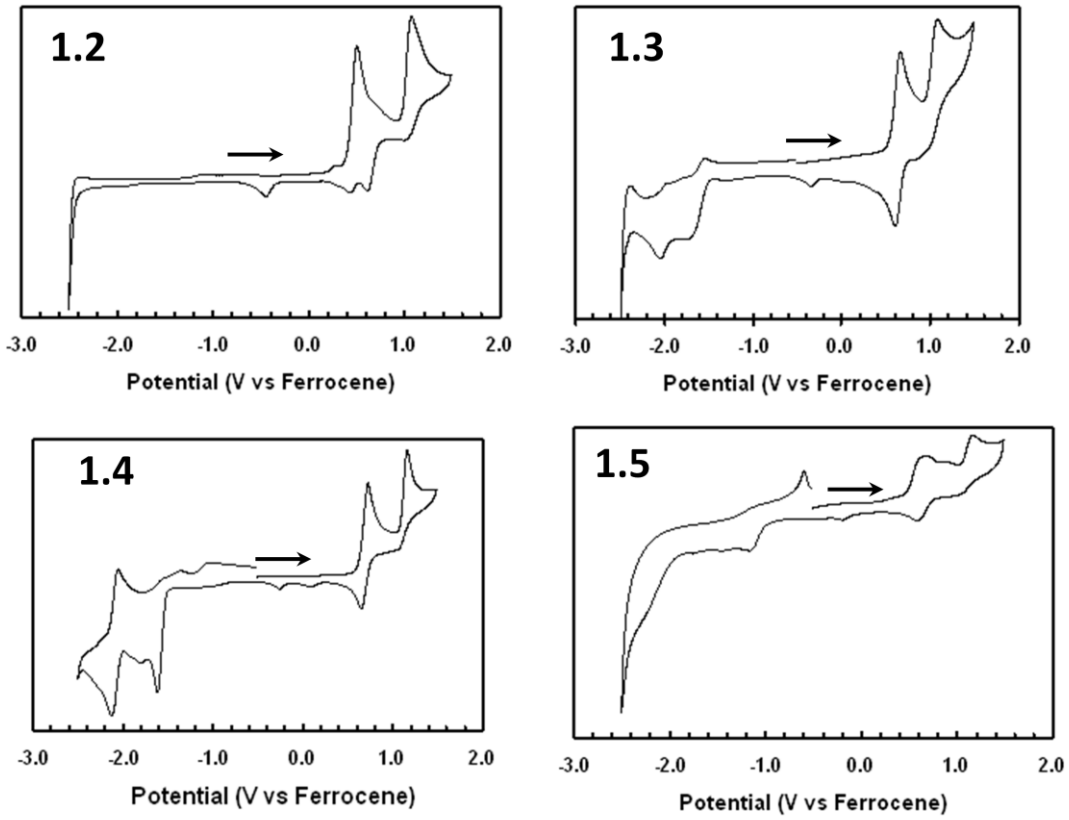

Figure 66: Cyclic voltammograms of 10^{-3} M solutions of **1.2 – 1.5** in acetonitrile containing 0.1 M Bu_4NPF_6. Scan rate 100 mV/s.

Compound	E'_{ox1} (V)	E'_{ox2} (V)
1.2	+0.5	+1.0
1.3	+0.6 (rev)	+1.0
1.4	+0.7 (rev)	+1.1
1.5	+0.6 (rev)	+1.1

Table 2: Selected electrochemical data for **1.2 – 1.5**.

1.3.1.3.1.2 UV-visible spectroscopy.

The UV spectra (**Figure 67**) of ligand **1.2** features an intense absorption at about 350 nm which is attributed to multiple n-π* transitions which is typical for triarylamines[56, 63, 97d] as well as other higher energy transitions. The complexes **1.3-1.5** exhibit similar absorption patterns which altogether resemble the UV-spectra of ligand **1.2** except the red-shift of the major absorption band in **1.2** from 350 nm to 420 nm.

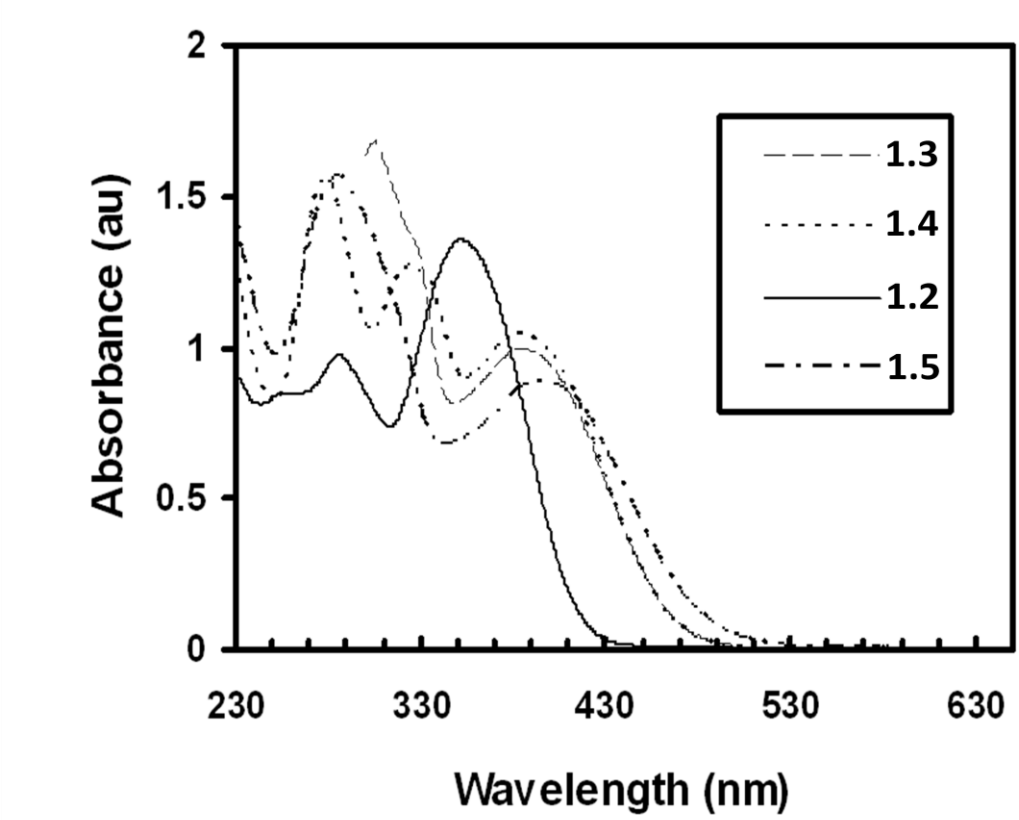

Figure 67: UV-vis spectra of **1.2-1.5** at RT in CH_2Cl_2.

1.3.1.3.1.3 Spectroelectrochemical measurements.

Spectroelectrochemical spectra (**Figure 68**) were recorded for complexes **1.3-1.5** by applying a potential of approximately 1 V (versus silver wire) to solutions of

the complexes in CH_2Cl_2 (containing 0.1 M $^nBu_4NPF_6$) while simultaneously recording the time dependent absorption spectra between 250 and 1000 nm. In all three cases absorption bands assigned to the starting neutral complexes decreased in absorption intensity (down arrows) over the course of the oxidation while new bands appeared (up arrows) which are assigned to the single electron oxidized radical-cation complexes. In particular, new bands at wavelengths of 446, 615 and 820 nm have been observed in other reported free and coordinated triarylamminum radical cations.[63, 99] Isosbestic points are noted in all spectra, indicating clean oxidative processes and the presence of only two species in solution over the course of the oxidation

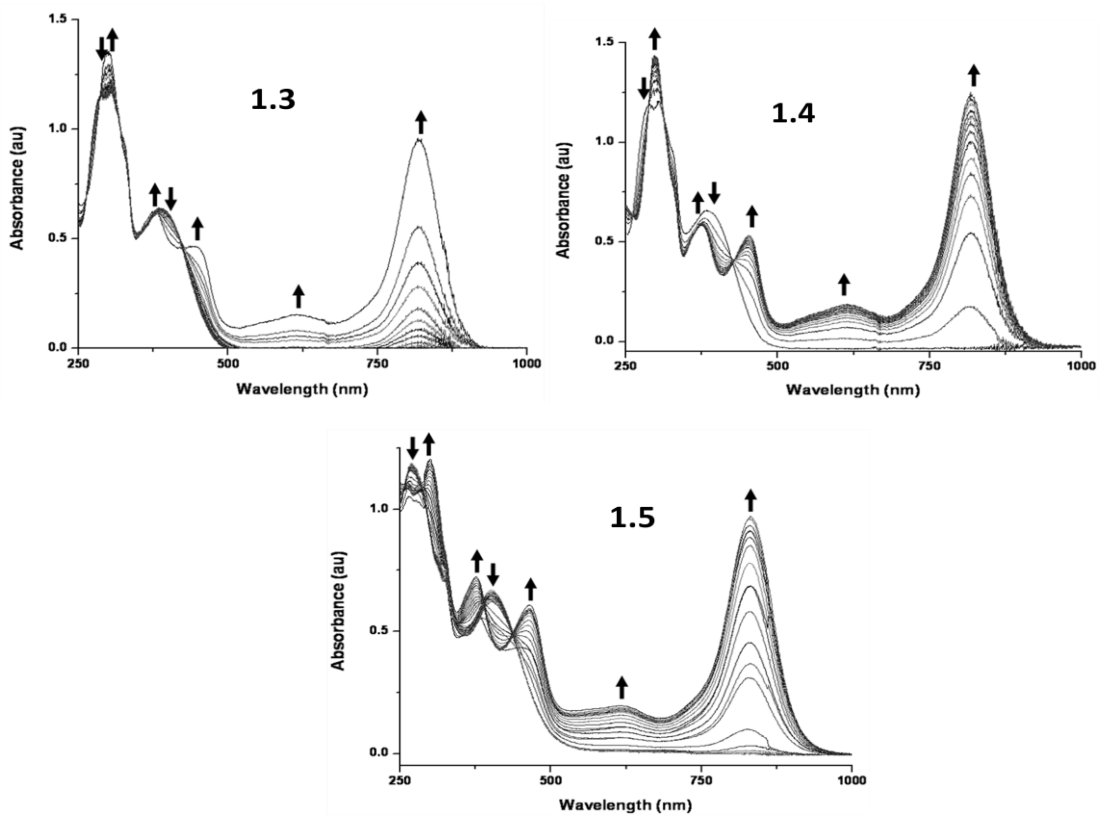

Figure 68: Spectroelectrochemistry of **1.3 – 1.5** at RT in CH_2Cl_2 solution containing 0.1M $^nBu_4NPF_6$. Black arrows indicate increase (up pointing) and decrease (down pointing) in absorbance over the course of the oxidation.

1.3.1.3.2 Variable Temperature Magnetic Susceptibility

The solid-state temperature dependent magnetic properties of neutral complexes **1.3-1.5** were investigated using SQUID magnetometry (**Figure 69**). As anticipated, nearly ideal Curie behaviour is noted for all complexes with approximately temperature independent magnetic moments that are typical for isolated monometallic Mn, Ni, and Cu complexes, with only very small deviations noted at the lowest temperatures.

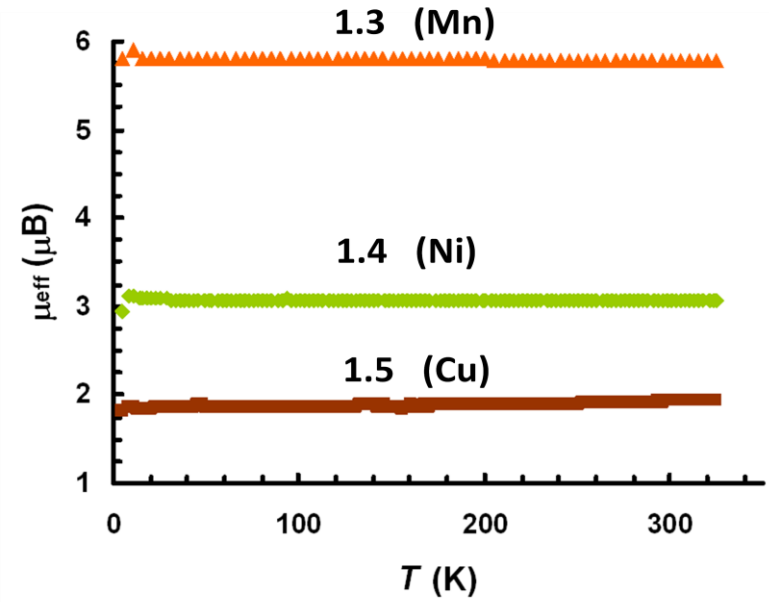

Figure 69: Temperature dependence of μ_{eff} values for **1.3-1.5**. Data obtained by SQUID-magnetometry.

The magnetic properties of the one electron oxidized radical cations of **1.3** and **1.4** were measured in solution using the Evans method (**Figure 70**). For comparison, the magnetic moments for neutral complexes **1.3** and **1.4** were also measured by this technique. Data was recorded from 300 to 244 K for **1.3** and **1.3**$^{+\bullet}$ and from 325 to 244 K for **1.4** and **1.4** $^{+\bullet}$ (low temperature data collection is limited to temperatures above the melting point of acetonitrile). The data for neutral **1.3** is very similar to

that recorded in the solid state, with a magnetic moment of 5.9 BM at 300 K, which is the anticipated value for a magnetically dilute Mn^{2+} complex. However, the magnetic moment of the singly oxidized **1.3**$^{+\bullet}PF_6$- complex is higher, approaching 6.4 BM. This value is also higher than the theoretical value anticipated for non-interacting $\boldsymbol{S} = \frac{5}{2}$ Mn^{2+} and a coordinated radical ($\boldsymbol{S} = \frac{1}{2}$), which is 6.16 BM, and suggests the presence of ferromagnetic coupling between Mn^{2+} and the radical. While at low temperature, a freshly prepared solution of **1.4**$^{+\bullet}$ was placed in the spectrometer and the identical Evans experiment was run from low to higher temperatures. The initial magnetic moment of the sample was 3.1 BM, which is a little lower than the anticipated value (3.3 BM) for non-interacting $\boldsymbol{S} = \mathbf{1}$ (Ni^{2+}) and a coordinated radical ($\boldsymbol{S} = \frac{1}{2}$). The data supports the presence of weak Ni^{2+}-radical antiferromagnetic coupling. For comparison, Evans data was acquired for an acetonitrile solution of neutral complex **1.4**, and the data is very similar to that obtained from the solid-state experiment. The magnetic properties of oxidized **1.5** were not investigated because the cyclic voltammetry results for this complex indicated an unclean oxidation.

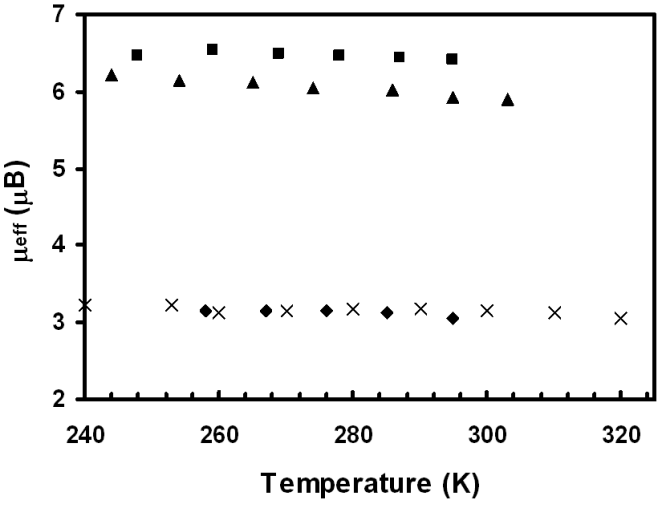

Figure 70: Temperature dependence of μ_{eff} values for **1.3** (▲), 1.3$^{+\bullet}PF_6^-$ (■), **1.4** (×), and **1.4**$^{+\bullet}PF_6^-$ (♦) measured in solution by the Evans method.

1.3.1.3.3 Spin density calculations

Density functional calculations at the B3LYP/TZVP level were used to calculate the structures and spin density distributions for the ground state singly oxidized radical cation complexes. The ground state spin density distributions within the radical cation complexes of **1.3-1.5** are shown in (**Figure 71** and **Figure 72**). For complex $\mathbf{1.3}^{+\cdot}$ a substantial positive π spin density is noted at the amminium nitrogen atom, and the π spin distribution around each atom of the adjacent bipyridine ring alternates between negative and positive. The coordinating nitrogen atoms of the 2,2′-bipyridine feature a significant amount of negative π spin density, which results in positive d_π spin density at Mn^{2+}, which produces an overall ferromagnetic interaction between the radical and Mn^{2+} ion. On the other hand, complexes $\mathbf{1.4}^{+\cdot}$, and $\mathbf{1.5}^{+\cdot}$ feature metal ions with d_σ spin density of the same sign as the π spin density at the coordinate nitrogen atom and the net interaction with the radical in each case is antiferromagnetic. These results are similar to the studies of Iwamura, which demonstrated the spin polarization mechanism behind the magnetic coupling in a series of $M(hfac)_2$ complexes featuring differentially substituted pyridine or 2,2′-bipyridine containing nitroxide radicals.[69, 108]

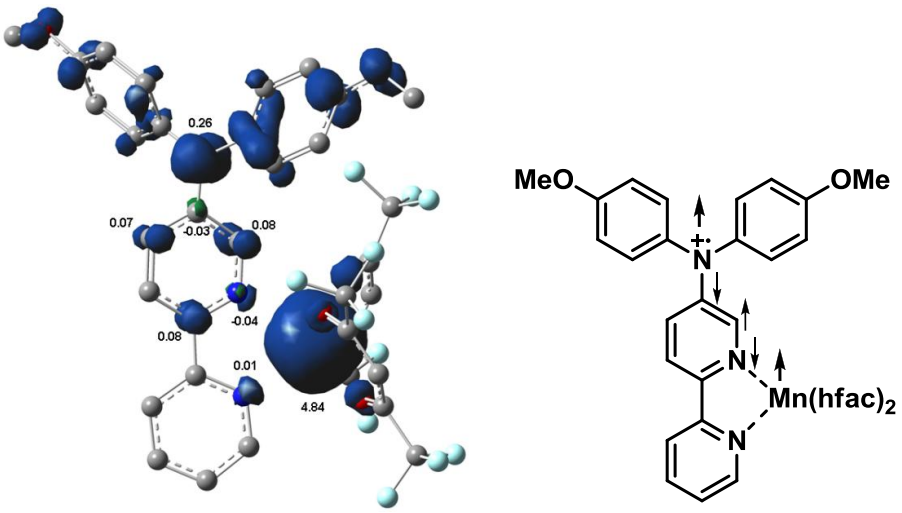

Figure 71: Calculated spin density (left) and spin polarization modelling (right) for $\mathbf{1.3}^{+\cdot}$.

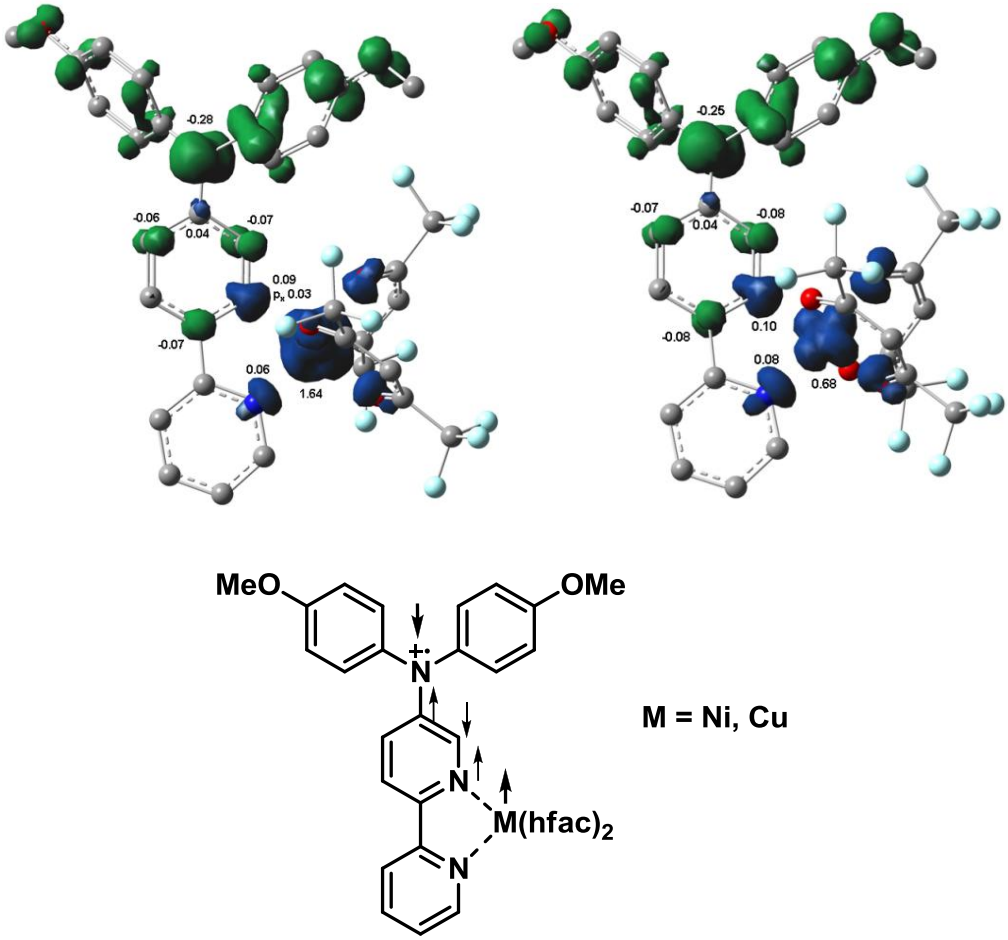

Figure 72: Calculated spin density for **1.4**$^{+\cdot}$ (top left) and **1.5**$^{+}$ (top right) and their spin polarization modelling (bottom).

1.3.1.4 Conclusion and future work

The results presented have demonstrated our efforts towards exploring the coordination chemistry of triarylamminium radical cation. Ligand **1.2** with short distance between triarylamminium and metal binding sites was synthesized and coordinated with manganese, nickel and copper ions in attempt to observe strong metal-radical exchange coupling. The ferromagnetic interactions for manganese and antiferromagnetic interactions for nickel and copper oxidized complexes were discovered. This work has a large potential for engineering ferromagnetic interactions with metals containing d_σ magnetic orbitals by synthetic adjustment of ligand structure via changing the position of radical site linkage to the bipyridine ring. For example, based on the spin polarization model proved to be correct for these systems, the ligand, synthesized through the attachment of triarylamminium site to the 4^{th} or 6^{th} position onto bipyridine upon coordination to copper and nickel ions should produce metal complexes exhibiting ferromagnetic metal-radical interactions. The stability of oxidized complexes may be enhanced by use of ligands modified with various substituents through steric protection of the spin density rich sites, which could make possible the isolation and study of solid-state structures and magnetic susceptibility measurements.

1.3.2 Synthesis and study of bimetallic complexes.

1.3.2.1 Goals and objectives

After encouraging results with monometallic complexes our goal was to obtain bimetallic radical-cation complexes with high ground state numbers and strong metal-radical and metal-metal magnetic interactions.

1.3.2.2 Ligand synthesis and coordination chemistry

Although we had a reliable technique for the production of functionalized bipyridines via Negishi coupling [106] in hand, the high price of the key reagent, 2-pyridylzinc bromide solution, was a main reason for us to explore alternative synthetic pathways.

1.3.2.2.1 Failed route.

Suggested route (**Scheme 2**) would result in 4-substituted bipyridine, not 5-substituted as in ligand **1.2** for monometallic compound synthesis. However, it would still suit our needs, since, as mentioned in previous part, we could obtain ferromagnetically coupled complexes with copper and nickel ions.

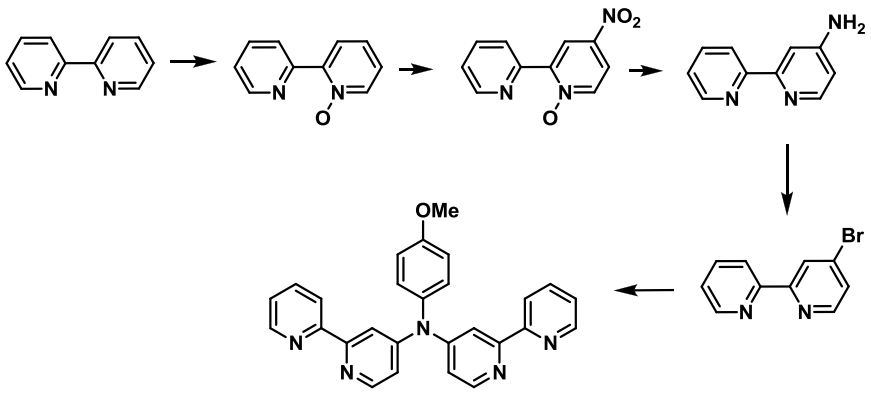

Scheme 2: Attempted synthetic route for ditopic ligand.

N-oxide was produced from 2,2-bipyridine through oxidation with mCPBA [109] with reasonable yield (~ 30%). Higher yields could be achieved through the use of distilled hydrogen peroxide and fluorine-containing acids[110] but the procedure was hazardous. Our attempts to conduct oxidation with hydrogen peroxide (36%) in glacial acetic acid [111] did not lead to the desired product. Nitration of the obtained N-oxide was performed with potassium nitrate in concentrated sulfuric acid.[109, 112] The low yield of nitrate (~ 10%) was attributed to its high solubility in water and issues with its extraction. The product of the next step, reduction of nitro-group with $SnCl_2$, had the same isolation problems. It was decided to choose an alternative bidentate ligand structure and change the synthetic pathway.

1.3.2.2.2 Final route.

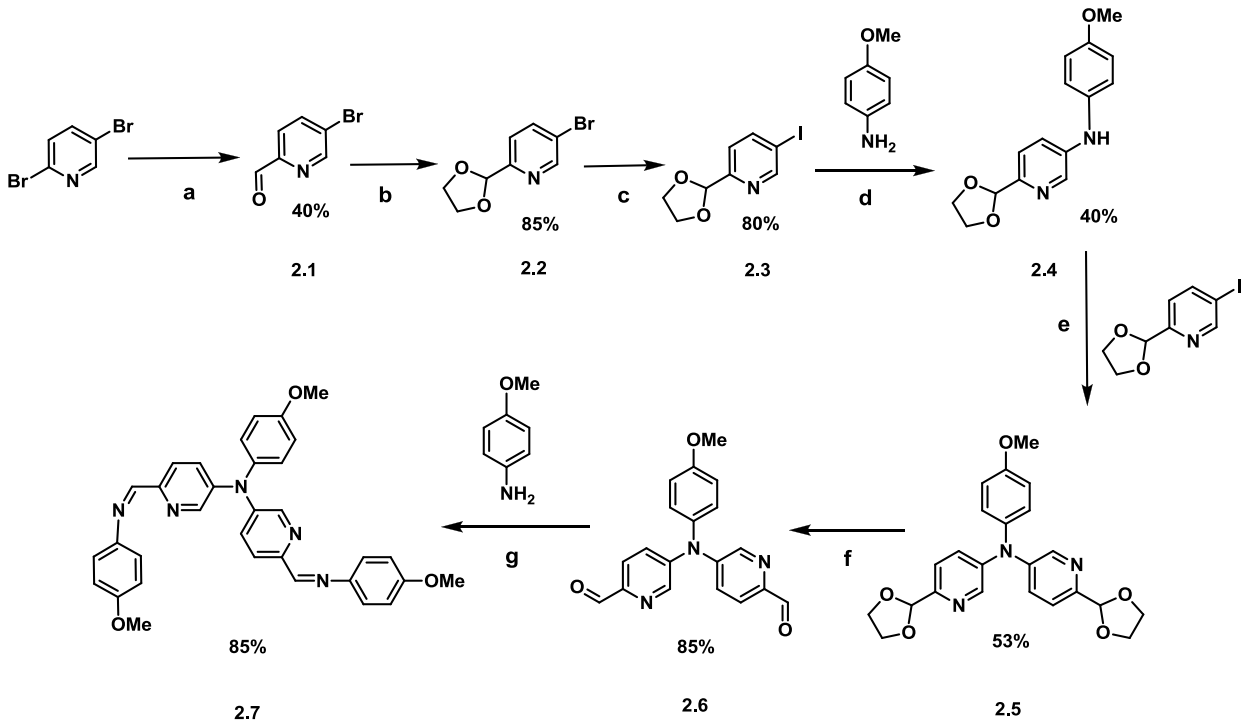

Scheme 3: Actual synthetic rout for ditopic ligand **2.7**. Reagents and conditions: a - BuLi, Toluene, -78^{o}C, DMF, b - Ethylene glycol, TosOH, Toluene, c - CuI, NaI, DMEDA, Dioxane, d - $Pd(OAc)_2$, BINAP, Cs_2CO_3, Toluene, 50^{o}C, e - $Pd(OAc)_2$, BINAP, Cs_2CO_3, Toluene, 90^{o}C, f - HCl, THF, rt, g - $MgSO_4$,THF, rt.

We used conditions found in literature to obtain aldehyde **2.1** from 2,5-dibromopyridine [113] and protected it with the dioxolane group.[114] Since the bromo-derivative was not successful towards C-N coupling, we changed the bromo-substituent for iodo.[115] In all attempted reactions under Buchwald-Hartwig conditions[116] at 90 ^{o}C, significant amounts of both secondary and tertiary amine were produced, including also a large proportion of dehalogenated **2.3**. Unfortunately, we were unable to separate the mixture of amines by column chromatography and so attempted the preparation of **2.5** in two steps. Starting with a single equivalent of **2.3**, we could readily prepare pure secondary amine **2.4** in a reasonable yield at 50 ^{o}C. Reaction between **2.4** and a second equivalent of **2.3** at elevated temperatures produced pure tertiary amine **2.5**, which was then deprotected and reacted with two equivalents of anisidine to produce the condensation product **2.7** as a hydrolytically unstable yellow powder. Storage of **2.7** in an inert environment is necessary to prevent decomposition.

Bimetallic complexes containing ligand **2.7** were readily produced by combining two equivalents of hydrated M(hfac)$_2$ salts (M = Mn, Ni, Cu) with **2.7** in CH_2Cl_2 solution (**Scheme 4**), which produced analytically pure, microcrystalline precipitates of complexes **2.8** (Mn), **2.9** (Ni), and **2.10** (Cu). Complex **2.10** produced what appeared to be X-ray diffraction quality crystals via slow evaporation of concentrated methanol solutions but in all our attempts to acquire an X-ray structure data collection was extremely weak due to poor crystal diffraction.

The structures of complexes **2.8**-**2.10** were confirmed by spectral data and elemental analysis.

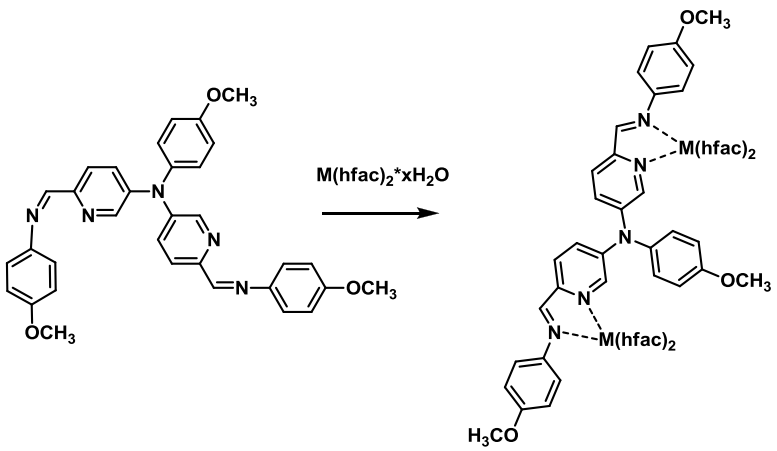

Scheme 4: Coordinating ligand **2.7** with metal ions to produce **2.8** (M=Mn (II)), **2.9** (M=Ni (II)) and **2.10** (M=Cu (II)).

1.3.2.3 Study of properties.

1.3.2.3.1 Electronic properties.

The electronic properties of ligand **2.7** and complexes **2.8** – **2.10** were investigated via electronic absorbance spectroscopy and cyclic voltammetry.

1.3.2.3.1.1 ***Electronic absorption***

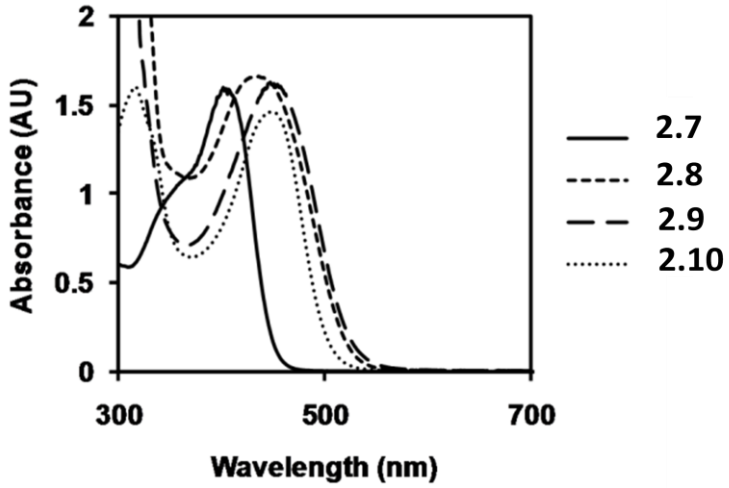

Figure 73: Electronic absorption spectra of **2.7** – **2.10** (acetonitrile solution).

The electronic absorption spectra of **2.7 - 2.10** in CH_3CN solution is shown in **Figure 73**. Ligand **2.7** features a dominant visible absorption band centered at 410 nm, which is n-π* in origin. Complexes **2.8-2.10** each exhibit this same ligand centered transition but at slightly longer wavelengths in all cases relative to **2.7**. No bands in the visible region of the spectra can be attributed to metal-centered d-d transitions or metal-ligand charge transfer.

1.3.2.3.1.2 Electrochemistry

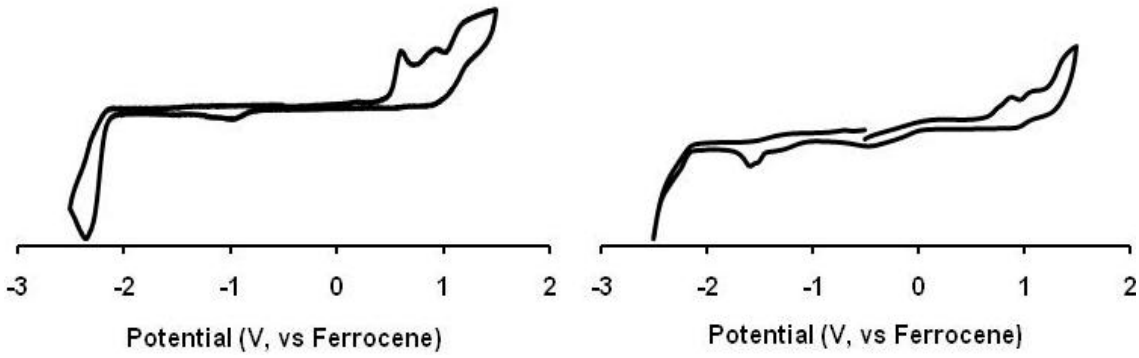

Figure 74: Cyclic voltammograms of ligand **2.7** (left) and complex **2.10** (right) in acetonitrile solution containing 10^{-3} M $^{n}Bu_4NPF_6$. 100 mV/s scan rate.

Cyclic voltammograms (**Figure 74**) were acquired for **2.7** and complexes **– 2.8 - 2.10** in acetonitrile solution. Toward positive potentials ligand **2.7** exhibits three closely spaced and irreversible waves centered at +0.6, 0.9 and 1.2 V (vs. ferrocene). The first and second waves likely represent production of radical-cation and dication, respectively. The third wave is of an unknown origin, but may represent a metal-centered oxidation (for complexes **2.8 – 2.10**), or oxidation of a decomposition product formed from one of the first two oxidation processes. Toward negative potentials the CV of **2.7** is unremarkable, featuring an irreversible imine reduction centered at -2.3 V. In complexes **2.8 – 2.10** the same pattern of three irreversible

oxidative processes are noted, but are shifted to higher potentials relative to **2.7** (**Figure 74**, right). The waves are also more closely spaced than in **2.7**, with the first two waves separated by only approximately 100 mV. This is in stark contrast to ligand **1.2** and its monometallic complexes **1.3 – 1.5**, in which $M(hfac)_2$ coordination stabilized the radical-cation and produces reversible electrochemistry at potentials lower than in the free ligand. Complexes **2.8** – **2.10** also exhibit irreversible cathodic waves at potentials centered at -1.6 and -2.4 V, which represent hfac and imine reductions, respectively.

1.3.2.3.2 Magnetic measurements

The variable temperature magnetic properties of **2.8** – **2.10** were investigated by SQUID magnetometry over a temperature range of 300 – 5 K, in an external field of 2000 Oe (**Figure 75**). For each complex, the data were fitted [117] to numerical expressions derived from the van Vleck equation for simple bimetallic complexes containing Mn, Ni or Cu, based upon the following isotropic spin Hamiltonian:

$$\widehat{H} = J\widehat{S}_M\widehat{S}_M \qquad \textbf{(20)}$$

All variable temperature magnetic data fitting was carried out using the fitting program Magmun.[117] The best fit parameters for **2.8** (g = 2.0, J_{MnMn} = -0.025 cm^{-1}, ρ = 0.025, θ = -0.4 K, R = 0.0086) and **2.9** (g = 2.26, J_{NiNi} = -0.20 cm^{-1}, TIP = 900×10^{-6} cm^3 mol^{-1} K^{-1}, θ = -0.9 K, R = 0.028) each include very weak intra- and intermolecular antiferromagnetic coupling terms. However, only very slightly poorer fits can also be obtained with very small ferromagnetic coupling terms, so the actual sign of the coupling is not unambiguous.

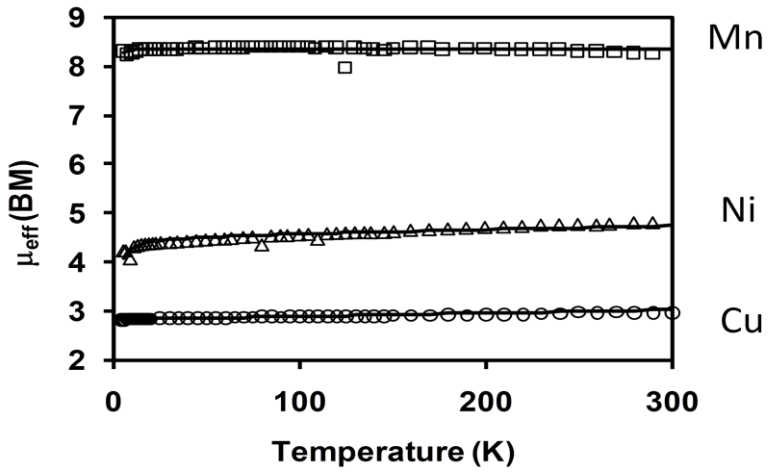

Figure 75: Effective magnetic moment versus temperature plots for complexes **2.8** (□), **2.9** (Δ), and **2.10** (○) (2000 Oe external field). The lines through the points represent best fits based on appropriate spin Hamiltonians with best fit parameters.

It is best to describe complexes **2.8** and **2.9** as very weakly coupled systems. On the other hand, the best fit parameters for complex **2.10** (**Figure 76**) suggest a weak, but measureable ferromagnetic coupling that may be operative been the copper ions (g = 2.30, J_{CuCu} = +2.0 cm^{-1}, ρ = 0.020, TIP = 500×10^{-6} cm^3 mol^{-1} K^{-1}, θ = -0.6 K, R = 0.0031).

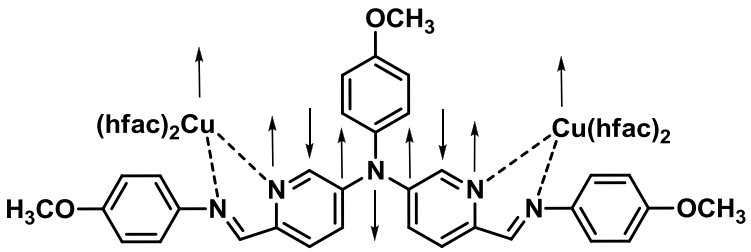

Figure 76: Proposed π-spin density distribution in **2.10**.

In an effort to confirm a ground triplet state for **2.10**, a low temperature (4K) magnetization versus field experiment was performed (**Figure 77**). While the

magnetization does not saturate up to 5 T, the experimental data points are similar to the theoretical curve calculated for a triplet state at 4 K (assuming a *g* parameter equal to that obtained from the fit of the magnetic susceptibility data).

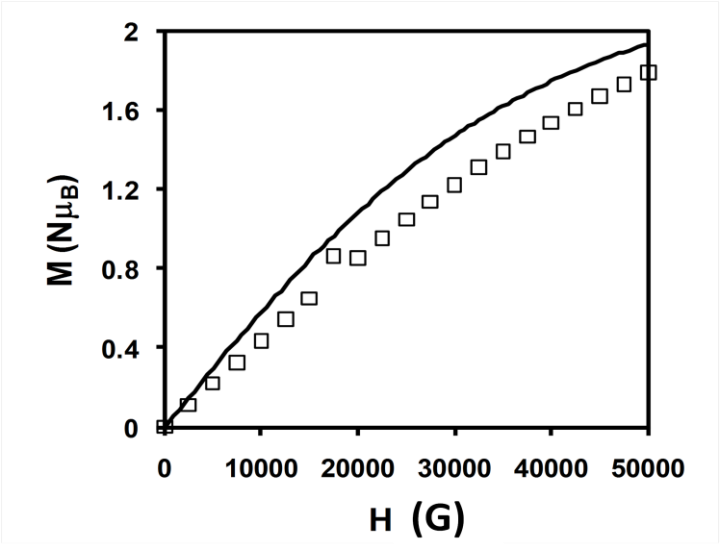

Figure 77: Reduced magnetization versus field data for complex **2.10** at 4K. The solid line represents the theoretical curve for an $S = 1$ state at 4 K ($g = 2.3$)

1.3.2.3.3 Oxidation

In an effort to produce the radical cation of ligand **2.7** and complexes **2.8 - 2.10**, chemical oxidations were carried out in acetonitrile solution by careful addition of $NOPF_6$ (one equivalent) at room temperature under anhydrous and aerobic conditions (**Figure 78** and **Figure 79**). Instantly, a color change to deep cherry red was noted in all reactions upon oxidant addition. With the exception of complex **2.9**, the visible absorption spectra of the oxidation products are all very similar and feature a longer wavelength band (relative to the neutral precursors) together with a higher energy shoulder. Of note, addition of a second (or more) equivalent of oxidant results in no other changes to the absorption spectra. In fact, these absorption spectra are very different from those produced by chemical oxidation of $M(hfac)_2$ complexes

containing **1.2** and the spectra of other reported triarylamminium radical cations and are in fact more representative of spectra produced from reported diamagnetic dicationic species.[56, 97d]

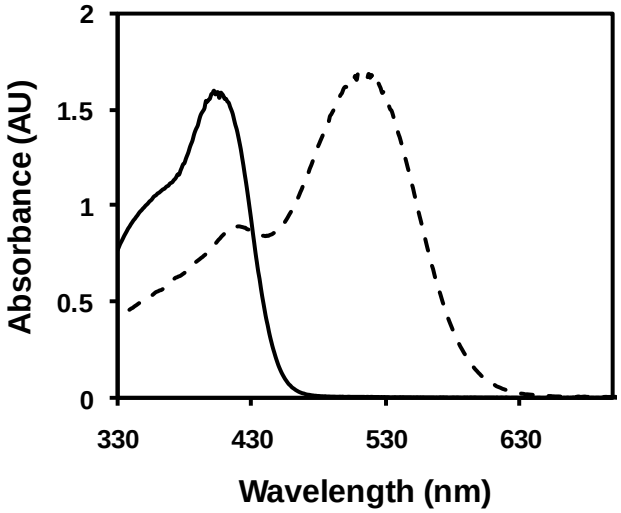

Figure 78: Visible absorption spectra of ligand **2.7** (solid line) and **2.7**$^{2+}$ (dashed line).

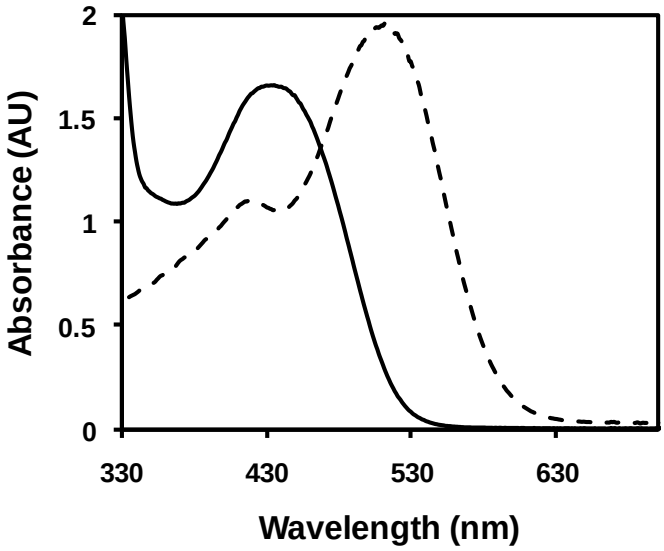

Figure 79: Visible absorption spectra of **2.8** (solid line) and **2.8**$^{2+}$ (dashed line).

Searching for any proof of radical presence we attempted to obtaine EPR spectra of oxidized ligand **2.7** and complex **2.8** at room temperature in acetonitrile.

No EPR spectrum of **2.7** was obtained and EPR spectra of neutral and oxidized **2.8** were identical (**Figure 80**).

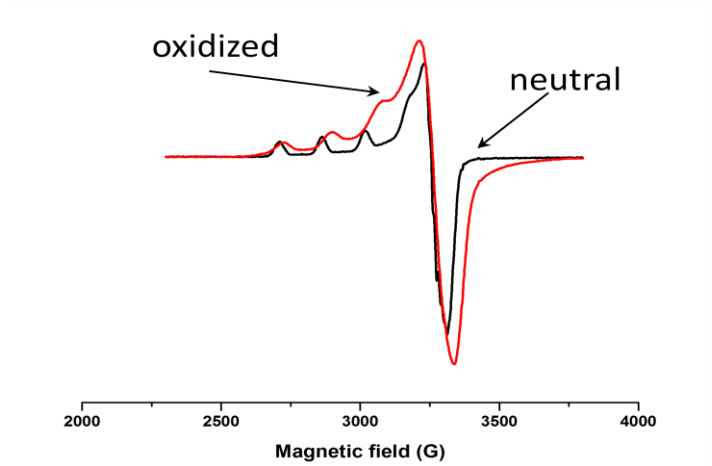

Figure 80: EPR spectra of neutral and oxidized **2.8**.

These results led us to the conclusion that no radical-cation formation occurs but production of stable dications takes place instead during oxidation of **2.7**, **2.8** and **2.10** (**Figure 81**) while oxidation of **2.9** results in decomposition.

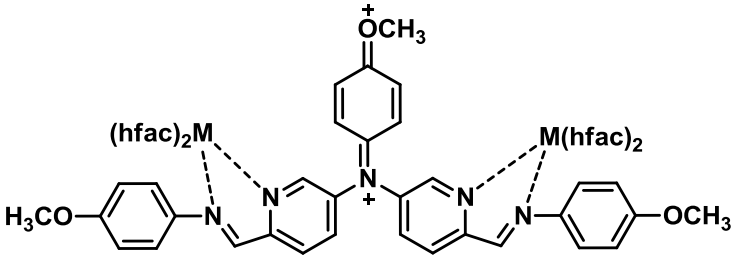

Figure 81: Proposed structure of dication complexes of **2.8** and **2.10**.

Given the irreversible nature and meagre separation (less than 200 mV) between the purported oxidation waves for radical cation and dication observed in the CV it is clear that isolating persistent radical cation complexes is not possible with the given system.

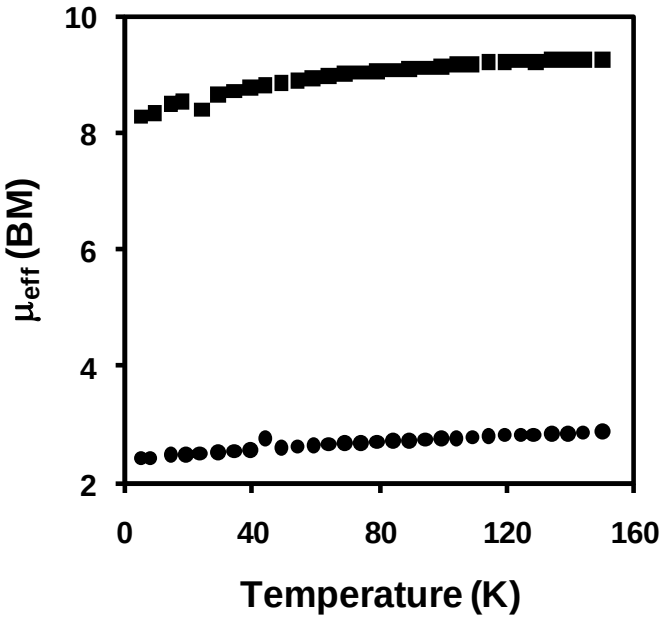

Figure 82: Effective magnetic moment versus temperature plots for the oxidation products of complexes **2.8** (■) and **2.10** (●) (2000 Oe external field).

The variable temperature magnetic properties of dication **2.8** and **2.10** were investigated by SQUID magnetometry over a narrow temperature range (5 – 150 K) and indicate essentially no coupling between the metal ions (**Figure 82**). Given the uncertainty in the mass and purity of these products we did not attempt to fit these data but the magnitude of the magnetic moments and curve profiles with decreasing temperature suggest extremely weak interactions at best.

1.3.2.3.4 DFT calculations

For comparison, the structures, relative energies and spin density distributions were calculated for hypothetical bimetallic $M(hfac)_2$ (M = Ni, Mn) containing the *radical cation* of ligand **2.7**. Calculations were performed on the S = 11/2 and 9/2 states of the $Mn(hfac)_2$ complex, which corresponds to manganese(II)–N-radical ferromagnetic or antiferromagnetic coupling, respectively. The spin density distributions for the two minimized structures are shown in **Figure 84** and **Figure 85**.

The individual Mn (II) ions are in the high-spin configuration and NPA-derived atomic spin densities for the manganese atoms are 4.74-4.75 for both S=11/2 and 9/2 states, respectively. It has been shown that manganese-ligands bonds have relatively low covalent profile,[118] which is in agreement with Mn-O and Mn-N bond orders (0.25 - 0.29 and 0.21 - 0.23, respectively).

The antiferromagnetically coupled manganese complex with S = 9/2 is calculated to have a lower energy than the complex with a ferromagnetic interaction (S = 11/2) by 91 cm^{-1}. This is in contrast to the reported $Mn(hfac)_2$ complex with the radical cation of **1.2**, which was demonstrated to exhibit a weak ferromagnetic Mn-radical interaction, which was rationalized on the basis of a π-spin polarization mechanism (supported by DFT calculations). The geometry and calculated π-spin density distribution in the bimetallic complex is different from $Mn(hfac)_2$**1.2**, including essentially zero spin density on the coordinate N atom of the pyridine ring or the C atom bonded to the amminium N atom. This result suggests that the same mechanism behind the observed coupling in $Mn(hfac)_2$ **1.2** complex (**Figure 83**) would not be operative in the bimetallic analogue. Calculated spin density distribution for manganese complex is shown on **Figure 84**.

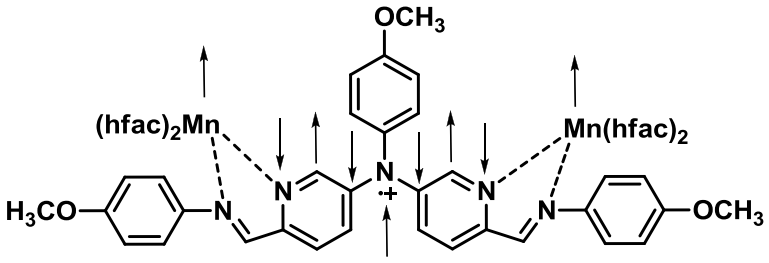

Figure 83: Suggested spin polarization in **2.8** based on results obtained for **1.3**.

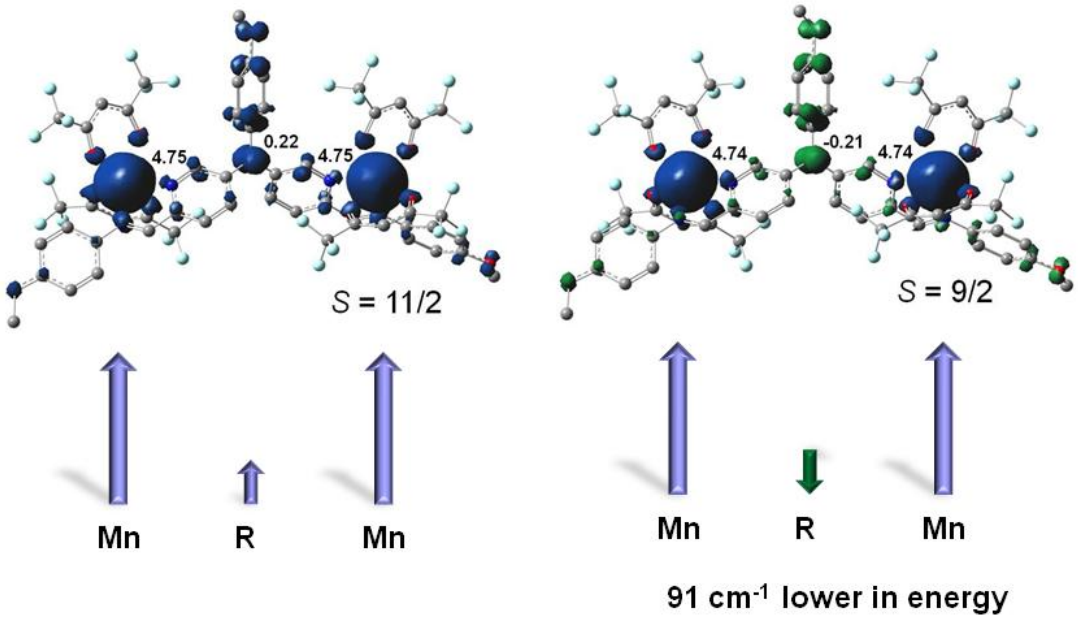

Figure 84: Calculated spin density distributions in optimized structures for the S=11/2 and 9/2 states of the radical cation of complex **2.8**. The NPA-derived atomic spin densities for the metal ions and the triarylamminium nitrogen are shown. Spin densities are shown with the isosurface contour value of 0.004

Calculations were also performed on the *S* = 5/2 or 3/2 states of the bimetallic Ni(hfac)$_2$ complex (**Figure 85**) of the same radical cation ligand of **2.7** and the results (geometry and spin density distribution) were similar to those observed from the bimetallic Mn(hfac)$_2$ complexes described above. NPA-derived atomic spin densities both Ni (II) spin states S = 5/2 and S = 3/2 result in the same value of 1.65. Compared to the bimetallic manganese complex, the Ni (II) – ligand bonds have stronger covalency as can be seen from the bond orders: 0.33-.35 for Ni-O and 0.33-0.34 for Ni-N. The energy of the *S* = 3/2 state (nickel-radical antiferromagnetic coupling) is lower by 56 cm^{-1} relative to the *S* = 5/2 state (ferromagnetically coupled). In both hypothetical complexes it is likely that a very weak superexchange pathway and not spin polarization would be responsible for any metal-radical exchange coupling.

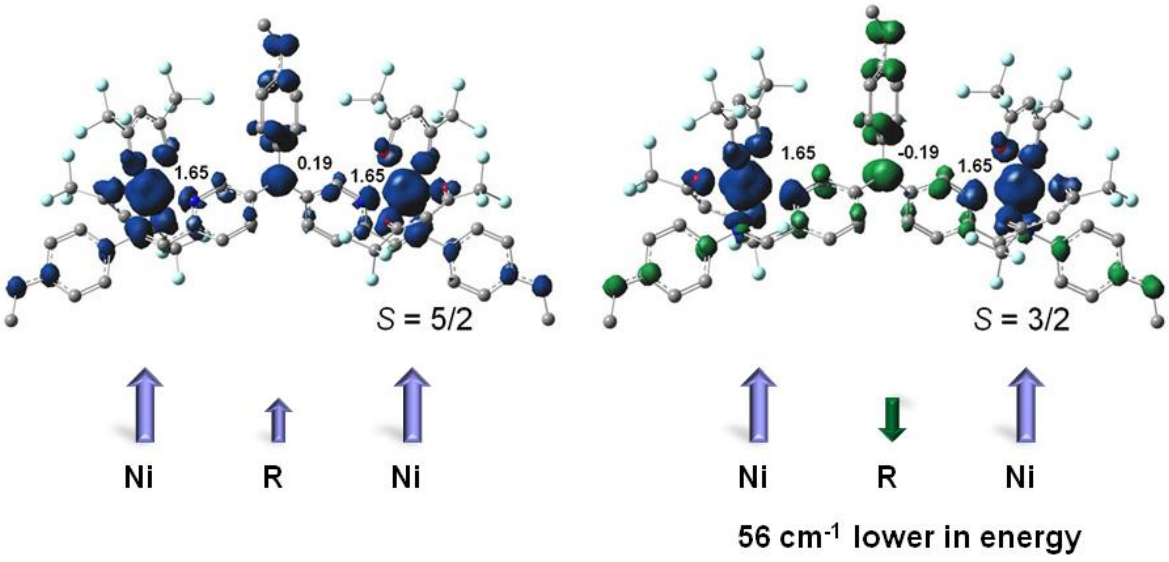

Figure 85: Calculated spin density distributions in optimized structures for the S=5/2 and 3/2 states of the radical cation of complex **2.9**. The NPA-derived atomic spin densities for the metal ions and the triarylamminium nitrogen are shown. Spin densities are shown with the isosurface contour value of 0.004

1.3.2.4 Conclusion and future work

The multistep synthesis of a new ditopic triarylamino-type ligand was conducted and the full characterization of bimetallic $M(hfac)_2$ complexes (M = Mn, Ni, Cu) containing this ligand was accomplished. In the neutral precursor complexes, very weak magnetic interactions persist between the coordinated metal ions; including a weak ferromagnetic interaction mediated by spin polarization when M = Cu. Chemical oxidation of the precursor complexes produces persistent complexes of the dication of **2.7**, which we could identify by UV-vis and EPR spectroscopies. Unfortunately, the complexes containing the radical cation of **2.7** could not be isolated, perhaps owing to the irreversible nature and poor separation of the first and second oxidation waves observed in the ligand. In fact, DFT calculations on a bimetallic $Mn(hfac)_2$ complex containing the dication of **2.7** indicate a lower energy than the analogous radical-cation complex.

It is possible that minor modifications of the ligand structure such as absence of electron donating group (**Figure 86**, left) may disfavour easy dication formation and improve the chances for isolation of the radical-cation.

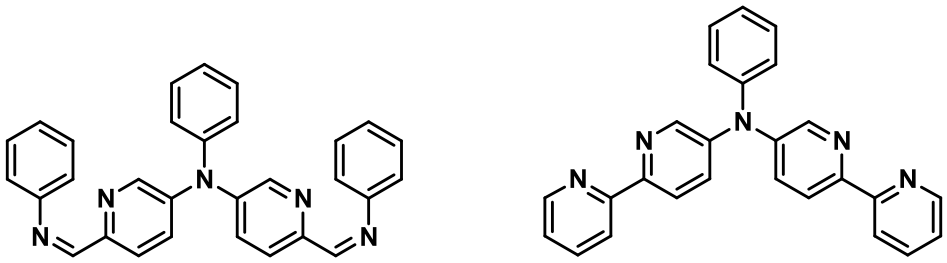

Figure 86: Suggested ligand structures: left - without electron donating groups, right – with bipyridine coordination sites.

Also it may be reasonable to return synthetic strategy to bipyridine pathway similar to the one used in the monometallic project (**Figure 86**, right). It is possible,

that coordination of metal ion to the 2,2-bipyridine system could provide better profile of electron density distribution and spin-spin coupling.

1.3.3 Synthesis of dendrimer ligand for polimetallic complexes.

1.3.3.1 Goals and objectives

The goal of this project was synthesis of a polytopic ligand and its complexes with manganese, nickel and copper. The complexes (example shown on **Figure 87**) were expected to demonstrate high ground state number and possible magnetic interaction between metal ions and between metal ions and radical-cation sites.

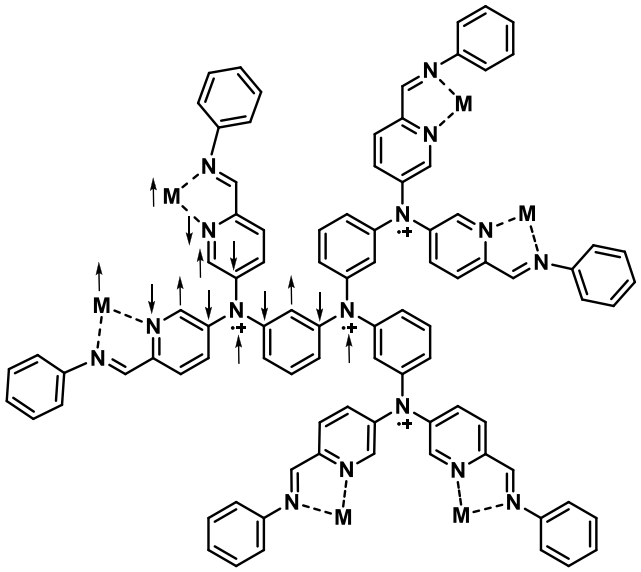

Figure 87: Proposed spin polarization in oxidized **3.12**, M = Mn (II)

$S_{predicted}=6\times(5/2)+3\times(1/2)+1/2=17$

1.3.3.2 Ligand synthesis.

Synthesis of the ligand is usually the largest part of the work on the way to the polymetallic complexes. In current project the original multistep route for ligand synthesis was proposed. In this chapter its description is broken down into the following parts: synthetic plan for ligand **3.11**, synthetic optimization for precursor **2.3**, synthesis of coordination site **3.4**, synthesis of the central unit **3.8**, attempted C-N

coupling of **3.4** and **3.8** and the final strategy for obtaining of **3.9** followed by its deprotection.

1.3.3.2.1 Original route for ligand 3.11 synthesis.

The original idea was to prepare bitopic secondary amine precursor **3.4** out of iodide **2.3** and primary amine **3.3**. This secondary amine part (3 equivalents) was to be connected to the central tris-iodide **3.8** via C-N coupling under Buchwald-Hartwig conditions to obtain **3.9.** Further deprotection of **3.9** would result in hexa-aldehyde **3.10** which upon condensation with aniline would give ligand **3.11.** Coordination of **3.11** to $M(hfac)_2 \cdot xH_2O$ salts, where M = Mn, Ni and Cu, would result in polymetallic complexes **3.12-3.14** (**Scheme 5**).

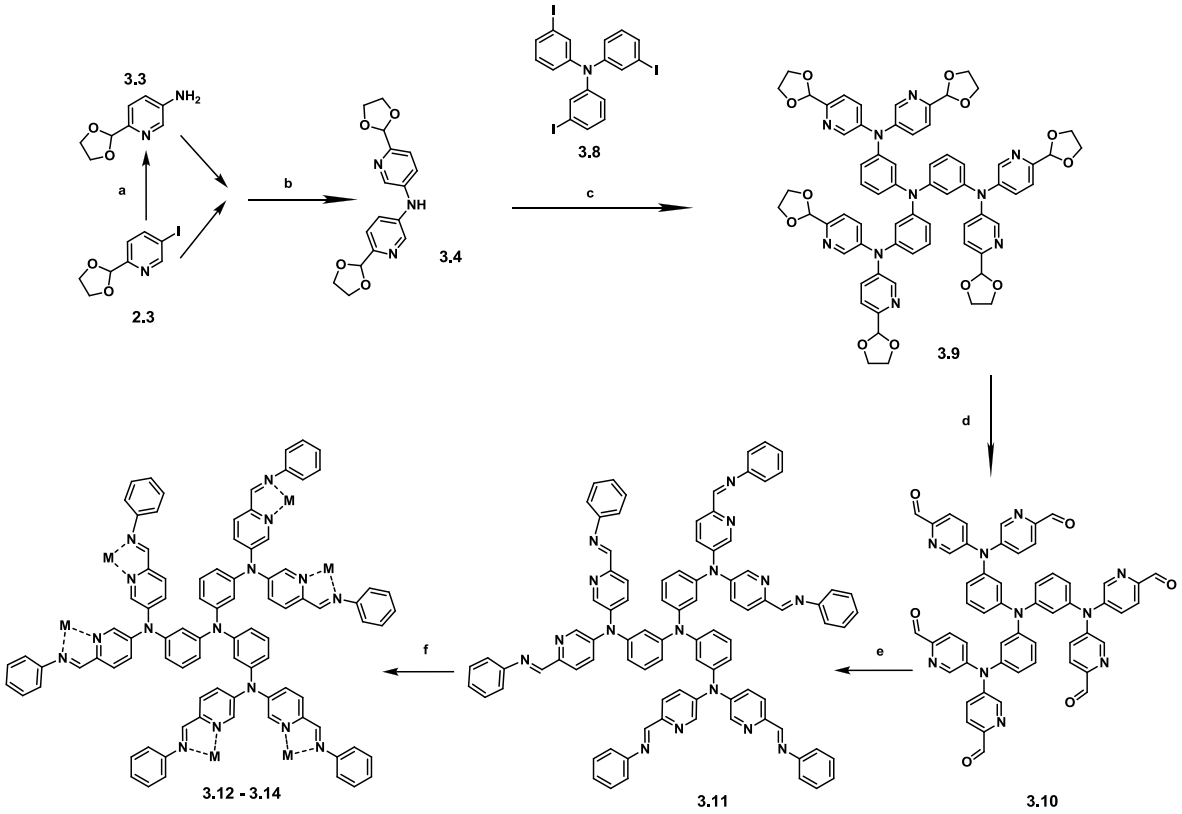

Scheme 5: Suggested synthetic pathway for **3.11** and **3.12-3.14**. Reagents and conditions: a – $NH_3 \cdot H_2O$, Cu_2O, Ethylene Glycol, DMEDA, b and c – $Pd(OAc)_2$, Cs_2CO_3, BINAP, Toluene, d – HCl, THF, e – $C_6H_5NH_2$, $MgSO_4$, THF, f – $M(hfac)_2 \cdot xH_2O$ (M=Mn, Ni, Cu), CH_2Cl_2.

1.3.3.2.2 Aldehyde 2.1 synthetic pathway optimization.

Since synthetic pathway for the "iodide" precursor developed in the course of the bitopic ligand synthesis had a weak spot in its first step, an attempt to reach this compound in a more reliable method was investigated. Poorly reproducible and very sensitive reaction with n-butyl lithium and DMF used previously gave 40% yield of aldehyde **2.1** at best. Now the aldehyde was obtained through three highly efficient steps: 5-bromo-picolinic acid was converted into methyl ester **3.1** which was then selectively reduced to alcohol **3.2** with sodium borohydride. The alcohol was then carefully oxidized with manganese dioxide to yield aldehyde **2.1**. The overall yield of these three steps together was close to 60%, which is about 1.5 times higher and easier to reproduce than the one-step reaction we used in our previous project (**Scheme 6**).

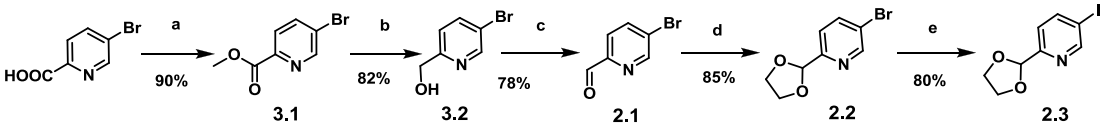

Scheme 6: Optimized synthetic pathway for **2.1**. Reagents and conditions: a - MeOH, H_2SO_4, 16 h, reflux, b - $NaBH_4$, MeOH:CH_2Cl_2 7:3, 25 h, c - MnO_2, CH_2Cl_2, 3 days, rt, d - Ethylene glycol, TosOH, Toluene, e - CuI, NaI, DMEDA, Dioxane.

1.3.3.2.3 Synthesis of coordination site 3.4.

Primary amine **3.3** was obtained from iodide **2.3** through the direct amination procedure (**Scheme 5**).[119] Under Buchwald-Hartwig conditions secondary amine **3.4** was produced with reasonable yield.

1.3.3.2.4 Central amminium site.

The central site of ligand molecule was synthesized stepwise out of *m*-nitroaniline. First, *m*-iodonitrobenzene **3.5** was obtained through Sandmeyer conditions[120], then tris-m-nitrophenylamine **3.6** was produced via Ullmann coupling

and resulted product was reduced to **3.7**, which was converted into tris-iodide **3.8** with another Sandmeyer reaction (**Scheme 7**).

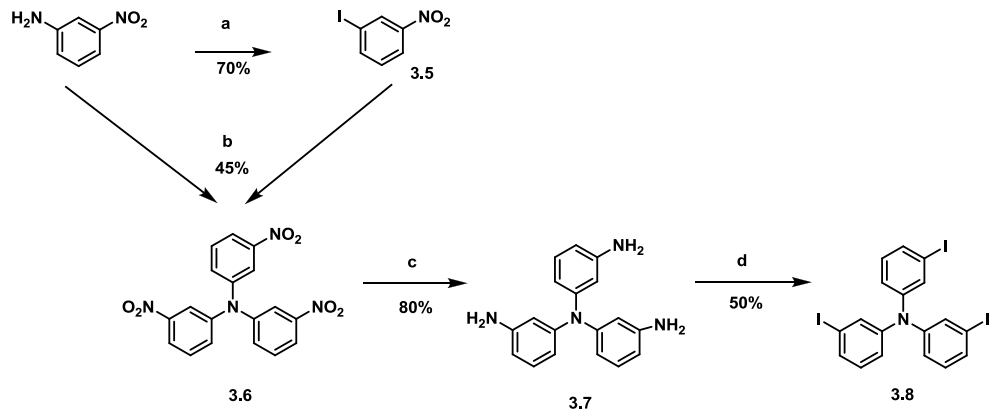

Scheme 7: Synthesis of precursor for central site. Reagents and conditions: a - $NaNO_2$, KI,CH_3COOH, H_2SO_4, b -Cu, 18-crown-6, K_2CO_3, xylene, c - Sn, HCl, EtOH, d - $NaNO_2$, KI,CH_3COOH, H_2SO_4

1.3.3.2.5 Assembling.

Unfortunately, due to steric hindrance none of C-N coupling reactions between 2^o amine **3.4** and tris-iodide precursor **3.8** led to the desired product, although multiple sets of Buchwald-Hartwig and Ullmann conditions were tested.

1.3.3.2.6 Final route for C-N coupling and deprotection.

Surmising that 2^o amine **3.4** was too bulky for this reaction, we tried to react 6 equivalents of iodide with 1 equivalent of **3.7** under Ullmann conditions with commercially available copper powder as catalyst and obtained minimal quantities of desired product (~ 2% yield). Few methods of copper catalyst preactivation by removing oxide layer from the surface of copper powder particles were attempted with no success. Finally, we were fortunate to find the original procedure of copper catalyst preparation by Piccard and Larsen[121] from 1917. Their method based on copper salt reduction in solution was developed in attempt to produce copper catalyst

with properties analogous to the famous at the time "Naturkupfer C" or "Kupferbronze" patented reagent produced in Germany. The technique was used with minor changes in our laboratory. To our surprise the yield of Ullmann reaction with this catalyst was close to 30%, which is relatively good taking into account that this one reaction includes six C-N coupling steps in it. Also it must be taken into account the numerous nitrogen sites rendering the molecule very polar, purification of **3.9** via silica gel column chromatography results in some inevitable loss. An interesting observation about the catalyst was made. The catalyst activity depended crucially on the source of zinc used as a reducing agent for conversion of Cr^{3+} into Cr^{2+} which reduced Cu^{2+} into Cu^{0} followed by precipitation of fresh copper powder. We found that neither zinc powder nor zinc mossy but only zinc pellets could be used to obtain active catalyst. Unless pellets were used, the shape, size and color of copper particles were visibly different from the very fine shiny red powder which showed remarkable activity. The elemental analysis of powder showed ppm-level presence of other metals, such as nickel and chromium. It is possible that this small metal impurity participates in the catalytic reaction.

The compound **3.9** was then deprotected with hydrochloric acid to give the hexaaldehyde **3.10**.

1.3.3.3 Conclusion and future work.

The final route for the synthesis of dendritic ligand **3.11** is presented on **Scheme 8**. The condensation reaction to convert **3.10** into **3.11** can be conducted the same way as it was done in the final step of ligand synthesis in the previous project. The oxidation of neutral polymetallic complexes can be achieved analogously to the oxidation of mono- and bimetallic complexes.

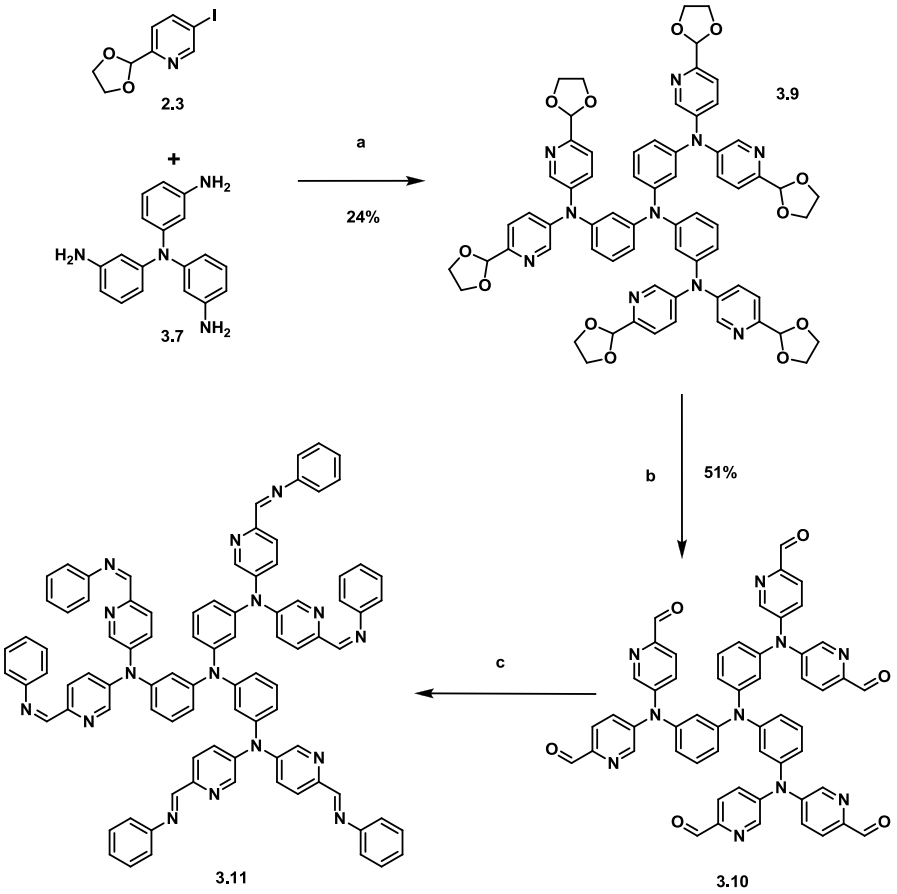

Scheme 8: Final synthetic pathway to **3.11**. Reagents and conditions: a - Cu (freshly made), K_2CO_3, 18-crown-6, Toluene, 90 ^oC, 7 days, b - HCl, THF, rt, c - $C_6H_5NH_2$, $MgSO_4$, THF.

Although the final objections were not completed, this project features a reliable synthetic approach and shows a large potential for future work in the development of high spin polymetallic complexes. The ligand structure provides a lot of opportunities for variations with electron-donating, electron-withdrawing or simply bulky substituents. The central part of the ligand can be easily modified by using para-substituted **3.15** to result in alternative **3.16** ligand structure (**Figure 88**).

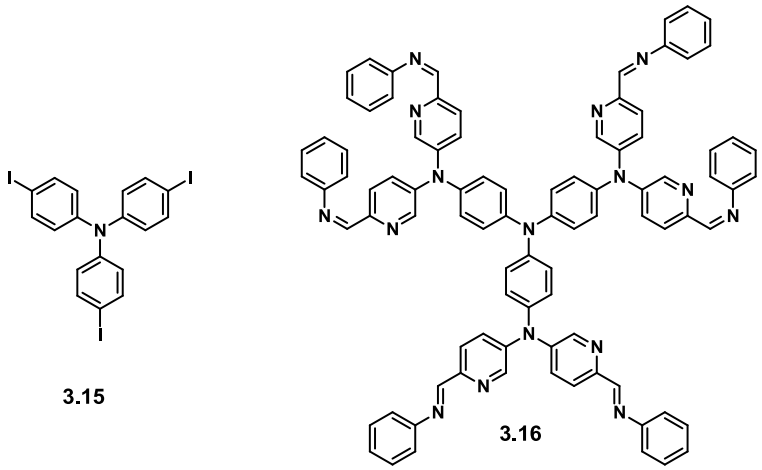

Figure 88: Alternative central triarylaminnium site precursor **3.15** and ligand **3.16**.

If the suggested spin polarization model for complex **3.17** (**Figure 89**) was observed, resulting in $S_{predicted}=6\times(5/2)+3\times(1/2)-1/2=16$ with M = Mn(II), then both ligands **3.11** and **3.16** as well as their complexes could make an excellent workbench for studying spin polarization mechanisms and methods for spin alignment tuning in large molecules as well as it would be one of the first examples of high spin polymetallic triarylamminium complexes.

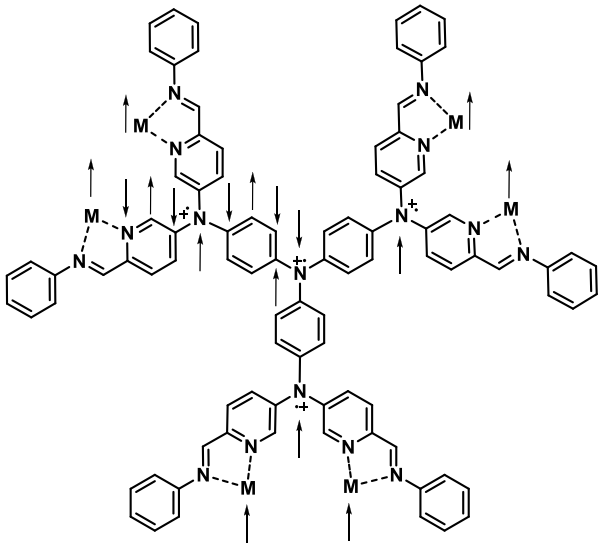

Figure 89: Suggested spin polarization in complex **3.17**.

In case if complexes with ligands **3.11** and **3.16** did not exhibit expected magnetic properties, the bipyridine-based ligand structures **3.18** and **3.19**, analogous to ligand **1.2**, could be considered as alternative ways due to their improved planarity and regularity of π-systems arrangement (**Figure 90**).

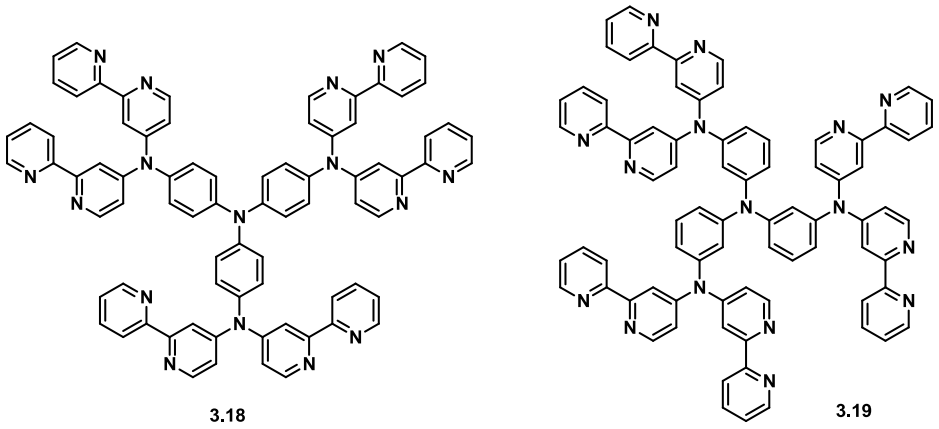

Figure 90: Bipyridine-based dendritic ligands.

1.4 Conclusion for Triarylamminium radical-cation metal complexes projects.

In these three projects we showed the possibility of producing triarylamminium radical-cation complexes with strong spin-spin interactions between metal ions and radical-cation sites. We also faced difficulties with ligand design leading to low metal-metal and metal-radical interactions as well as oxidation problems. Strategies for solving these problems by changing the ligand structure were suggested. The successful synthesis of polytopic ligand precursor for polymetallic high spin complexes was accomplished leaving a substantial base for the development of polymetallic complexes.

1.5 Experimental.

1.5.1 General

All reagents were commercially available and used as received unless otherwise stated. Deaerated and anhydrous solvents were obtained from a Puresolve PS MD-4 solvent purification system, and all air and/or moisture sensitive reactions were carried out using standard Schlenk techniques. $^{1}H/^{13}C$-NMR spectra were recorded on a Bruker Avance 300 MHz spectrometer with a 7.05 T Ultrashield magnet using deuterated solvents. FT-IR spectra were recorded on a Shimadzu IRAffinity spectrometer as thin films deposited by evaporation of CH_2Cl_2 solutions on KBr plates. EI/FAB mass spectra were obtained using a Kratos Concept 1S High Resolution E/B mass spectrometer. UV-Vis measurements were recorded on a Shimadzu 3600 UV-Vis-NIR spectrophotometer in CH_2Cl_2 solution using quartz cuvette cells. Elemental analyses were carried out by Canadian Microanalytical Services, LTD, Surrey, BC, Canada, or Guelph Chemical Laboratories LTD, Guelph, ON, Canada.

Electrochemical Measurements. Cyclic voltammetry (CV) experiments were performed with a Bioanalytical Systems Inc. Epsilon electrochemical workstation. Compounds were dissolved in anhydrous solvent (CH_3CN), filtered, and then deareated by sparging with N_2 gas for 20 minutes. Analyte concentrations were approximately 10^{-3} M containing 0.1 M supporting electrolyte (Bu_4NPF_6). A typical three-electrode set-up was used including a glassy carbon working electrode, Ag/AgCl reference electrode, and a platinum wire counter electrode. Ferrocene was used in all cases as an internal standard to calibrate the reference electrode and was

oxidized at a potential of +0.51 V in our set up. The scan rate for all CV experiments was 100 mV/s or as otherwise stated in the text.

Spectroelectrochemical Measurements. Spectroelectroelectrochemical experiments were performed in CH_2Cl_2 solution with 10^{-5} M of studied complexes concentration, containing approximately 0.1 M supporting electrolyte (Bu_4NPF_6) using a Bioanalytical Systems Inc. Epsilon electrochemical workstation. A special thin layer quartz glass cuvette containing the above solution in addition to a small platinum gauze working electrode, platinum wire counter electrode, and silver wire reference electrode was loaded into a Shimadzu UV-3600 and a constant potential of 1.0 V (versus ferrocene) was applied. UV-visible spectra were recorded in repeat mode (250 – 1000 nm), until subsequent runs no longer resulted in any significant spectral changes

Variable Temperature Magnetic Susceptibility Measurements and EPR Spectroscopy. Solid state variable temperature magnetic susceptibility measurements were recorded on a superconducting quantum interference device (SQUID) magnetometer (Quantum Design MPMS) with a 5.5 T magnet (temperature range 1.8 to 400 K) in an external field of 0.5 T. Samples were carefully weighed into gelatin capsules, which were loaded into plastic straws, and attached to the sample transport rod. The magnetization of the samples was scanned over a temperature range of 5 to 325 K and then back to 5 K. Diamagnetic corrections to the paramagnetic susceptibilities were accomplished using Pascal's constants. Solution magnetic moments were obtained using the Evans method. For example, in a typical experiment, 29.1 mg of complex **1.3** was dissolved in exactly 4.0 mL of dry acetonitrile. Under N_2, one equivalent of $NOPF_6$ dissolved in exactly 1.0 mL of

acetonitrile was added, resulting in a color change to dark green. The solution was stirred for approximately 10 min, and then a small portion was withdrawn by syringe under N_2 and loaded into a special narrow coaxial NMR tube assembly. This narrow tube was inserted into another NMR tube containing an approximately 1:1 mixture of CH_3CN and CD_3CN and ^1H NMR spectra were immediately recorded at a series of different temperatures. Mass susceptibility (χ_g) was calculated from Equation 21:

$$\chi_g = \frac{3\Delta\upsilon}{4\pi\upsilon c} \qquad \textbf{(21)}$$

Where $\Delta\nu$ is the difference in absorption frequency between CH_3CN in the outer and inner tubes, ν is the spectrometer frequency (600.32 MHz) and c is the concentration (g/mL) of the paramagnetic complex. Molar susceptibility was calculated in the typical manner and corrections for the diamagnetism of the complex and solvent were calculated using Pascal's constants. The temperature dependent density changes of the acetonitrile solvent were accounted for using published values and the required corrections were made to the paramagnetic solution concentrations. EPR spectra were recorded as toluene solutions at room temperature in quartz tubes on a Bruker Elexsys E580 pulsed and CW X-band (9 GHz) spectrometer.

Computational Details. All DFT calculations were performed using the Gaussian 03 package using the B3LYP hybrid functional and the TZVP basis set for all atoms.[122] Tight SCF convergence criteria were used for all calculations. The converged wave functions were tested to confirm that they correspond to the ground-state surface. The evaluation of atomic charges and spin densities was performed using the natural population analysis (NPA).[123] The analysis of molecular orbitals in terms of fragment orbital contributions were carried out using the AOMix program.[124]

Time-dependent DFT (TD-DFT) calculations at the B3LYP/TZVP level were performed to calculate the absorption spectra as previously described.[125]

1.5.2 Monometallic complexes.

X-ray Structure Determination. Crystals of suitable size were mounted on a glass fibre. Data were collected at room temperature (100 K) on a SMART APEX II diffractometer with MoKα radiation (λ = 0.71073 Å) located at the McMaster Analytical X-ray Diffraction Facility (MAX). Data were processed using APEX v2.2.0 and solved by direct methods (SHELXS-97). Data were refined using least-squares techniques on F2. The data were solved in the monoclinic space group P2, and checked by Platon AddSymm for additional symmetry. All non-hydrogen atoms were refined anisotropically except for those that were disordered. Hydrogen atoms were generated and treated as riding on their constituent atoms with updates after each cycle of refinement. A 2-fold twin law was applied, with a resultant BASF of 0.13(2). The disordered groups for molecule 1 (Cu1) include CF3 (F1, F2 and F3), rotationally disordered over two positions in a 75:25 ratio, and the F atoms were restrained with EADP. The other disordered portion of molecule 1 is the anisole ring starting with C18, with a ring shift and methyl ether disorder of 80:20. These atoms were also restrained with EADP and refined isotropically. Similarly, for molecule 2 there are two CF3 groups with rotational disorder: F13, F14 and F15 at a ratio of 56:44, and F22, F23 and F24, at 41:59 ratio. One of the anisole rings in this molecule was also disordered similar to that in molecule 1, at 45:55. All disordered atoms in molecule 2 were also refined isotropically. In the final stages of refinement, two peaks of residual electron density were located. The first was associated with O4 of the non-disordered ring of molecule 1, and the second with C113 of the non-disordered anisole of molecule 2. Attempts to refine these as atoms did not result in

reasonable results, and it is assumed that these peaks are possibly "shadows" from the heavy atoms in a second crystal.

formula	$C_{34}H_{23}CuF_{12}N_3O_6$
fw	861.09
dimensions (mm)	0.266 × 0.135 × 0.095
a (Å)	10.2632(16)
b (Å)	30.851(5)
c (Å)	11.4269(18)
cryst syst	Monoclinic
α (deg)	90
β (deg)	104.555(3)
γ (deg)	90
volume ($Å^3$)	3502.0(10)
space group	*Pc*
Z	4
μ (mm^{-1})	0.738
T (K)	100(2)
independent reflections	10497 (R_{int} = 0.0830)
number of parameters	964
R_1 [$F^2 > 2\sigma(F^2)$]	0.0848
wR_2 (F^2)[a]	0.2239

[a] $w = 1/[\sigma^2(F_o^2) + (0.069P)^2 + 0.2902P]$ where $P = (F_o^2 + 2F_c^2)/3$

Table 3: Crystallographic data for **1.5**.

5-(4,4′-dimethoxydiphenylamino)-2,2′-bipyridine (1.2).

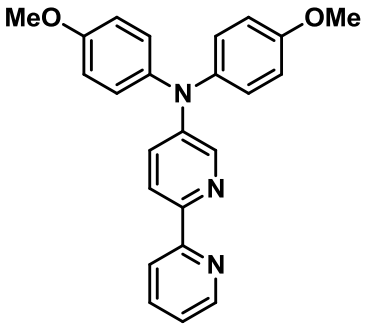

5-bromo-2,2′-bipyridine **1.1**, obtained by procedure[106] (0.104 g, 0.442 mmol), *N*,*N*′-(4,4′-dimethoxydiphenyl)amine (0.125 g, 0.546 mmol), Cs_2CO_3 (0.202 g, 0.620 mmol), palladium(II) acetate (0.0055 g, 0.0245 mmol), and BINAP (0.015 g, 0.024 mmol) were combined under N_2 into a dry Schlenk flask and slurried into dry toluene (20 mL). The solution was purged with N_2 for 20 min and then heated to 95°C. Total consumption of starting materials was noted after 35 h at which time the reaction was cooled to room temperature. The cooled reaction contents were filtered and the precipitate was washed with $CHCl_3$. The filtrate and washing were rotovaped down to a brown oil, which was chromatographed over neutral Al_2O_3 (12" × 1"), eluting with 9:1 hex/EtOAc, followed by 7:3 hex/EtOAc (R_f = 0.6) to collect the bright yellow zone. Pure fractions were combined and concentrated to a white solid, yield 130 mg (77%).

^{1}H NMR ($CDCl_3$): δ 8.63 (d, 1H, *J* = 4 Hz), 8.31 (d, 1H, *J* = 3 Hz), 8.28 (d, 1H, *J* = 8 Hz), 8.19 (d, 1H, *J* = 9 Hz), 7.76 (dd, 1H, *J* = 8, 2 Hz), 7.32 (dd, 1H, *J* = 9, 3 Hz), 7.23 (dd, 1H, *J* = 8, 2 Hz), 7.12 (d, 4H, *J* = 9 Hz), 6.89 (d, 4H, *J* = 9 Hz), 3.83 ppm (s, 6H). ^{13}C NMR ($CDCl_3$): δ 156.6, 156.0, 149.0, 147.4, 145.2, 140.9, 139.6, 136.7, 126.8, 126.3, 122.5, 121.0, 120.1, 115.0, 55.5 ppm. Anal. Calc'd for $C_{24}H_{21}N_3O_2$ (Found): C: 75.16 (74.82); H: 5.52 (5.61); N: 10.96 % (10.89%). MS

(EI +): *m*/*z* 383 (M^+, 100%), 368 (M-CH_3, 30%). FT-IR (film, KBr): 3045 (w), 3001 (w), 2930 (w), 2833 (w), 1568 (m), 1541 (s), 1458 (s), 1435 (w), 1327 (m), 1242 (s), 1165 (w), 1033 (m), 827 (m), 739 (m), 638 (w), 581 cm^{-1} (w). UV-vis (CH_2Cl_2): λ_{max} (ε): 352 nm (2.1×10^4 cm^{-1} M^{-1}).

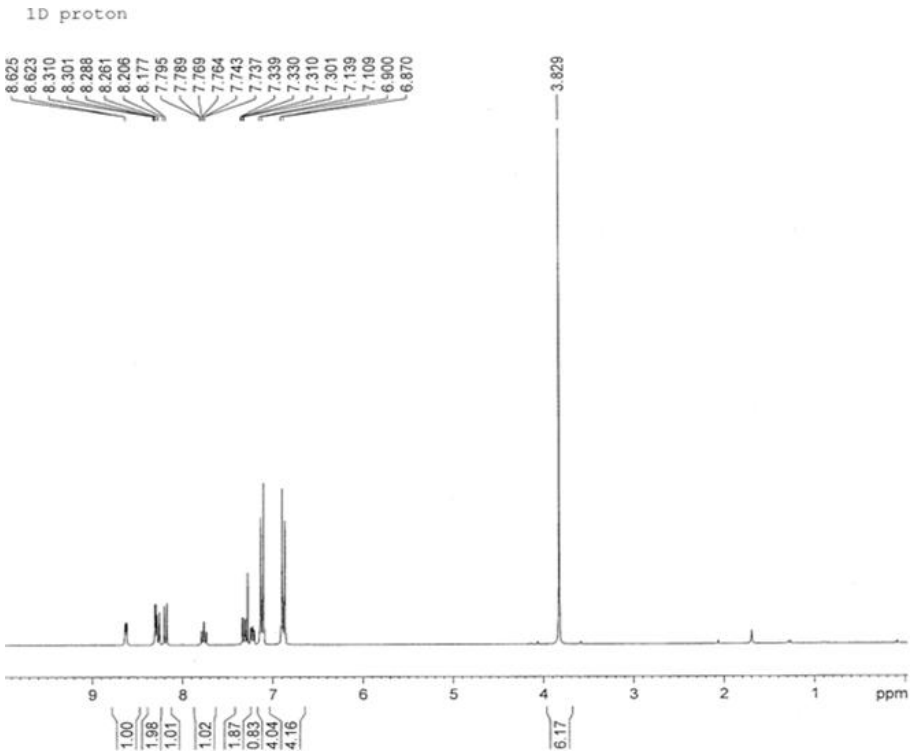

^{1}H NMR of ligand **1.2** ($CDCl_3$, 300 MHz).

Mn(hfac)$_2$(1.2) (1.3).

Mn(hfac)$_2$·3H_2O (0.22 g, 0.42 mmol) was dissolved in a solvent mixture containing hexanes (5 mL) and MeOH (2 mL) and combined with a CH_2Cl_2 solution (5 mL) of **1.2** (0.15 g, 0.39 mmol). The solution was stirred at room temperature for 1 hr to produce a clear, orange solution. The solution was filtered and let stand at room temperature. Over a period of days, orange, rod-shaped crystals were observed, which were isolated by vacuum filtration, yield 0.14 g, (41%).

Anal. Calcd for $C_{34}H_{23}N_3O_6F_{12}Mn$ (Found): C, 47.88 (48.05); H, 2.72 (2.43); N, 4.93 (4.98). MS (FAB +): 852 (M^+, 2), 645 (M-hfac, 50), 383 (**1**, 100%). FT-IR (film, KBr): 1651 (m), 1589 (w), 1557 (m), 1508 (s), 1470 (s), 1442 (m), 1344 (m), 1252 (s), 1196 (s), 1142 (s), 1082 (w), 1032 (w), 833 (w), 795 (m), 662 (m), 583 cm^{-1} (w). UV-vis (CH_2Cl_2): λ_{max} (ε): 385 nm (1.8×10^4 cm^{-1} M^{-1}).

Ni(hfac)$_2$(1.2) (1.4).

Ni(hfac)2×2H2O (0.13 g, 0.26 mmol) was slurried in 7 mL of hexanes and combined with a CH_2Cl_2 solution (4 mL) of **1.2** (0.10 g, 0.26 mmol). The solution was stirred at room temperature overnight to produce a clear, golden solution. The solution was concentrated to a crusty golden residue, which was dissolved into hot hexanes (12 mL). Upon cooling to room temperature, a green microcrystalline powder precipitated, which was isolated by vacuum filtration, yield 0.14 g (61%).

Anal. Calc'd for $C_{34}H_{23}N_3O_6F_{12}Ni$ (Found): C: 47.67 (47.86); H: 2.71 (2.78); N: 4.91 (4.95). MS (EI +): 648 (M-hfac, 10%), 383 (**1**, 100%). FT-IR (film, KBr): 1643 (m), 1590(w), 1556 (m), 1506 (s), 1471 (s), 1441 (m), 1346 (m), 1256 (s), 1202 (s), 1148 (s), 1097 (m), 1034 (m), 833 (w), 791 (m), 671 (m), 586 cm^{-1} (m). UV-vis (CH_2Cl_2):λ_{max} (ε): 383 nm (1.8×10^4 cm^{-1} M^{-1}).

Cu(hfac)$_2$(1.2) (1.5).

Cu(hfac)$_2$·×H_2O (0.068 g, 0.14 mmol) was slurried in 7 mL of 2:1 hexanes:CH_2Cl_2 and combined with a CH_2Cl_2 solution (2 mL) of **1.2** (0.055 g, 0.14 mmol). The solution was stirred at room temperature for 3 h to produce a clear red-brown solution. The solution was concentrated to dryness, producing a lime colored residue, which was dissolved into a minimum of hot methanol. The solution was left

open to the atmosphere and slow evaporation provided brown rod crystals, which were isolated by vacuum filtration, yield 0.060 g (51%).

Anal. Calc'd for $C_{34}H_{23}N_3O_6F_{12}Cu$ (Found): C: 47.40 (47.30); H: 2.69 (2.74); N: 4.88 (4.87). MS (FAB +): 653 (M-hfac, 100), 446 (M-2hfac, 30), 383 (**1**, 55%). FT-IR (film, KBr): 1653 (m), 1589(w), 1548 (m), 1508 (s), 1471 (s), 1442 (m), 1348 (w), 1254 (s), 1200 (s), 1144 (s), 1082 (m), 1031 (w), 833 (w), 791 (m), 665 (m), 586 cm^{-1} (w). UV-vis (CH_2Cl_2): λ_{max} (ε): 394 nm (1.6×10^4 cm^{-1} M^{-1}).

1.5.3 Experimental. Synthesis of bimetallic complexes.

5-bromo-2-pyridinecarboxaldehyde (2.1).

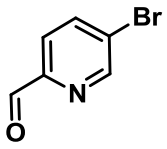

Following general procedure of Wang and co-workers[113], a solution of BuLi (2.5M in hexanes, 10.0 mL, 25.3 mmol) was slowly added to a solution of 2,5-dibromopyridine (5.0 g, 21 mmol) in dry toluene (250 mL) at -78^{o}C and the mixture was stirred for 5 h. Next, dry DMF (2.15 mL, 27.6 mmol) was added. After stirring for 1 h at -78^{o}C, the solution was warmed up to -10^{o}C and the reaction was quenched with saturated NH_4Cl aqueous solution. The organic phase was separated and the aqueous phase was washed twice with ethyl acetate. All organic fractions were collected, dried over $MgSO_4$ and the solvent was removed by rotary evaporation. Column chromatography (silica gel, hexane/ethyl acetate 15:1) produced pure **2.1** (1.8 g, 45%). All characterization is consistent with the literature values.

5-bromo-2-(1,3-dioxolan-2-yl)pyridine (2.2).

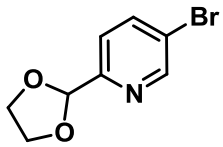

Ethylene glycol (2.0 ml, 36 mmol) and *p*-toluenesulfonic acid (400 mg, 2.30 mmol) were added to a solution of 5-bromo-2-pyridinealdehyde **2.1** (4.0 g, 22 mmol) in toluene (30 ml) and reaction mixture was refluxed with Dean-Stark apparatus for 2 days. After cooling to room temperature, the mixture was quenched with 10% Na_2CO_3 aqueous solution and extracted with ethyl acetate. Organic fractions were washed with water, brine, and then dried over $MgSO_4$. Solvent was removed by

rotary evaporation. The product was purified by column chromatography (silica gel, hexane/ethyl acetate 15:1) to produce 4.2 g (85%) of a pure brown oil.

^{1}H NMR (300 MHz, $CDCl_3$) δ 8.64 (d, 1H, *J* = 2.3 Hz), 7.83 (dd, 1H, *J* = 8.3 Hz, 2.3 Hz), 7.40 (d, 1H, *J* = 8.3 Hz), 5.78 (s, 1H), 4.07 ppm (m, 4H). (Consistent with literature data.)

5-iodo-2-(1,3-dioxolan-2-yl)pyridine (2.3).

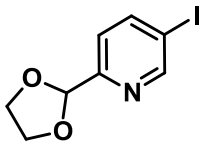

5-bromo-2-(1,3-dioxolan-2-yl)pyridine **2.2** (0.90 g, 3.9 mmol) and *N*,*N*'-dimethylethylenediamine (34 mg, 0.39 mmol) were added to a solution of copper (I) iodide (37 mg, 0.19 mmol) and sodium iodide (1.17 g, 7.8 mmol) in 10 ml 1,4-dioxane (prior to the reaction inorganic salts were recrystallized and dried in vacuo). The reaction mixture was refluxed for 3 days. After cooling to room temperature the reaction was diluted with 25% NH_4OH aqueous solution and extracted with $CHCl_3$. The organic fractions were washed with brine and dried over $MgSO_4$. Column chromatography (silica gel, hexane/ethyl acetate 15:1), which gave yellow-white shiny crystals (865 mg, 80%).

^{1}H NMR (300 MHz, $CDCl_3$): δ 8.81 (d, 1H, *J* = 1.9 Hz), 8.04 (dd, 1H, *J* = 7.9, 1.9 Hz), 7.32 (d, 1H, *J* = 8.*3* Hz), 5.79 (s, 1H), 4.10 ppm (m, 4H). ^{13}C NMR (75.5 MHz, $CDCl_3$): δ 156.0, 155.4, 145.1, 122.5, 103.1, 93.7, 65.6 ppm. HRMS, calculated for $C_8H_8NO_2I$: 276.9599, found: 276.95949. FT-IR (KBr): 3449 (w), 2965 (w), 2896 (m), 2875 (m), 2750 (w), 1840 (w), 1635 (w), 1572 (m), 1552 (w), 1468 (w), 1381 (s), 1364 (s), 1206 (m), 1129 (m), 1024 (m), 1004 (s), 975 (s), 943 (s), 862 (m), 825 (m), 753 (w), 717 (w), 668 (m), 624 cm^{-1} (m).

6-(1,3-dioxolan-2-yl)-N-(4-methoxyphenyl)pyridin-3-amine (2.4).

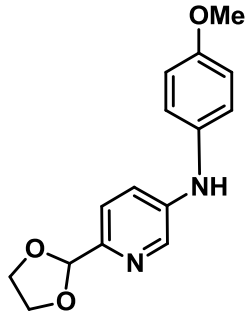

A Schlenk flask charged with 5-iodo-2-(1,3-dioxolan-2-yl)pyridine (72 mg, 0.26 mmol), *p*-anisidine (16 mg, 0.13 mmol), palladium (II) acetate (3 mg, 0.013 mmol), BINAP (16 mg, 0.026 mmol) and Cs_2CO_3 (170 mg, 0.52 mmol) was evacuated and back-filled with dinitrogen (3×). Next, dry toluene (2 ml) was syringed into the flask and the reaction was stirred at 50°C for 2 days. Conversion of starting material was monitored by TLC (product R_f = 0.36 eluent, EtOAc). After complete consumption of starting material was noted the reaction mixture was cooled to room temperature, filtered and the solvent was removed by rotary evaporation. The product was purified by column chromatography (hexane/EtOAc, 5:1) to produce a dark oil, 28 mg (40%).

^{1}H NMR (300 MHz, $CDCl_3$): δ 8.21 (d, 1H, J = 2.3 Hz), 7.33 (d, 1H, J = 8.7 Hz), 7.19 (dd, 1H, J = 8.3, 2.6 Hz), 7.06 (m, 2H), 6.86 (m, 2H), 5.77 (s, 1H), 5.65 (s, 1H), 4.10 (m, 4H), 3.79 ppm (s, 3H). ^{13}C NMR (150 MHz, $CDCl_3$): δ 156.1, 147.1, 142.1, 137.6, 134.0, 123.0, 121.2, 121.2, 114.8, 103.8, 65.4, 55.5 ppm. HRMS, calculated for $C_{15}H_{16}O_3N_2$: 272.11609, found: 272.11595. FT-IR (KBr): 3397 (w), 3267 (w), 2955 (w), 2890 (w), 2834 (w), 1593 (m), 1577 (m), 1511 (s), 1465 (w), 1440 (w), 1388 (w), 1330 (w), 1287 (w), 1244 (m), 1180 (w), 1132 (w), 1090 (m), 1032 (m), 987 (w), 943 (w), 829 (s), 751 (s), 518 cm^{-1} (s).

***N*-(6-(1,3-dioxolan-2-yl)pyridin-3-yl)-6-(1,3-dioxolan-2-yl)-N-(4-methoxyphenyl)pyridin-3-amine (2.5)**.

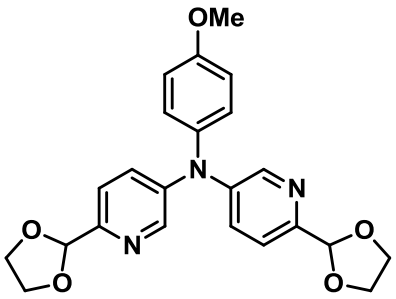

A Schlenk flask charged with 6-(1,3-dioxolan-2-yl)-N-(4-methoxyphenyl)pyridin-3-amine **2.4** (0.15 g, 0.55 mmol), 5-iodo-2-(1,3-dioxolan-2-yl)pyridine (0.15 g, 0.55 mmol), palladium (II) acetate (6.0 mg, 0.027 mmol), BINAP (34.3 mg, 0.055 mmol) and Cs_2CO_3 (0.36 g, 1.1 mmol) was evacuated and back-filled with dinitrogen (3×). Dry toluene (2 ml) was syringed into the flask and the reaction was stirred at 95^{o}C for 3 days. The reaction mixture was cooled to room temperature, filtered and the solvent was removed by rotary evaporation. Column chromatography (hexane/EtOAc, 5:1) produced **2.5** as a brown oil 123 mg (53%).

^{1}H NMR (300 MHz, $CDCl_3$): δ 8.31 (d, 2H, J = 0 Hz), 7.36 (m, 4H), 7.04 (d, 2H, J = 8.7 Hz), 6.86 (d, 2H, J = 8.7 Hz), 5.79 (s, 2H), 4.11 (m, 8H), 3.79 ppm (s, 3H). ^{13}C NMR (150 MHz, $CDCl_3$): δ 157.5, 143.8, 138, 135.3, 129.4, 127.6, 121.2, 120.9, 115.4, 103.3, 65.6, 55.5 ppm. HRMS, calculated for $C_{23}H_{23}O_5N_3$: 421.16377, found: 421.16402. FT-IR (KBr): 3423 (s), 3061 (w), 2965 (m), 2890 (m), 2362 (w), 2328 (w), 1762 (w), 1636 (m), 1585 (w), 1569 (w), 1531 (w), 1508 (s), 1437 (w), 1388 (m), 1315 (m), 1294 (m), 1246 (s), 1166 (w), 1135 (m), 1091 (s), 1026 (s), 943 (m), 898 (w), 875 (w), 829 (m), 750 (m), 722 (m), 700 (m), 642 (w), 524 cm^{-1} (m).

5,5'-(4-methoxyphenylazanediyl)dipicolinaldehyde (2.6).

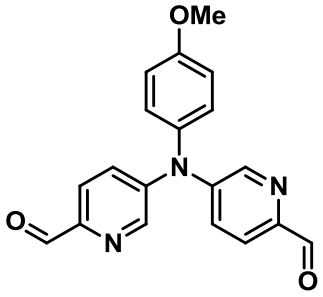

N-(6-(1,3-dioxolan-2-yl)pyridin-3-yl)-6-(1,3-dioxolan-2-yl)-N-(4-methoxyphenyl)pyridin-3-amine **2.5** (0.10 g, 0.24 mmol) was stirred with 5% HCl (3 ml) in THF (5ml) for 2 days. The reaction mixture was made basic with NaOH pellets and extracted into ethyl acetate. The organic layer was dried over $MgSO_4$ and the solvent was removed by rotary evaporation. A pure, yellow product was obtained by column chromatography (silica gel, hexane/EtOAc, 4:1), 68 mg (85%).

^{1}H NMR (300 MHz, $CDCl_3$): δ 9.96 (s, 2H), 8.49 (d, 2H, J = 2.3 Hz), 7.86 (d, 2H, J = 8.7 Hz), 7.47 (dd, 2H, J = 8.7, 2.3 Hz), 7.12 (m, 2H), 6.96 (m, 2H), 3.84 ppm (s, 3H). ^{13}C NMR (300 MHz, $CDCl_3$): δ 191.7, 159.1, 147.4, 146, 143.4, 136.2, 128.6, 128.2, 122.7, 116, 55.6 ppm. HRMS, calculated for $C_{19}H_{15}N_3O_3$: calculated 333.11134, found 333.11055. FT-IR (KBr): 3429 (w), 3045 (w), 3008 (w), 2929 (w), 2812 (w), 2709 (w), 2507 (w), 2359 (w), 2034 (w), 1702 (s), 1555 (s), 1480 (s), 1387 (w), 1319 (s), 1287 (s), 1247 (s), 1211 (s), 1030 (s), 819 (s), 736 (w), 669 (w), 617 (w), 547 cm^{-1} (w).

N-(4-methoxyphenyl)-6-((4-methoxyphenylimino)methyl)-N-(6-((Z)-(4-methoxyphenylimino)methyl)pyridin-3-yl)pyridin-3-amine (2.7)

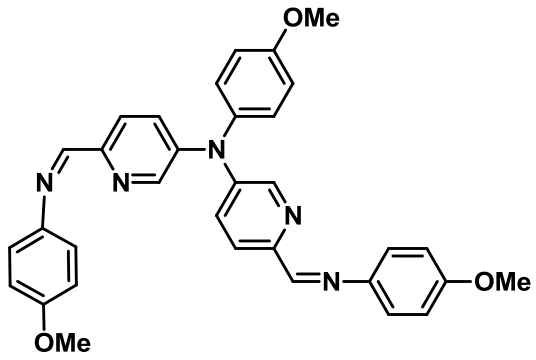

2.6 (0.20 g, 0.60 mmol) was stirred with 2 equivalents of *p*-anisidine (0.15 mg, 1.2 mmol) and dry $MgSO_4$ (0.15 g) in DCM (5 ml) for 2 days. The reaction mixture was then filtered and the solvent was removed by rotary evaporation. Crude purification was first carried out by column chromatography (silica gel, hexane/EtOAc, 5:1). Further purification of **2.7** was accomplished by dissolving the chromatographed product into isopropanol (2 mL) and precipitating it out with weak HCl solution. The product was filtered off, shaken with 10% NaOH solution and then extracted into ethyl acetate. The solvent was removed by rotary evaporation to produce a yellow powder, 280 mg (85%). This product is mildly susceptible to hydrolysis and was stored under an inert atmosphere in the refrigerator.

^{1}H NMR (300 MHz, $CDCl_3$): δ 8.56 (s, 2H), 8.42 (d, 2H, J = 2.6 Hz), 8.06 (d, 2H, J = 9.1 Hz), 7.45 (dd, 2H, J = 8.3, 2.6 Hz), 7.30 (m, 4H), 7.13 (d, 2H, J = 9.1 Hz), 8.93 (m, 6H), 3.84 (s, 3H), 3.83 ppm (s, 6H). ^{13}C NMR (150 MHz, $CDCl_3$): δ 158.7, 158.1, 157.4, 149.0, 144.1, 144.0, 143.4, 137.5, 128.8, 128.1, 122.6, 122.2, 115.6, 114.4, 55.5, 30.9 ppm. Anal. Calc'd for $C_{33}H_{29}O_3N_5$ (found): C, 72.93 (73.17); H, 5.34 (5.58); N, 12.89 (12.73%). HRMS, calculated for $C_{33}H_{29}O_3N_5$: 543.22704, found 543.22773. FT-IR (KBr): 3448 (w), 1618 (w), 1560 (w), 1506 (s), 1477 (m), 1319 (w), 1246 (m), 1260 (w), 1031 (w), 829 cm^{-1} (w).

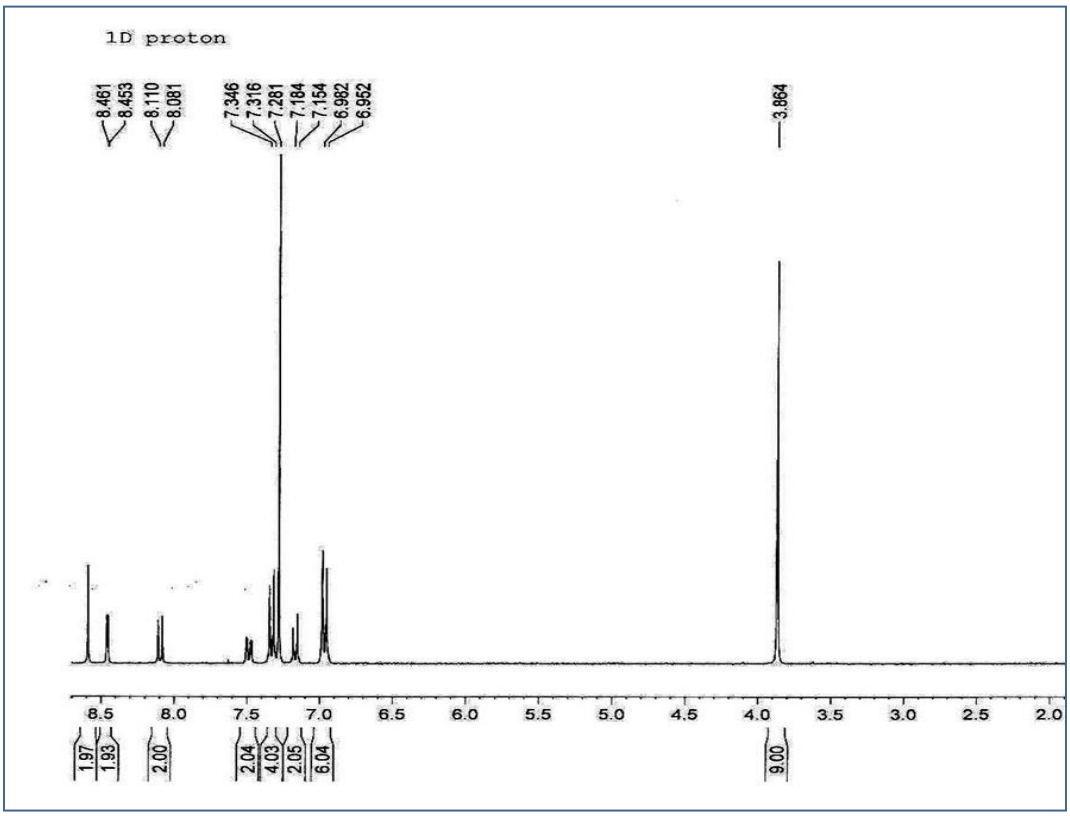

^{1}H NMR of ligand **2.7** ($CDCl_3$, 300 MHz).

[Mn(hfac)$_2$]$_2$(2.7) (2.8).

Mn(hfac)$_2$·3H$_2$O (96.3 mg, 0.184 mmol) was dissolved in a mixture of DCM (2 mL) and MeOH (~0.5 mL) and combined with a solution of **2.7** (50 mg, 0.092 mmol) in DCM (5 ml). The mixture was stirred for 2 days at room temperature. The solvent volume was reduced to 2 mL and after several hours, precipitation of bright brown-orange solid was observed. The product was collected by vacuum filtration, and dried. Yield, 68 mg (50%).

Anal. Calc'd for $C_{53}H_{33}N_5O_{11}F_{24}Mn_2$ (found): C, 42.94 (43.14); H, 2.25 (2.09); N, 4.73 (4.79). MS (FAB -): *m/z* 1481 (M^-, 0.3%), 262 [Mn(hfac), 2.5%], 207 (hfac, 100%). FT-IR (KBr): 3448 (s), 2364 (w), 1647 (m), 1617 (w), 1559 (w), 1500 (m), 1316 (w), 1256 (s), 1201 (m), 1146 (s),1096 (m), 1032 (m), 797 (w), 664 (w), 583 cm^{-1} (w).

[Ni(hfac)$_2$]$_2$(2.7) (2.9).

Ni(hfac)$_2$·H$_2$O (87 mg, 0.184 mmol) was dissolved in a mixture of hexanes (3 mL) and DCM (3 mL) and combined with a DCM solution of **2.7** (50 mg, 0.092 mmol). After stirring at room temperature for approximately 12 h the solvent volume was reduced to 2 ml and the reaction mixture was cooled on ice. An orange-brown precipitate was collected by vacuum filtration and dried. Yield 75 mg (55%).

Anal. Calc'd for $C_{53}H_{33}N_5O_{11}F_{24}Ni_2$ (found): C, 42.73 (42.73); H, 2.23 (1.98); N, 4.70 (4.72). MS (FAB -): *m/z* 1489 (M^-, 0.3%), 472 [Ni(hfac)$_2$, 26.3%], 207 (hfac, 100%). FT-IR (KBr): 3431 (s), 2921 (w), 2363 (w), 2339 (w), 1644 (m), 1617 (w), 1559 (w), 1507 (m), 1490 (w), 1424 (w), 1317 (w), 1256 (s), 1202 (m), 1149 (s), 1089 (m), 1059 (m), 1033 (m), 870 (w), 837 (w), 794 (w), 668 (w), 586 (w), 558 (w), 467 cm^{-1} (w).

[Cu(hfac)$_2$]$_2$(2.7) (2.10).

Cu(hfac)$_2$·H$_2$O (91.3 mg, 0.184 mmol) was dissolved in DCM (3 mL) and added to DCM solution of **2.7** (50 mg, 0.092 mmol). After stirring at room temperature for 12 h precipitation of a red-brown microcrystalline solid was noted, which was isolated by vacuum filtration and dried. Yield 80 mg (58%).

Anal. Calc'd for $C_{53}H_{33}N_5O_{11}F_{24}Cu_2$ (found): C, 42.45 (43.14); H, 2.22 (2.09); N, 4.67 (4.79). MS (FAB -): *m/z* 477 [Cu(hfac)$_2$, 62%], 207 (hfac, 100%). FT-IR (KBr): 3432 (m), 2364 (w), 1648 (m), 1617 (w), 1582 (w), 1546 (m), 1508 (s), 1425 (w), 1368 (w), 1305 (w), 1256 (s), 1202 (s), 1147 (s), 1084 (w), 1032 (w), 943 (w), 896 (w), 836 (w), 794 (w), 741 (w), 667 (w), 586 (w), 527 (w), 419 cm^{-1} (w).

Chemical oxidation of 2.7-2.10: 15 mg each of **2.7-2.10** were dissolved in 2 or 3 mL of dry, deoxygenated CH_3CN in a 25 mL round bottom flask. One equivalent of $NOPF_6$ solution (CH_3CN) was added by syringe to produce in all cases but complex **2.10**, a clear red solution. The solutions were stirred under a dinitrogen atmosphere for 10 minutes and then the solvent was removed *in vacuo* to produce solids that were immediately loaded into gel caps for squid magnetometry experiments.

1.5.4 Synthesis of dendrimer ligand for polimetallic complexes

Methyl-5-bromopicolinate (3.1).

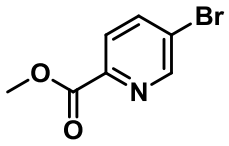

5-Bromopicolinic acid (4.8 g, 23.8 mmol) and 20 ml (0.5 mol) of absolute methanol were refluxed with 4 ml of concentrated sulfuric acid for 16 h. The reaction was then cooled in the ice bath and slowly neutralized with solid sodium carbonate. The extraction of reaction mixture with ethyl acetate gave 4.6 g of pure product (yield 90%). All characterization was consistent with literature values.[126]

(5-bromopyridin-2-yl)methanol (3.2).

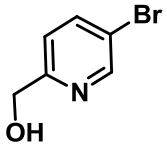

Sodium borohydride (1.46 g, 38.5 mmol) was slowly added to a solution of methyl-5-bromopicolinate **3.1** (3.5 g, 16.2 mmol) in 50 ml of degassed 7:3 mixture methanol:dichloromethane at 0^{o}C. After 1 h of stirring at 0^{o}C the reaction mixture was slowly warmed to room temperature and stirring was continued for 24 h. The reaction was quenched with 10 ml of saturated NH_4Cl solution, and then the solvent was evaporated *in vacuo*. The solid residue was shaken with dichloromethane and filtered. The evaporation of filtrate gave 2.5 g (13.3 mmol) of pure product. Yield: 82%. All characterization was consistent with literature values.[127]

5-bromopicolinaldehyde (2.1).

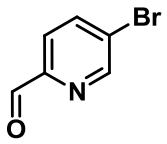

Manganese dioxide (3g, 0.346 mol) was added to a solution of 5-bromopyridin-2-yl)methanol **3.2** (3.25 g, 17.3 mmol) in degassed dichloromethane and stirred under inert atmosphere at room temperature for 3 days. The reaction mixture was filtered through celite filter plug. Evaporation of solvent *in vacuo* gave 2.5 g (13.44 mmol) of product. No further purification was required. Yield: 78%. All characterization was consistent with the literature values.[128, 129]

5-bromo-2-(1, 3-dioxolan-2-yl)pyridine (2.2). See experimental for bimetallic project, p. 103.

5-iodo-2-(1, 3-dioxolan-2-yl)pyridine (2.3). See experimental for bimetallic project, p. 104.

6-(1, 3-dioxolan-2-yl)pyridin-3-amine (3.3).

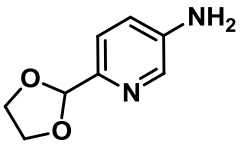

5-iodo-2-(1,3-dioxolan-2-yl)pyridine **2.3** (0.6 g, 2.16 mmol), Cu_2O (17 mg0.12 mmol), K_2CO_3 (420 mg, 3 mmol) and N,N'-dimethylethylenediamine (18 mg, 0.2 mmol) were mixed with 3 ml of ethylene glycol in a sealed vial and reaction mixture was purged with nitrogen gas. Then ammonium hydroxide (3 ml) was added under the nitrogen gas stream and vial was tightly sealed. The reaction was stirred under 60^{o}C for 16 h and then quenched with water and solid NaOH. The quenched

solution was further extracted with diethyl ether and ethyl acetate. The product was purified by column chromatography (silica gel, start with EtOAc:Hexanes 1:2, then EtOAc) to produce yellow oil (175 mg, yield 50%) which crystallized under vacuum. All characterization was consistent with the literature values.[130]

Bis(6-(1,3-dioxolan-2-yl)pyridin-3-yl)amine (3.4).

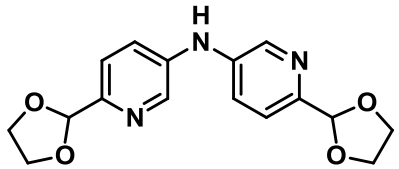

A Schlenk flask charged with 5-iodo-2-(1,3-dioxolan-2-yl)pyridine **2.3** (166.9 mg, 0.6 mmol), 6-(1 ,3-dioxolan-2-yl)pyridin-3-amine **3.3** (100 mg,0.6 mmol), palladium acetate (6.7 mg, 0.03 mmol), BINAP (18.7 mg, 0.03 mmol) and cesium carbonate (391 mg, 1.2 mmol) was evacuated and backfilled with dinitrogen (3 times). Dry toluene was syringed into the flask and reaction was stirred at 100^{o}C for 2 days. The reaction mixture was concentrated in vacuo and the product was purified by column chromatography (methanol:dichloromethane 1:30). Yield: 50 mg (27%).

^{1}H NMR (300 MHz, $CDCl_3$) δ 8.37 (m, 2H), 7.43 (m, 4H), 6.02 (s, 1H), 5.80 (s, 2H), 4.11 (m, 8H). ^{13}C NMR (300 MHz, $CDCl_3$): δ 149.9, 139.9, 138.8, 124.4, 121.3, 103.5, 65.5. HRMS, calculated for $C_{16}H_{17}N_3O_4$: 315.1219, found: 315.12242.

1-iodo-3-nitrobenzene (3.5).

The general procedure of Sandmeyer reaction used by Hodgson and Walker in 1933 [120] was followed with some changes. A solution of 3-nitroaniline (1g, 7.25 mmol) in hot glacial acetic acid (12 ml) was rapidly cooled to room temperature and

gradually stirred into a solution of sodium nitrite (7.98 mmol, 550 mg) in concentrated sulfuric acid (3.5 ml). The mixture was cooled on the ice bath and added to a saturated solution of potassium iodide (2g). The reaction mixture was stirred at 0^{o}C for one hour and then slowly warmed up and left stirred overnight at room temperature. Reaction was slowly quenched with saturated aqueous solution of sodium sulfite and product was extracted with ethyl acetate (3×100 ml). Organic fractions were dried over $MgSO_4$ and solvent was removed in vacuo. No further purification was required. Yield: 1.3 g (70%). All characterization was consistent with the literature values.[131, 132]

Tris(3-nitrophenyl)amine (3.6).

The procedure described in [133] was used with minor changes. A Schlenk flask charged with 3-nitroaniline (41 mg, 0.3 mmol), 1-iodo-3-nitrobenzene, copper powder (51.6 mg, 0.8 mmol) and 18-crown-6 (8 mg, 0.03 mmol) was evacuated 3 times and backfilled with dinitrogen gas. Toluene (2 ml) was syringed into the flask and the reaction was refluxed for 20 h. The reaction mixture was cooled to room temperature. Solid components were filtered off, the filtrate was evaporated. Column chromatography (silica gel. 1:10 EtOAc : Hexanes) gave pure product with 45 % yield (60 mg). All characterization was consistent with the literature values.[133]

Tris(3-aminophenyl)amine (3.7).

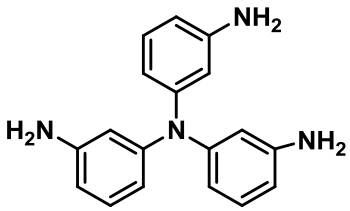

A mixture of tris(3-nitrophenyl)amine **3.6** (160 mg, 0.42 mmol), tin mossy (400 mg, 3.4 mmol) and 2 ml HCl was refluxed in ethanol for 2 h. After cooling down to room temperature the reaction mixture was neutralized with sodium hydroxide and concentrated in vacuo. The residue was extracted with ethyl acetate (3 × 100 ml). Organic fractions were dried over $MgSO_4$ and evaporated. Yield: 82% (100 mg).

^{1}H NMR (300 MHz, $CDCl_3$): δ 6.99 (m, 3H), 6.47 (d, 3H, J = 6.8 Hz), 6.40 (s, 3H), 6.31 (d, 3H, J = 7.5 Hz), 3.48 (s, 6H) HRMS, calculated for $C_{18}H_{18}N_4$: 290.1531, found: 290.15336. All characterization is consistent with the literature values.[133]

Tris(3-iodophenyl)amine (3.8).

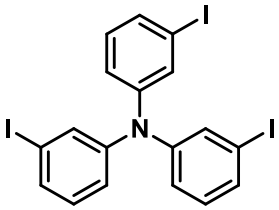

100 mg (0.35 mmol) of tris(3-aminophenyl)amine **3.7** was dissolved in 2 ml of 25% H_2SO_4 acid and stirred into a solution of sodium nitrite (79 mg (1.14 mmol) in 2 ml H_2O. The mixture was stirred for 30 min and added to the solution of 1 g KI in 2 ml H_2O on ice. The reaction was stirred at 0^{o}C for 2 h, 83 mg (1.38 mmol) of

carbamide was added and after quick stirring the mixture was poured into ice cold solution of potassium iodide. The reaction was warmed up to room temperature and stirred for 5 h. Then the suspension was cooled to 4^{o}C and dark precipitate was filtered off, washed with water, dried and then refluxed in THF with charcoal. Yield: 50% (217 mg).

^{1}H NMR (600 MHz, $CDCl_3$): δ 7.38 (m, 4H), 7.35 (m, 4H), 6.99 (m, 4H), 6.97 (m, 4H). ^{13}C NMR (600 MHz, $CDCl_3$): δ 148.0, 132.9, 132.7, 130.9, 123.5, 94.7. HRMS, calculated for $C_{18}H_{12}NI_3$: 622.8104, found: 622.81075. FT-IR (KBr): 3963 (w), 3426 (s), 2973 (w), 2924 (w), 2104 (w), 1636 (w), 1574 (s), 1466 (s), 1425 (w), 1309 (w), 1282 (w), 1258 (w), 1164 (w), 1089 (m), 1050 (m), 991 (w), 948 (w), 877 (w), 805 (w), 771 (w), 696 (m), 436 (w).

N1,N1-bis(6-(1,3-dioxolan-2-yl)pyridin-3-yl)-N3,N3-bis(3-(bis(6-(1,3-dioxolan-2-yl)pyridin-3-yl)amino)phenyl)benzene-1,3-diamine (**3.9**).

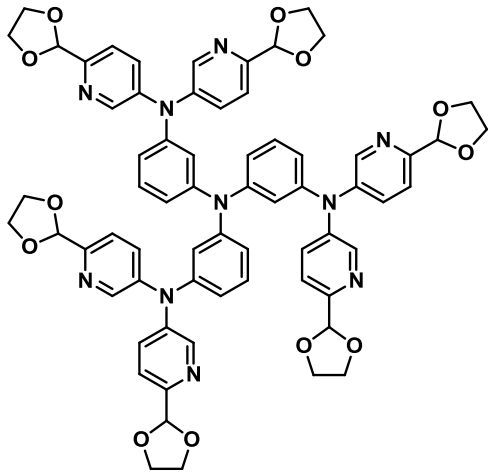

The Schlenk flask charged with 5-iodo-2-(1,3-dioxolan-2-yl)pyridine **(2.3)** (222 mg (0.8 mmol), tris(3-aminophenyl)amine (**3.7**) (21 mg, 0.072 mmol), K_2CO_3 (420 mg, 3 mmol), 18-crown-6 (78 mg, 0.3 mmol) and copper catalyst powder (60 mg, 0.94 mmol) was evacuated and backfilled with dinitrogen gas (3 times), then dry toluene was syringed in. The reaction was stirred under nitrogen at 90^{o}C for 7 days. Formation of desired product was monitored by TLC. After 7 days the reaction was cooled to room temperature. Solid components were filtered off and washed with ethyl acetate. Combined organic fractions were concentrated *in vacuo* and pure product was obtained by flush chromatography (silica gel plug, unreacted chemicals and byproducts were eluted with ethyl acetate/hexane 1:1, then 12 was washed from the column with ethyl acetate/methanol 1/1 solvent system). Evaporation of final solvent fractions gave 22 mg of **3.9**. Yield: 23.8%.

^{1}H NMR(600 MHz, $CDCl_3$): δ: 8.29 (m, 6H), 7.39 (m, 6H), 7.35 (m, 6H), 7.12 (t, J = 7.9 Hz, 3H), 6.74 (m, 6H), 6.63 (m, 3H), 5.75 (s, 6H), 4.09 (m, 24H) ppm. ^{13}C NMR (600 MHz, $CDCl_3$): δ: 151.1, 148.12, 146.56, 144.52, 143.32, 130.83,

130.72, 121.32, 120.29, 119.84, 119.45, 103.31, 65.51 ppm. FT-IR (KBr): 3423 (m), 2894 (m), 2827 (w), 1970 (w), 1637 (w), 1585 (m), 1481 (m), 1386 (w), 1351 (m), 1286 (m), 1251 (m), 1105 (s), 1024 (w), 962 (s), 896 (w), 838 (m), 702 (w), 530 (w).

MALDI Spectrum: protonated peak 1185, sodiated peak 1207 (calculated molar mass 1184)

5,5',5'',5''',5'''',5'''''-(3,3',3''-nitrilotris(benzene-3,1-diyl)tris(azanetriyl))hexapicolinaldehyde (**3.10**).

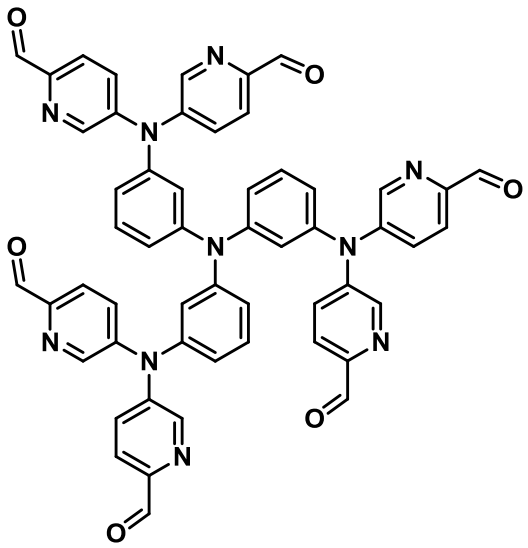

20 mg (0.017 mmol) of **3.9** were stirred in degassed dichloromethane with 1 ml of 42% aqueous solution of H_3PO_4 under inert atmosphere for 2 days. Then solvent was removed in vacuo, the mixture was basified with NaOH and extracted with EtOAc (3×100). Evaporation of solvent gave pure product. Yield: 51% (8 mg).

^{1}H NMR(600 MHz, $CDCl_3$): δ: 9.86 (s, 6H), 8.38 (m, 6H), 7.84 (d, J = 8.3 Hz, 6H), 7.50 (m, 6H), 7.30 (t, J = 7.9 Hz, 3H), 6.95 (m, 6H), 6.80 (m, 3H).

^{13}C NMR (600 MHz, $CDCl_3$): δ :191.34, 148.27, 147.87, 145.46, 145.20, 144.02, 131.91, 128.95, 122.68, 122.37, 121.76, 121.46. FT-IR (KBr) : 2341 (w), 1768 (w), 1704 (s), 1559 (s), 1481 (s), 1317 (m), 1289 (m), 1215 (s), 1160 (w), 1122 (m), 1015 (w), 947 (w), 917 (w), 823 (w), 736 (w), 671 (w), 618 (w), 598 (w), 421 (w).

Copper catalyst preparation method is based on the technique described by Piccard and Larssen [121] with some changes. Chromium (III) chloride hexahydrate (15g, 0.056 mol) was dissolved in the mixture of 60 ml H_2O and 20 ml conc. H_2SO_4 under inert atmosphere. Then excess of zinc pellets (10 g, 0,15 mol) was added into reaction in portions followed by 30 ml HCl. Reaction was stirred for 1 h. Intense bubbling and heating was observed, solution gradually changed color from dark green to bright blue which indicated formation of chromium 2+ ions. When most of zinc was dissolved and the blue color was deep and stable, the reaction was filtered under inert atmosphere through the filtration column with frit glass to remove non-dissolved zinc. Any contact with air causes undesirable oxidation of Cr^{+2} into Cr^{+3} (may be observed by color change) which is crucial for copper reduction process and affects yield very negatively. Clear blue filtrate was cooled on ice bath and cold degassed aqueous solution of $CuSO_4 \times 5H_2O$ was syringed dropwise into the flask while stirring. The precipitation of bright red very fine copper powder occurred immediately. The copper precipitate was quickly filtered, washed with water and ethanol and dried *in vacuo*. It was stored under inert atmosphere in a glove box to prevent particle aggregation and oxidation. Yield: 25.6% (1.28 g).

2 Base-catalyzed hydrosilylation

This work was conducted under the supervision of Prof. G. Nikonov at Brock University and published in *Chemistry - a European Journal* (just accepted, DOI:10.1002/chem.201302728)

2.1 Introduction

Transition metal-catalyzed hydrosilylation is a well-known approach for reduction of aldehydes, ketones, esters, carboxylic acids, amides, alkenes, alkynes. The range of metals used in this reaction is wide and includes titanium,[134] copper,[135] iron,[136,137,138] platinum,[139] indium,[140] iridium,[141] ruthenium,[142] rhenium,[143] to name just a few. The use of transition metals has certain advantages, such as unique chemo-, regio- and stereoselectivity, but is compromised by the high cost and toxicity of the usually used catalysts. At the same time, industrial demand of an efficient but nontoxic, environment-friendly and low-cost catalyst is still very high. In this context, the development of metal-free hydrosilylation is an appealing alternative but reports on organo-catalytic version of this reaction are scarce. The goal of this project was to explore transition metal-free reductive hydrosilylation and develop a green, safe and inexpensive reduction method.

2.2 Historical

2.2.1 Hydrosilylation catalysts based on main group elements.

Since metal-catalyzed hydrosilylation has been developed for a very wide range of metals, ligands and substrates and occurs by mechanisms which are substantially different from the one found in this study, this historical part does not have its goal to review the metal catalysis. Instead, the non-metal induced hydrosilylation will be discussed.

2.2.1.1 Borane catalysts.

The story of borane-catalyzed hydrosilylation started in 1970-s. In 1976 Doyle *et al.* reported reduction of aromatic aldehydes and ketones into alcohols and ethers as well as reduction of cyclic aliphatic ketones into hydrocarbons with boron trifluoride etherate as a Lewis acid and triethylsilane as the reductant.[144] It was postulated that the reaction proceeded via complexation of the Lewis acid to the carbonyl oxygen followed by hydride transfer from the silane. The silicon co-product was the fluorosilane formed upon fluoride abstraction from the borane adduct by the silylium cation formed in situ. Related reduction of alcohols into alkanes with BF_3 and Et_3SiH was reported the same year by Fry *et al.*[145] The latter group also independently studied the reduction of aldehydes and ketones with triethylsilane and gaseous boron trifluoride.[146] Although harsh conditions were avoided, the reaction set up cannot be considered as practical due to complications caused by the gaseous nature of boron trifluoride.

A very interesting study, with reliable yields, on the reduction of activated arenes, ketones, carboxylic acids, and heterocycles with boron trifluoride hydrate and triethyl silane was published in 1979 by Larsen and Chang.[147] Selected results from

this work are presented in **Table 4**. Later, a similar $BF_3 \cdot 2CF_3CH_2OH$ complex was used in analogous reduction of various ketones and aromatics.[148]

Entry	Substrate	Product	Isolated yield, %
1	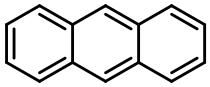	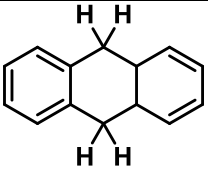	89
2	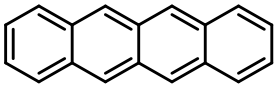	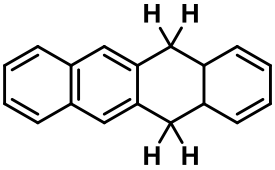	88
3	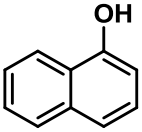	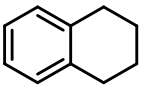	52
4	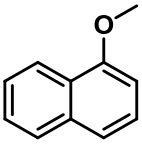	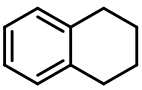	37
5	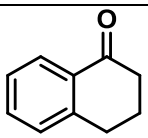	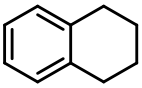	67
6	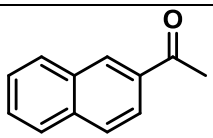	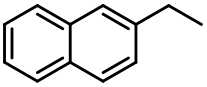	70
7	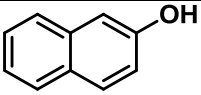	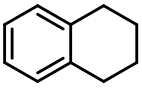	37
8	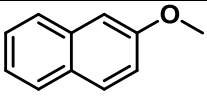	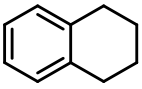	26

9	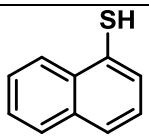	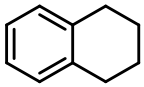	13
10	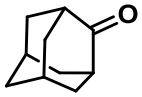		78

Table 4: Hydrosilylation catalyzed by $BF_3 \cdot H_2O$ at 25 ^oC.[147]

The interest in borane catalysis renewed two decades later when Piers et al. showed in 1996 that the highly electrophilic borane $B(C_6F_5)_3$ can be an active catalyst in the hydrosilylation of aromatic aldehydes, ketones and esters under mild reaction conditions (room temperature, 1-4 mol % of catalyst, 1 equivalent of $PhSiH_3$).[149] It is interesting to note that the borane $B(C_6F_5)_3$ had been prepared already in 1963,[150] but its chemistry remained almost dormant until mid-90s. Although initial mechanistic data were consistent with the conventional mechanism of carbonyl activation by the Lewis acid (pathway A in **Scheme 9**), the rate law obtained was consistent with the pathway B (**Scheme 9**). In the latter novel mechanism the borane activates the silane by means of formation of a three centre-two electron Si-H-B bond followed by a reaction with the carbonyl substrate. The free borane was generated in the mixture by reversible dissociation of the borane-substrate adduct. And therefore, less basic substrates showed increased activity as they maintained higher concentration of the active catalyst (free borane) in the solution.

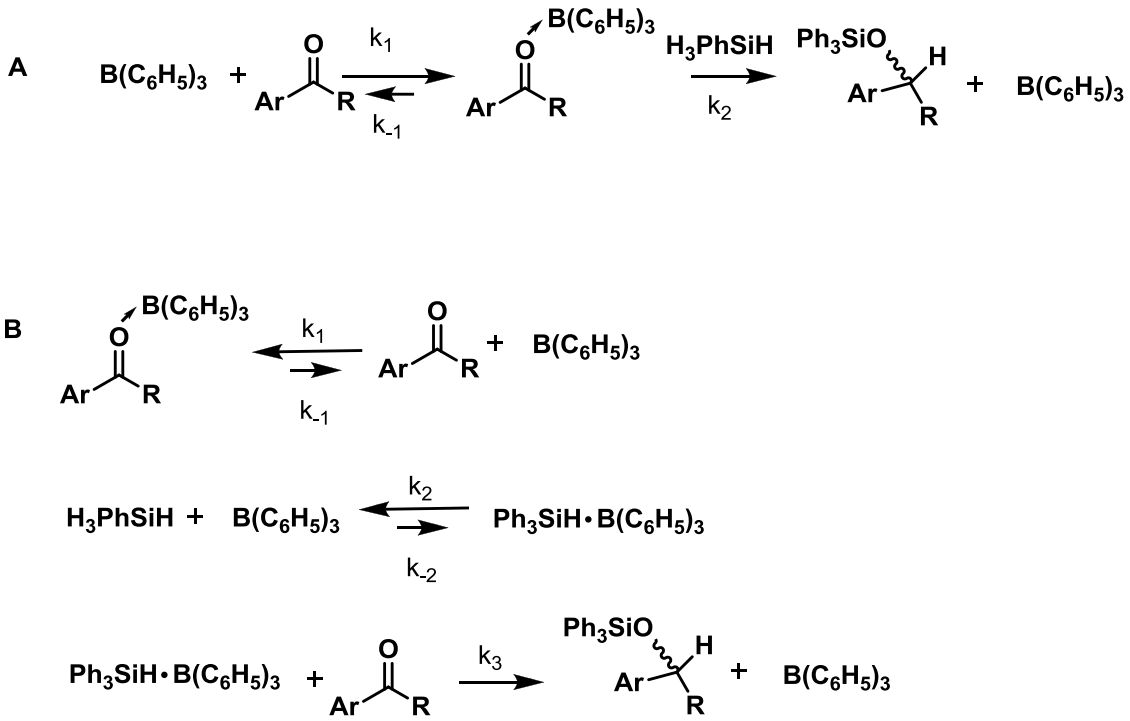

Scheme 9: Possible mechanistic pathways in borane-catalysed hydrosilylation. [149]

This mechanism was further elaborated in subsequent mechanistic studies[151] and the field has been recently reviewed by Piers *et al.*[152] The original suggestion of borane dissociation from an adduct with carbonyl and activation of silane was extended to the statement that a cationic silicon species, a silylium ion, forms which then coordinates to the most basic site of the substrate and thereby activates it. The borate $[HB(C_6F_5)_3]^-$ formed upon hydride abstraction from the silane works as a reducing agent by transferring the hydride to the silylated substrate. Although a borane-silane adduct could not be detected directly by NMR because its concentration was very small, its presence was deduced from the observation of $B(C_6F_5)_3$ -catalyzed H/D exchange between Et_3SiH and Ph_3SiD, broadening of Si-H resonance upon addition of borane, and the fact that "Piers' borane" $HB(C_6F_5)_2$ was produced in the reaction between $B(C_6F_5)_3$ and Et_3SiH.[152-153] In the latter process the intermediate

$[Et_3Si]^+[HB(C_6F_5)_3]^-$ was postulated. DFT calculations on the adduct between $B(C_6F_5)_3$ and Et_3SiH showed that its electronic energy is lower than that for reactants.[152, 154]

The stereochemical aspects of borane-catalyzed hydrosilylation were elaborated in an elegant study by the Oestreich group. In particular, Oestreich et al. prepared a series of chiral silanes, whose application allowed them to propose an S_N2 type mechanism for $B(C_6F_5)_3$-catalyzed hydrosilylation.[152, 155] The main characteristics of this mechanism are the inversion of configuration of the silane stereoprobe at the second step upon transfer of the silylium ion from the silane-borane adduct to carbonyl substrate and the retention of this configuration in the product formed upon addition of DIBAL-H (**Scheme 10**).

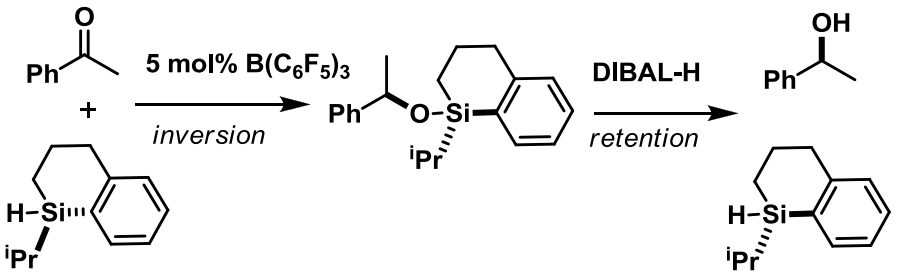

Scheme 10: A two-step inversion/retention pathway according to Oestreich *et al*.[155b]

The same year, Kawakami *et al.* reported similar observations for the $B(C_6F_5)_3$-catalyzed silylation of alcohols, silanols and methoxysilanes with optically active methyl(1-naphthyl)phenylsilane.[156]

The perfluoroarylborane-catalyzed hydrosilylation was extended from carbonyls to imines. In 2000 Piers *et al.* reported reduction of a series of

benzaldimines. Analysis of intermediates allowed them to propose a reaction mechanism similar to that one for the reduction of carbonyls (**Scheme 11**).[157]

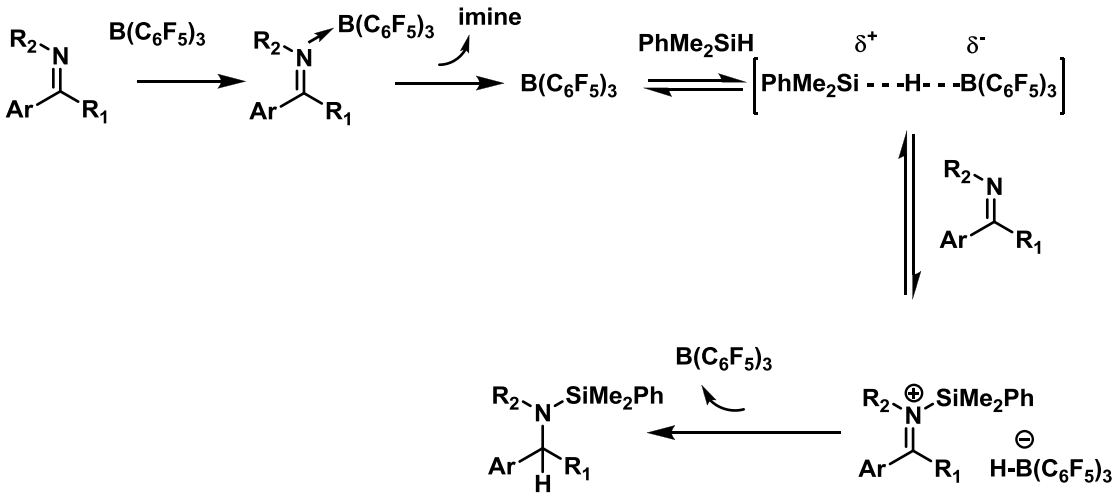

Scheme 11: Proposed mechanism for the hydrosilylation of imines.[157]

An example of $B(C_6F_5)_3$-catalyzed reduction of imines with ferrocene-stabilized silylium ions has been reported recently.[158] A study of stereochemical effects in the $B(C_6F_5)_3$-catalyzed hydrosilylation of ketones caused by presence of an alkynyl group was published in 2002 by Yamamoto.[159] It was shown that syn-selectivity in the reduction of β-alkynyl ketones is supported by σ–π-chelation of R_3Si^+ in which the carbonyl lone pair (σ) and π-electrons of C≡C bond coordinate to the silylium ion.

Despite the apparent similarity between the reduction mechanisms for carbonyls and imines developed by Piers *et al.*, first efforts to observe an analogous stereogenity pattern for imines by using enantiomerically pure silanes failed.[160] In 2012 Klankermayer et al. succeeded in enantioselective hydrosilylation of carbonyls and imines by using chiral Frustrated Lewis Pairs (**Figure 91**), synthesized by the reaction of Piers' borane with a chiral alkene.[161] While the obtained borane itself

(**Figure 91**, left) gives a racemic amine product in imine reduction, in combination with Lewis basic phosphines (**Figure 91**, center and right) it forms a catalyst, which directs the reaction towards higher enantioselectivity. A similar reduction pattern was observed in the reduction of acetophenone, although only a moderate enantioselectivity was achieved.[161]

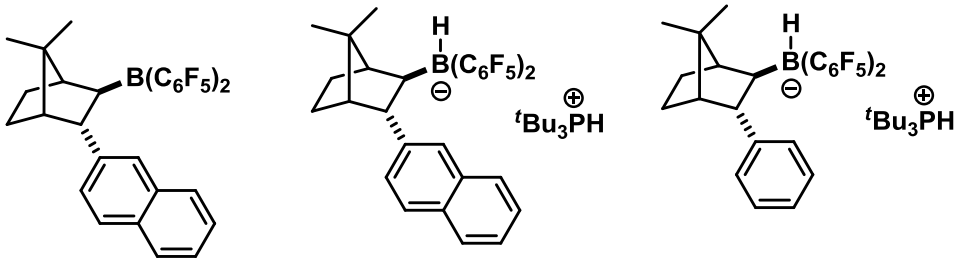

Figure 91: Chiral borane (left) and phosphonium hydridoboranes (center, right).[161]

A recent study by Oestreich et al. with an axially chiral borane and silane shown in Figure 88 finally put the end to speculations on the mechanism of borane-catalyzed hydrosilylation of imines. It was concluded that the S_N2- mechanisms for carbonyl and imine reduction are indeed essentially identical.[162] It is interesting, though, that while the axially chiral borane (**Figure 92**, a) activates the Si-H bond, it does not provide an asymmetric induction in carbonyl hydrosilylation[163]. This borane showed promising enantioselectivity results towards imine reduction but, unlike the Klankermayer's case,[161] no phosphines were required. It was observed that imine substrates with electron-donating substituents on the nitrogen tend to react slower, presumably because of formation of a more stable imine-borane adduct. At the same time, imines with bulkier groups on nitrogen are reduced faster. These two observations allow for the conclusion that the mechanism should follow the Si-H activation pathway rather than Lewis acid activation.[162]

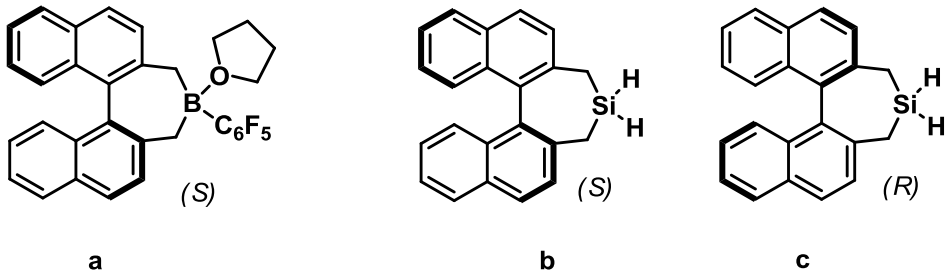

Figure 92: Axially chiral borane (a) and silanes (b, c) as stereochemical probes. [162]

From the practical application point of view, the scope of substrates and products in borane-catalyzed hydrosilylation is very wide. Hydrolysis of hydrosilylation products in the reduction of aldehydes and ketones[149, 151] allows for the preparation of alcohols. Reduction of imines, mentioned above, gives amino products.[157, 160, 162] Boron catalysed hydrosilylation of olefins, alkynes and allenes was reported by Gevorgyan *et al.*[164]

A recent work of Dussault and co-workers published in 2010 presented the $B(C_6F_5)_3$-promoted tandem OH silylation and intramolecular alkene hydrosilylation of enols, which resulted in their diastereoselective reduction into alcohols.[165]

Reduction of alcohols to alkanes and cleavage of ethers was first described by Gevorgyan et al. in 1999,[164b] and later was extended to the reduction of acyl chlorides, esters, aliphatic aldehydes and carboxylic acids into methyl groups.[166] Reduction of secondary and tertiary alcohols into their corresponding alkanes was also achieved.[167] Very recently, Brookhart *et al.* reported $B(C_6F_5)_3$–catalyzed hydrosilylative reduction of carboxylic acids into aldehydes.[168] Hydrosilylative reduction of α-diketones to silyl-protected 1,2-diols[169] was achieved by the Rosenberg group. These workers also reported the synthesis of polysilanes containing thiolato side chains by $B(C_6F_5)_3$-catalyzed hydrosilylation.[170]

Borane-catalyzed hydrosilylation was successfully applied in solving such a challenging problem as reduction of carbon dioxide. Piers *et al.* demonstrated FLP-catalyzed deoxygenative hydrosilylation of CO_2, which allows for a step-wise transformation of CO_2 into CH_4 (**Scheme 12**).[171]

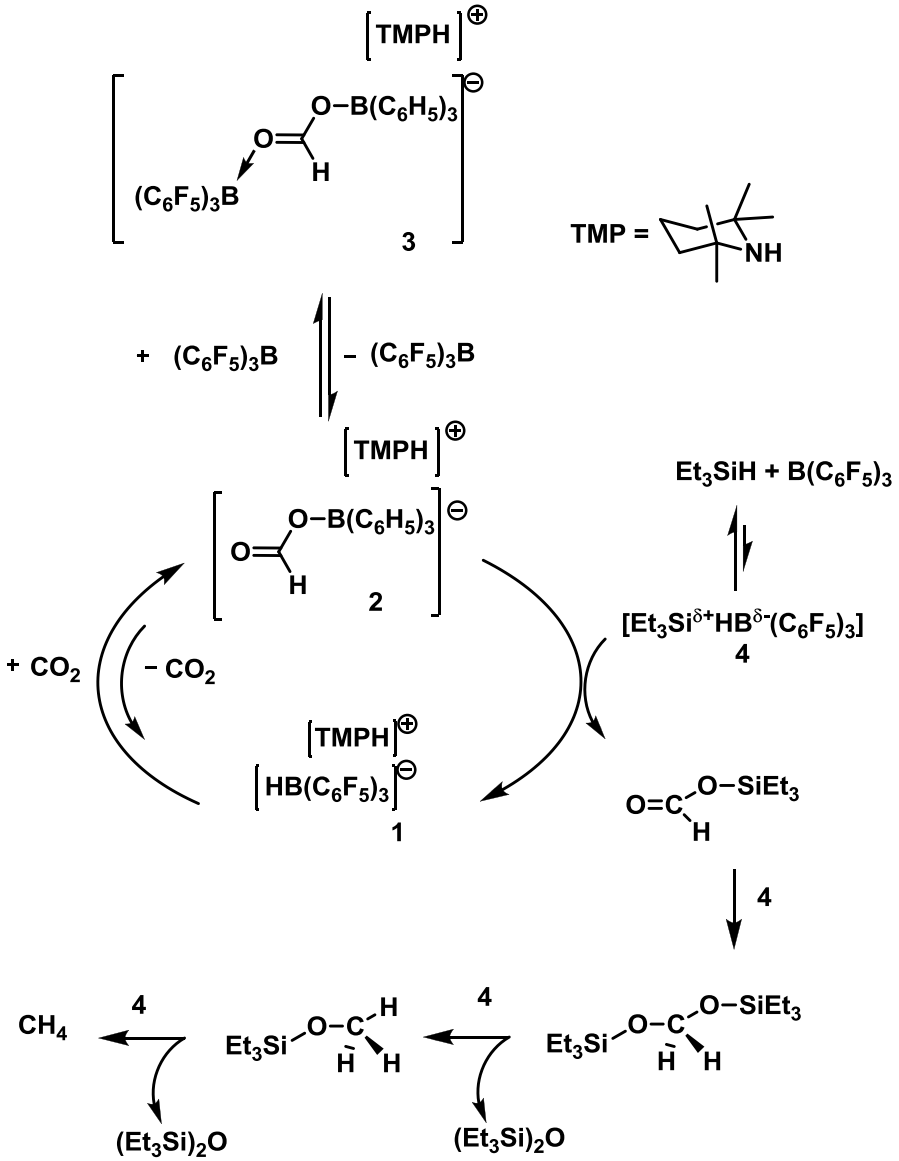

Scheme 12: Transformation of CO_2 into CH_4. Adapted from reference [171a].

A recent study of fluoroarylboranes showed that out of three species, B(*o*-$HC_6F_4)_3$, B(*p*-$HC_6F_4)_3$, and B($C_6F_5)_3$, it is B($C_6F_5)_3$ that has the strongest Lewis acidity.[172]

While being very stable reactants and excellent hydrosilylation catalysts, perfuoroboranes do have some drawbacks, the most serious being their high cost and practical difficulties in handling. Perfuoroboranes are highly hydrophilic and their high Lewis acidity transforms into strong Brønsted acidity when a borane contacts water, which may be a crucial factor for catalyzed reaction.[152, 173]

2.2.1.2 Aluminum catalysts.

After the earlier work on Lewis acid catalysed hydrosilylation of allenes[174] and alkynes[174-175] with $AlCl_3$, the research on aluminum catalysed hydrosilylation has been surprisingly scarce. Only one example of hydrosilylation catalyzed by a pyrazolylborate aluminum complex (**Scheme 13**) was reported by Bergman and Koller in 2012.[176] High yields of hydrosilylation products were achieved in reactions with aldehydes, ketones, enones and imines with a low load (1-2.5 mol %) of the catalyst, but the mode of catalytic action was not established.

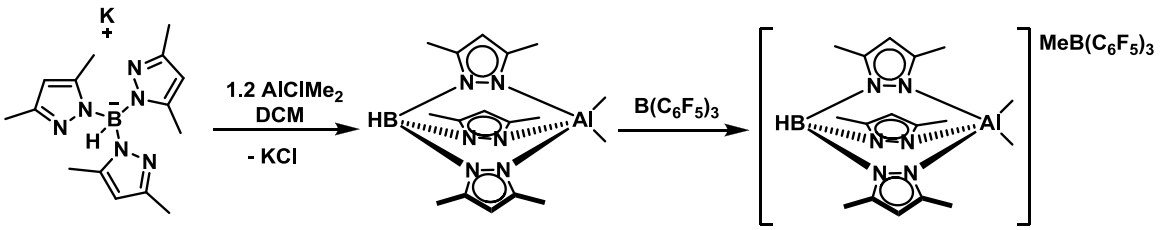

Scheme 13: Synthesis of aluminum catalyst.[176]

2.2.1.3 Fluorides as catalysts.

One of the first reports on reduction by silanes mediated by a fluorinated compound goes back to 1966, when Kursanov *et al.* performed ionic hydrogenation of alkenes into alkanes and ketones into alcohols with triethyl silane in excess of trifluoroacetic acid.[177] Five decades later this field is still getting attention and newer

papers are being published, such as the recent report on hydroamination with PMHS and trifluoroacetic acid.[178]

Extensive work on fluoride- and base-catalyzed hydrosilylation and silane rearrangements was done by Corriu and coworkers in 1970-s - 1990-s. What started as an early questioning of the existence of the "siliconium" ion R_3Si^+,[179] developed into a study of processes occurring on silicon centres, such as nucleophilic activation[180] and formation of pentaco-ordinate silicon species.[181] The latter have a direct relevance to the hydrosilylation catalysis, as will be discussed below.

Reduction of aldehydes, ketones and esters into alcohols was achieved via a reaction of either polymethylhydrosiloxane (PMHS) or diethoxymethylsilane and potassium or caesium fluorides as catalysts. The aldehydes were reduced more readily than ketones, and ketones were reduced faster than esters. Slow reduction of amides and acide chlorides was observed, as well as non-selective partial reduction of conjugated double bonds. But no reaction occurred with the nitro groups, bromides, nitriles, imides and isolated double bonds.[180c, 182] A heterogeneous variant of this reaction without a solvent was also reported.[183] The CsF/silane system was found effective in the Michael additions of monoketones and arylacetonitriles to different kinds of Michael acceptors, such as α, β - unsaturated ketones, esters and nitriles, with stoichiometric amounts of silane and fluoride under solvent-free conditions.[184] The formation of pentaco-ordinate fluorosilicates (for example, see **Scheme 14**) is believed to be essential for this type of hydrosilylation.[180c, 183]

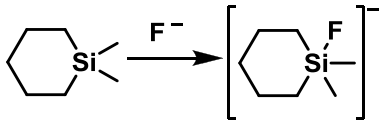

Scheme 14: Formation of a fluorosilicate.[180c]

Hiyama and Fujita reported reduction of aldehydes and ketones, as well as diastereoselective synthesis of 1,2-diols and 2-amino alcohols via hydrosilylation catalyzed by tetrabutyl ammonium fluoride (TBAF) and tris(diethylamino)sulfonium difluorotrimethylsilicate (TASF).[185]

Kobayashi *et al.* reported a very similar reductive hydrosilylation of ketones into alcohols with PMHS and catalytic amounts of TBAF.[186] The mechanism suggested for hydrosilylation (**Scheme 15**) involves the formation of a pentaco-ordinate silicate center while retaining the PMHS chain structure.

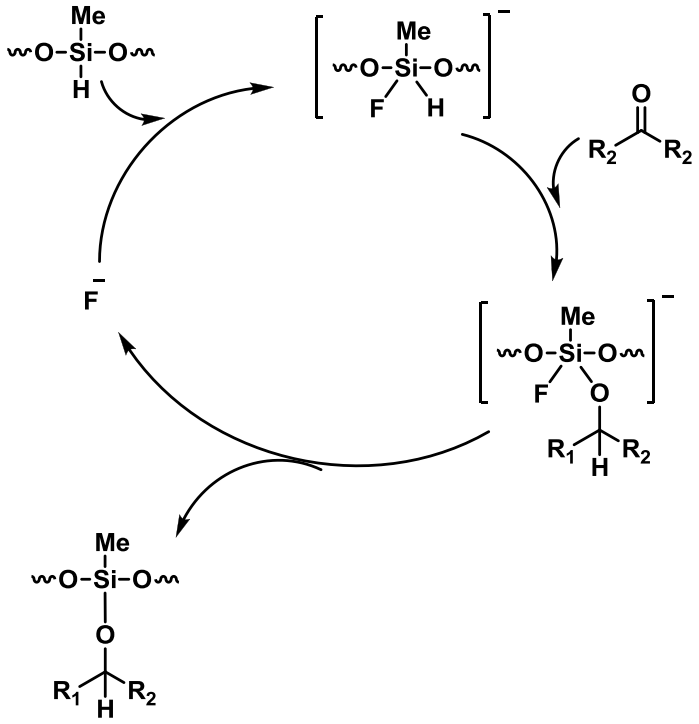

Scheme 15: Mechanism of TBAF-catalyzed hydrosilylation, suggested by Kobayashi et al.[186]

Analogous method for selective reduction of ketones and esters with silanes and TBAF was published by Lawrence *et al.* in 1997.[187] These authors proposed a "zipper" mechanism for reduction with PMHS, where, once again, the chain structure of the polysiloxane was retained. It was suggested that the silicate centre "migrates" along the chain due to nucleophile (fluoride, alkoxide etc) shift from one hydride site to another (**Scheme 16**).[187]

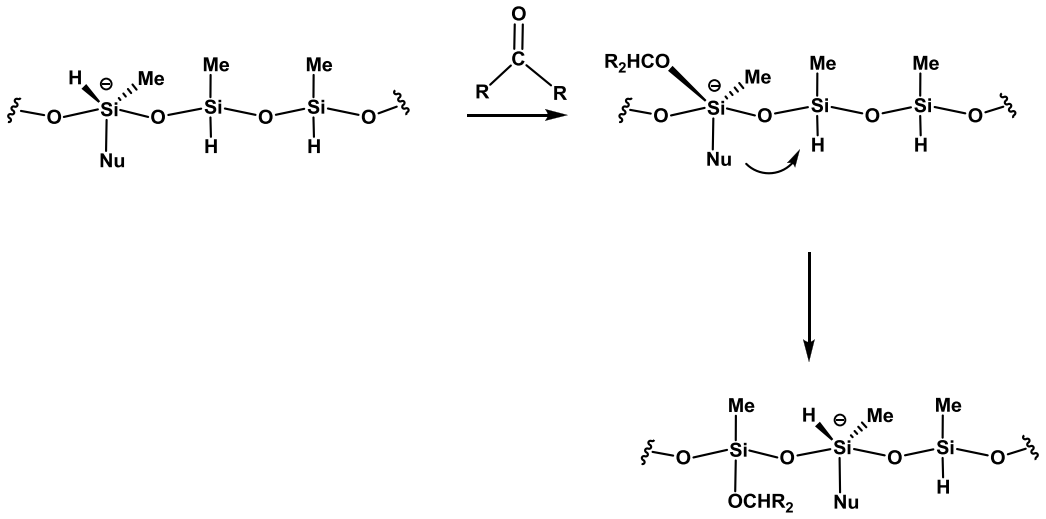

Scheme 16: The "zipper" mechanism for nucleophile catalyzed reduction by PMHS. [187b]

The chiral ammonium fluoride salts and triethoxysilane were used for asymmetric reduction of ketones by the same group (**Scheme 17**).[188] High yields (up to 100%) were achieved as well as good ee values: 51% for salt **b**, 39% for **d** and 53% for **f** (**Scheme 17**).

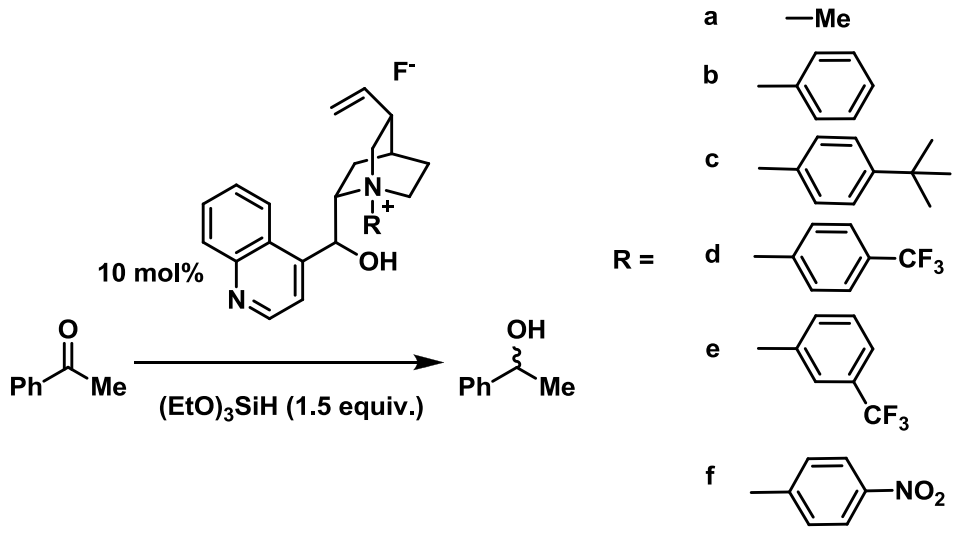

Scheme 17: Enantioselective reduction of acetophenone. [188]

Beller's group was able to selectively reduce primary amides into corresponding nitriles by hydrosilanes in the presence of TBAF and at temperatures up to 100 ^{o}C.[189] They also achieved reasonable conversions with KF and KOtBu as the catalysts. Recently this technique has been extended to the reduction of aromatic nitriles into amines catalyzed by TBAF at room temperature.[190] The selectivity studies showed that nitriles are reduced less readily than esters and ketones.

2.2.1.4 Bases as the catalysts for hydrosilylation.

There are only a few reports of hydrosilylation catalysis with simple bases, such as alkali metal alkoxides and hydroxides.

The rearrangement of hydrido- and alkoxysilanes in the presence of bases was discussed extensively by Corriu *et al.*[181a, 181d, 191-192] The reactions were postulated to proceed via hypervalent silicon species, and indeed a five-co-ordinate hydridosilicate was obtained in the reaction of triethoxysilane with potassium ethoxide (**Scheme 18**).[181a]

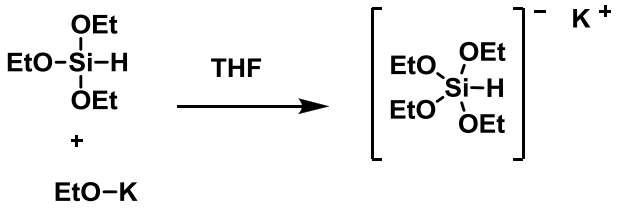

Scheme 18: Formation of pentacoordinate silicate. [181a]

Similar experiments were conducted with dihydridosilanes and metal hydrides, such as KH and NaH, when the exchange of silicon-carbon and silicon-hydrogen bonds was observed.[191b] A thorough study of hydridosilicates was conducted by McGrady and Steed and co-workers who were the first to isolate and obtain the X-ray structure of a penta-coordinate hydrosilicate species.[193] It was established, that the hypercoordinate silicon center it interacts with metal cation electrostatically via the silicon-bound hydride.[193]

Direct hydride transfer between tetra- and pentaco-ordinate species, important for the understanding of silane rearrangement processes, was reported in 1992 (**Scheme 19**).[194]

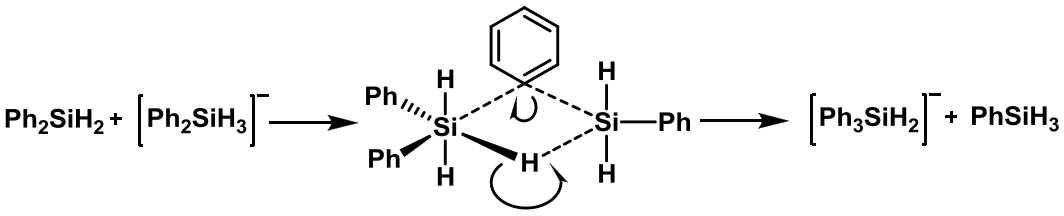

Scheme 19: Hydride transfer between silicate and silane. [194]

The intrinsic reducing ability of polycoordinate silicate species was established in the hydrosilylation of carbonyls by a tetraalkoxysilicate in the absence of additional catalyst (**Scheme 20**).[181d]

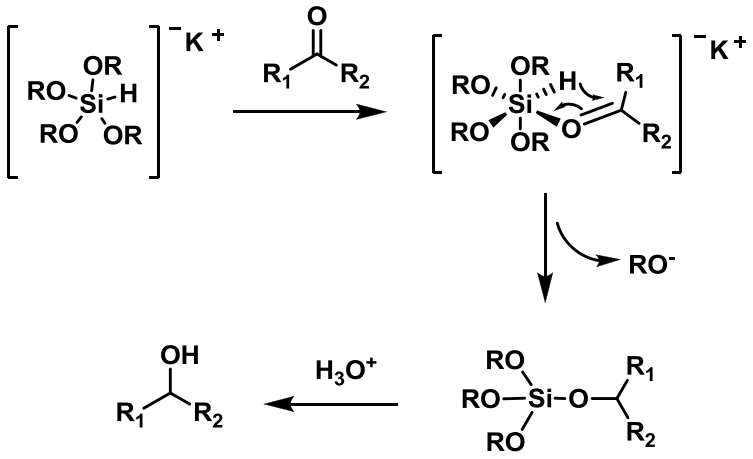

Scheme 20: Carbonyls reduction with polycoordinate silicates.[181d]

In 1986, the hydrosilylation of aldehydes and ketones with trimethoxysilane and stoichiometric amounts of lithium methoxide was reported by Hosomi et al.[195] This discovery was extended to asymmetric reduction of carbonyls[196] and imines[197] by use of chiral bases, such as lithium salts of 2-aminoalcohols. The stereoselectivity in the reduction of α,β–epoxyketones with trimethoxysilane and catalytic amounts of lithium methoxide was reported in 1995, where the keto- group was selectively reduced.[198] Esters and lactones were successfully reduced with this silane/alkoxide system as well.[199]

Hydrosilylation of acetophenone catalyzed by sodium or potassium tert-butoxides was further reported by Beller's group in 2010.[200]

Very recently Grubbs *et al.* reported on reductive opening of aryl ethers by silanes.[201] A variety of silyl group addition products (**Scheme 21**) were obtained, with the product ratio strongly depending on the solvent and the base used.

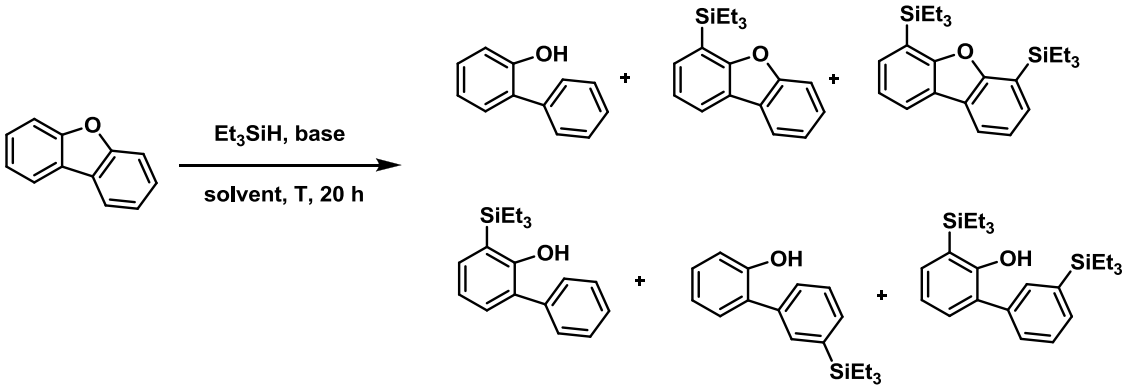

Scheme 21: Base-catalyzed hydrosilylation of aryl ethers.[201]

In the most recent report from Nolan`s group, a solvent-free base-catalyzed hydrosilylation of esters into alcohols and tertiary amides into amines was achieved at room temperature.[202] Potassium hydroxide was used as catalyst and acidic work-up conditions were applied to obtain high isolated yields.[202] In a paper of Cui *et al.* from November 2013, a solvent-free procedure for the reduction of various tertiary amides into amines with phenyl silane and catalytic amounts of cesium carbonate in good to excellent yields is reported.[68c] The authors assume that a pentaco-ordinate silicate intermediate plays the key role in the reduction mechanism, while the choice of the base, cesium carbonate vs sodium and potassium carbonates, is due to the higher solubility of the catalyst in the silane-substrate reaction mixture.

2.2.2 Reduction of heterocycles.

Heterocyclic compounds are abundant among natural products, and therefore, reduction of aromatic heterocycles is of great importance for pharmaceutical and agrochemical industries. Chemo- and regioselective reduction of heteroarenes presents a significant challenge, so we became interested in the application of catalytic hydrosilylation to this problem. Reduction chemistry of hetroarenes is a

fastly developing field of research but not so many examples of catalytic reductions have been reported. Thus we elected not to limit our discussion to the main group catalysis only. Instead, selected examples of hydroboration, direct and transfer hydrogenation will be given along with the discussion of hydrosilylation approach. Most of the known literature examples run under harsh reaction conditions, such as high pressure (for hydrogenation by H_2) and/or elevated temperatures, and the use of expensive rhodium or iridium catalysts.

Earlier efforts in reduction of heterocycles relied on the application of lithium aluminum hydride.[203] The addition of hydride to quinoline gives dihydroquinoline upon aqueous work-up. Similar dihydroproducts were obtained from pyridine, phenazine, acridine and benzimidazole, while the reduction of quinoxaline and 2,3-dimethylquinoxaline resulted in tetrahydroproducts (**Scheme 22**).[203a]

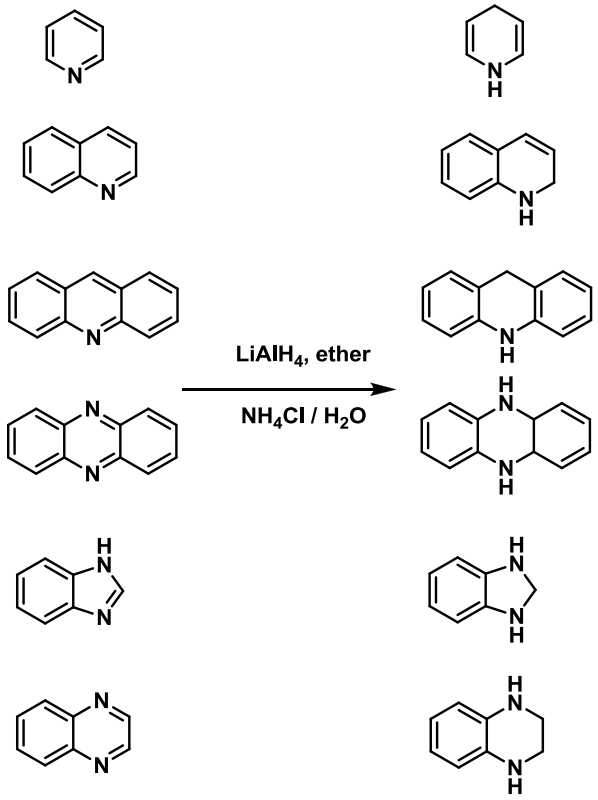

Scheme 22: Reduction of heterocyclic compounds with lithium aluminum hydride.[203a]

While being simple and reliable, the lithium aluminum hydride method has such issues as the lack of variability, the cost of reagent, and serious safety concerns for scaling-up.

Recent reports from Hill's group established the key role of *in situ* generated magnesium hydrides in the reduction of heterocycles.[204] Thus, hydrosilylation[204a] and hydroboration[204b] catalyzed by β-diketiminato n-butyl magnesium complex allows for dearomatization of pyridine and quinoline derivatives (**Scheme 23**).

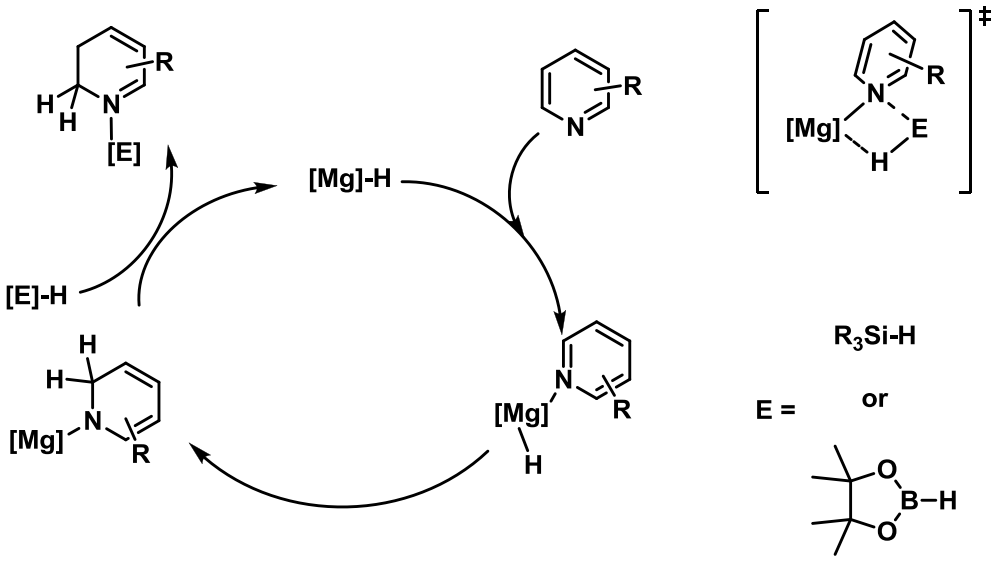

Scheme 23: Hydrosilylative dearomatization of pyridines.[204]

Regioselective hydrogenation of quinolines was conducted under hydrogen atmosphere (4 atm) with rhodium and iridium mono-, di- and tri-dentated phosphine complexes prepared *in situ*.[205] Solvent dependent regioselective hydrogenation of substituted quinolines was observed by Fache in 2004.[206] While using methanol as solvent leads to the formation of tetrahydro products (**Scheme 24**), reactions conducted in hexafluoroisopropanol tend to result in decahydro product.[206]

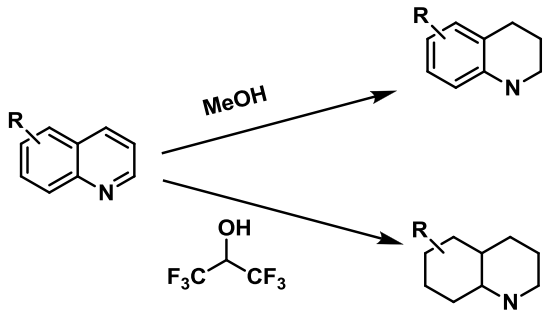

Scheme 24: Hydrogenation of quinolines. Conditions: room temperature, 50 bar H_2, Rh/Al_2O_3.[206]

Complete reduction of the *N*-ring of quinolines and isoquinolines with high isolated yields was conducted by Murahashi *et al.* under water-gas shift conditions with rhodium-carbonyl clusters as catalysts.[207] Heterogeneous catalytic hydrogenation with gold nanoparticles supported on TiO_2 was recently shown to result in the *N*-ring reduction of quinolines.[208] The *N*-ring reduction was observed by Chin *et al.* in reactions with acridines and quinolines catalyzed by an iridium-triphenylphosphine complex, whereas a reaction with indol resulted in the reduction of both its rings.[209] Hydrogenation of quinolines and benzothiophenes under homogeneous catalysis by osmium, iridium, rodium and ruthenium complexes was reported in 1989,[210] followed by examples of Rh-catalyzed hydrogenation of heteroatom-bearing rings of indoles, benzofuranes, substituted quinolines and benzoquinolines, acridines and benzothiophenes.[211] The same reduction pattern was demonstrated by Zhou *et al.* who used a ruthenium catalyst activated by iodine.[212] The Zhou group also reported the first example of asymmetric hydrogenation with a catalytic system consisting of an iridium complex, a phosphine ligand, iodine and the Hantzsch ester.[213] An air-stable iridium-phosphine catalytic system for asymmetric hydrogenation of quinolines was reported in 2007.[214] Following the same approach, chiral bisphosphine ligands were used together with iridium[215] and rhodium[216]

complexes for asymmetric reduction of the *N*-ring of indoles. In all these examples, complete reduction of the ring takes places.

Partial hydrosilylation of quinoline was reported by Crabtree *et al.* in 2008 (**Scheme 25**). Interestingly, the 1,2-dihydroquinoline was obtained with excellent regioselectivity.[217] The same group also reported complete reduction of the *N*-ring by transfer hydrogenation.

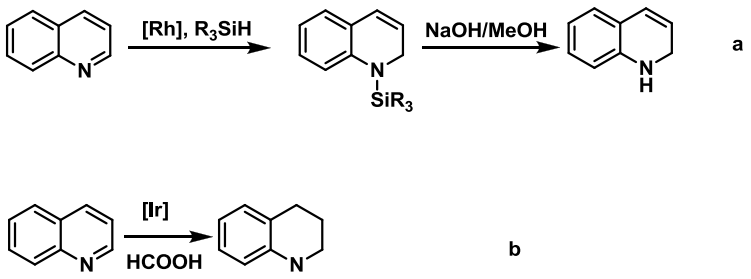

Scheme 25: Hydrosilylation (a) and transfer hydrogenation (b) of quinolines.[217a]

Chemoselective monoreduction of pyridines was achieved by Nikonov and Gutsulyak with a ruthenium catalyst (**Scheme 26**).[218] Importantly, the regiospecific 1,4-hydrosilylation to give *N*-silyldihydropyridine-1,4 was observed.

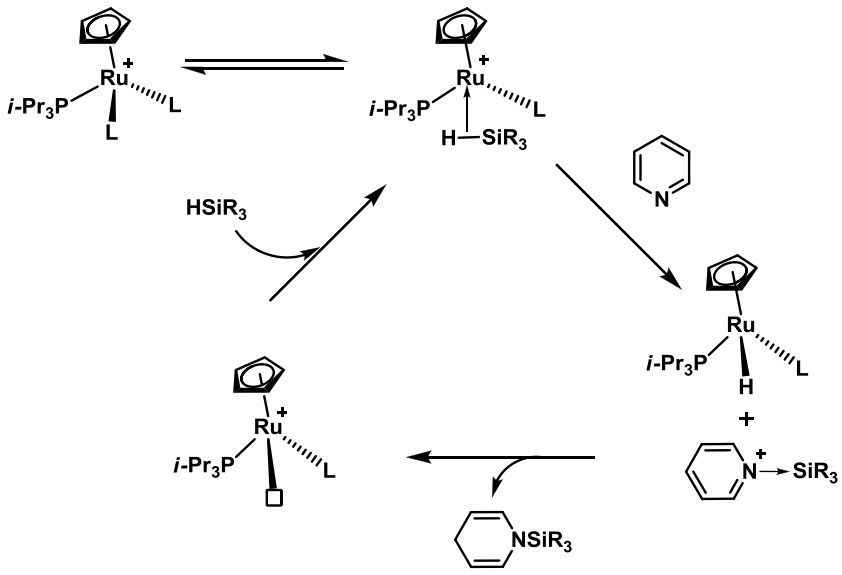

Scheme 26: Proposed mechanism for hydrosilylation of pyridines.[218a]

A very recent study of Oestreich *et al.* reports 1,4-hydrosilylation of pyridines with a thiolate ruthenium catalyst and dimethylphenylsilane.[219] The first example of enantioselective Lewis base-catalysed hydrosilylation of benzoxazinones and quinoxalines (**Scheme 27**) was presented by Zhang *et al.* in 2010.[220]

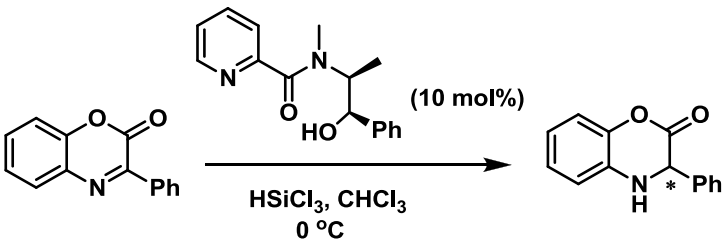

Scheme 27: Lewis Base organocatalyzed hydrosilylation.[220]

Reduction of *N*-containing heterocycles by hydroborates usually results in complete reduction of the *N*-ring. The examples include the application of sodium cyanoborohydride/boron trifluoride etherate by Srikrishna[221] and a zinc borohydride by Ranu.[222]

There are a few recent examples of using perfluoroarylboranes for the reduction of heterocyclic compounds. In particular, Stephan *et al.* developed the first metal-free hydrogenation of aniline with $B(C_6F_5)_3$ to give a *N*-cyclohexylammonium hydridoborate salt.[223] This breakthrough report was followed by an example of metal-free hydrogenation of *N*-containing heterocycles (**Scheme 28**).[224]

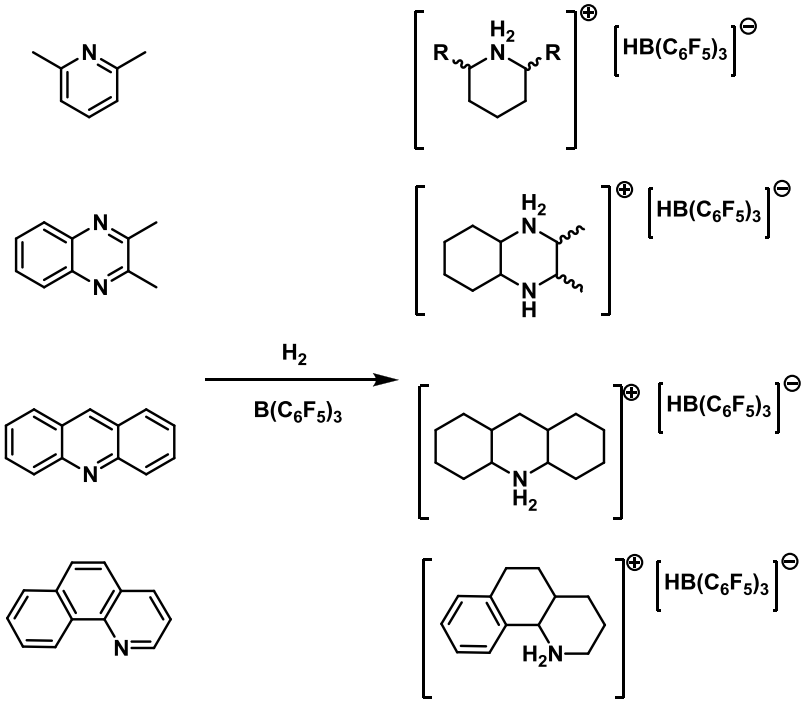

Scheme 28: Hydrogenation of N-containing heterocycles.[224]

A variation of this method with alkyl borane produced *in situ* was developed by Du (**Scheme 29**).[225]

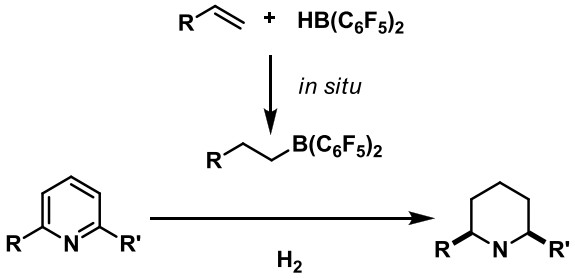

Scheme 29: Hydrogenation of pyridine derivatives.[225]

Asymmetric hydrogenation of thiophenes and benzothiophenes with a Ru-NHC catalyst was developed by Glorius *et al*. (**Scheme 30**).[226]

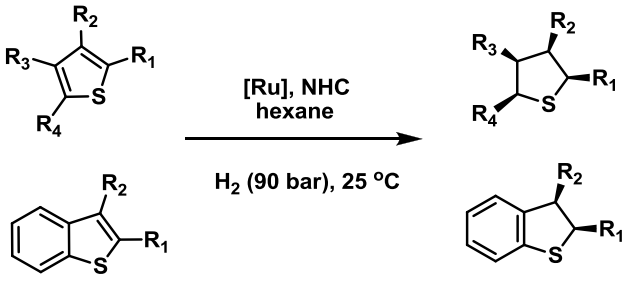

Scheme 30: Reduction of thiophenes and benzothiophenes.[226]

Enantioselective reduction of C=N bonds in various *N*-containing heterocycles was achieved via hydrogenation with iridium-phosphine-phospite complexes (**Scheme 31**).[227]

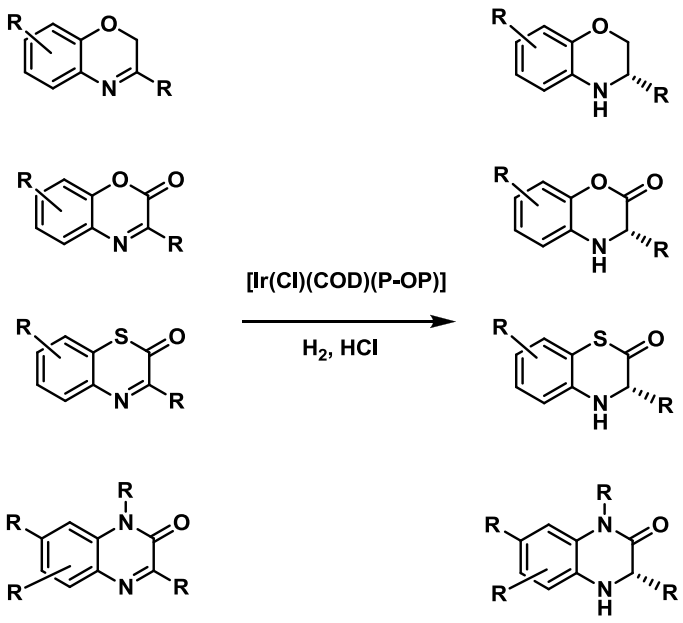

Scheme 31: Reduction of C=N bond in heterocycles.[227a]

Current efforts towards reduction of heterocycles are focused on the search for low-cost, efficient and environment-friendly methods.[228]

2.2.3 Silanes used for hydrosilylation.

Since the current project was aimed at the development of an industrially "friendly" hydrosilylation method, such parameters as the cost, availability, safety, and environmental impact of all reactants were considered important. The data on the most often used silanes are presented in **Table 5**.

Phenyl silane is among the most efficient reducing agents, but its usage is compromised by the high cost and sensitivity to moisture. Triethoxysilane is much less expensive and is used very often in small-scale reactions, but its employment on a larger or industrial scale cannot be considered as safe, since it easily forms significant amounts of pyrophoric SiH_4 as a result of disproportionation.[229]

Compared to other common reagents, the toxicity of most silanes is much lower, but it is still considered to be significant by MSDS. The production of silane does impact the environment and increase the overall level of pollution. On the other hand, polymethylhydrosiloxane (PMHS) is obtained as a by-product of Direct Synthesis[230] of silanes, and is non-toxic[187b] and very inexpensive (see **Table 5**). The application of PMHS in the reduction of carbonyls[187b, 188, 231] and imines[232] as well as dehalogenation of organohalides[233] has been reported. While the application of PMHS requires some adjustment in hydrosilation procedures, its use seems very prospective both from the environmental and economical point of view.

Table 5: Characteristics of silanes.

Silane	Molar mass, g/mol	Estimated N_H [a] (number of hydride units per gram), g^{-1}	Price	Stability (air, moisture) [c,d]	Physical state parameters[c,d]	Toxicity[d]	Safety (MSDS[d])	Known application
SiH_4	32	$7.5*10^{22}$	\$80/kg [b]	Very unstable, pyrophoric	m.p. -185 °C b.p. -111.4 °C	Highly toxic	Spontaneous flammability	Silicon layers coating, Semiconductor manufacturing
Et_3SiH	116	$5.2*10^{21}$	\$324/250 g [c] \$525/500 g [d]	Moisture sensitive	m.p. -157 °C b.p. 108 °C	Toxic, irritant	Highly flammable,	Reducing agent
$PhMe_2SiH$	136	$4.4*10^{21}$	\$112/50 g [c] \$112/25 g [d]	-	m.p. -124 °C b.p. 156 °C	Irritant	Flammable	Reducing agent
Ph_2MeSiH	198	$3.0*10^{21}$	\$56/25 g [c]	-	b.p. 266 °C	Irritant	Not flammable	Reducing agent
Ph_3MeSiH	260	$2.3*10^{21}$	\$124/50 g [d]	Moisture and air sensitive	m.p. 42 °C b.p. 152 °C [e]	Toxic, irritant	Not flammable	Reducing agent
$PhSiH_3$	108	$1.7*10^{22}$	\$812/100 g [c] \$267/25 g [d]	Air and moisture sensitive	b.p. 120 °C	Toxic	Flammable, violently reacts with water	Reducing agent

$Me(EtO)_2SiH$	134	$4.5*10^{21}$	\$247/50 g [c] \$121/10 g [d]	-	b.p. 94 °C	Toxic, irritant	Flammable	Reducing agent
$(EtO)_3SiH$	164	$3.7*10^{21}$	\$406/250 g [c] \$136/50 g [d]	Moisture sensitive	m.p. -170 °C b.p. 134 °C	Fatal if inhaled, strong irritant	Flammable, forms SiH_4	Reducing agent
TMDS	134	$9.0*10^{21}$	\$378/500 g [c] \$688/500 g [d]	Moisture sensitive	m.p. -78 °C b.p. 70 °C	Toxic	Highly flammable	Reducing agent
PMHS	60 per unit, average M = 1700-3200	$1.0*10^{22}$	\$137/1000g [c] \$61/250 g [d]	Stable	Flash point 204 °C	Non-toxic	Not flammable	Low-cost and safer alternative to $(EtO)_3SiH$

a – $N(H) = \frac{n*N_A}{M}$, where n - number of H in R_xSiH_n, molecule $^{-1}$; N_A - Avogadro number, $^{molecule}/_{mol}$; M – molar mass, $^{g}/_{mol}$.

b – Price at http://www.diytrade.com/china/pd/7816087/Silane_SiH4.html

c - Alfa Aesar (http://www.alfa.com),

d – Sigma-Aldrich (http://www.sigmaaldrich.com)

e –under 2 mm Hg

2.3 Results and discussion.

2.3.1 The discovery of silane-base system.

This project started as a study of carbonyl hydrosilylation catalyzed by the Schwartz`s reagent $(C_5H_5)_2ZrHCl$. Since the Schwartz`s reagent is air-sensitive and insoluble in non-polar solvents, we attempted its generation *in situ* from the readily accessible compound $(C_5H_5)_2ZrCl_2$ upon treatment with an alkoxide followed by addition of a hydrosilane. Our reasoning was that a zirconium alkoxide would be formed upon chloride displacement which would be converted into a hydride upon addition of silane. Both steps have many precedents in the chemistry of early transition metals. Initial catalytic tests were very positive as fast conversions of carbonyl substrates (benzaldehyde, acetophenone etc) were observed. However, much to our surprise, an immediate carbonyl reduction was observed in blank experiments without any zirconium complexes added, when the substrate was mixed only with the phenyl silane and 5% KOtBu, which was originally believed to serve merely as a co-activator of the metal catalyst (**Scheme 32**).

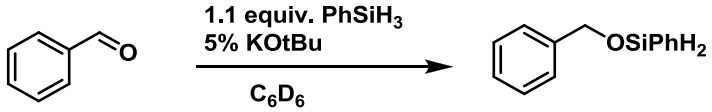

Scheme 32: Base catalysed hydrosilation of benzaldehyde.

With this result in hand, the activity of different silanes in the hydrosilylation of acetophenone was studied. The results are summarized in **Table 6**. Phenyl silane and triethoxysilane showed the shortest reaction times. The use of TMDS and PMHS required heating and extended periods of time. Diethoxymethyl silane was virtually inactive.

Entry	Silane/amount	Base	Temp.	Time	Conversion, % (NMR)
1	$PhSiH_3$, 1.1 equiv.	KO*t*Bu, 0.1%	RT	< 10 min	98
2	$HSi(OEt)_3$, 1.1 equiv.	KO*t*Bu, 5%	RT	15 min	98
3	$HSi(OEt)_3$, 1.1 equiv.	KO*t*Bu, 0.1%	RT	5.5 h	98
4	$HSi(OEt)_2Me$, 1.1 equiv.	KO*t*Bu, 5%	RT	4 days	0
5	TMDS, 3 equiv.	KO*t*Bu, 5%	70°C	2 days	98
6	PMHS, 5 equiv.	KO*t*Bu, 5%	RT	7 h	98
7	PMHS, 2.5 equiv.	KOH, 5%	RT	2 days	98 (66 – isolated yield)

Table 6: Base catalyzed hydrosilylation of acetophenone.

2.3.2 Silane rearrangement studies.

During these preliminary hydrosilylation experiments the appearance of additional peaks in ^1H NMR spectra was noted, which could be assigned to silane redistribution products, a process known from the literature.[181a, 191b] For example, upon contact with a base triethoxysilane forms the silane SiH_4.[229, 234] In fact, such a silane redistribution is the major obstacle for the industrial use of $(EtO)_3SiH$ since SiH_4 is highly explosive.

2.3.2.1 Phenyl silane

Mechanistic studies for the reaction of H_3SiPh with *t*BuOK at low temperature provided a further significant insight into the nature of the hydrosilylation reaction. In particular, several silicate species were observed and characterized. The ^{29}Si and ^1H

NMR spectra are shown in **Figure 93**, and a possible route for silane rearrangement is sketched in **Scheme 33**.

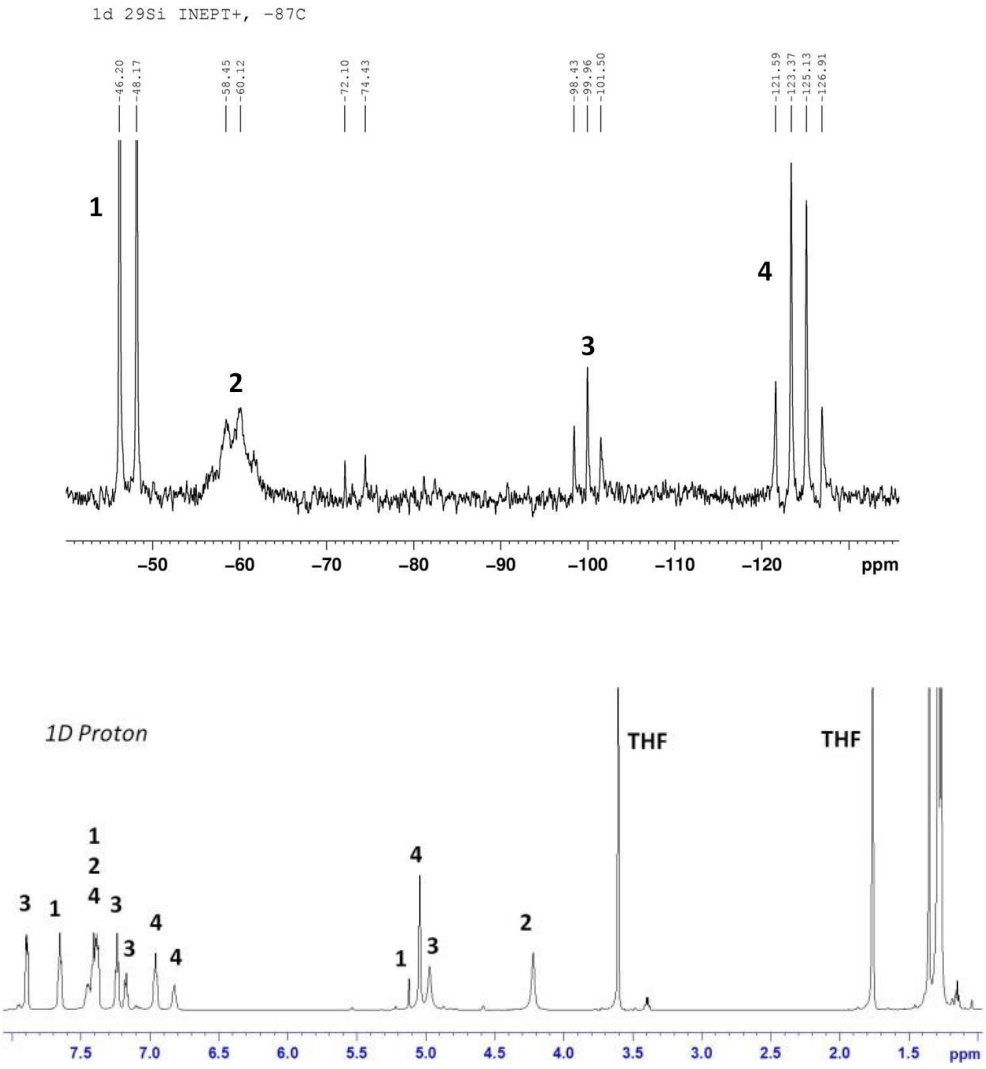

Figure 93: 1D ^{29}Si INEPT NMR (top) at -87 ^{o}C and ^{1}H NMR (bottom) at -40 ^{o}C. 1-$[Ph_2(O\mathit{t}Bu)_2SiH]^-$, 2 – $[PhSiH_4]^-$ and $[SiH_5]^-$, 3-[$Ph(O\mathit{t}Bu)_2SiH_2]^-$, 4 – $[Ph(OtBu)SiH_3]^-$

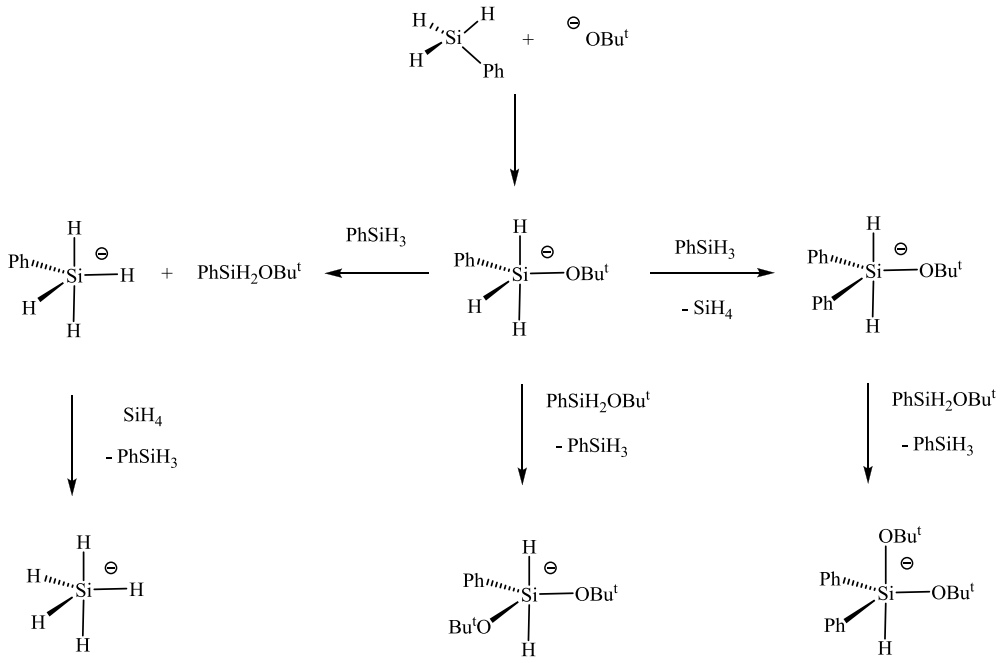

Scheme 33: Reaction of $PhSiH_3$ with *t*BuOK.

A reaction between $PhSiH_3$ and *t*BuOK in THF-d_8 at -70 °C gives the silicate $[Ph(tBuO)SiH_3]K$ (**Scheme 33**), which upon warming to -40 °C decomposes to a mixture of $[Ph(tBuO)SiH_3]K$, $[Ph(tBuO)_2SiH_2]K$, $[Ph_2(tBuO)_2SiH]K$, $[PhSiH_4]K$, and $[SiH_5]K$ (**Figure 93**, bottom). The latter two species are in a very fast exchange, giving rise to a broad SiH signal at 4.22 ppm. At lower temperatures this peak broadens but the signals proved impossible to decoalesce even at – 87 ºC. An EXSY NMR experiment further established a fast equilibrium at -40 °C between the SiH signal of $[Ph(tBuO)SiH_3]K$ at 5.05 ppm and the signal at 4.22 ppm.

$$ln\frac{k}{T} = -\frac{\Delta H^{\neq}}{R} * \frac{1}{T} + ln\frac{k_B}{h} + \frac{\Delta S^{\neq}}{R} \qquad \textbf{(22)}$$

The Eyring-Polanyi equation (**Equation 22**, where k is the exchange rate constant, T – temperature, $R = N_A k_B$, k_B- Boltzmann constant, h – Planck constant, $\Delta H^{\neq}$ - enthalpy, $\Delta S^{\neq}$ - enthalpy) was used for the calculation of enthalpy and entropy

in the exchange mechanism. The data were linearized in the coordinates $-\boldsymbol{ln}\frac{\boldsymbol{k}}{\boldsymbol{T}}$ vs $\frac{\mathbf{1}}{\boldsymbol{T}}$, (**Figure 94**), allowing us to determine the activation parameters (the line slope equals to $\frac{\Delta \boldsymbol{H}^{\neq}}{\boldsymbol{R}}$). Therefore, activation parameters for this process ($\Delta \boldsymbol{H}^{\neq}$ = 29.2 kJ.mol^{-1}, $\Delta \boldsymbol{S}^{\neq}$ = -96.2 kJ·mol^{-1}·K^{-1}) suggested an associative mechanism of exchange.

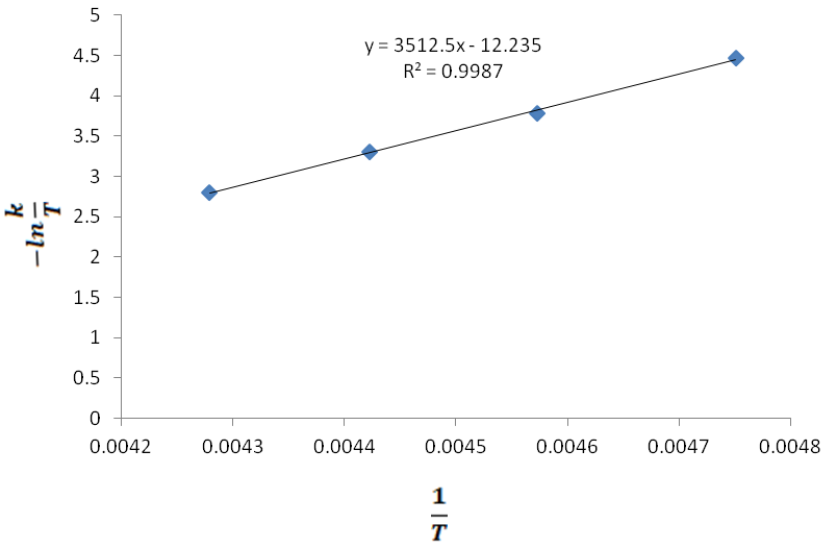

Figure 94: Eyring plot for activation parameters.

In the ^{29}Si INEPT+ spectrum, compounds [Ph(tBuO)SiH$_3$]K, [Ph(tBuO)$_2$SiH$_2$]K, and [Ph$_2$(tBuO)$_2$SiH]K give rise to up-field signals at -124.0 (q, J(H-Si)= 211.0 Hz), -99.8 (t, J(H-Si)= 124.4 Hz) and -47.3 (d, J(H-Si)= 124.3 Hz), respectively, confirming their silicate nature (**Figure 93**, top). Upon a gentle increase of temperature, [Ph(tBuO)SiH$_3$]K further decomposes into [Ph(tBuO)$_2$SiH$_2$]K, [Ph$_2$(tBuO)$_2$SiH]K and [PhSiH$_4$]K via hydride/alkoxy and Ph/alkoxy exchanges. At room temperature broad featureless signals are observed, suggesting a fast equilibrium. Unfortunately, reactions of these silicates with acetophenone are too fast even at -40 °C to allow for accurate kinetic measurements.

2.3.2.2 Base-mediated disproportionation of hydrosiloxanes

The skeletal changes of siloxanes PMHS and TMDS were observed by NMR upon addition of a base (**Figure 95**). Most interestingly, the base-induced rearrangement of PMHS produces methyl silane $MeSiH_3$, whereas dimethyl silane is obtained from TMDS. Both silanes are gases under normal conditions and are difficult to generate and manipulate by using conventional preparative strategies of hydrosilane syntheses. In contrast, the rearrangement reactions are fast at room temperature, require only catalytic amounts of base, are reproducible, and most importantly utilise inexpensive siloxanes, which are by-products of the Direct Synthesis of silanes.[229b, 230a, 234]

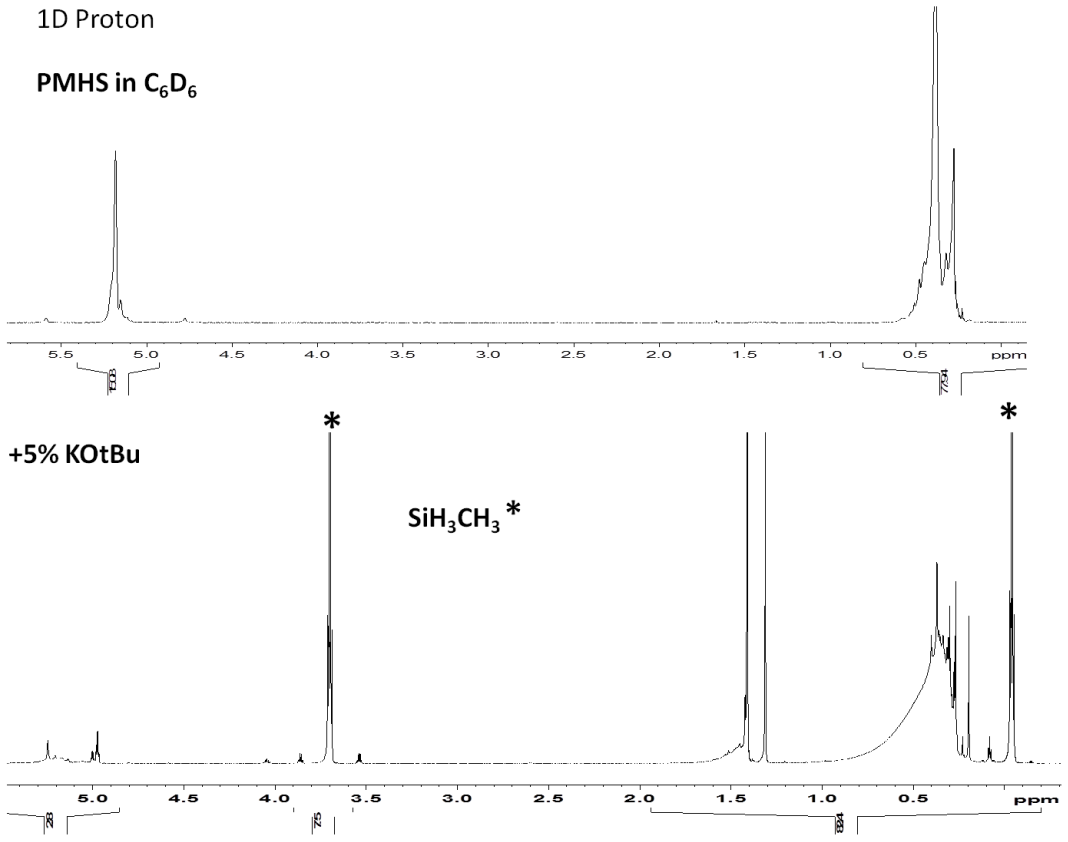

Figure 95: NMR-spectra of PMHS sample before (top) and after (bottom) addition of KO*t*Bu

To probe the zipper-mechanism suggested by Lawrence *et al.*[187-188], an experiment with PMHS and TBAF was carried out, which also lead to the formation Me_3SiH_3. Therefore, this study shows convincingly that the zipper mechanism is not applicable to the hydrosilylation catalysis simply because the siloxane backbone of PMHS is not maintained in the presence of fluoride. The importance of this siloxane-to-silane rearrangement was further probed when a base-catalyzed reduction by PMHS was attempted under inert atmosphere in an open flask system (**Figure 96**, left). No product of reduction was formed. Conducting a similar, open-system experiment under hydrogen atmosphere (**Figure 96**, right) did not lead to the reduction either.

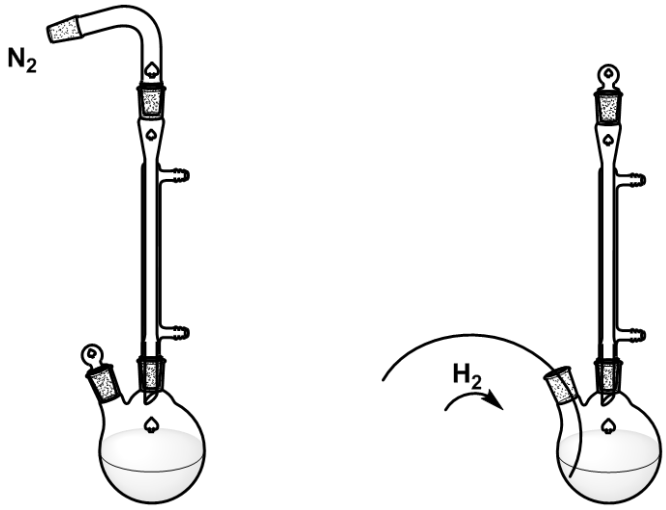

Figure 96: Reaction setups: open system under the nitrogen atmosphere (left) and open system under hydrogen atmosphere, H_2 is bubbled through the reaction mixture (right).

Finally, removal of volatiles from the PMHS/base mixture prior to the addition of a substrate, resulted in no reduction either. Altogether these facts allow for the conclusion that reduction by PMHS proceeds via formation of the volatile (bp -57.5°C) silane H_3SiMe which upon further reactions with a strong nucleophile (e.g.

fluoride, hydroxide, *tert*-butoxide anions, etc.) forms a reducing silicate species, as it has been established for the closely related silane H_3SiPh. A possible mechanism of PMHS disproportionation is offered in **Scheme 34**.

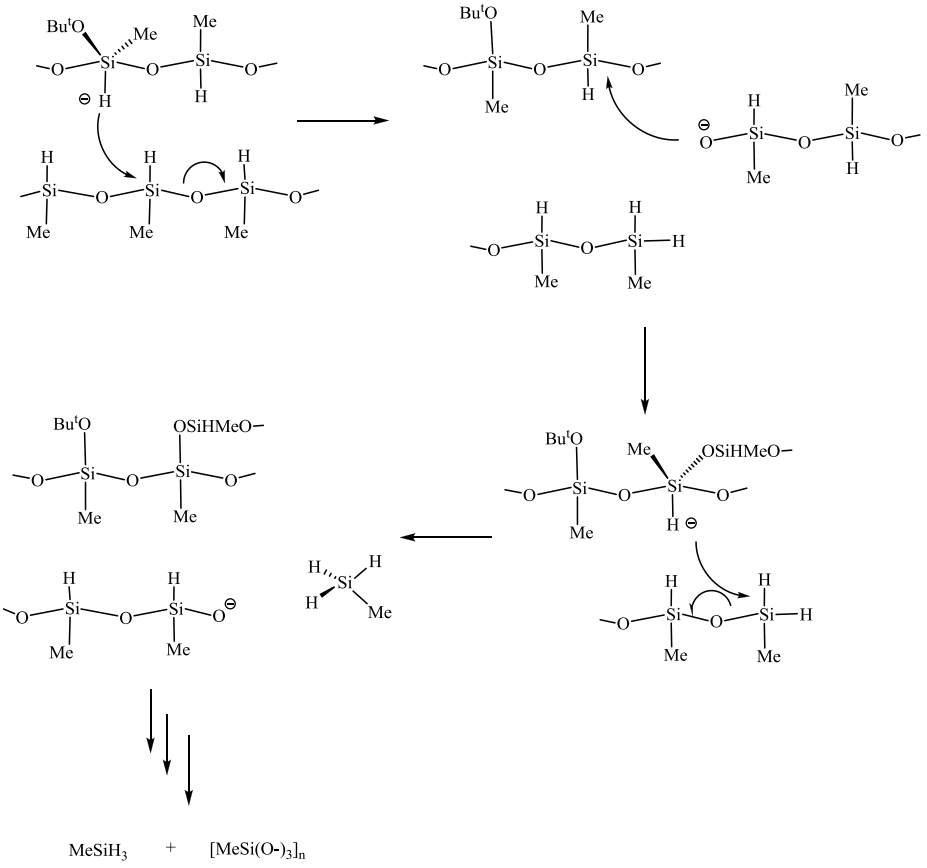

Scheme 34: Base-catalyzed rearrangement of PMHS to $MeSiH_3$

2.3.3 Reduction of aldehydes and ketones.

The silane/base system was then used for reduction of a series of carbonyl substrates on the NMR and millimole scales. The results of hydrosilylation of aldehydes and ketones are shown in **Table 7**. All reactions proceed well at room temperature, and product isolation was relatively easy.

Table 7: Base-catalyzed hydrosilylation of aldehydes and ketones by PMHS. Room temperature.

Entry	Substrate	Silane	Base	Time	Conversion[a], %
1	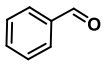	PMHS, 5 eq	KO*t*Bu, 5%	< 10 min	98
2		PMHS, 5 eq	KO*t*Bu, 5%	40 min	98 (aldehyde)
3	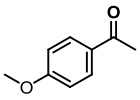	PMHS, 5 eq	KO*t*Bu, 5%	14 h	98 (ketone)
4		PMHS, 2.5 eq	KOH, 5%	2 days	98 (74)[b]
5	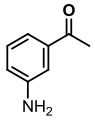	PMHS, 5 eq	KO*t*Bu, 5%	9 h	98
6	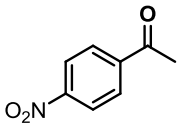	PMHS, 5 eq	KO*t*Bu, 5%	45 h	98
7		PMHS, 2.5 eq	KOH, 5%	2 days	98(27) (ketone)
8	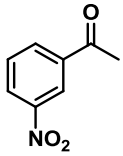	PMHS, 2.5 eq	KOH, 5%	2 days	98 (48) (ketone)
9	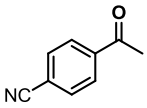	PMHS, 2.5 eq	KOH, 5%	2 days	98 (89)
10					
11		PMHS, 2.5 eq	KOH, 5%	2 days	98 (89)
12	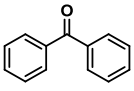	PMHS, 2.5 eq	KOH, 5%	2 days	98 (82)
13		PMHS, 5 eq	KO*t*Bu, 5%	20 min	98
14		$PhSiH_3$, 1.1 eq	KO*t*Bu, 5%	20 min	80

[a] Isolated yields of alcohols after basic work-up in brackets

2.3.4 Reduction of esters, tertiary amide and aldimine.

2.3.4.1 Methyl silane generation.

In contrast to the reduction of aldehydes and ketones, the hydrosilylation of esters with PMHS required elevated temperatures. At 70 ^{o}C a significant part of PMHS transforms into a silicone "gum" which has a dense structure and is hard to break even upon intensive stirring and additional heating during the basic work-up procedure.

To circumvent this drawback, methylsilane was used as a reducing agent. Since the $MeSiH_3$ has a low boiling point (- 57.5 C), a custom-made glassware unit for its production and transfer was employed (**Figure 97**).

Figure 97: A custom-made glassware unit for the production and separation of methylsilane (left compartment) and substrate reduction (right compartment).

To our delight, we observed that the silicone gum formed in reductions by methylsilane has a light structure and, thus, the isolation of reduction products from

the reaction mixture became easier and afforded higher yields than in experiments with PMHS.

2.3.4.2 Reaction substrate scope.

The results of NMR and preparative (2 mmol) scale reactions with $PhSiH_3$, TMDS, PMHS and $MeSiH_3$ are compiled in **Table 8**.

Table 8: Base-catalyzed hydrosilylation of esters, aldimines, and amides.

Entry	Substrate	Silane[a]	Base	Time	Conversion[b], %
1	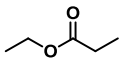	$PhSiH_3$, 1.1 equiv.	KO*t*Bu, 5%	< 10 min	98
2		$PhSiH_3$, 1.1 equiv.	KO*t*Bu, 0.5%	2 days	98
3		TMDS, 5 equiv.	KO*t*Bu, 5%	4 days	85
4		PMHS, 5 equiv.	KO*t*Bu, 5%	38 h	98
5	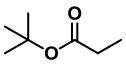	$PhSiH_3$, 1.1 equiv.	KO*t*Bu, 5%	46 h	98
6	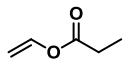	$PhSiH_3$, 1.1 equiv.	KO*t*Bu, 5%	24 h	98
7	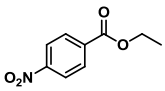	$PhSiH_3$, 1.1 equiv.	KO*t*Bu, 5%	24 h	0
8		PMHS, 5 equiv.	KO*t*Bu, 5%	45 h	98
9	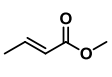	$PhSiH_3$, 1.1 equiv.	KO*t*Bu, 5%	12 min	98
10		PMHS, 5 equiv.	KO*t*Bu, 5%	1 day	98

11	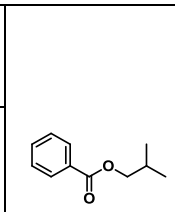	PMHS, 3 equiv.	KO*t*Bu, 5%	3 days	98
12		PMHS, 3 equiv.	KOH, 5%	2 days	98 (56)
13		$MeSiH_3$, 3 equiv.	KO*t*Bu, 5%	2 days	98 (93)
14	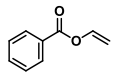	PMHS, 3 equiv.	KO*t*Bu, 5%	1 day	98
15	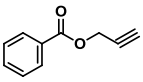	PMHS, 3 equiv.	KO*t*Bu, 5%	15 min	98
16	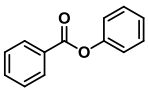	PMHS, 3 equiv.	KO*t*Bu, 5%	3 days	98
17	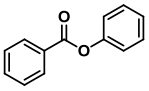	PMHS, 3 equiv.	KOH, 5%	2 days	98 (70)
18		$MeSiH_3$, 3 equiv.	KO*t*Bu, 5%	2 days	98 (76)
19	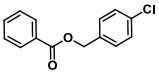	PMHS, 3 equiv.	KO*t*Bu, 5%	3 days	98
20		PMHS, 3 equiv.	KOH, 5%	2 days	98 (64)
21		$MeSiH_3$, 3 equiv.	KO*t*Bu, 5%	2 days	98 (46)
22	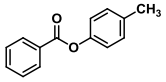	PMHS, 3 equiv.	KO*t*Bu, 5%	3 days	98
23		PMHS, 3 equiv.	KOH, 5%	2 days	98 (28)
24		$MeSiH_3$, 3 equiv.	KO*t*Bu, 5%	2 days	98 (51)
25	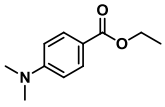	PMHS, 3 equiv.	KO*t*Bu, 5%	3 Days	98

26	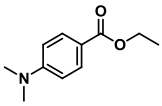	PMHS, 3 equiv.	KOH, 5%	2 days	98 (3.3)
27		$MeSiH_3$, 3 equiv.	KO*t*Bu, 5%	2 days	98 (12)
28	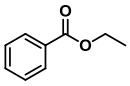	PMHS, 3 equiv.	KO*t*Bu, 5%	2 Days	98
29		PMHS, 3 equiv.	KOH, 5%	2 days	98 (50)
30		$MeSiH_3$, 3 equiv.	KO*t*Bu, 5%	2 days	98 (93)
31	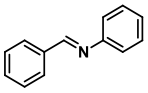	PMHS, 3 equiv.	KO*t*Bu, 5%	2 days	98[c]
32		PMHS, 3 equiv.	KOH, 5%	2 days	98 (82)[c]
33		$PhSiH_3$, 1.1 equiv.	KO*t*Bu, 5%	15 h	98[c]
34	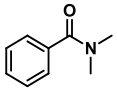	PMHS, 3 equiv.	KOH, 5%	2 days	98 (14)[d]
35[f]		$PhSiH_3$, 1.1 equiv.	KO*t*Bu, 5%	18 h	98

[a] For the generation of $MeSiH_3$, see the procedure described above. [b] Conversion to alcohol determined by NMR, isolated yield in brackets. [c] amine product. [d] benzyl alcohol product. [e] room temperature. [f] heating at 70 ^oC.

In addition to aldehydes, ketones and esters, the activity of the silane-base system was shown to be sufficient for the reduction of aldimines and tertiary amides (results also shown in **Table 8**). The amide reduction on the 2 mmol scale (entry 34) resulted in a mixture of products, of which only benzyl alcohol was isolated.

Unfortunately, there were no reactions with primary and secondary amides and ketimines.

These results differ from those obtained by Nolan and Cui, where tertiary amides were reduced into amines under solvent-free conditions.[68c, 202]

2.3.5 Selectivity.

The hydrosilylation of multifunctional substrates, containing both the aldehyde and ketone groups, by a 1/3 molar equivalent of H_3SiPh showed chemoselective reduction of the aldehyde functionality. This result is consistent with previous literature observations that aldehydes are more reactive substrates in hydrosiylation. Under the same conditions of a careful control of hydride content, the reduction of $MeO_2CC_6H_4C(=O)Me$ gave exclusively the product of ketone hydrosilylation, with complete retention of the ester group (**Scheme 35**).

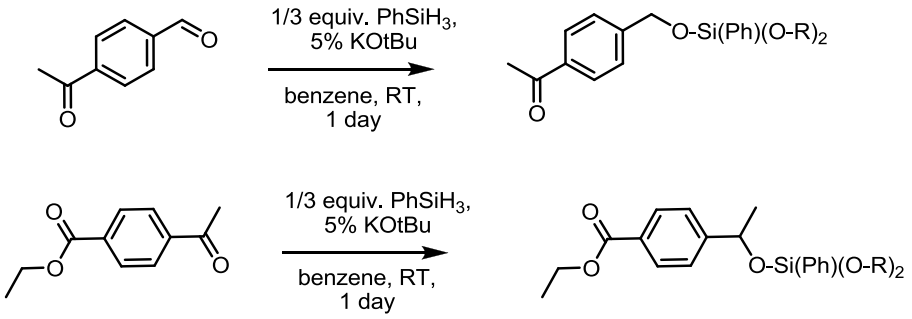

Scheme 35: Reduction of bifunctional substrates. Only one hydrosilylation product is shown, however a mixture of alkoxy silanes was observed in due to substituent rearrangement at the silicone center.

The C=C double bonds (entries 6, 9, 10 and 14 of **Table 8**) and C≡C triple bonds (entry 15 of **Table 8**) are tolerated under these reaction conditions. Although

attempts to isolate products on the 2 mmol scale failed, our additional experiments with 1-hexene and 3-hexyne showed that isolated double and triple bonds do not react.

The tolerance to the nitro-group (entries 7-8 of **Table 8**) was also confirmed by an experiment with nitrobenzene, which resulted in the retention of this functionality.

In the reaction with 4-cyclohexen-1-one, the reduction of keto group tolerated the presence of the double bond which remained intact. However, the isolated yield was low, either because of the formation of multiple product or due to retention of the product in the silicon gum.

Reaction with styrene oxide resulted in a complex mixture of products without retaining of the epoxy group.

2.3.6 Reduction of heterocycles.

Reduction of heterocycles by base-activated silanes was attempted on both NMR and preparative (2 mmol) scales. While the NMR scale reactions showed high consumption of such substrates as quinoline, iso-quinoline, various substituted quinolines, quinoxaline, pyrimidine and triazine (**Table 9**), apparently the products formed were too strongly bound to the insoluble silicon "gum", so that interpretation of spectra was not possible. This is also the reason why the term "consumption" is used instead of "conversion", since the conversion products could not be assigned.

In the 2 mmol-scale reactions complex mixtures of products were formed which proved difficult for separation by column chromatography. Also, an efficient work-up protocol for these reactions still has to be developed, since the problem of

product binding to the silicon "gum", encountered in the NMR-scale reactions, remains unsolved even in cases when methylsilane was used as the reducing reagent.

Table 9: Reduction of heterocyclic compounds with base-activated silanes on NMR-scale.

Entry	Substrate	Silane	Base	Temp.	Time	Conversion, %
1	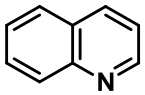	PMHS, 5 equiv.	KOtBu, 5%	70°C	7 days	100 (no starting material signal)
2		PMHS, 5 equiv.	KOtBu, 5%	70°C	3 days	0
3		$PhSiH_3$, 5 equiv.	KOtBu, 5%	70°C	3 days	0
4	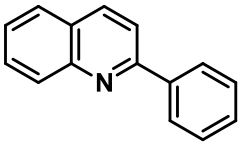	PMHS, 5 equiv.	KOtBu, 5%	70°C	16 h	80% consumption of substrate, no data for product characterization available
5		PMHS, 5 equiv.	KOtBu, 5%	70°C	16 h	100 (no starting material signal)
6	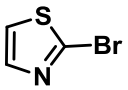	PMHS, 5 equiv.	KOtBu, 5%	70°C	16 h	100 (no starting material signal)
7	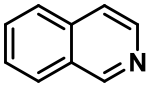	PMHS, 5 equiv.	KOtBu, 5%	70°C	6 days	90

8	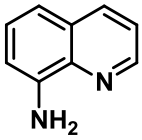	PMHS, 5 equiv.	KOtBu, 5%	70°C	6 days	100 (no starting material signal)
		PMHS, 5 equiv.	KOtBu, 5%	120°C	4 days	99
	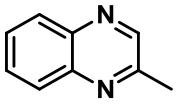	PMHS, 5 equiv.	KOtBu, 5%	120°C	4 days	85
	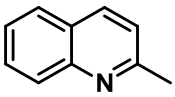	PMHS, 5 equiv.	KOtBu, 5%	120°C	4 days	80% no data for product characterization available
		PMHS, 5 equiv.	KOtBu, 5%	70°C	16 h	100 (no starting material signal)

2.4 Conclusion

A simple base-catalyzed reduction of ketones, esters, aldimines and tertiary amides by PMHS was discovered and mechanistic aspects of this process were revealed. NMR- and 2 mmol-scale reactions were conducted and isolated yields are reported.

It was found that the base catalyst causes a rearrangement of hydrosiloxanes into light silanes (e.g. H_2SiMe_2, H_3SiMe), and a very practical method of generating and using these compounds as reducing agents was developed. Further reaction of thus produced silanes with a base results in silicates, which are the actual reducing species.

For the silane H_3SiPh having a labile Si-aryl bond, the formation of several silicate species stemming from the H/OR, H/Ph, and Ph/OR exchange was identified by NMR. Kinetic measurements by EXSY NMR for the exchange between [Ph(*t*BuO)SiH_3]K and [$PhSiH_4$]K/ [SiH_4]K suggest that the exchange proceeds via an associative mechanism, likely including a doubly-bridged six-coordinated silicon centers.

Reduction of heterocyclic compounds was attempted. While NMR-scale reactions showed promising results with the consumption of substrates, not much success was achieved in larger scaled reactions mostly likely because of problems with isolation.

2.5 Experimental

General.

Unless otherwise stated, all manipulations were carried out by using conventional inert atmosphere glove-box and Schlenk techniques. Dry diethyl ether, toluene, and hexanes, were obtained, using Grubbs-type purification columns, other solvents were dried by distillation from appropriate drying agents. Column chromatography was performed using silica gel 70-230 mesh, 60Å, purchased from Aldrich. Solvents for chromatography were technical grade. Analytical thin-layer chromatography (TLC) was performed on silica gel 60 plates with F_{254} UV-active indicator purchased from EMD. TLC was visualised with UV-irradiation. NMR spectra were obtained with a Bruker DPX-300 and Bruker DPX-600 instruments (^{1}H: 300 and 600 MHz; ^{13}C: 75.5 and 151 MHz; ^{29}Si: 59.6 and 119.2 MHz). NMR analysis was done at room temperature unless specified. All NMR tube reactions and kinetic experiments were done under nitrogen atmosphere using J. Young type NMR tubes equipped with Teflon valves. 1D EXSY experiments were carried as previously described. [235] $PhSiCl_3$, $HSi(OEt)_3$, TMDS were purchased from Aldrich. PMHS was obtained from Alfa Aesar. Aldehydes and ketones were purchased from Aldrich, except pyridine-3-carboxaldehyde and 4-chloroacetophenone which were purchased from Alfa Aesar. Esters were from Aldrich, except ethyl benzoate, phenyl benzoate, ethyl-4-dimethylaminobenzoate and ethyl-4-nitrobenzoate which were purchased from Alfa Aesar. Heterocyclic compounds were obtained in Alfa Aesar, except quinoline and isoquinoline were purchased from Aldrich. $PhSiH_3$ was prepared from $PhSiCl_3$ by treatment with $LiAlH_4$ followed by hydrolysis and vacuum distillation.

General procedure for NMR reactions. In the glove box an J. Young type NMR tube was loaded with the solution of substrate (0.072 mmol) and KO*t*Bu (5% of

silane) in dry deuterated or non-deuterated solvent (D_2O insert was used in this case). Then a silane (1.1-2.5 eq) was added into the tube by syringe and the cap was immediately sealed. The reaction was monitored by NMR. Depending on the experimental conditions, some of the tubes were heated up to 70^{o}C in the oil bath for the time periods given in Tables 6-9.

General procedure for the reduction of aldehydes and ketones. In the glove box, a vial equipped with a septum cap was loaded with a substrate (2 mmol), KOH (14 mg, 0.25 mmol) and 5 ml of dry THF. Then the vial was capped and PMHS (5 mmol, 300 μl) was syringed into the reaction mixture. The reaction was stirred at room temperature for 2 days. A gas formation was observed. After 2 days the reaction was quenched with KOH and methanol solution and stirred at room temperature for 2 more hours. Then the solvent was removed in *vacuo* and the residue was extracted with diethyl ether (50 ml× 3). Combined organic fractions were dried to yield a pure product. No further purification was required.

General procedure for ester reduction with PMHS. In the glove box, a vial equipped with a septum cap was loaded with a substrate (2 mmol), KOH (14 mg, 0.25 mmol) and 5 ml of dry THF. Then the vial was capped and PMHS (5 mmol, 300 μl) was syringed into the reaction mixture. The reaction was stirred at 70^{o}C for 2 days. A gas formation was observed. After 2 days an aliquot was taken from the reaction mixture to check the conversion yield by NMR. Then the reaction was quenched with KOH, water and methanol solution and stirred at 70^{o}C overnight. The solvent was removed in *vacuo* and the residue was extracted with diethyl ether (50 ml×3). Combined organic fractions were dried to yield pure product. No further purification was required in cases when the substrate was an ethanol derivative. Products of other

derivatives were purified by silica gel column chromatography (EtOAc : Hexanes 1:4).

General procedure for ester reduction with $MeSiH_3$. The reaction was performed in a custom made glassware unit consisting of two ampoules equipped with Teflon stopcocks and interconnected through a Teflon valve (Fig. 2). The first compartment was loaded with KO*t*Bu (112 mg, 1 mmol) and dry THF (10 ml) and frozen with liquid nitrogen. PMHS (20 mmol, 1.2 ml) was added under a stream of nitrogen. The ampoule was closed, warmed to room temperature and heated at 70 ^{o}C for 2 h. Meanwhile the second ampoule was loaded with a substrate (2 mmol), KO*t*Bu (0.35 mmol, 40 mg) and 5 ml of dry THF. When the heating of the first ampoule finished, the second part was frozen with liquid nitrogen and the connecting valve was opened. The $MeSiH_3$, formed in the first part was transferred and condensed into the second ampoule. When the transfer was complete, the valve was closed and the reaction mixture was warmed to room temperature and then heated at 70^{o}C for two days. After 2 days the reaction was quenched with aqueous solution of KOH and stirred at room temperature overnight. Then the solvent was removed *in vacuo* and the residue was extracted with diethyl ether (50 ml×3). Combined organic fractions were washed with water and brine, dried over $MgSO_4$ and evaporated to yield the pure product. No further purification was required in cases when the substrate was an ethanol derivative. Products of other derivatives were purified by silica gel column chromatography (EtOAc : Hexanes 1:4).

2.5.1 Product characterization for 2 mmol-scale reactions

Ketones reduction.

Substrate: acetophenone, 2 mmol (234 μl).

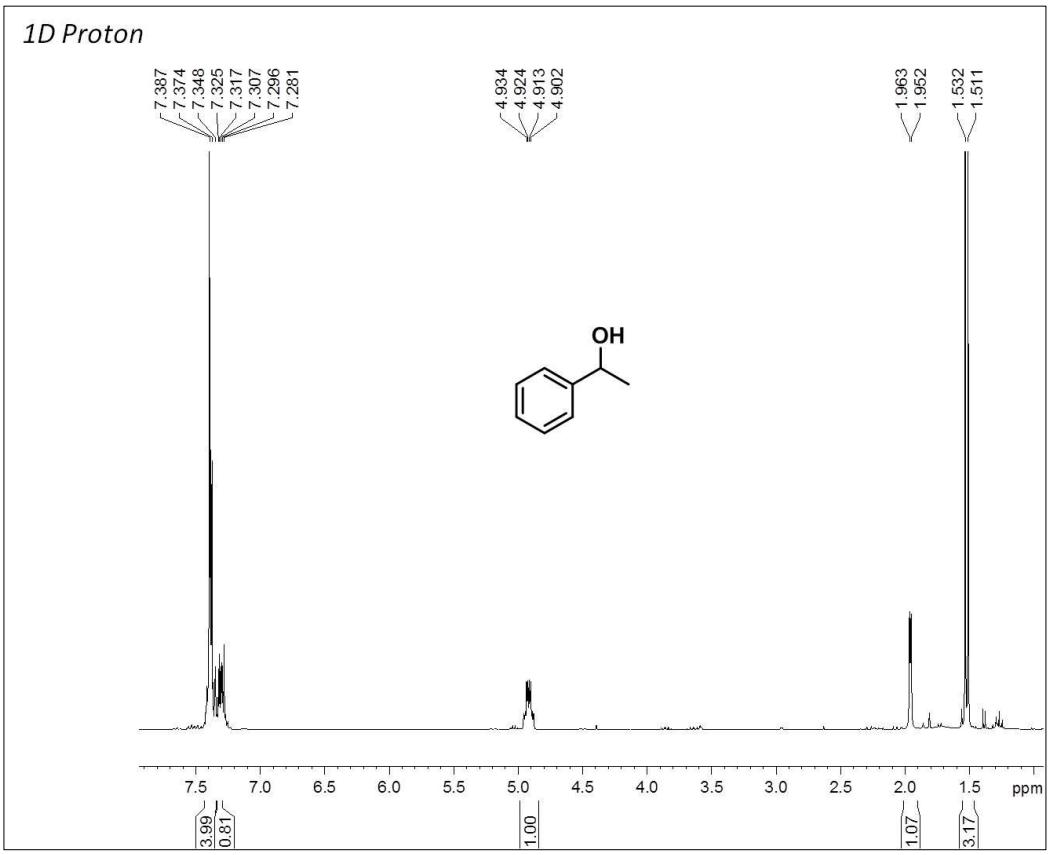

^{1}H NMR (300 MHz, $CDCl_3$): δ 7.37 (m, 4H), 7.29 (m, 1H), 4.92 (m, 1H), 1.95 (d, 3.36 Hz), 1.52 (d, 6.49 Hz, 3H). Data is consistent with literature values.[236]

Substrate: p-nitroacetophenone, 2 mmol, 330 mg.

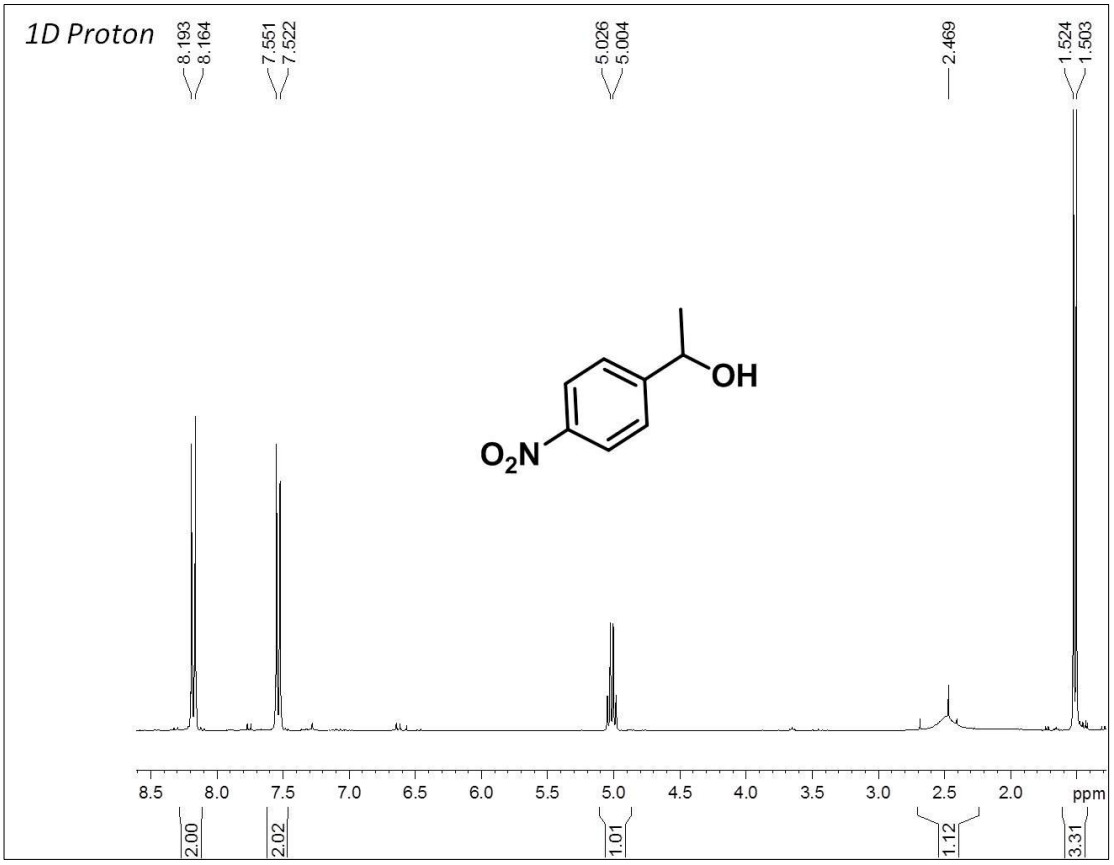

^{1}H NMR (300 MHz, $CDCl_3$): δ 8.17 (d, J = 9.1 Hz, 2H), 7.53 (d, J = 9.1 Hz, 2H), 5.01 (q, J = 7.1 Hz, 1H), 2.47 (br. s, 1H), 1.51 (d, J = 6.6 Hz, 3H). Data is consistent with literature values. [237]

Substrate: 2-acetopyridine, 2 mmol, 240µl.

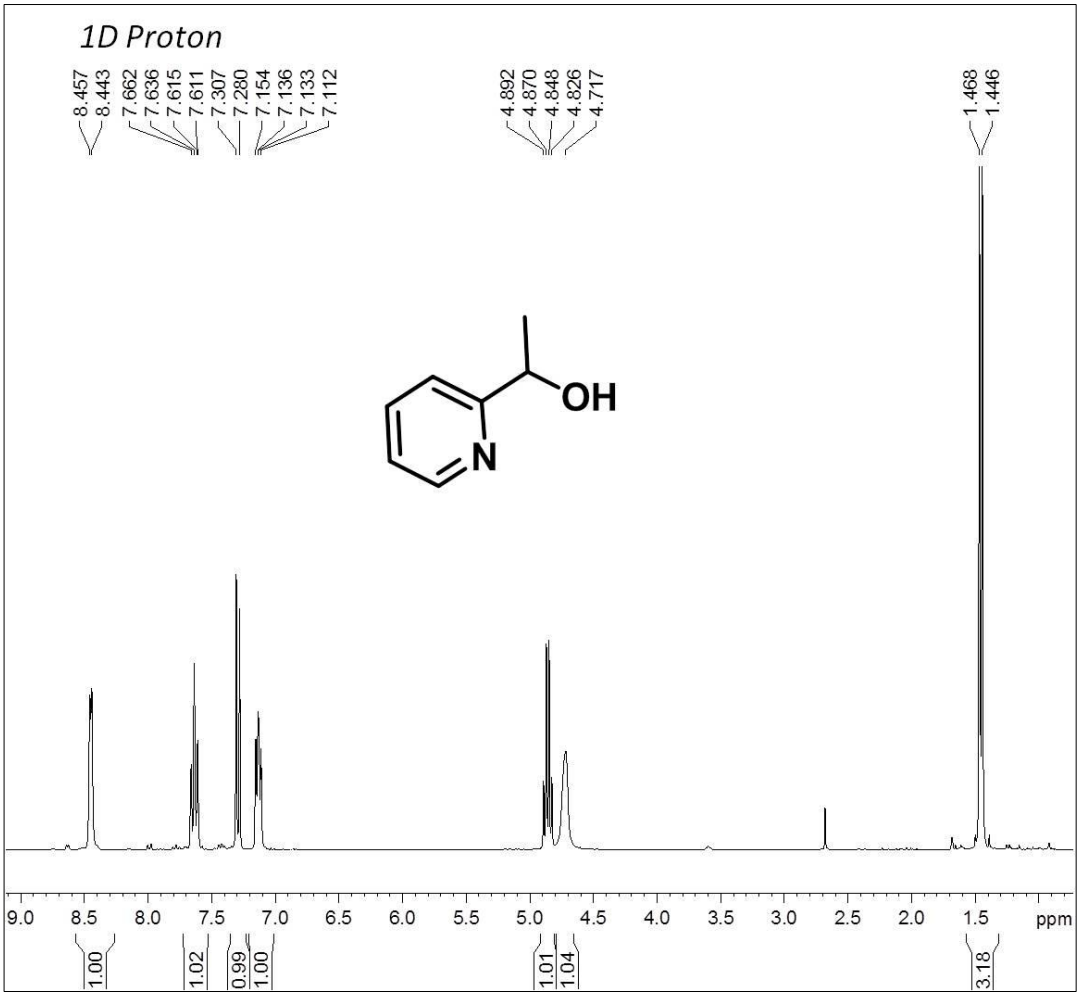

^{1}H NMR (300 MHz, $CDCl_3$): δ 8.45 (d, J = 3.7, 1H), 7.63 (t, J = 7.5, 1H), 7.29 (d, J = 7.5 Hz, 1H), 7.13 (m, 1H), 4.85 (q, J = 6.5 Hz, 1H), 4.71 (br.s., 1H), 1.45 (d, J = 6.5Hz, 3H). Data is consistent with literature values.[238]

Substrate: m-nitroacetophenone, 2 mmol, 330 mg.

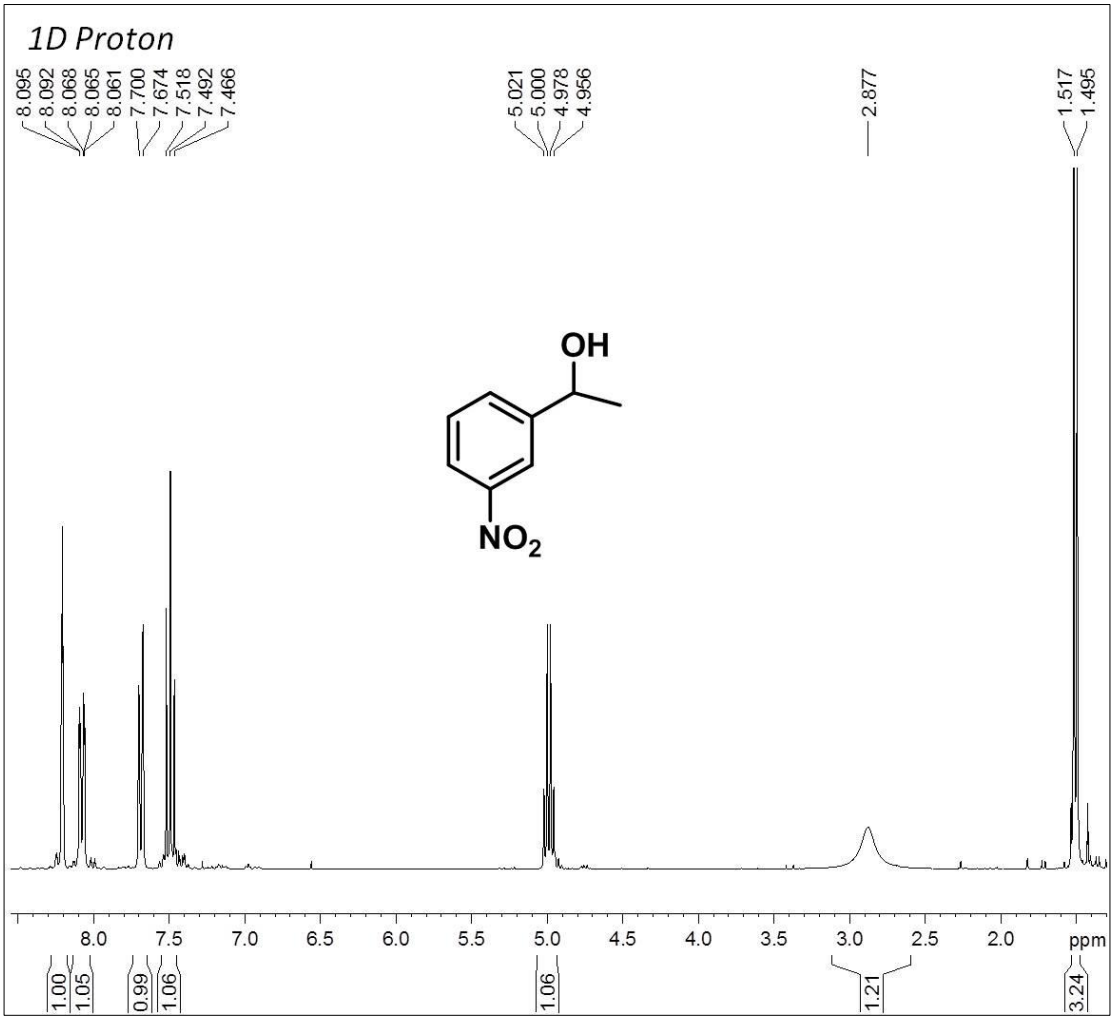

^{1}H NMR (300 MHz, $CDCl_3$): δ 8.21 (m, 1H), 8.07 (m, 1H), 7.68 (d, J = 7.6 Hz, 1H), 7.49 (m, 1H), 5.01 (q, J = 6.5 Hz, 1H), 2.88 (br s, 1H), 1.50 (d, J = 6.3 Hz, 3H). Data is consistent with literature values. [239]

Substrate: p-methoxyacetophenone,2 mmol, 300 mg.

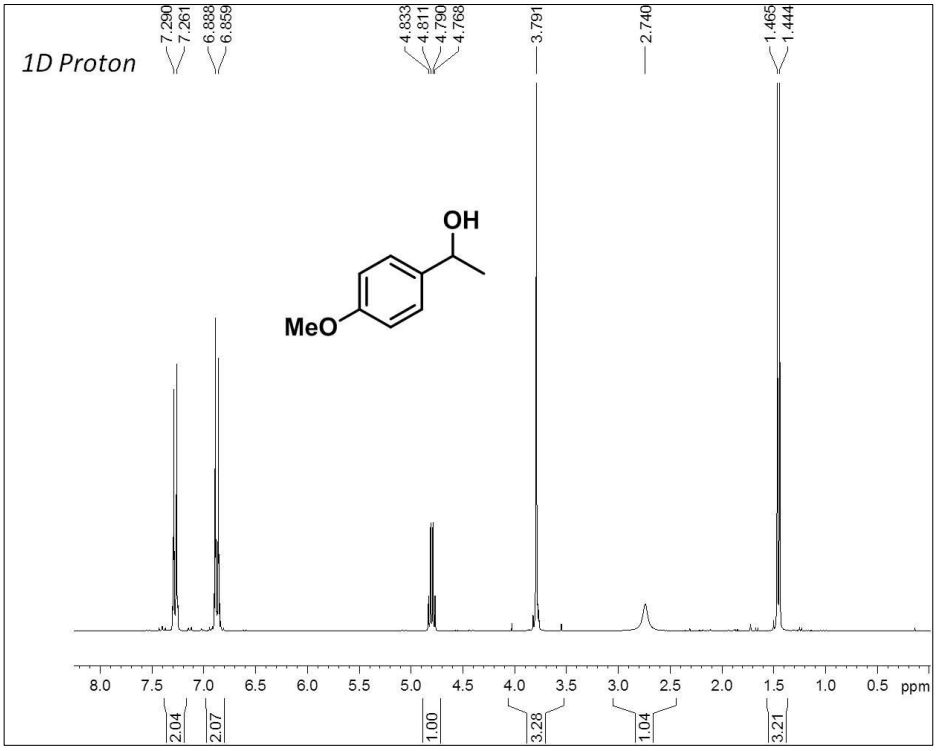

^{1}H NMR (300 MHz, $CDCl_3$): δ 7.27 (d, J = 8.5 Hz, 2H), 6.87 (d, J = 8.8 Hz, 2H), 4.80 (q, J = 6.5 Hz, 1H), 3.79 (s, 3H), 2.74 (br s, 1H), 1.45 (d, J = 6.3 Hz, 3H). Data is consistent with literature values.[238]

Substrate: benzophenone, 2 mmol, 364 mg.

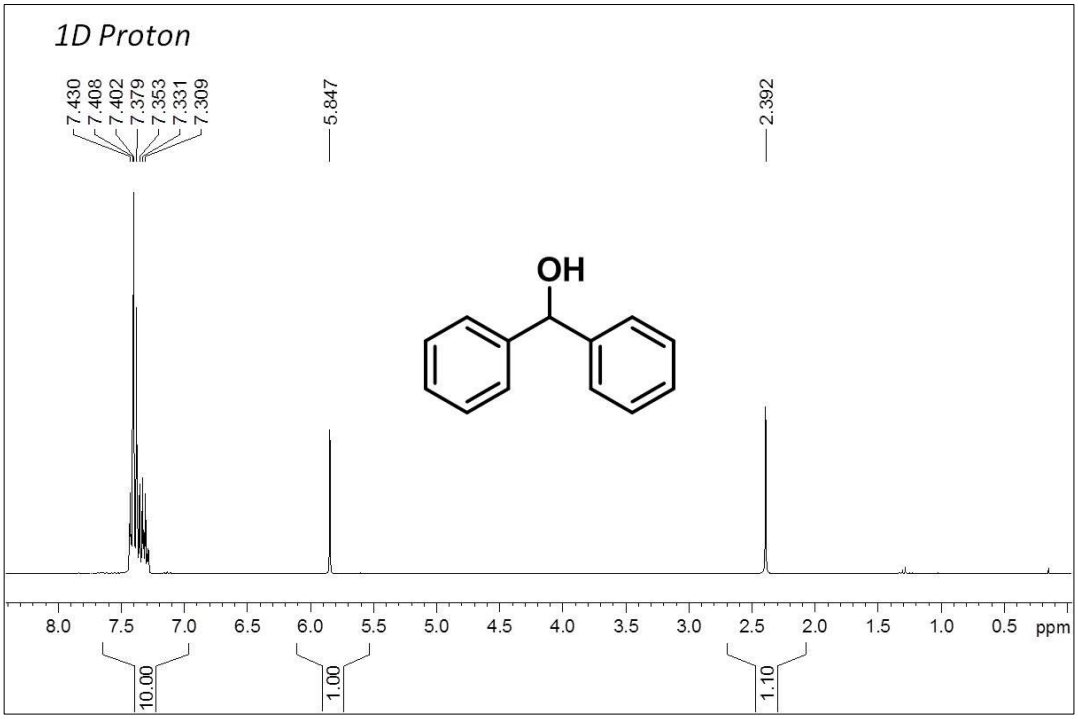

^{1}H NMR (300 MHz, $CDCl_3$): δ 7.30-7.43 (m, 10H), 5.85 (s, 1H), 2.39 (s, 1H). Data is consistent with literature values.[240]

Esters reduction (2 mmol scale).

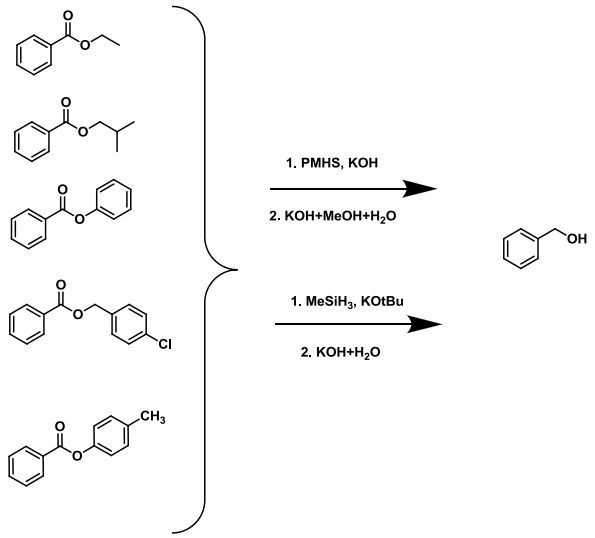

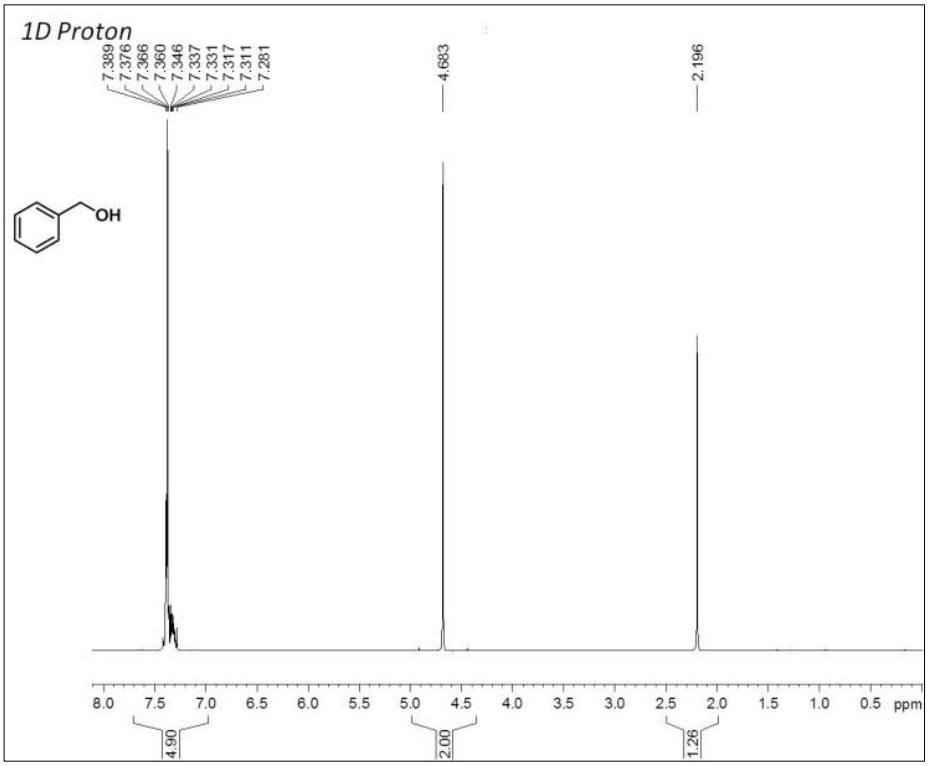

^{1}H NMR (300 MHz, $CDCl_3$): δ 7.33(m, 5H), 4.68 (s, 2H), 2.20 (s, 1H). Characterization is consistent with literature values.[241]

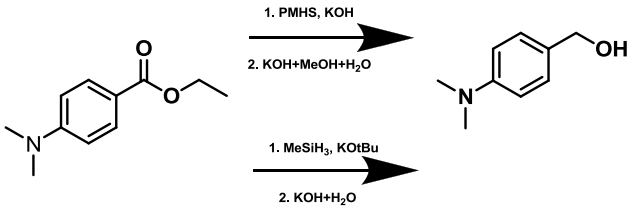

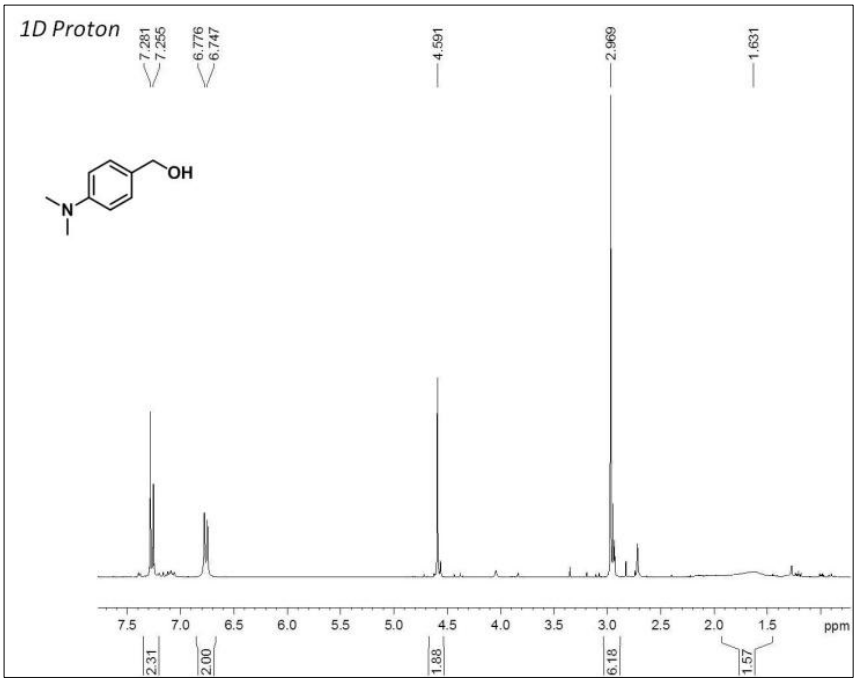

^{1}H NMR (300 MHz, $CDCl_3$): δ 7.26 (m, 2H), 6.76 (m, 2H), 4.59 (s, 2H), 2.97 (s, 6H), 1.63 (br.s., 1H). Data is consistent with literature values.[242]

Aldimine reduction, 2 mmol.

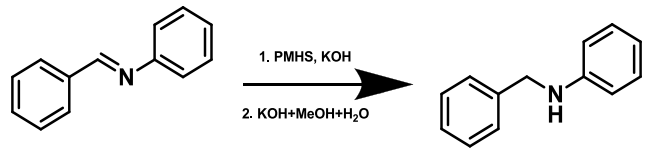

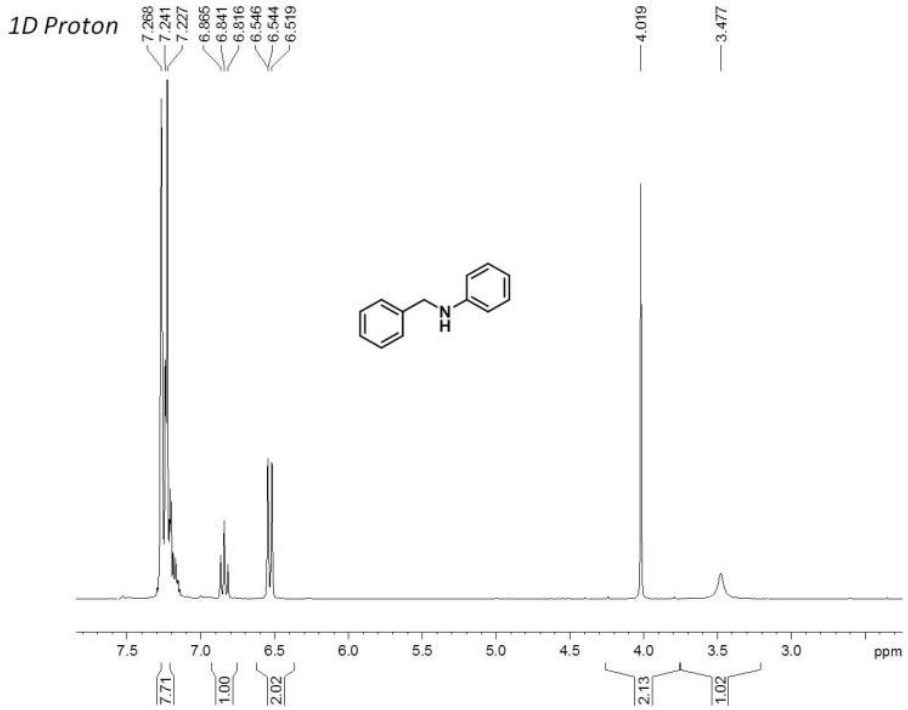

^{1}H NMR (300 MHz, C_6D_6): δ 7.25 (m, 7H), 6.84 (m, 1H), 6.53 (d, J = 7.8 Hz, 2H), 4.02 (s, 2H), 3.48 (br. s., 1H). Data is consistent with literature values.[243]

Tertiary amide reduction, 2 mmol.

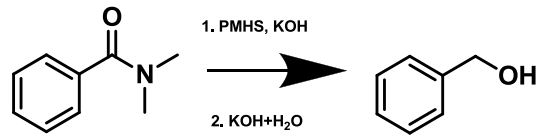

For product data see esters reduction.

3 References

1. Inc., G. I. Global Market for Magnetic Materials to Reach $33 Billion by 2018. (accessed 13/05/2013).

2. Miller, J. S.; Epstein, A. J.*MRS Bull.* **2000,** *25*, 21-30.

3. Yakhmi, J. V.*Bull. Mater. Sci.* **2009,** *32*, 217-225.

4. (a) Yakhmi, J. V.*Macromol. Symp.* **2004,** *212*, 141-158; (b) Lemaire, M. T.*Pure Appl. Chem.* **2011,** *83*, 141-149.

5. Coey, J. M. D., *Magnetism and Magnetic Materials*. Cambridge University Press: New York, 2010.

6. Miller, J. S.; Epstein, A. J.*Angew. Chem. Int. Ed.* **1994,** *33*, 385-415.

7. Caneschi, A.; Gatteschi, D.; Sessoli, R.; Rey, P.*Acc. Chem. Res.* **1989,** *22*, 392-398.

8. (a) Iwamura, H.*Pure Appl. Chem.* **1986,** *58*, 187-196; (b) Sugawara, T.; Murata, S.; Kimura, K.; Iwamura, H.; Sugawara, Y.; Iwasaki, H.*J. Am. Chem. Soc.* **1985,** *107*, 5293-5294.

9. Iwamura, H.*Pure Appl. Chem.* **1993,** *65*, 57-64.

10. Rajca, A.*Chem. Rev.* **1994,** *94*, 871-893.

11. Bleaney, B.; Bowers, K. D.*Proc. R. Soc. London, Ser. A* **1952,** *214*, 451-465.

12. Maurer, J. A. I. Structure-function analysis of the mechanosensitive channel of large conductance. II. Design of novel magnetic materials using crystal engineering. PhD, California Institute of Technology, Pasadena, USA, 2003.

13. Cullity, B. D.; Graham, C. D., *Introduction to magnetic materials*. John Wiley&Sons: Hoboken, 2009.

14. W.G. Jenks; S.S.H. Sadeghi ; J. P.Wikswo.*J. Phys. D: Appl. Phys.* **1997,** *30*, 293–323.

15. (a) Evans, D. F.*J. Chem. Soc.* **1959**, 2003-2005; (b) Evans, D. F.; Fazakerley, G. V.; Phillips, R. F.*J. Chem. Soc. A* **1971**, 1931-1934; (c) Evans, D. F.; Jakubovic, D. A.*J. Chem. Soc., Dalton Trans.* **1988**, 2927-2933.

16. (a) Naklicki, M. L.; White, C. A.; Plante, L. L.; Evans, C. E. B.; Crutchley, R. J.*Inorg. Chem.* **1998,** *37*, 1880-1885; (b) Turner, J. W.; Schultz, F. A.*Inorg. Chem.* **2001,** *40*, 5296-5298.

18. (a) Evans, D. F.*J. Chem. Soc. A* **1967**, 1670-1671; (b) Saunderson, A.*Phys. Ed.* **1968,** *3*, 272-275; (c) Viswanadham, P.*J. Chem. Educ.* **1978,** *55*, 54.

19. Gütlich, P.; Bill, E.; Trautwein, A. X., *Mössbauer Spectroscopy and Transition Metal Chemistry*. Springer-Verlag: Berlin Heidelberg, 2011.

20. Kalska-Szostko, B. Mössbauer Spectroscopy on Selected Magnetic Compounds. PhD Dissertation, Uppsala University, Uppsala, 2000.

21. Gütlich, P.; Bhattacharjee, A.; Seredyuk, M.; Gaspar, A. B.*Hyperfine Interact.* **2009,** *189*, 3–19.

22. McMillan, F.; Evans, D. Introduction to Mössbauer Spectroscopy. (accessed 2013).

23. Klingele, M. H.; Moubaraki, B.; Cashion, J. D.; Murray, K. S.; Brooker, S.*Chem. Commun.* **2005**, 987-989.

24. (a) Bagai, R.; Christou, G.*Chem. Soc. Rev.* **2009,** *38*, 1011-1026; (b) Epstein, A. J.*MRS Bull.* **2000,** *25*, 33-40.

25. (a) Sessoli, R., Gatteschi, D., Caneschi, A., Novak, M. A.*Nature* **1993,** *365*, 141-143; (b) Christou, G.; Gatteschi, D.; Hendrickson, D. N.; Sessoli, R.*MRS Bull.* **2000,** *25*, 66-71.

26. (a) Sessoli, R.; Powell, A. K.*Coord. Chem. Rev.* **2009,** *253*, 2328-2341; (b) Sessoli, R.; Tsai, H. L.; Schake, A. R.; Wang, S.; Vincent, J. B.; Folting, K.;

Gatteschi, D.; Christou, G.; Hendrickson, D. N.*J. Am. Chem. Soc.* **1993,** *115*, 1804-1816.

27. Sun, W.-B.; Han, B.-L.; Lin, P.-H.; Li, H.-F.; Chen, P.; Tian, Y.-M.; Murugesu, M.; Yan, P.-F.*J. Chem. Soc., Dalton Trans.* **2013,** *42*, 13397-13403.

28. Fortier, S.; Le Roy, J. J.; Chen, C.-H.; Vieru, V.; Murugesu, M.; Chibotaru, L. F.; Mindiola, D. J.; Caulton, K. G.*J. Am. Chem. Soc.* **2013,** *135*, 14670-14678.

29. Siladke, N. A.; Meihaus, K. R.; Ziller, J. W.; Fang, M.; Furche, F.; Long, J. R.; Evans, W. J.*J. Am. Chem. Soc.* **2011,** *134*, 1243-1249.

30. Feng, X.; Mathonière, C.; Jeon, I.-R.; Rouzières, M.; Ozarowski, A.; Aubrey, M. L.; Gonzalez, M. I.; Clérac, R.; Long, J. R.*J. Am. Chem. Soc.* **2013,** *135*, 15880-15884.

31. Bogani, L.; Vindigni, A.; Sessoli, R.; Gatteschi, D.*J. Mater. Chem.* **2008,** *18*, 4750-4758.

32. (a) Glauber, R. J.*J. Math. Phys.* **1963,** *4*, 294-307; (b) Caneschi, A.; Gatteschi, D.; Lalioti, N.; Sangregorio, C.; Sessoli, R.; Venturi, G.; Vindigni, A.; Rettori, A.; Pini, M. G.; Novak, M. A.*Angew. Chem. Int. Ed.* **2001,** *40*, 1760-1763.

33. Fehlhammer, W. P.; Fritz, M.*Chem. Rev.* **1993,** *93*, 1243-1280.

34. Sieklucka, B.; Podgajny, R.; Korzeniak, T.; Nowicka, B.; Pinkowicz, D.; Kozieł, M.*Eur. J. Inorg. Chem.* **2011,** *2011*, 305-326.

35. Entley, W. R.; Girolami, G. S.*Science* **1995,** *268*, 397-400.

36. Holmes, S. M.; Girolami, G. S.*J. Am. Chem. Soc.* **1999,** *121*, 5593-5594.

37. Wang, S.; Ding, X.-H.; Zuo, J.-L.; You, X.-Z.; Huang, W.*Coord. Chem. Rev.* **2011,** *255*, 1713-1732.

38. Beltran, L. M. C.; Long, J. R.*Acc. Chem. Res.* **2005,** *38*, 325-334.

39. Berseth, P. A.; Sokol, J. J.; Shores, M. P.; Heinrich, J. L.; Long, J. R.*J. Am. Chem. Soc.* **2000,** *122*, 9655-9662.

40. Sokol, J. J.; Shores, M. P.; Long, J. R.*Inorg. Chem.* **2002,** *41*, 3052-3054.

41. Sieklucka, B.; Szklarzewicz, J.; Kemp, T. J.; Errington, W.*Inorg. Chem.* **2000,** *39*, 5156-5158.

42. Zhong, Z. J.; Seino, H.; Mizobe, Y.; Hidai, M.; Fujishima, A.; Ohkoshi, S.-i.; Hashimoto, K.*J. Am. Chem. Soc.* **2000,** *122*, 2952-2953.

43. Ratera, I.; Veciana, J.*Chem. Soc. Rev.* **2012,** *41*, 303-349.

44. (a) Gomberg, M.*J. Am. Chem. Soc.* **1900,** *22*, 757-771; (b) Gomberg, M.*J. Am. Chem. Soc.* **1901,** *23*, 496-502; (c) Gomberg, M.*Chem. Rev.* **1924,** *1*, 91-141.

45. (a) Domingo, V. M.; Castaner, J.*Chem. Commun.* **1995**, 895-896; (b) Armet, O.; Veciana, J.; Rovira, C.; Riera, J.; Castaner, J.; Molins, E.; Rius, J.; Miravitlles, C.; Olivella, S.; Brichfeus, J.*J. Phys. Chem.* **1987,** *91*, 5608-5616.

46. (a) Koivisto, B. D.; Hicks, R. G.*Coord. Chem. Rev.* **2005,** *249*, 2612-2630; (b) Train, C.; Norel, L.; Baumgarten, M.*Coord. Chem. Rev.* **2009,** *253*, 2342-2351.

47. Tamura, M.; Nakazawa, Y.; Shiomi, D.; Nozawa, K.; Hosokoshi, Y.; Ishikawa, M.; Takahashi, M.; Kinoshita, M.*Chem. Phys. Lett.* **1991,** *186*, 401-404.

48. Chiarelli, R. N., M. A.; Rassat, A.; Tholence, J. L.*Nature* **1993,** *363*, 147-149.

49. Ishida, T.; Shinozuka, K.; Kubota, M.; Ohashi, M.; Nogami, T.*Chem. Commun.* **1995**, 1841-1842.

50. Nakasuji, K.; Yamaguchi, M.; Murata, I.; Yamaguchi, K.; Fueno, T.; Ohya-Nishiguchi, H.; Sugano, T.; Kinoshita, M.*J. Am. Chem. Soc.* **1989,** *111*, 9265-9267.

51. Goto, K.; Kubo, T.; Yamamoto, K.; Nakasuji, K.; Sato, K.; Shiomi, D.; Takui, T.; Kubota, M.; Kobayashi, T.; Yakusi, K.; Ouyang, J.*J. Am. Chem. Soc.* **1999,** *121*, 1619-1620.

52. Sarkar, A.; Itkis, M. E.; Tham, F. S.; Haddon, R. C.*Chem. - Eur. J.* **2011,** *17*, 11576-11584.

53. Yoshioka, T.; Watanabe, K.; Ohya-Nishiguchi, H.*Bull. Chem. Soc. Jpn.* **1975,** *48*, 2533-2537.

54. Pearson, G. A.; Walter, R. I.*J. Am. Chem. Soc.* **1977,** *99*, 5262-5268.

55. Rajca, A.; Utamapanya, S.; Xu, J.*J. Am. Chem. Soc.* **1991,** *113*, 9235-9241.

56. Bushby, R. J.; Taylor, N.; Williams, R. A.*J. Mater. Chem.* **2007,** *17*, 955-964.

57. (a) Ito, A.; Urabe, M.; Tanaka, K.*Angew. Chem. Int. Ed.* **2003,** *42*, 921-924; (b) Hirao, Y.; Urabe, M.; Ito, A.; Tanaka, K.*Angew. Chem. Int. Ed.* **2007,** *46*, 3300-3303.

58. Seeger, D. E.; Berson, J. A.*J. Am. Chem. Soc.* **1983,** *105*, 5144-5146.

59. Ito, A.; Hata, K.; Kawamoto, K.; Hirao, Y.; Tanaka, K.; Shiro, M.; Furukawa, K.; Kato, T.*Chem. - Eur. J.* **2010,** *16*, 10866-10878.

60. Rajca, A.; Utamapanya, S.; Thayumanavan, S.*J. Am. Chem. Soc.* **1992,** *114*, 1884-1885.

61. Rajca, A.; Utamapanya, S.*Mol. Cryst. Liq. Cryst. Sci. Technol., Sect. A* **1993,** *232*, 305-312.

62. Rajca, A.; Wongsriratanakul, J.; Rajca, S.*Science* **2001,** *294*, 1503-1505.

63. Bushby, R. J.; Kilner, C. A.; Taylor, N.; Vale, M. E.*Tetrahedron* **2007,** *63*, 11458-11466.

64. Fukuzaki, E.; Nishide, H.*J. Am. Chem. Soc.* **2005,** *128*, 996-1001.

65. Yen, H.-J.; Lin, H.-Y.; Liou, G.-S.*Chem. Mater.* **2011,** *23*, 1874-1882.

66. Vostrikova, K. E.*Coord. Chem. Rev.* **2008,** *252*, 1409-1419.

67. (a) Anderson, O. P.; Kuechler, T. C.*Inorg. Chem.* **1980,** *19*, 1417-1422; (b) Bencini, A.; Benelli, C.; Gatteschi, D.; Zanchini, C.*J. Am. Chem. Soc.* **1984,** *106*,

5813-5818; (c) Grand, A.; Rey, P.; Subra, R.*Inorg. Chem.* **1983,** *22*, 391-394; (d) Caneschi, A.; Gatteschi, D.; Laugier, J.; Rey, P.*J. Am. Chem. Soc.* **1987,** *109*, 2191-2192; (e) Caneschi, A.; Gatteschi, D.; Grand, A.; Laugier, J.; Pardi, L.; Rey, P.*Inorg. Chem.* **1988,** *27*, 1031-1035.

68. (a) Caneschi, A.; Gatteschi, D.; Rey, P.; Sessoli, R.*Inorg. Chem.* **1988,** *27*, 1756-1761; (b) Fegy, K.; Sanz, N.; Luneau, D.; Belorizky, E.; Rey, P.*Inorg. Chem.* **1998,** *37*, 4518-4523; (c) Xie, W.; Zhao, M.; Cui, C.*Organometallics* **2013, DOI: 10.1021/om400951n**.

69. Kumada, H.; Sakane, A.; Koga, N.; Iwamura, H.*J. Chem. Soc., Dalton Trans.* **2000,** *0*, 911-914.

70. Brook, D. J. R.; Lynch, V.; Conklin, B.; Fox, M. A.*J. Am. Chem. Soc.* **1997,** *119*, 5155-5162.

71. Hicks, R. G.; Lemaire, M. T.; Thompson, L. K.; Barclay, T. M.*J. Am. Chem. Soc.* **2000,** *122*, 8077-8078.

72. Barclay, T. M.; Hicks, R. G.; Lemaire, M. T.; Thompson, L. K.*Inorg. Chem.* **2001,** *40*, 5581-5584.

73. Hearns, N. G. R.; Preuss, K. E.; Richardson, J. F.; Bin-Salamon, S.*J. Am. Chem. Soc.* **2004,** *126*, 9942-9943.

74. Britten, J.; Hearns, N. G. R.; Preuss, K. E.; Richardson, J. F.; Bin-Salamon, S.*Inorg. Chem.* **2007,** *46*, 3934-3945.

75. Hearns, N. G. R.; Fatila, E. M.; Clérac, R.; Jennings, M.; Preuss, K. E.*Inorg. Chem.* **2008,** *47*, 10330-10341.

76. Hearns, N. G. R.; Clerac, R.; Jennings, M.; Preuss, K. E.*J. Chem. Soc., Dalton Trans.* **2009**, 3193-3203.

77. Jennings, M.; Preuss, K. E.; Wu, J.*Chem. Commun.* **2006**, 341-343.

78. Wu, J.; MacDonald, D. J.; Clérac, R.; Jeon, I.-R.; Jennings, M.; Lough, A. J.; Britten, J.; Robertson, C.; Dube, P. A.; Preuss, K. E.*Inorg. Chem.* **2012,** *51*, 3827-3839.

79. Fatila, E. M.; Goodreid, J.; Clerac, R.; Jennings, M.; Assoud, J.; Preuss, K. E.*Chem. Commun.* **2010,** *46*, 6569-6571.

80. Fatila, E. M.; Clerac, R.; Rouzieres, M.; Soldatov, D. V.; Jennings, M.; Preuss, K. E.*Chem. Commun.* **2013,** *49*, 6271-6273.

81. Arzberger, S.; Soper, J.; Anderson, O. P.; la Cour, A.; Wicholas, M.*Inorg. Chem.* **1999,** *38*, 757-761.

82. Kirk, M. L.; Shultz, D. A.*Coord. Chem. Rev.* **2013,** *257*, 218-233.

83. Shultz, D. A.; Bodnar, S. H.; Vostrikova, K. E.; Kampf, J. W.*Inorg. Chem.* **2000,** *39*, 6091-6093.

84. Shultz, D. A.; Vostrikova, K. E.; Bodnar, S. H.; Koo, H.-J.; Whangbo, M.-H.; Kirk, M. L.; Depperman, E. C.; Kampf, J. W.*J. Am. Chem. Soc.* **2003,** *125*, 1607-1617.

85. Kirk, M. L.; Shultz, D. A.; Habel-Rodriguez, D.; Schmidt, R. D.; Sullivan, U.*J. Phys. Chem. B* **2010,** *114*, 14712-14716.

86. (a) Yang, N. C.; Castro, A. J.*J. Am. Chem. Soc.* **1960,** *82*, 6208-6208; (b) Caneschi, A.; Dei, A.; Mussari, C. P.; Shultz, D. A.; Sorace, L.; Vostrikova, K. E.*Inorg. Chem.* **2002,** *41*, 1086-1092; (c) Shultz, D. A.; Boal, A. K.; Farmer, G. T.*J. Org. Chem.* **1998,** *63*, 9462-9469; (d) Shultz, D. A.; Bodnar, S. H.; Lee, H.; Kampf, J. W.; Incarvito, C. D.; Rheingold, A. L.*J. Am. Chem. Soc.* **2002,** *124*, 10054-10061.

87. Shultz, D. A.; Fico, R. M.; Bodnar, S. H.; Kumar, R. K.; Vostrikova, K. E.; Kampf, J. W.; Boyle, P. D.*J. Am. Chem. Soc.* **2003,** *125*, 11761-11771.

88. (a) Kirk, M. L.; Shultz, D. A.; Stasiw, D. E.; Habel-Rodriguez, D.; Stein, B.; Boyle, P. D.*J. Am. Chem. Soc.* **2013,** *135*, 14713-14725; (b) Kirk, M. L.; Shultz, D. A.; Stasiw, D. E.; Lewis, G. F.; Wang, G.; Brannen, C. L.; Sommer, R. D.; Boyle, P. D.*J. Am. Chem. Soc.* **2013,** *135*, 17144-17154.

89. Miller, J. S.; Calabrese, J. C.; Epstein, A. J.; Bigelow, R. W.; Zhang, J. H.; Reiff, W. M.*Chem. Commun.* **1986**, 1026-1028.

90. Manriquez, J. M.; Yee, G. T.; McLean, R. S.; Epstein, A. J.; Miller, J. S.*Science* **1991,** *252*, 1415-1417.

91. (a) Harvey, M. D.; Crawford, T. D.; Yee, G. T.*Inorg. Chem.* **2008,** *47*, 5649-5655; (b) Pokhodnya, K. I.; Lefler, B.; Miller, J. S.*Adv. Mat.* **2007,** *19*, 3281-3285.

92. Broderick, W. E.; Thompson, J. A.; Day, E. P.; Hoffman, B. M.*Science* **1990,** *249*, 401-403.

93. Motokawa, N.; Matsunaga, S.; Takaishi, S.; Miyasaka, H.; Yamashita, M.; Dunbar, K. R.*J. Am. Chem. Soc.* **2010,** *132*, 11943-11951.

94. Vickers, E. B.; Giles, I. D.; Miller, J. S.*Chem. Mater.* **2005,** *17*, 1667-1672.

95. Taliaferro, M. L.; Palacio, F.; Miller, J. S.*J. Mater. Chem.* **2006,** *16*, 2677-2684.

96. Ballesteros-Rivas, M.; Zhao, H.; Prosvirin, A.; Reinheimer, E. W.; Toscano, R. A.; Valdés-Martínez, J.; Dunbar, K. R.*Angew. Chem. Int. Ed.* **2012,** *51*, 5124-5128.

97. (a) Dapperheld, S.; Steckhan, E.; Brinkhaus, K.-H. G.; Esch, T.*Ber.* **1991,** *124*, 2557-2567; (b) Lambert, C.; Amthor, S.; Schelter, J.*J. Phys. Chem. A* **2004,** *108*, 6474-6486; (c) Seibt, J.; Schaumlöffel, A.; Lambert, C.; Engel, V.*J. Phys. Chem. A* **2008,** *112*, 10178-10184; (d) Amthor, S.; Noller, B.; Lambert, C.*Chem. Phys.* **2005,** *316*, 141-152; (e) Amthor, S.; Lambert, C.*J. Phys. Chem. A* **2005,** *110*, 1177-1189.

98. (a) Takashi Kurata, Y.-J. P., and Hiroyuki Nishide.*Polym. J.* **2007,** *39*, 675–683; (b) Murata, H.; Takahashi, M.; Namba, K.; Takahashi, N.; Nishide, H.*J. Org. Chem.* **2004,** *69*, 631-638; (c) Michinobu, T.; Kato, F.; Inui, J.; Nishide, H.*J. Polym. Sci., Part A: Polym. Chem.* **2009,** *47*, 4577-4586.

99. Bushby, R. J.; Kilner, C.; Taylor, N.; Williams, R. A.*Polyhedron* **2008,** *27*, 383-392.

100. Yano, M.; Inoue, K.; Motoyama, T.; Azuma, Y.; Tatsumi, M.; Yamauchi, O.; Oyama, M.; Sato, K.; Takui, T.*Polyhedron* **2005,** *24*, 2112-2115.

101. Yano, M.; Fujita, M.; Miyake, M.; Tatsumi, M.; Yajima, T.; Yamauchi, O.; Oyama, M.; Sato, K.; Takui, T.*Polyhedron* **2007,** *26*, 2174-2178.

102. Yano, M.; Manabe, M.; Tatsumi, M.; Oyama, M.; Sato, K.; Takui, T.*Polyhedron* **2009,** *28*, 1935-1939.

103. Kocyigit, O.*Synth. React. Inorg. Met.-Org. Chem.* **2012,** *42*, 196–204, .

104. Adugna, S.; Revunova, K.; Djukic, B.; Gorelsky, S. I.; Jenkins, H. A.; Lemaire, M. T.*Inorg. Chem.* **2010,** *49*, 10183-10190.

105. Revunova, K.; Gorelsky, S. I.; Lemaire, M. T.*Polyhedron* **2013,** *52*, 1118-1125.

106. Fang, Y.-Q.; Hanan, G. S.*Synlett* **2003,** *2003*, 0852-0854.

107. Villamena, F. A.; Horak, V.; Crist, D. R.*Inorg. Chim. Acta* **2003,** *342*, 125-130.

108. (a) Kitano, M.; Ishimaru, Y.; Inoue, K.; Koga, N.; Iwamura, H.*Inorg. Chem.* **1994,** *33*, 6012-6019; (b) Ishimaru, Y.; Kitano, M.; Kumada, H.; Koga, N.; Iwamura, H.*Inorg. Chem.* **1998,** *37*, 2273-2280; (c) Shimada, T.; Ishida, T.; Nogami, T.*Polyhedron* **2005,** *24*, 2593-2598.

109. Wenkert, D.; Woodward, R. B.*J. Org. Chem.* **1983,** *48*, 283-289.

110. (a) Dayan, S.*Synthesis* **1999,** *1999*, 1427-1430; (b) Joachim Demnitz, F. W.; D'Heni, M. B.*Org. Prep. Proced. Int.* **1998,** *30*, 467-469.

111. Antonini, I.; Claudi, F.; Cristalli, G.; Franchetti, P.; Grifantini, M.; Martelli, S.*J. Med. Chem.* **1981,** *24*, 1181-1184.

112. Trécourt, F.; Gervais, B.; Mongin, O.; Le Gal, C.; Mongin, F.; Quéguiner, G.*J. Org. Chem.* **1998,** *63*, 2892-2897.

113. Wang, X.; Rabbat, P.; O'Shea, P.; Tillyer, R.; Grabowski, E. J. J.; Reider, P. J.*Tetrahedron Lett.* **2000,** *41*, 4335-4338.

114. Landa, A.; Minkkilä, A.; Blay, G.; Jørgensen, K. A.*Chem. - Eur. J.* **2006,** *12*, 3472-3483.

115. Goodbrand, H. B.; Bender, T. P.; Gaynor, R. E.; Murphy, L. Process for preparing iodoaromatic compounds. 2005.

116. (a) Louie, J.; Hartwig, J. F.*Tetrahedron Lett.* **1995,** *36*, 3609-3612; (b) Guram, A. S.; Rennels, R. A.; Buchwald, S. L.*Angew. Chem. Int. Ed.* **1995,** *34*, 1348-1350.

117. Thompson, L. K.; Xu, Z. Memorial University of Newfoundlend, St. John's, Canada, 2005.

118. Gorelsky, S. I.; Basumallick, L.; Vura-Weis, J.; Sarangi, R.; Hodgson, K. O.; Hedman, B.; Fujisawa, K.; Solomon, E. I.*Inorg. Chem.* **2005,** *44*, 4947-4960.

119. Xia, N.; Taillefer, M.*Angew. Chem. Int. Ed.* **2009,** *48*, 337-339.

120. Hodgson, H. H.; Walker, J.*J. Chem. Soc.* **1933**, 1620-1621.

121. Piccard, J.; Larsen, L. M.*J. Am. Chem. Soc.* **1917,** *39*, 2006-2009.

122. Schafer, A.; Huber, C.; Ahlrichs, R.*The Journal of Chemical Physics* **1994,** *100*, 5829-5835.

123. (a) Godbout, N.; Salahub, D. R.; Andzelm, J.; Wimmer, E.*Can. J. Chem.* **1992,** *70*, 560-571; (b) Reed, A. E.; Curtiss, L. A.; Weinhold, F.*Chem. Rev.* **1988,** *88*, 899-926.

124. Gorelsky, S. I. AOMix, version 6.46; University of Ottawa, Ottawa, 2010.

125. Gorelsky, S. I.; Lever, A. B. P.*J. Organomet. Chem.* **2001,** *635*, 187-196.

126. Chambers, R. J.; Marfat, A.*Synth. Commun.* **1997,** *27*, 515-520.

127. Habermeyer, B.; Takai , A.; Gros, C. P.; El Ojaimi , M.; Barbe, J.-M.; Fukuzumi , S.*Chem. - Eur. J.* **2011,** *17*, 10670-10681.

128. Song, J. J.; Yee, N. K.; Tan, Z.; Xu, J.; Kapadia, S. R.; Senanayake, C. H.*Org. Lett.* **2004,** *6*, 4905-4907.

129. Mandal, A. B.; Augustine, J. K.; Quattropani, A.; Bombrun, A.*Tetrahedron Lett.* **2005,** *46*, 6033-6036.

130. Liu, M. C.; Lin, T. C.; Sartorelli, A. C.*J. Med. Chem.* **1992,** *35*, 3672-3677.

131. Olah, G. A.; Wang, Q.; Sandford, G.; Surya Prakash, G. K.*J. Org. Chem.* **1993,** *58*, 3194-3195.

132. Hubbard, A.; Okazaki, T.; Laali, K. K.*J. Org. Chem.* **2007,** *73*, 316-319.

133. J. Bushby, R.; R. Mcgill, D.; M. Ng, K.; Taylor, N.*J. Mater. Chem.* **1997,** *7*, 2343-2354.

134. (a) Carter, M. B.; Schiott, B.; Gutierrez, A.; Buchwald, S. L.*J. Am. Chem. Soc.* **1994,** *116*, 11667-11670; (b) Hoyos, M.; Sprick, R. S.; Wang, C.; Turner, M. L.; Navarro, O.*J. Polym. Sci., Part A: Polym. Chem.* **2012,** *50*, 4155-4160; (c) Berk, S. C.; Buchwald, S. L.*J. Org. Chem.* **1992,** *57*, 3751-3753.

135. Appella, D. H.; Moritani, Y.; Shintani, R.; Ferreira, E. M.; Buchwald, S. L.*J. Am. Chem. Soc.* **1999,** *121*, 9473-9474.

136. (a) Misal Castro, L. C.; Li, H.; Sortais, J.-B.; Darcel, C.*Chem. Commun.* **2012,** *48*, 10514-10516; (b) Bézier, D.; Venkanna, G. T.; Castro, L. C. M.; Zheng, J.; Roisnel, T.; Sortais, J.-B.; Darcel, C.*Adv. Synth. Catal.* **2012,** *354*, 1879-1884.

137. Junge, K.; Wendt, B.; Zhou, S.; Beller, M.*Eur. J. Org. Chem.* **2013,** *2013*, 2061-2065.

138. Das, S.; Li, Y.; Junge, K.; Beller, M.*Chem. Commun.* **2012,** *48*, 10742-10744.

139. Igarashi, M.; Kobayashi, T.; Sato, K.; Ando, W.; Matsumoto, T.; Shimada, S.; Hara, M.; Uchida, H.*J. Organomet. Chem.* **2013,** *725*, 54-59.

140. (a) Xing, P.; Zang, W.; Huang, Z.-g.; Zhan, Y.-x.; Zhu, C.-j.; Jiang, B.*Synlett* **2012,** *23*, 2269-2273; (b) Sakai, N.; Usui, Y.; Ikeda, R.; Konakahara, T.*Adv. Synth. Catal.* **2011,** *353*, 3397-3401.

141. Cheng, C.; Brookhart, M.*Angew. Chem. Int. Ed.* **2012,** *51*, 9422-9424.

142. Matsubara, K.; Iura, T.; Maki, T.; Nagashima, H.*J. Org. Chem.* **2002,** *67*, 4985-4988.

143. Toh, C. K.; Sum, Y. N.; Fong, W. K.; Ang, S. G.; Fan, W. Y.*Organometallics* **2012,** *31*, 3880-3887.

144. Doyle, M. P.; West, C. T.; Donnelly, S. J.; McOsker, C. C.*J. Organomet. Chem.* **1976,** *117*, 129-140.

145. Adlington, M. G.; Orfanopoulos, M.; Fry, J. L.*Tetrahedron Lett.* **1976,** *17*, 2955-2958.

146. Fry, J. L.; Orfanopoulos, M.; Adlington, M. G.; Dittman, W. P.; Silverman, S. B.*J. Org. Chem.* **1978,** *43*, 374-375.

147. Larsen, J. W.; Chang, L. W.*J. Org. Chem.* **1979,** *44*, 1168-1170.

148. Prakash, G. K. S.; Mathew, T.; Marinez, E. R.; Esteves, P. M.; Rasul, G.; Olah, G. A.*J. Org. Chem.* **2006,** *71*, 3952-3958.

149. Parks, D. J.; Piers, W. E.*J. Am. Chem. Soc.* **1996,** *118*, 9440-9441.

150. Massey, A. C.; Park, J.; Stone, F. G. A.*Proc. Chem. Soc.* **1963**, 212.

151. Parks, D. J.; Blackwell, J. M.; Piers, W. E.*J. Org. Chem.* **2000,** *65*, 3090-3098.

152. Piers, W. E.; Marwitz, A. J. V.; Mercier, L. G.*Inorg. Chem.* **2011,** *50*, 12252-12262.

153. (a) Parks, D. J.; Piers, W. E.; Yap, G. P. A.*Organometallics* **1998,** *17*, 5492-5503; (b) Peuser, I.; Fröhlich, R.; Kehr, G.; Erker, G.*Eur. J. Inorg. Chem.* **2010,** *2010*, 849-853.

154. Chojnowski, J.; Rubinsztajn, S.; Cella, J. A.; Fortuniak, W.; Cypryk, M.; Kurjata, J.; Kaźmierski, K.*Organometallics* **2005,** *24*, 6077-6084.

155. (a) Oestreich, M.*Synlett* **2007,** *2007*, 1629-1643; (b) Rendler, S.; Oestreich, M.*Angew. Chem. Int. Ed.* **2008,** *47*, 5997-6000.

156. Shinke, S.; Tsuchimoto, T.; Kawakami, Y.*Silicon Chem* **2007,** *3*, 243-249.

157. Blackwell, J. M.; Sonmor, E. R.; Scoccitti, T.; Piers, W. E.*Org. Lett.* **2000,** *2*, 3921-3923.

158. Müther, K.; Mohr, J.; Oestreich, M.*Organometallics* **2013**.

159. Asao, N.; Ohishi, T.; Sato, K.; Yamamoto, Y.*Tetrahedron* **2002,** *58*, 8195-8203.

160. Hog, D. T.; Oestreich, M.*Eur. J. Org. Chem.* **2009,** *2009*, 5047-5056.

161. Chen, D.; Leich, V.; Pan, F.; Klankermayer, J.*Chem. - Eur. J.* **2012,** *18*, 5184-5187.

162. Mewald, M.; Oestreich, M.*Chem. - Eur. J.* **2012,** *18*, 14079-14084.

163. Mewald, M.; Fröhlich, R.; Oestreich, M.*Chem. - Eur. J.* **2011,** *17*, 9406-9414.

164. (a) Rubin, M.; Schwier, T.; Gevorgyan, V.*J. Org. Chem.* **2002,** *67*, 1936-1940; (b) Gevorgyan, V.; Liu, J.-X.; Rubin, M.; Benson, S.; Yamamoto, Y.*Tetrahedron Lett.* **1999,** *40*, 8919-8922.

165. Shchepin, R.; Xu, C.; Dussault, P.*Org. Lett.* **2010,** *12*, 4772-4775.

166. Gevorgyan, V.; Rubin, M.; Liu, J.-X.; Yamamoto, Y.*J. Org. Chem.* **2001,** *66*, 1672-1675.

167. Nimmagadda, R. D.; McRae, C.*Tetrahedron Lett.* **2006,** *47*, 5755-5758.

168. Bézier, D.; Park, S.; Brookhart, M.*Org. Lett.* **2013,** *15*, 496-499.

169. Skjel, M. K.; Houghton, A. Y.; Kirby, A. E.; Harrison, D. J.; McDonald, R.; Rosenberg, L.*Org. Lett.* **2009,** *12*, 376-379.

170. Lee, P. T. K.; Skjel, M. K.; Rosenberg, L.*Organometallics* **2013,** *32*, 1575-1578.

171. (a) Berkefeld, A.; Piers, W. E.; Parvez, M.*J. Am. Chem. Soc.* **2010,** *132*, 10660-10661; (b) Berkefeld, A.; Piers, W. E.; Parvez, M.; Castro, L.; Maron, L.; Eisenstein, O.*Chem. Sci.* **2013,** *4*, 2152-2162.

172. Morgan, M. M.; Marwitz, A. J. V.; Piers, W. E.; Parvez, M.*Organometallics* **2012,** *32*, 317-322.

173. Bergquist, C.; Bridgewater, B. M.; Harlan, C. J.; Norton, J. R.; Friesner, R. A.; Parkin, G.*J. Am. Chem. Soc.* **2000,** *122*, 10581-10590.

174. Sudo, T.; Asao, N.; Gevorgyan, V.; Yamamoto, Y.*J. Org. Chem.* **1999,** *64*, 2494-2499.

175. (a) Asao, N.; Sudo, T.; Yamamoto, Y.*J. Org. Chem.* **1996,** *61*, 7654-7655; (b) Kato, N.; Tamura, Y.; Kashiwabara, T.; Sanji, T.; Tanaka, M.*Organometallics* **2010,** *29*, 5274-5282.

176. Koller, J.; Bergman, R. G.*Organometallics* **2011,** *31*, 2530-2533.

177. Kursanov, D. N.; Parnes, Z. N.; Bassova, G. I.; Loim, N. M.; Zdanovich, V. I.*Tetrahedron* **1967,** *23*, 2235-2242.

178. Patel, J. P.; Li, A.-H.; Dong, H.; Korlipara, V. L.; Mulvihill, M. J.*Tetrahedron Lett.* **2009,** *50*, 5975-5977.

179. Corriu, R. J. P.; Henner, M.*J. Organomet. Chem.* **1974,** *74*, 1-28.

180. (a) Corriu, R. J. P.; Dabosi, G.; Martineau, M.*J. Organomet. Chem.* **1978,** *154*, 33-43; (b) Corriu, R. J. P.; Guerin, C.*J. Organomet. Chem.* **1980,** *198*, 231-320; (c) Corriu, R. J. P.; Perz, R.; Reye, C.*Tetrahedron* **1983,** *39*, 999-1009; (d) Corriu, R. J. P.; Dabosi, G.; Martineau, M.*J. Organomet. Chem.* **1980,** *186*, 25-37.

181. (a) Becker, B.; Corriu, R.; Guerin, C.; Henner, B.; Wang, Q.*J. Organomet. Chem.* **1989,** *359*, C33-C35; (b) Boyer, J.; Breliere, C.; Corriu, R. J. P.; Kpoton, A.; Poirier, M.; Royo, G.*J. Organomet. Chem.* **1986,** *311*, C39-C43; (c) Boyer, J.; Corriu, R. J. P.; Kpoton, A.; Mazhar, M.; Poirier, M.; Royo, G.*J. Organomet. Chem.* **1986,** *301*, 131-135; (d) Corriu, R.; Guérin, C.; Henner, B.; Wang, Q.*J. Organomet. Chem.* **1989,** *365*, C7-C10; (e) Corriu, R. J. P.*J. Organomet. Chem.* **1990,** *400*, 81-106.

182. Chuit, C.; Corriu, R. J. P.; Perz, R.; Reyé, C.*Synthesis* **1982,** *1982*, 981-984.

183. Boyer, J.; Corriu, R. J. P.; Perz, R.; Reye, C.*Tetrahedron* **1981,** *37*, 2165-2171.

184. Boyer, J.; Corriu, R. J. P.; Perz, R.; Reye, C.*Tetrahedron* **1983,** *39*, 117-122.

185. (a) Fujita, M.; Hiyama, T.*J. Am. Chem. Soc.* **1984,** *106*, 4629-4630; (b) Fujita, M.; Hiyama, T.*J. Org. Chem.* **1988,** *53*, 5405-5415.

186. Kobayashi, Y.; Takahisa, E.; Nakano, M.; Watatani, K.*Tetrahedron* **1997,** *53*, 1627-1634.

187. (a) Drew, M. D.; Lawrence, N. J.; Fontaine, D.; Sehkri, L.; Bowles, S. A.; Watson, W.*Synlett* **1997,** *1997*, 989-991; (b) J. Lawrence, N.; D. Drew, M.; M. Bushell, S.*J. Chem. Soc., Perkin Trans. 1* **1999,** *0*, 3381-3391.

188. Drew, M. D.; Lawrence, N. J.; Watson, W.; Bowles, S. A.*Tetrahedron Lett.* **1997,** *38*, 5857-5860.

189. Zhou, S.; Junge, K.; Addis, D.; Das, S.; Beller, M.*Org. Lett.* **2009,** *11*, 2461-2464.

190. Bornschein, C.; Werkmeister, S.; Junge, K.; Beller, M.*New J. Chem.* **2013,** *37*, 2061-2065.

191. (a) Becker, B.; Corriu, R. J. P.; Guérin, C.; Henner, B.; Wang, Q.*J. Organomet. Chem.* **1989,** *368*, C25-C28; (b) Becker, B.; Corriu, R. J. P.; Guérin, C.; Henner, B. J. L.*J. Organomet. Chem.* **1989,** *369*, 147-154; (c) Corriu, R.; Guérin, C.; Henner, B.; Wang, Q.*Inorg. Chim. Acta* **1992,** *198–200*, 705-713.

192. Denmark, S. E.; Beutner, G. L.*Angew. Chem. Int. Ed.* **2008,** *47*, 1560-1638.

193. Prince, P. D.; Bearpark, M. J.; McGrady, G. S.; Steed, J. W.*J. Chem. Soc., Dalton Trans.* **2008**, 271-282.

194. Corriu, R. J. P.; Guerin, C.; Henner, B. J. L.; Wang, Q.*J. Organomet. Chem.* **1992,** *439*, C1-C5.

195. Hosomi, A.; Hayashida, H.; Kohra, S.; Tominaga, Y.*Chem. Commun.* **1986,** *0*, 1411-1412.

196. Kohra, S.; Hayashida, H.; Tominaga, Y.; Hosomi, A.*Tetrahedron Lett.* **1988,** *29*, 89-92.

197. Nishikori, H.; Yoshihara, R.; Hosomi, A.*Synlett* **2003,** *2003*, 0561-0563.

198. Hojo, M.; Fujii, A.; Murakami, C.; Aihara, H.; Hosomi, A.*Tetrahedron Lett.* **1995,** *36*, 571-574.

199. Hojo, M.; Murakami, C.; Fujii, A.; Hosomi, A.*Tetrahedron Lett.* **1999,** *40*, 911-914.

200. Addis, D.; Zhou, S.; Das, S.; Junge, K.; Kosslick, H.; Harloff, J.; Lund, H.; Schulz, A.; Beller, M.*Chemistry – An Asian Journal* **2010,** *5*, 2341-2345.

201. Fedorov, A.; Toutov, A. A.; Swisher, N. A.; Grubbs, R. H.*Chem. Sci.* **2013**.

202. Fernandez-Salas, J. A.; Manzini, S.; Nolan, S. P.*Chem. Commun.* **2013,** *49*, 9758-9760.

203. (a) Bohlmann, F.*Ber.* **1952,** *85*, 390-394; (b) Stout, D. M.; Meyers, A. I.*Chem. Rev.* **1982,** *82*, 223-243.

204. (a) Hill, M. S.; Kociok-Kohn, G.; MacDougall, D. J.; Mahon, M. F.; Weetman, C.*J. Chem. Soc., Dalton Trans.* **2011,** *40*, 12500-12509; (b) Arrowsmith, M.; Hill, M. S.; Hadlington, T.; Kociok-Köhn, G.; Weetman, C.*Organometallics* **2011,** *30*, 5556-5559.

205. Rosales, M.; Vallejo, R.; Soto, J.; Chacón, G.; González, Á.; González, B.*Catal Lett* **2006,** *106*, 101-105.

206. Fache, F.*Synlett* **2004,** *2004*, 2827-2829.

207. Murahashi, S.-I.; Imada, Y.; Hirai, Y.*Bull. Chem. Soc. Jpn.* **1989,** *62*, 2968-2976.

208. Ren, D.; He, L.; Yu, L.; Ding, R.-S.; Liu, Y.-M.; Cao, Y.; He, H.-Y.; Fan, K.-N.*J. Am. Chem. Soc.* **2012,** *134*, 17592-17598.

209. Chin, C.; Park, Y.; Lee, B.*Catal Lett* **1995,** *31*, 239-243.

210. Sánchez-Delgado, R. A.; González, E.*Polyhedron* **1989,** *8*, 1431-1436.

211. Baralt, E.; Smith, S. J.; Hurwitz, J.; Horvath, I. T.; Fish, R. H.*J. Am. Chem. Soc.* **1992,** *114*, 5187-5196.

212. Lu, S.-M.; Han, X.-W.; Zhou, Y.-G.*J. Organomet. Chem.* **2007,** *692*, 3065-3069.

213. Wang, D.-W.; Zeng, W.; Zhou, Y.-G.*Tetrahedron: Asymmetry* **2007,** *18*, 1103-1107.

214. Chan, S. H.; Lam, K. H.; Li, Y.-M.; Xu, L.; Tang, W.; Lam, F. L.; Lo, W. H.; Yu, W. Y.; Fan, Q.; Chan, A. S. C.*Tetrahedron: Asymmetry* **2007,** *18*, 2625-2631.

215. Kuwano, R.; Kashiwabara, M.; Sato, K.; Ito, T.; Kaneda, K.; Ito, Y.*Tetrahedron: Asymmetry* **2006,** *17*, 521-535.

216. (a) Mršić, N.; Jerphagnon, T.; Minnaard, A. J.; Feringa, B. L.; de Vries, J. G.*Tetrahedron: Asymmetry* **2010,** *21*, 7-10; (b) Maj, A. M.; Suisse, I.; Méliet, C.; Agbossou-Niedercorn, F.*Tetrahedron: Asymmetry* **2010,** *21*, 2010-2014.

217. (a) Voutchkova, A. M.; Gnanamgari, D.; Jakobsche, C. E.; Butler, C.; Miller, S. J.; Parr, J.; Crabtree, R. H.*J. Organomet. Chem.* **2008,** *693*, 1815-1821; (b) Lee, S.-H.; Gutsulyak, D. V.; Nikonov, G. I.*Organometallics* **2013,** *32*, 4457-4464.

218. (a) Gutsulyak, D. V.; van der Est, A.; Nikonov, G. I.*Angew. Chem. Int. Ed.* **2011,** *50*, 1384-1387; (b) Osakada, K.*Angew. Chem. Int. Ed.* **2011,** *50*, 3845-3846.

219. Königs, C. D. F.; Klare, H. F. T.; Oestreich, M.*Angew. Chem. Int. Ed.* **2013,** *52*, 10076-10079.

220. Xue, Z.-Y.; Jiang, Y.; Peng, X.-Z.; Yuan, W.-C.; Zhang, X.-M.*Adv. Synth. Catal.* **2010,** *352*, 2132-2136.

221. Srikrishna, A.; Jagadeeswar Reddy, T.; Viswajanani, R.*Tetrahedron* **1996,** *52*, 1631-1636.

222. Ranu, B. C.; Jana, U.; Sarkar, A.*Synth. Commun.* **1998,** *28*, 485-492.

223. Mahdi, T.; Heiden, Z. M.; Grimme, S.; Stephan, D. W.*J. Am. Chem. Soc.* **2012,** *134*, 4088-4091.

224. Mahdi, T.; del Castillo, J. N.; Stephan, D. W.*Organometallics* **2013,** *32*, 1971-1978.

225. Liu, Y.; Du, H.*J. Am. Chem. Soc.* **2013,** *135*, 12968-12971.

226. Glorius, F.*Org. Biomol. Chem.* **2005,** *3*, 4171-4175.

227. (a) Núñez-Rico, J. L.; Vidal-Ferran, A.*Org. Lett.* **2013,** *15*, 2066-2069; (b) Fernández-Pérez, H.; Etayo, P.; Panossian, A.; Vidal-Ferran, A.*Chem. Rev.* **2011,** *111*, 2119-2176; (c) Núñez-Rico, J. L.; Fernández-Pérez, H. c.; Benet-Buchholz, J.; Vidal-Ferran, A.*Organometallics* **2010,** *29*, 6627-6631.

228. Constable, D. J. C.; Dunn, P. J.; Hayler, J. D.; Humphrey, G. R.; Leazer, J. J. L.; Linderman, R. J.; Lorenz, K.; Manley, J.; Pearlman, B. A.; Wells, A.; Zaks, A.; Zhang, T. Y.*Green Chem.* **2007,** *9*, 411-420.

229. (a) Parshina, L. N.; Oparina, L. A.; Khil'ko, M. Y.; Trofimov, B. A.*J. Organomet. Chem.* **2003,** *665*, 246-249; (b) Suzuki, E.; Nomoto, Y.; Okamoto, M.; Ono, Y.*Catal Lett* **1997,** *48*, 75-78.

230. (a) Rochow, E. G.*J. Am. Chem. Soc.* **1945,** *67*, 963-965; (b) Bazant, V.*Pure Appl. Chem.* **1969,** *19*, 473-488; (c) Clarke, M. P.; Davidson, I. M. T.*J. Organomet. Chem.* **1991,** *408*, 149-156.

231. (a) Lipshutz, B. H.; Frieman, B. A.*Angew. Chem. Int. Ed.* **2005,** *44*, 6345-6348; (b) Voigtritter, K. R.; Isley, N. A.; Moser, R.; Aue, D. H.; Lipshutz, B. H.*Tetrahedron* **2012,** *68*, 3410-3416; (c) Deutsch, C.; Krause, N.; Lipshutz, B. H.*Chem. Rev.* **2008,** *108*, 2916-2927.

232. Hansen, M. C.; Buchwald, S. L.*Tetrahedron Lett.* **1999,** *40*, 2033-2034.

233. (a) Pri-Bar, I.; Buchman, O.*J. Org. Chem.* **1986,** *51*, 734-736; (b) Pri-Bar, I.; Buchman, O.*J. Org. Chem.* **1984,** *49*, 4009-4011.

234. Suzuki, E.; Nomoto, Y.; Okamoto, M.; Ono, Y.*Appl. Catal., A* **1998,** *167*, 7-10.

235. Khalimon, A. Y.; Shirobokov, O. G.; Peterson, E.; Simionescu, R.; Kuzmina, L. G.; Howard, J. A. K.; Nikonov, G. I.*Inorg. Chem.* **2012,** *51*, 4300-4313.

236. Lee, J. M.; Park, E. J.; Cho, S. H.; Chang, S.*J. Am. Chem. Soc.* **2008,** *130*, 7824-7825.

237. Bheeter, L. P.; Henrion, M.; Brelot, L.; Darcel, C.; Chetcuti, M. J.; Sortais, J.-B.; Ritleng, V.*Adv. Synth. Catal.* **2012,** *354*, 2619-2624.

238. Castro, L. C. M.; Bézier, D.; Sortais, J.-B.; Darcel, C.*Adv. Synth. Catal.* **2011,** *353*, 1279-1284.

239. Nogueira Fernandes, J. L.; de Souza, M. C.; Souza Brenelli, E. C.; Brenelli, J. A.*Synthesis* **2009,** *2009*, 4058-4062.

240. Zhang, B.; Zhu, S.-F.; Zhou, Q.-L.*Tetrahedron* **2013,** *69*, 2033-2037.

241. (a) Nagendra, G.; Madhu, C.; Vishwanatha, T. M.; Sureshbabu, V. V.*Tetrahedron Lett.* **2012,** *53*, 5059-5063; (b) Terent'ev, A. O.; Krylov, I. B.; Sharipov, M. Y.; Kazanskaya, Z. M.; Nikishin, G. I.*Tetrahedron* **2012,** *68*, 10263-10271.

242. Jiang, F.; Bézier, D.; Sortais, J.-B.; Darcel, C.*Adv. Synth. Catal.* **2011,** *353*, 239-244.

243. Singh, R.; Allam, B. K.; Raghuvanshi, D. S.; Singh, K. N.*Tetrahedron* **2013,** *69*, 1038-1042.